The Dissertation Committee for Raman Kumar Jha Certifies that this is the approved version of the following dissertation:

Investigation of Local Mixing and Its Influence on Core Scale Mixing (Dispersion)

Committee:

Steven L. Bryant, Supervisor

Larry W. Lake, Co-supervisor

Russell T. Johns

James W. Jennings

Todd J. Arbogast

Investigation of Local Mixing and Its Influence on Core Scale Mixing (Dispersion)

by

Raman Kumar Jha, M.S., B. Tech.

Dissertation

Presented to the Faculty of the Graduate School of

The University of Texas at Austin

in Partial Fulfillment

of the Requirements

for the Degree of

Doctor of Philosophy

The University of Texas at Austin

August, 2008

Dedication

To all the researchers who contribute to the growth of human knowledge.

Acknowledgements

I am grateful to my supervisor Dr. Steven L. Bryant for his support, guidance and continuous encouragement without which this work would not have been possible. His guidance helped me think rationally about complex problems. I also thank him for encouraging me to develop independent thinking and giving me complete freedom to explore on my own.

It has been a pleasure and privilege to work closely with Dr. Larry W. Lake. I thank him for taking keen interest in the project and giving valuable comments and suggestions throughout. His vast knowledge and experience have played an important role in success of this project.

I would like to extend my most sincere appreciation to the members of my dissertation committee, Dr. Russell T. Johns, Dr. James W. Jennings and Dr. Todd J. Arbogast for taking time to review my dissertation. I would also like to thank them for their valuable comments especially during my proposal defense. They had a significant impact on the outcome of the project.

Special thanks go to my friends and the fellow graduate students Abraham John and Gholamreza Garmeh for their technical discussions and suggestions. I thank them for being supportive and good friends. I would like to thank Abraham especially for introducing me to multi-physics modeling using FEMLAB which forms a major part of this research. I would also like to thank Ms. Cynthia Thane for providing coordinates of

random packing of spheres. That served as the starting point for quantifying dispersion in realistic pore space.

I would like to thank Roger Terzian for paying immediate attention to my computer and software related needs. His helpful attitude is deeply appreciated.

I would also like to thank my colleagues and friends at The University of Texas: Navanit, Raushan, Siyavash, Liying, Jitendra, Narayan and Vishal for technical discussion on various topics, their support and encouragement. Their camaraderie has made these years at Austin the most memorable time of my life.

I also thank my parents and sister for their love, affection and patience during this study. It would not have been possible without their support.

The funding provided for the project by the US Department of Energy (DOE grant # DE-FC26-04NT15534) is also deeply acknowledged.

Investigation of Local Mixing and Its Influence on Core Scale Mixing (Dispersion)

Publication No._____

Raman Kumar Jha, Ph. D.

The University of Texas at Austin, 2008

Supervisor: Steven L. Bryant

Co-supervisor: Larry W. Lake

Local displacement efficiency in miscible floods is significantly affected by mixing taking place in the medium. Laboratory experiments usually measure flow-averaged ("cup mixed") effluent concentration histories. The core-scale averaged mixing, termed as *dispersion*, is used to quantify mixing in flow through porous media. The dispersion coefficient has the contributions of convective spreading and diffusion lumped together. Despite decades of research there remain questions about the nature and origin of dispersion.

The main objective of this research is to understand the basic physics of solute transport and mixing at the pore scale and to use this information to explain core-scale mixing behavior (dispersion). We use two different approaches to study the interaction

between convective spreading and diffusion for a range of flow conditions and the influence of their interaction on dispersion.

In the first approach, we perform a direct numerical simulation of pore scale solute transport (by solving the Navier Stokes and convection diffusion equations) in a surrogate pore space. The second approach tracks movement of solute particles through a network model that is physically representative of real granular material. The first approach is useful in direct visualization of mixing in pore space whereas the second approach helps quantify the effect of pore scale process on core scale mixing (dispersion).

Mixing in porous media results from interaction between convective spreading and molecular diffusion. The converging-diverging flow around sand grains causes the solute front to stretch, split and rejoin. In this process the area of contact between regions of high and low solute concentrations increases by an order of magnitude. Diffusion tends to reduce local variations in solute concentration inside the pore body. If the fluid velocity is small, diffusion is able to homogenize the solute concentration inside each pore. On the other hand, in the limit of very large fluid velocity (or no diffusion) local mixing because of diffusion tends to zero and dispersion is entirely caused by convective spreading.

Flow reversal provides insights about mixing mechanisms in flow through porous media. For purely convective transport, upon flow reversal solute particles retrace their path to the inlet. Convective spreading cancels and echo dispersion is zero. Diffusion, even though small in magnitude, causes local mixing and makes dispersion in porous

media irreversible. Echo dispersion in porous media is far greater than diffusion and as large as forward (transmission) dispersion.

In the second approach, we study dispersion in porous media by tracking movement of a swarm of solute particles through a physically representative network model. We developed deterministic rules to trace paths of solute particles through the network. These rules yield flow streamlines through the network comparable to those obtained from a full solution of Stokes' equation. In the absence of diffusion the paths of all solute particles are completely determined and reversible. We track the movement of solute particles on these paths to investigate dispersion caused by purely convective spreading at the pore scale. Then we superimpose diffusion and study its influence on dispersion. In this way we obtain for the first time an unequivocal assessment of the roles of convective spreading and diffusion in hydrodynamic dispersion through porous media. Alternative particle tracking algorithms that use a probabilistic choice of an out-flowing throat at a pore fail to quantify convective spreading accurately.

For Fickian behavior of dispersion it is essential that all solute particles encounter a wide range of independent (and identically distributed) velocities. If plug flow occurs in the pore throats a solute particle can encounter a wide range of independent velocities because of velocity differences in pore throats and randomness of pore structure. Plug flow leads to a purely convective spreading that is asymptotically Fickian. Diffusion superimposed on plug flow acts independently of convective spreading causing dispersion to be simply the sum of convective spreading and diffusion. In plug flow hydrodynamic dispersion varies linearly with the pore-scale Peclet number.

For a more realistic parabolic velocity profile in pore throats particles near the solid surface of the medium do not have independent velocities. Now purely convective spreading is non-Fickian. When diffusion is non-zero, solute particles can move away from the low velocity region near the solid surface into the main flow stream and subsequently dispersion again becomes asymptotically Fickian. Now dispersion is the result of an interaction between convection and diffusion and it results in a weak non-linear dependence of dispersion on Peclet number. The dispersion coefficients predicted by particle tracking through the network are in excellent agreement with the literature experimental data.

We conclude that the essential phenomena giving rise to hydrodynamic dispersion observed in porous media are (i) stream splitting of the solute front at every pore, thus causing independence of particle velocities purely by convection, (ii) a velocity gradient within throats and (iii) diffusion. Taylor's dispersion in a capillary tube accounts for only the second and third of these phenomena, yielding a quadratic dependence of dispersion on Peclet number. Plug flow in the bonds of a physically representative network accounts for the only the first and third phenomena, resulting in a linear dependence of dispersion upon Peclet number.

Table of Contents

List of Tables xv

List of Figures xvi

List of Figures xvi

Chapter 1: Introduction 1

1.1 Importance of mixing in porous media 1

1.2 Mixing in porous media 2

1.3 Description of mixing 5

1.4 Quantification of mixing 5

1.5 Objective 10

1.6 Method 10

1.7 Organization of the dissertation 15

References 16

Chapter 2: Investigation of Local Mixing through Pore Scale Simulation 19

2.1 Introduction 19

2.2 Method 20

2.3 Model description 21

2.4 Comment on solute breakthrough curves 23

2.5 Basic mechanism of local mixing 24

2.6 simulations on an ordered pack 25

2.7 Simulations on a disordered pack 29

2.8 Effect of peclet number on mixing: simulations on a regular pack 33

2.9 Conclusions 36

References 36

Chapter 3: Flow Reversal and Mixing 38

3.1 Introduction 38

3.2 Method 40

3.3 Mixing mechanisms and effect of flow reversal on mixing 41
3.4 Discussion on local mixing mechanism.....48
3.5 Flow reversibility simulations in a disordered pack (with a correlated heterogeneity) 50
3.6 Effect of depth of penetration on irreversibility of mixing.....54
3.7 Flow reversibility simulations in an ordered pack.....55
3.8 Flow reversibility simulations in a disordered pack without correlated heterogeneity.....59
3.9 Comment on flow reversal studies at field scale 61
3.10 Conclusions.....61
3.11 Limitations 62
References.....63

Chapter 4: Preparing a Physically Representative Network Model.....65
4.1 Introduction.....65
4.2 Description of dense random packing of spheres 68
4.3 Discretizing the pore space 69
4.4 Grouping together neighbors of a cell 71
4.5 Calculating bond conductance connecting two neighbors.....77
4.6 Solving for potentials in the network.....90
4.7 Effect of spatial correlations in pore structure.....99
4.8 Summary.....100
References.....100

Chapter 5: Deterministic Rules for Tracking Solute Particle through a Physically Representative Network Model 102
5.1 Introduction.....102
5.2 Deterministic rules for choosing an out-flowing bond 103
5.3 Mapping an incoming point to an out-flowing bond 112
5.4 Particle movement in the network 114
5.5 Particle tracking in a tube with convection and diffusion.....115
5.7 Validation of particle tracking algorithm.....120
5.8 Algorithm for tracking particle through the network.....122

5.8 Summary 123

References 124

Chapter 6: Quantitative Investigation of Dispersion in a Dense, Random Packing of Spheres 125

6.1 Introduction 125

6.2 Convective spreading as a diffusive process 126

6.3 Particle tracking in a physically representative network model with plug flow in bonds (without diffusion) 129

6.4 Effect of diffusion on particle statistics 135

6.5 Analytical expression for dispersion coefficient 139

6.6 Particle tracking with a probabilistic choice of out-flowing bond at pore bodies 141

6.7 Simulation with a parabolic velocity profile in bonds 143

6.8 Convective spreading with parabolic velocity profile in bonds 146

6.9 Effect of diffusion on particle statistics 149

6.10 Discussion 159

Summary and conclusions 162

Chapter 7: Effect of Medium Geometry on Dispersion 167

7.1 Introduction 167

7.2 Dispersion in spatially ordered porous media (staggered srray of disks) 168

7.3 Dispersion in random porous media 170

7.4 Discussion 172

7.5 Effect of porosity on dispersion 175

7.6 Conclusions 178

Chapter 8: Summary, Conclusions and Future Work 181

8.1 Summary and conclusions 181

8.2 Future work 184

Appendix 185

A1. Marking a segment of a circular tube carrying a known fraction of total flow 185

A2. Determining geometric centers of flow segments.....189

A3. Marking segments of a circular tube splitting into three streams 191

A4. Determining relative distance from boundary and angle from reference vector.....192

A5. Rotating a point on a horizontal circle in any arbitrary direction and vice versa 196

List of Symbols.....201

Bibliography 203

Vita….....212

List of Tables

Table 4.1: Sphere indices forming a cell and coordinates of sphere centers. Radius of spheres = 2.1918. 73

Table 4.2: Sphere indices forming the four faces of a cell. The sphere indices for a face are sorted in ascending order. 74

Table 4.3: Sphere indices forming the four faces of a cell put one below other along with the cell number. 75

Table 4.4: Sphere indices vertically sorted in ascending order. The neighbors sharing a face (highlighted) get lined up one below another. 76

Table 4.5.1: Calculation of conductance of bonds connecting two cells. 85

Table 4.5.2: Calculation of conductance of bonds connecting two cells. 86

Table 4.5.3: Calculation of conductance of bonds connecting two cells. 87

Table 4.5.4: Calculation of conductance of bonds connecting two cells. 88

Table 4.6: Neighbors of a cell grouped together and the corresponding bond conductances. Cells with only three neighbors are located at an outer boundary of the network. 89

Table 4.7: Bond conductances for the schematic network. 94

Table 5.1: Comparison of simulated dispersion in a capillary tube with Taylor's experiments 121

List of Figures

Figure 1.1: Attenuation of a miscible solvent slug as a result of mixing in the reservoir. 1

Figure 1.2: Transmission dispersion experiment. A step change in solute concentration is made at the inlet face and effluent concentration monitored at the outlet face. 6

Figure 1.3: Convective spreading hypothesis. 7

Figure 1.4: Local mixing hypothesis. 8

Figure 2.1: Simulated velocity field for an ordered pack. The fluid velocity is large near the edge of the pack because of high local permeability. Inset: magnified view of the local velocity field inside the medium. The local velocity is higher at the pore throat than in the pore body. 22

Figure 2.2: Stretching and splitting of a solute slug around an impervious disk. Because of the increase in contact area between regions of high and low solute concentrations diffusion becomes an effective mixing mechanism. 24

Figure 2.4: (a) Simulated concentration profile (at t = 60 s) and (b) local dispersion at the indicated sections for $D_o = 10^{-10}\ m^2/s$. Diffusion enhances local mixing and reduces the effect of permeability heterogeneity on local dispersion. Inset: magnified view of local concentration profile. Diffusion eliminates the transverse variation in local concentration caused because of splitting and rejoining of streams and homogenizes solute concentration inside a pore body. 28

Figure 2.6: (a) Solute concentration profile and (b) local dispersion at the indicated sections for $D_o = 10^{-11}\ m^2/s$. Local dispersion varies significantly with position. Inset: magnified view of local concentration profile. The streams splitting, rejoining and diffusion homogenizing local concentration can be seen. 31

Figure 2.7: (a) Solute concentration profile and (b) local dispersion at the indicated sections for $D_o = 10^{-9}\ m^2/s$. Diffusion enhances local mixing and reduces the effect of permeability heterogeneity on local mixing. Inset: magnified view of local concentration profile. Diffusion eliminates the radial variation in local concentration caused because of splitting and rejoining of streams and homogenizes solute concentration inside a pore body..... 32

Figure 2.8: Concentration profiles for slug injection at $t_D = 0.684$ (*a*) $vD_p/D_o = 1$ (*b*) $vD_p/D_o = 10$ (*c*) $vD_p/D_o = 100$ (*d*) $vD_p/D_o = 1000$. There is a complete local mixing for smaller values of local Peclet number, vD_p/D_o. Local mixing becomes increasingly more incomplete as the local Peclet number increases. 35

Figure 3.1: Echo dispersion experiment. Echo dispersion (indicated by dotted curves) is the same as the transmission dispersion in a homogeneous medium and smaller than the transmission dispersion in a heterogeneous medium. 39

Figure 3.3: Solute concentration profiles for a slug with parabolic velocity (a) five seconds after injection, (b) at the time of flow reversal and (c) five seconds before exit. Stretching of solute front enhances mixing due to diffusion. However, convective spreading dominates mixing caused by diffusion. Upon flow reversal the convective mixing cancels and dispersion is largely reversible. A large

difference in (d) forward solute concentration history and (e) backward solute concentration history also suggests largely reversible dispersion is occurring. (1 PV ≈ 200 s). 44

Figure 3.5: Solute concentration profiles for solute slug flowing around a sand grain (a) five seconds after injection, (b) at the time of flow reversal and (c) five seconds before exit. Splitting around sand grain increases area for diffusion and enhances local mixing. (d) Forward concentration history and (e) backward concentration history. (1 PV ≈ 200 s). 46

Figure 3.6: Solute concentration profiles for flow of solute slug around three grains (a) five seconds after injection, (b) at the time of flow reversal and (c) five seconds before exit. More grains correspond to more splitting of solute slug and hence enhanced local mixing and more irreversibility of dispersion. (d) Forward concentration history and (e) backward concentration history. (1 PV ≈ 200 s). .. 47

Figure 3.6: Comparison of backward solute concentration histories at the original inlet ($D_o = 10^{-11}\ m^2/s$) after flow reversal. The falling peak of concentration indicates more local mixing. 49

Figure 3.7: Comparison of backward solute concentration histories with a smaller diffusion coefficient ($D_o = 10^{-12}\ m^2/s$). Less diffusion causes greater reversibility of dispersion. 49

Figure 3.8: Comparison of backward solute concentration histories with larger diffusion coefficient ($D_o = 10^{-10}\ m^2/s$). Because of irreversibility of mixing, all the curves look the same. 50

Figure 3.9: Velocity profile in a disordered pack. The pack has correlated regions of high velocity because of inhomogeneity of packing..... 51

Figure 3.10: Solute concentration profiles for a slug in an irregular arrangement of disks (a) five seconds after injection, (b) at the time of flow reversal and (c) five seconds before exit. Similarity in shapes of concentration profiles in parts (a) and (c) indicate cancellation of convective spreading. (1 PV ≈ 110 s). 52

Figure 3.11: Comparison of solute concentration histories for a slug in a medium with irregular packing ($D_o = 10^{-11}\ m^2/s$). Forward curve (at original outlet) is non-Gaussian because of the heterogeneous nature of the medium. The backward curve (at original inlet) on the other hand is Gaussian as it results from local mixing. 53

Figure 3.12: Comparison of solute concentration histories for a slug in a medium with irregular packing ($D_o = 10^{-9}\ m^2/s$). Higher diffusion coefficient reduces effect of inhomogeneity on mixing. For a diffusion dominated processes the forward and backward dispersions are the same. 53

Figure 3.13: Continuous solute injection in a long core. The flow was reversed from four different depths of penetration shown by the four arrows. 54

Figure 3.14: Comparison of backward concentration histories from different penetration depths with the forward concentration history. Forward curve is non-Gaussian. Backward curves are Gaussian. Greater depth of penetration corresponds to greater local mixing and more irreversibility of dispersion. 55

Figure 3.16: Forward and backward solute concentration histories for flow in a uniform pack ($D_o = 10^{-11}\ m^2/s$). Dispersion is irreversible. 58

Figure 3.17: Solute concentration histories for flow in a uniform pack at forty times smaller effective diffusion coefficient. The backward curve shows partial reversibility of dispersion. 58

Figure 3.18: Solute concentration profiles for a slug in a random arrangement of disks (a) five seconds after injection, (b) at the time of flow reversal and (c) five seconds before exit. The mixing mechanism is same as that in case of ordered arrangement of disks. The role of solute front-splitting, rejoining and local mixing enhances the effective diffusion coefficient. The slug behaves the same way on its way back as it would have done while flowing forward. Dispersion is irreversible. For a random medium without correlated heterogeneity a very small diffusion coefficient is able to homogenize solute concentration in the transverse direction. …….59

Figure 3.19: Forward and backward solute concentration histories for flow in a random pack ($D_o = 10^{-12}\ m^2/s$). Dispersion is irreversible. 60

Figure 4.1: A dense random packing of 10000 spheres, formed by stacking two copies of a periodic packing of 5000 spheres. 69

Figure 4.3: (a) A Delaunay cell having sand grains and void space. The body of the cell can be visualized as pore body. (b) A converging-diverging path connecting two neighboring pores. (c) The faces are the areas of narrowest constriction (throats) that connect the cell to neighboring cells. r_c is the radius of the largest

circle that can fit in the constriction. r_e is the radius of the circle having same area as that of the void space. Arithmetic average of r_c and r_e is a good estimate of the equivalent radius of the bond that describes its hydraulic conductivity. 70

Figure 4.4: Throat radius on a face of a Delaunay cell. 78

Figure 4.5: Histogram of throat radii in a sphere pack. 80

Figure 4.6: Histogram of equivalent bond radii in a sphere pack. 83

Figure 4.7: Histogram of path lengths in a sphere pack. 83

Figure 4.7: Schematic diagram for a network of resistors. The numbers indicate the junction number. 90

Figure 4.8: System of linear equations for determining node potentials. 93

Figure 4.9: Potential at each pore in the network for steady-state single-phase flow in the *z* direction, with no-flow boundaries on the *x* and *y* faces. 96

Figure 4.11: Removing overlapping of bonds near a pore body. A sphere can be placed at the cell center. The momentum loss in the sphere is ignored. 98

Figure 5.1: Intersecting bonds at a pore body. 104

Figure 5.2: Faces of four bonds at a pore junction. They are displaced along their bond axes for finding flow configuration and calculating reference points and then moved back to their original location. 105

Figure 5.3: (a) Flow configuration with one in-flowing and three out-flowing bonds. The in-flowing stream splits into three segments. (b) Face of the in-flowing bond. ……...105

Figure 5.4: Flow configuration with three in-flowing and one out-flowing bonds. The out-flowing stream consists of flow from all the three in-flowing streams. 107

Figure 5.5: Flow configuration with two in-flowing and two out-flowing bonds. Third bond is the farthest from bond 1 and flow in bond 4 is greater than that in bond 1……..... 108

Figure 5.6: Flow configuration with two in-flowing and two out-flowing bonds. Third bond is the farthest from bond 1 and flow in bond 4 is smaller than that in bond 1. ……...109

Figure 5.7: Flow configuration with two in-flowing and two out-flowing bonds. The fourth bond is farthest from bond 1. 110

Figure 5.8: Flow configuration with two in-flowing and two out-flowing bonds. The second bond is the farthest from bond 1. In this configuration, both the in-flowing bonds feed both the out-flowing ones. 111

Figure 5.9: Marking the outgoing point based on reference angle and relative radial distance of the incoming point. 113

Figure 5.10: Marking the outgoing point on a horizontal segment. 114

Figure 5.11: Forward and backward paths of two solute particles in the network. The solute particles retrace their path in the absence of diffusion. 115

Figure 5.12: Movement of a solute particle in a randomly oriented tube. 115

Figure 5.13: Solute particle reflecting at tube wall. 118

Figure 5.14: Comparison of simulated dispersion in a capillary tube with Taylor's theory…. 121

Figure 6.1: Paths of five different pairs of neighboring particles with no diffusion. Particles split their paths after traveling together for a few pores. 127

Figure 6.2: Paths of several particles starting at different positions in the same pore. Particles paths are independent of each other. If each convective step is independent and has the same global statistics, solute particle displacements will be normally distributed. 128

Figure 6.3: Mean flow velocity distribution in bonds. There are many bonds perpendicular to the flow direction that have small velocity. 130

Figure 6.4: Comparison of core-scale averaged (thick curve) and pore-scale averaged (thin curves) solute concentration histories in absence of diffusion. .. 131

Figure 6.5: Cumulative distribution of path lengths of solute particles. 132

Figure 6.6: Figure 6.6: (a)-(e) Scanned spatial distribution of solute particles. Plug flow is assumed in the network bonds and $D_o = 0\ m^2/s$. Normally distributed curves having same mean and standard deviation as the actual data are also shown for comparison. (f) Dispersion coefficient as evaluated from spatial and temporal statistics. 134

Figure 6.7: Effect of diffusion on spatial statistics of solute particles for the plug flow profile in bonds. Diffusion has negligible impact on the particle statistics unless its magnitude becomes significant compared to the mechanical dispersion. All diffusion coefficients shown in the legend are in m^2/s. 137

Figure 6.8: Variation of dispersion coefficient vs. diffusion coefficient for the plug flow velocity profile in bonds in a physically representative network. Dispersion

coefficient does not change with diffusion unless diffusion becomes significant in magnitude compared to mechanical dispersion. 138

Figure 6.9: Comparison of simulated dimensionless dispersion coefficient with plug flow in bonds in a physically representative network of bead pack (bead radius = 2.1918×10^{-4} m) and experimental data in the literature. 138

Figure 6.10: Effect of diffusion in case of plug flow in a bond. Diffusion acts independently of velocity..... 139

Figure 6.11: Comparison of simulated dispersion coefficient with plug flow in bonds and linear model fit. A close match between the two suggests that the simulated dispersion coefficient is the sum of convective spreading and diffusion. 141

Figure 6.12: Effect of flow reversal on dispersion for probabilistic choice of out-flowing bond. Probabilistic rules introduce an artificial diffusion. Dispersion is an irreversible process even when input diffusion is zero. 142

Figure 6.13: Comparison of dispersion without diffusion (assuming plug flow in bonds) with probabilistic and deterministic choice of out-flowing bonds at a pore junction.. 143

Figure 6.14: Comparison of simulated dimensionless dispersion coefficient with parabolic flow in bonds and the literature experimental data. The simulated data matches quantitatively with the experimental data for all range of Peclet numbers. ……..145

Figure 6.15: Comparison of the simulated dispersion coefficients using a parabolic velocity profile in bonds with a power law model fit. 146

Figure 6.16: (a)-(e) Spatial distribution of solute particles. Parabolic flow is assumed in the network bonds and $D_o = 0\ m^2/s$. The first peak in the distribution corresponds to particles in the slow velocity regions near the pore walls. Other particles that are free to move form a second peak. Dispersion is not Fickian in this case. (f) Dispersion coefficient as evaluated from spatial statistics..... 147

Figure 6.17: (a)-(e) Scanned spatial distribution of solute particles. Parabolic flow is assumed in the network bonds and $D_o = 10^{-13}\ m^2/s$. The first peak which corresponds to particles in the slow velocity regions near the pore walls starts falling because of diffusion. Dispersion becomes Fickian at large times. (f) Dispersion coefficient as evaluated from spatial statistics. 151

Figure 6.18: (a)-(e) Scanned spatial distribution of solute particles. Parabolic flow is assumed in network bonds and $D_o = 10^{-12}\ m^2/s$. The first peak corresponding to particles in the slow velocity regions near the pore walls disappears quicker for larger diffusion. (f) Dispersion coefficient as evaluated from spatial statistics. 152

Figure 6.19: (a)-(e) Scanned spatial distribution of solute particles. Parabolic flow is assumed in network bonds and $D_o = 10^{-11}\ m^2/s$. The first peak corresponding to particles in the slow velocity regions near the pore walls disappears quicker for larger diffusion. (f) Dispersion coefficient as evaluated from spatial statistics. 153

Figure 6.20: (a)-(e) Scanned spatial distribution of solute particles. Parabolic flow is assumed in the network bonds and $D_o = 10^{-10}\ m^2/s$. (f) Dispersion coefficient as evaluated from spatial statistics. 154

Figure 6.21: (a)-(e) Scanned spatial distribution of solute particles. Parabolic flow is assumed in network bonds and $D_o = 10^{-9}\ m^2/s$. (f) Dispersion coefficient as evaluated from spatial statistics. 155

Figure 6.22: (a)-(e) Scanned spatial distribution of solute particles. Parabolic flow is assumed in network bonds and $D_o = 10^{-8}\ m^2/s$. (f) Dispersion coefficient as evaluated from spatial statistics. 156

Figure 6.23: (a)-(e) Scanned spatial distribution of solute particles. Parabolic flow is assumed in network bonds and $D_o = 10^{-7}\ m^2/s$. At high diffusion coefficient, some solute particles enter bonds with low velocities and get stuck there for long times. Particle distribution starts deviating from normal at longer times. (f) Dispersion coefficient as evaluated from spatial statistics. 157

Figure 6.24: Effect of diffusion on spatial statistics of solute particles for parabolic velocity profile in bonds. 158

Figure 6.25: Variation of asymptotic dispersion coefficient vs. diffusion coefficient for parabolic velocity profile in bonds. Dispersion coefficient decreases with diffusion unless diffusion becomes significant in magnitude as compared to mechanical dispersion. 159

Figure 6.26: Effect of flow reversal on dispersion for $D_o=10^{-13}\ m^2/s$. Irreversibility of dispersion increases with residence time in the medium. 161

Figure 6.27: Effect of flow reversal on dispersion for $D_o=10^{-10}\ m^2/s$. Greater diffusion enhances mixing and results in greater irreversibility of dispersion. .. 162

Figure 7.1: Solute concentration profile (upper) and streamlines (lower panel) in the flow domain in an ordered porous medium. Flow in this case is essentially unidirectional. Because of symmetry of the velocity field, there is a stagnant region of zero flow between the sand grains. Solute particles can enter this region only by diffusion. 168

Figure 7.2: Dimensionless dispersion coefficient vs. pore scale Peclet number for an ordered porous medium of Figure 7.1. The open circles show all the data points, whereas the filled diamonds show data points corresponding to high *Pe*. The asymptotic exponent is close to two, suggesting a mixing mechanism similar to that in a capillary tube. 170

Figure 7.3: Solute concentration profile (upper panel) and streamlines in the flow domain (lower panel) in a random porous medium. Streamlines can carry solute particles in the transverse direction by convection alone. Diffusion is important in carrying solute particles from no-velocity regions near the pore walls. 171

Figure 7.4: Dimensionless dispersion coefficient vs. pore scale Peclet number for the random porous medium of Figure 7.3. The exponent is close to unity, indicating that mechanical dispersion is the dominant dispersion mechanism. . 172

Figure 7.5: Dimensionless dispersion coefficient vs. pore scale Peclet number for an ordered porous medium with reduced porosity (43.5%). Porosity has small impact on mixing mechanism as long as flow geometry remains the same. 176

Figure 7.6: Solute concentration profile (upper panel) and streamlines (lower panel) in flow domain in a random porous medium with high porosity (90.2%). There is

no change in flow geometry and therefore mixing mechanism does not change. ……...177

Figure 7.7: Dimensionless dispersion coefficient vs. pore scale Peclet number for a random porous medium with high porosity (90.2%) as shown in Figure 7.6. Porosity does not have any significant impact on mixing mechanism as long as flow geometry remains same. 178

Figure A.1: Marking a segment of a circular tube carrying a known fraction of total flow ……...185

Figure A.2: Marking a segment of a circular tube carrying a known fraction of total flow wit parabolic velocity profile ……187

Figure A.3: Comparison of angles subtended at the center by a segment carrying a known fraction of total flow with plug flow and parabolic flow profiles……...189

Figure A.4: Marking segments of a circular tube splitting into three streams…...….191

Figure A.5: Determining relative distance of a point from chord. ……....192

Figure A.6: Determining relative distance of a point from arc……...……194

Figure A.7: Determining relative distance of a point in the mid-section of a circular tube. ……..……..195

Chapter 1: Introduction

1.1 IMPORTANCE OF MIXING IN POROUS MEDIA

A solvent slug injected for miscible enhanced oil recovery process mixes with the reservoir fluid at its leading edge and with the chase fluid at its trailing edge. This mixing dilutes the slug and reduces its effectiveness.

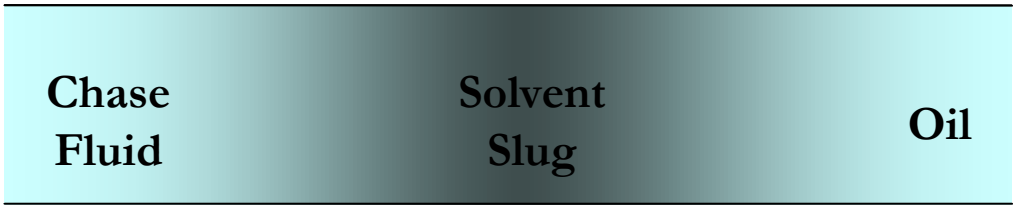

Figure 1.1: Attenuation of a miscible solvent slug as a result of mixing in the reservoir.

In first contact miscible (FCM) floods, the injected solvent mixes with the reservoir fluid on contact. The optimal slug size in such floods increases due to mixing and resulting dilution of the slug.

In multi contact miscible (MCM) floods, gas enriched with intermediate components is injected into the reservoir to achieve a multi contact miscible displacement of oil. For dispersion free displacements, minimum miscibility enrichment (MME) is the optimum enrichment for getting a single phase flow in the reservoir and a highly efficient displacement. Increase in oil recovery by enriching the injected gas beyond the MME is minimal (Johns et al., 1999).

Dispersion causes an MCM displacement to develop two-phase flow, which reduces recovery. For greater levels of dispersion, the gas enrichment needs to be much greater than MME to obtain the optimum recovery. The sensitivity of oil recovery on dispersion depends on the shape and size of the two-phase region. For a given enrichment, dispersion may cause a difference in oil recovery up to 15% of initial oil in place (Johns et al., 2000; Solano et al., 2001).

Because the local displacement efficiency is one of the primary factors that govern ultimate recovery, it is very important to understand and quantify how mixing of oil and gas in reservoirs can adversely impact the displacement efficiency of the MCM process.

Dispersion may also have some beneficial influence by reducing the effect of channeling during miscible floods and thus improving its sweep efficiency. Dispersion can also damp out the viscous fingers. Therefore, it is very important to understand these processes (Perkins and Johnston, 1963).

1.2 MIXING IN POROUS MEDIA

Mixing in porous media originates from a complex interplay of *molecular diffusion* and *convective spreading (mechanical dispersion)*.

Molecular Diffusion:

Molecules in the liquid or vapor states are in continuous random motion even if the bulk fluid velocity is zero. It results in a net movement of solute particles from regions of high solute concentrations to regions of low solute concentrations. The diffusive flux is described by Fick's law:

$$J = -D_o \frac{dC}{dx},$$

where D_o is diffusion coefficient and the derivative is concentration gradient.

Fick's (first) law describes instantaneous diffusive flux across a cross-section. It does not describe how solute concentration changes with time and space due to diffusion.

From mass conservation we know that

$$\frac{\partial C}{\partial t} = -\frac{\partial J}{\partial x}.$$

Differentiating Fick's equation with respect to x and using the mass balance equation, we get

$$\frac{\partial C}{\partial t} = D_o \frac{\partial^2 C}{\partial x^2}.$$

This is Fick's second law of diffusion. It describes how the solute concentration varies with time and space due to diffusion. Diffusion results in a normal distribution of solute concentration across the area of contact of two first contact miscible fluids.

In case of diffusion through a porous medium, the cross-sectional area for diffusion is reduced. Moreover, the path length for diffusion is increased because of the tortuous path through the medium. Noting that laws governing electrical conductivity and diffusion in porous media are analogous, it is shown that diffusion coefficient in porous media is related to formation resistivity factor by

$D = \frac{D_o}{F\phi} = \frac{D_o}{\tau}$ (Perkins and Johnston 1963; Lake, 1989),

where F is formation resistivity factor and for clean rocks a function of pore geometry only. τ is the tortuosity of the porous medium and D is the effective diffusion coefficient.

Convective Spreading (Mechanical Dispersion):

When a solute slug moves through a porous medium, there is additional mixing due to convection. The complex network of interconnected pores causes solute particles to take tortuous paths. Variations in local velocity, both in magnitude and direction, along the tortuous flow paths cause solute particles to spread. This is called convective spreading and it is governed by the pore structure. Two solute particles starting close to each other become widely separated because of convective spreading.

Mechanical dispersion is considered to be "diffusion –like"; a statistically random process. This hypothesis holds well in homogeneous (on REV scale) porous media and the miscible displacement process in that case is called "Fickian". In the conventional Fickian representation, mechanical dispersion is treated in the same manner as diffusion.

If the travel time for a solute particle becomes much larger than the time interval during which successive velocities are still correlated, its total displacement may be considered as the sum of a large number of elementary displacements that are statistically independent. For such conditions, the probability distribution of the particles' total displacement should be normal according to the central limit theorem. It is this tendency for a cloud of solute particles to converge to a normal distribution in space and to spread with a variance proportional to time that makes it possible to treat convective spreading similar to diffusion (Bear, 1972).

1.3 DESCRIPTION OF MIXING

To describe the combined effects of diffusion and convective spreading, a term "dispersion coefficient" is used. The growth of the mixing zone with the combined effects of convective spreading (mechanical dispersion) and molecular diffusion in a Lagrangian reference frame (where the observer follows the fluid movement) can be described by:

$$\frac{\partial C}{\partial t} = D_L \frac{\partial^2 C}{\partial x^2},$$

where the diffusion coefficient has been replaced by the dispersion coefficient, D_L in Fick's second law. The dispersion coefficient includes the effects of molecular diffusion as well as convective spreading.

In Eulerian reference frame where observer's location is fixed, the overall transport and mixing of fluids in flow through permeable medium is described by convection-diffusion equation (Lake, 1989):

$$\frac{\partial C}{\partial t} + v\frac{\partial C}{\partial x} = D_L \frac{\partial^2 C}{\partial x^2}.$$

1.4 QUANTIFICATION OF MIXING

Traditionally, mixing properties of a porous medium are quantified by carrying out miscible displacement experiments in which one miscible fluid displaces another entirely (for example, brine displaces water) through a core sample. The flow averaged ("cup-mixed") effluent concentration is recorded as a function of time which is typically

an S-shaped curve. The effluent concentration history is analyzed using a solution to the one-dimensional convection-diffusion equation to obtain the longitudinal dispersion coefficient.

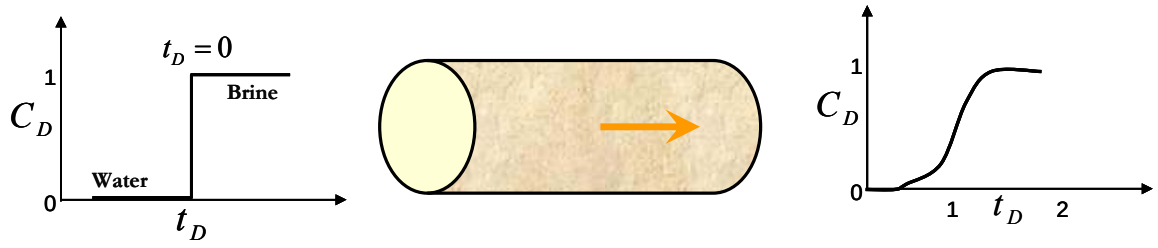

Figure 1.2: Transmission dispersion experiment. A step change in solute concentration is made at the inlet face and effluent concentration monitored at the outlet face.

The dispersion coefficient describes *apparent mixing* because it is averaged over the entire outlet and has contributions from convective spreading and diffusion lumped together. It does not give any information about their relative importance or how the two interact with each other.

It is well accepted in the literature that convective spreading is orders of magnitude larger than diffusion. Is core-scale mixing (dispersion) predominantly an artifact of convective spreading and diffusion categorically negligible (Coats et al., 2004), or does the role of diffusion become important in one limit or another?

We consider two scenarios for solute transport and mixing in homogeneous porous media which could explain the observed dispersion.

1. Convective Spreading Hypothesis: Solute particles travelling on a given streamline stay on that streamline until the exit. Diffusion being much smaller in magnitude can be neglected. Solute particles have no interaction with particles on adjacent streamlines. Solute particles do not move transverse to the streamlines. In this case averaged core scale mixing (dispersion) would be a result of convective spreading only (Figure 1.3). Diffusion being much smaller in magnitude can be neglected.

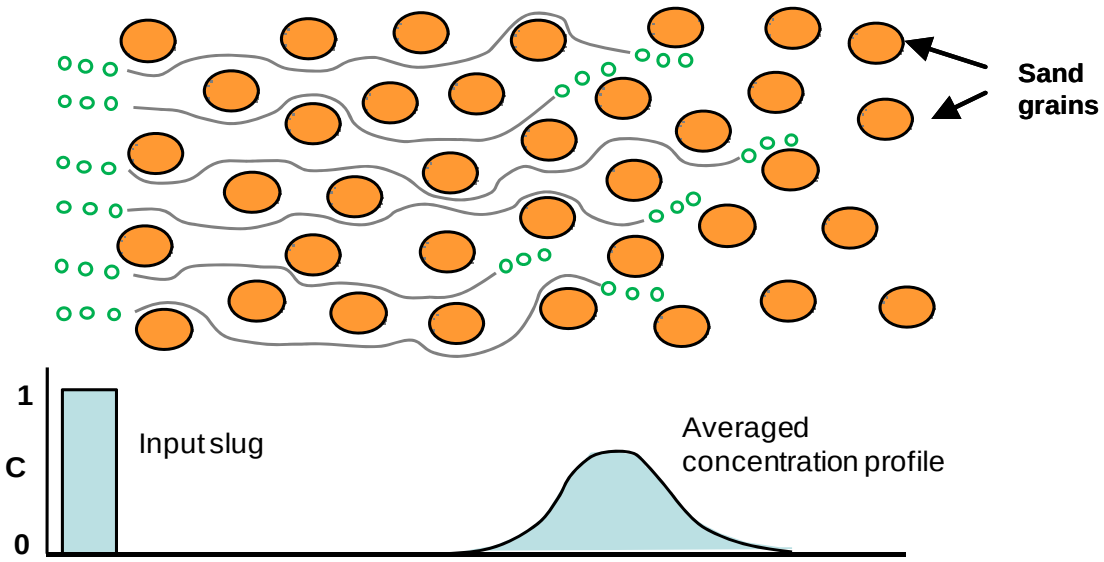

Figure 1.3: Convective spreading hypothesis.

2. Local Mixing Hypothesis: Solute particles travelling along a streamline jump to adjacent streamlines because of diffusion. Diffusion redistributes particles within the medium. The core scale mixing (dispersion) would be a result of interplay of

convective spreading and diffusion (Figure 1.4). Diffusion, being small in magnitude compared to the convective spreading has negligible effect on the overall spreading of the solute slug in the longitudinal direction.

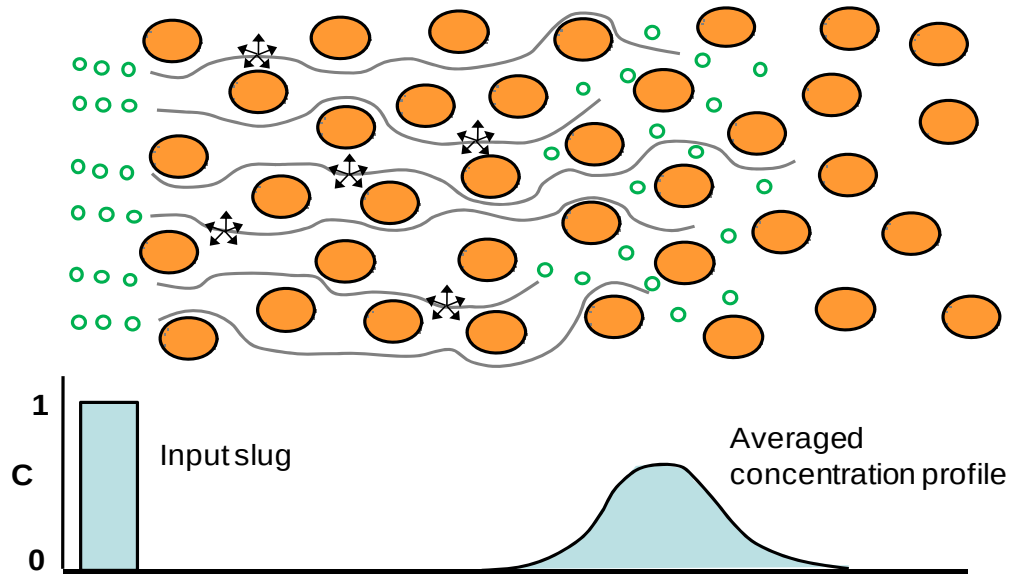

Figure 1.4: Local mixing hypothesis.

Both hypotheses predict normally distributed solute concentration profiles and histories and explain experimentally observed dispersion behavior but they have an important fundamental difference. In the first process solute particles are just getting spread, not getting mixed. Spreading is the change of shape of the slug as it gets distorted in a medium consisting of high and low velocity regions. The solute concentration anywhere within the slug is not reduced. Only when a cup-mixing average is taken does the concentration appear to be reduced. On the other hand, in the second case the solute

slug is undergoing local (in-situ) mixing and getting diluted. Local mixing is the true mixing and causes a reduction in the solute concentration at a point scale.

On the basis of an averaged breakthrough curve, one cannot distinguish between actual solute dilution, and variability of arrival times of solute particles travelling along different streamlines.

There are a few possible methods to distinguish between spreading and mixing:

1. Analyzing the solute breakthrough curve at a "point" within the domain gives additional information about the dilution of the tracer (Cirpka and Kitanidis, 2000). In case of purely convective spreading local solute breakthrough curve will show a step jump from initial concentration to the injected concentration. On the other hand, in case of local mixing the change in local solute concentration from initial concentration to injected concentration will be gradual (Jha et al. , 2006). An attempt to measure local solute concentration in a sand pack using a thin probe was made by Jha (2005). The results indicated that local mixing was taking place in the medium.

2. Local mixing can be described by prescribing degrees of resolution and uniformity. For example, by specifying a grid size (resolution) and bounds of composition within each box of the grid (uniformity). The difference between maximum and minimum solute concentrations in a grid should not exceed a specified limit. Moreover, in case of local mixing there should not be a sharp contrast in solute concentrations in two adjacent grids (Ottino, 1989).

3. Kitanidis (1994) introduced a dilution index to distinguish between spreading and mixing. The logarithm of dilution index is related to entropy. Like entropy mixing can only increase. Mixing is an irreversible process.

It is important for us to know the actual origin of core-scale mixing (dispersion) and individual roles played by convective spreading and diffusion for a range of flow conditions and pore geometries. If the convective spreading hypothesis is valid, upon flow reversal solute particles will retrace their path back to the inlet and we will recover the solute slug we had injected. On the other hand, if there is complete local mixing inside the pore space, the solute slug would keep mixing even after flow reversal.

1.5 OBJECTIVE

The main objective of this research is to understand the basic physics of solute transport and mixing at the pore scale and to use this information to explain the core-scale mixing (dispersion) behavior. We study the interaction between convective spreading and diffusion for a wide range of flow conditions and its influence on core scale mixing. We explain the mechanisms of mixing in pore space, the effects of flow reversal on dispersion and the dependence of dispersion coefficients on pore scale Peclet numbers. We explain several experimental observations regarding dispersion found in the literature from pore scale physics.

The research hypothesis is that core scale mixing (dispersion) can be predicted from pore scale mechanisms once the flow geometry is known.

1.6 METHOD

We use two different methods to study interaction between convective spreading and diffusion and its influence on dispersion.

1. Direct Numerical Simulation Using FEMLAB: In the first approach, we carry out pore scale simulation studies from first principles. We performed numerical simulations of pore scale solute transport using the multi-physics modelling software FEMLAB (now COMSOL). We simultaneously solve the Navier-Stokes and convection diffusion equations directly in a surrogate two-dimensional pore space for a range of flow velocities, diffusion coefficients and pore geometries. This allows investigation of solute transport and local mixing from first principles without making assumptions such as a Fickian model for mixing. The effect of various factors on solute transport and mixing can be directly visualized from the concentration profile. We also evaluate core scale mixing (dispersion) by computing velocity averaged solute concentrations at the outlet face and study the effect of local mixing on dispersion.

We also examine the effect of flow reversal on dispersion through pore scale simulation studies. In flow reversal studies the direction of flow is reversed after the solute slug has penetrated into the medium (but not exited) to a pre determined distance. Backward effluent concentration history obtained at the outlet (original inlet) is analyzed to obtain *echo dispersion coefficient*. Echo dispersion coefficient can determine relative significances of convective spreading and local mixing in the dispersion process and provide insights about its nature.

We carried out pore-scale simulations of flow reversal in several simple flow geometries to understand the mechanisms of local mixing and the factors influencing it. Then we use the insights gained to investigate effect of flow reversal on dispersion in more realistic models of porous media.

Based on our simulation studies, we explain the mixing mechanism and the reason for irreversibility of dispersion in porous media.

2. Particle Tracking in a Physically Representative Network Model: FEMLAB simulations, even though quite useful in explaining the pore scale mixing mechanisms, give us only qualitative results. We cannot compare these results quantitatively with the experimental data because these are two-dimensional models with unrealistically high porosities. Moreover, these simulations do not run in the absence of diffusion due to numerical issues.

Therefore, we use a different method to have a better quantitative comparison with the experimental data. We track movement of a swarm of 15000 solute particles through a three dimensional random pack of spheres which is a reasonable representation of sediment. We have center coordinates of a pack of 5000 spheres (with equal sphere radii) from Thane (2006). Knowledge of the sphere radii and the center coordinates completely specifies the micro-structure of the pore space. Thane pack is periodic and thus can be used as a building block to create an arbitrarily long pack of spheres. This is important in getting long enough streamlines to get reliable statistics of solute particles.

Continuum scale properties are governed by pore scale geometry and topology. However, it is very difficult to explicitly capture all the details of pore geometry. Therefore, most of the network models reported in the literature make some simplifying assumptions (Acharya et al., 2007, Bijeljic et al., 2004, Bruderer et al. 2001) such as (i) bond radii are picked randomly from an assumed distribution, (ii) all bonds have the same length, (iii) pores have some characteristic shape (e.g., circular or square cross section), and (iv) the network lattice is regular.

Most of these assumptions are found to be invalid in a dense random packing of spheres. The first geometrically characterized random packing was studied by Finney (1970). Flow path lengths calculated in a Finney pack are found to be almost uniformly distributed between zero and 0.8 sphere radii, with a few path lengths exceeding 1.0 sphere radii (Bryant et al., 1993). The assumption of a regular lattice is also invalid, since Mellor (1989) showed that the topology of the pore space network in the Finney pack is completely disordered. There has been found to be significant correlation in pore sizes, which has an important influence on macroscopic properties of the medium. The decorrelated network (with properties randomly redistributed from the Finney pack) had permeability 78% larger than that of the original network. Neglecting correlation may fail to account for physically significant features of porous media (Bryant et al., 1993). Since dispersivity is strongly affected by correlation of pore size, it is important to test whether the assumptions of conventional network models are adequate for studies of dispersion. The hypothesis of this work is that accounting for the structure of porous media more realistically will better explain core-scale mixing (dispersion) behavior quantitatively.

We prepared a physically representative network model of a dense random packing of spheres. The physically representative network model explicitly accounts for the connection of a pore with its unique set of neighbors. It has pore bodies located exactly at the same location as in the actual medium. The hydraulic conductance of the bond connecting any two neighbors is the same as that in the actual medium. Thus, this model preserves the geometry and topology of the pore space as well as spatial correlation in flow properties. This model is three dimensional and unstructured.

We evaluated hydraulic conductances of all the bonds in the network and obtain flow rates through them from mass balance at each pore.

One of the most common simplifying assumptions made in particle tracking through a network model reported in the literature is the probabilistic choice of an out-flowing bond. A solute particle arriving at a pore body (junction of bonds) is assigned to an out-flowing bond randomly with a flow rate weighted probability. However, we show that probabilistic choice of out-flowing bond is not realistic as it makes dispersion an irreversible process even in absence of diffusion. Moreover, it ignores spatial correlation in bond conductances which is one of the key features of the physically representative network models. Therefore, convective spreading cannot be modeled correctly with this approach.

To avoid these problems we developed deterministic rules to decide an out-flowing bond and to map the entrance point of the solute particle on this bond. These rules yield flow streamlines through the network comparable to those obtained from a full solution of Stokes' equation. In the absence of diffusion the paths of all solute particles are completely determined and reversible. We monitor spreading solute particles along these paths and explicitly quantify the convective spreading from spatial and temporal statistics.

Our algorithm captures the essential features of convective spreading and allows us to investigate it explicitly and rigorously in a realistic pore space. To the best of our knowledge it has not been previously attempted. We show that the paths of arbitrarily close pairs of particles become independent relatively quickly even in the absence of diffusion and even after accounting for spatial correlation of pore structure.

Next, diffusion is superimposed and movement of solute particles because of combined effects of convection and diffusion is monitored. Dispersion is quantified from spatial and temporal statistics of solute particles. With this framework we can quantitatively investigate the influence of increasing diffusion on dispersion. We explain the origin of core scale dispersion in terms of the interaction between convection and diffusion. The method predicts *a priori* the correct power law dependence of dispersion coefficient on pore scale Peclet number. All our predictions are consistent with the experimental results reported in the literature. Models more sophisticated than ours, e.g. a direct solution of the Stokes (or Navier-Stokes) equation in the pore space of a granular material coupled with a solution of the convection-diffusion equation, would also predict core-scale dispersion correctly. We propose that ours is the simplest model that captures the essential physics.

1.7 ORGANIZATION OF THE DISSERTATION

This dissertation presents the details of the methodology used and results obtained supported by relevant results from the literature. The second chapter presents results of pore scale simulation and investigates factors influencing local mixing. The third chapter studies the effect of flow reversal on mixing through pore scale simulation studies. The fourth chapter presents the details of calculations and methodology used in preparing a physically representative network model of a three dimensional random packing of spheres. It also shows calculation of flow rate through each pore for a given potential gradient. The fifth chapter presents the deterministic rules developed for tracing solute particles through the network. It also presents validation of the tracing algorithm for flow with diffusion by comparing simulation results in a capillary tube with Taylor's theory.

The sixth chapter presents the results obtained from the network calculations. It shows the influence of diffusion on dispersion and explains dependence of dispersion on pore scale Peclet number. The seventh chapter studies the influence of pore geometry on interaction between convection and diffusion. The eighth chapter summarizes all the results and conclusions.

REFERENCES

1. Acharya, R. C., van Dijke, M. I. J., Sorbie, K. S., Van der Zee, S. E. A. T. M. and Leijnse, A.: "Quantification of dispersion by upscaling Brownian motion of tracer displacement in a 3D pore-scale network model", Advances in Water Resources, 30 (2), 199 – 213, (2007).
2. Bear, Jacob: *Dynamics of Fluids in Porous Media*, Elsevier, New York, (1972).
3. Bijeljic, B., Muggeridge, A. H. and Blunt, M. J.: "Pore-scale modeling of longitudinal dispersion", Water Resources Research, Vol. 40, W11501 (2004).
4. Bruderer, C. and Y. Bernabe: "Network modeling of dispersion: Transition from Taylor dispersion in homogeneous networks to mechanical dispersion in very heterogeneous ones", Water Resources Research 37(4): 897-908 (2001).
5. Bryant, S. L., King, P. R. and Mellor, D. W.: "Network model evaluation of permeability and spatial correlation in a real random sphere packing", Transport in Porous Media, 11, 53-70, (1993).

6. Cirpka, O. A. and Kitanidis, P. K.: “Characterization of mixing and dilution in heterogeneous aquifers by means of local temporal moments”, Water Resources Research, 36 (5), 1211-1236, (May 2000).
7. Coats, K. H., C. H. Whitson and L.K. Thomas: "Modeling conformance as dispersion", paper SPE 90390 presented at the SPE Annual Technical Conference and Exhibition, Houston, TX, (Sep 26-29 2004).
8. FEMLAB Chemical Engineering Module Users Guide, (Oct. 2004).
9. Jha, R. K. : *Pore Level Investigation of Dispersivity*, MS Thesis, The University of Texas at Austin, (May, 2005).
10. Jha, R.K., Bryant, S.L., Lake, L.W. and John, A.: “Investigation of pore-scale (local) mixing**”,** paper SPE - 99782 presented at SPE Improved Oil Recovery Symposium, Tulsa, Oklahoma, (Apr. 2006).
11. Johns, R. T., Sah, P. and Subramanian, S.: “Effect of Gas Enrichment above the MME on Oil Recovery in Enriched-Gas Floods,” paper SPE 56826 presented at SPE ATCE held at Houston, Texas, (Oct. 1999).
12. Johns, R. T., Sah, P. and Solano, R.: “Effect of Dispersion on Local Displacement Efficiency for Multicomponent Enriched-Gas Floods above the MME”, paper SPE 64725 presented at SPE International Oil and Gas Conference and Exhibition in China held in Beijing, (Nov. 2000).
13. Kitanidis, P. K.: “The concept of dilution index”, Water Resources Research, 30 (7), 2011-2026, (Jul. 1994).
14. Lake, L. W.: *Enhanced Oil Recovery*, Prentice Hall, NJ, (1989). Available through the author.

15. Ottino, J. M.: “Mixing, chaotic advection and turbulence”, Annu. Rev. Fluid Mech., 22, 207-253, (1990).
16. Perkins, T. K. and Johnston, O. C.: “A Review of Diffusion and Dispersion in Porous Media”**,** SPE 480, SPE Journal, 3(3), 70-84, (Mar., 1963).
17. Solano, R., Johns, R.T. and Lake, L.W.: “Impact of reservoir mixing on recovery in enriched-gas drives above the minimum miscibility enrichment”, SPE Reservoir Evaluation and Engineering, Volume 4, Number 5, (Oct. 2001).

Chapter 2: Investigation of Local Mixing through Pore Scale Simulation

2.1 INTRODUCTION

Mixing in porous media mainly results from the interaction between convective spreading and molecular diffusion (Greenkorn and Kesseler, 1969). Laboratory experiments usually measure effluent concentration histories that are flow-averaged ("cup mixed") values over the entire outlet. The core-scale averaged mixing observed in flow through porous media usually termed as *dispersion* is used to quantify mixing. The averaged dispersion coefficient has the contributions of convective spreading and diffusion lumped together and gives no information about the underlying mechanisms of solute transport and mixing.

Local solute concentration measurements (at the length scale of a pore) using a thin conductivity probe indicate local mixing taking place (Jha, 2005). To corroborate the experimental observations and understand the mixing mechanisms over a wider range of flow conditions (than possible experimentally) we performed direct numerical simulation of solute transport at the pore scale using a multi-physics modeling software FEMLAB. We solve the Navier- Stokes and convection-diffusion equations directly in a surrogate pore space to simulate a single phase, incompressible, first-contact miscible flow in two-dimensional porous media (Auset and Keller, 2004). This allows investigation of solute transport and local mixing from first principles without making assumptions about a continuum model (such as a Fickian model) for mixing. We can directly visualize interplay of convective spreading and diffusion from concentration profiles. Computation

of local solute concentration histories averaged over a fraction of outlet and its comparison with core-scale averaged concentration history also gives an indication of the nature of solute transport.

This chapter presents the details of the pore scale simulations for a range of pore geometries and flow velocities and explains the mechanisms of solute transport and mixing at the pore-scale.

2.2 METHOD

FEMLAB (now COMSOL) is a multi-physics software that uses the finite element method to solve partial differential equations for the specified geometry and given initial and boundary conditions. It does not use streamlines. In this study we use FEMLAB to obtain solute concentration in the pore space as a solute slug moves through it.

Solving for solute concentration in the medium is a two step process. In the first step, we solve the Navier-Stokes equation to obtain local fluid velocity as each point in the medium. In the second step the convection-diffusion equation is solved in the flow domain to obtain solute concentration as a function of time and space. The convection-diffusion equation needs two parameters: fluid velocity and the diffusion coefficient. The equation uses local velocity obtained from the Navier-Stokes equation and the diffusion coefficient is supplied as an input. Solving the convection-diffusion equation as a time-dependent problem gives the solute concentration profile as a function of time. Effluent concentration history can be obtained by calculating the velocity weighted averaged solute concentration history at the outlet of the medium.

2.3 MODEL DESCRIPTION

Our two-dimensional porous medium consists of a rectangular plate with circular holes in it (Figure 2.1). The holes represent the sand grains and the fluid can flow through the pore space between them (Buyuktas and Wallender, 2004). The pore space is our flow domain. The grain diameter is usually taken as 50 micrometers. The length of the medium is about 40 grain diameters. We simulate water flow and solute transport through this medium.

Solving Navier Stokes Equation

The Navier-Stokes equation is solved to obtain the steady state flow velocity at each point inside the surrogate porous medium. Fluid is injected at a constant velocity of 10^{-5} m/s at the inlet face and the outlet face is maintained at atmospheric pressure. All other boundaries including the sand grain boundaries are the no-slip boundaries.

We create a fine mesh of 20,000 elements in the flow domain to reduce numerical error and solve the Navier-Stokes equation subject to the described boundary conditions. Figure 2.1 shows the simulated velocity profile for a staggered arrangement of disks (ordered porous medium). We can see higher fluid velocity near the edge of the medium. This is because of packing disorder at the boundary (Graton and Fraser, 1935). The fluid finds a straight uninterrupted path from the inlet to the outlet in this region. The fluid velocity inside the pack appears uniform on average. However, if we magnify we can see variations in fluid velocity within the pore space. Velocity at the throats is higher compared to that inside the pore bodies as shown in the inset of Figure 2.1.

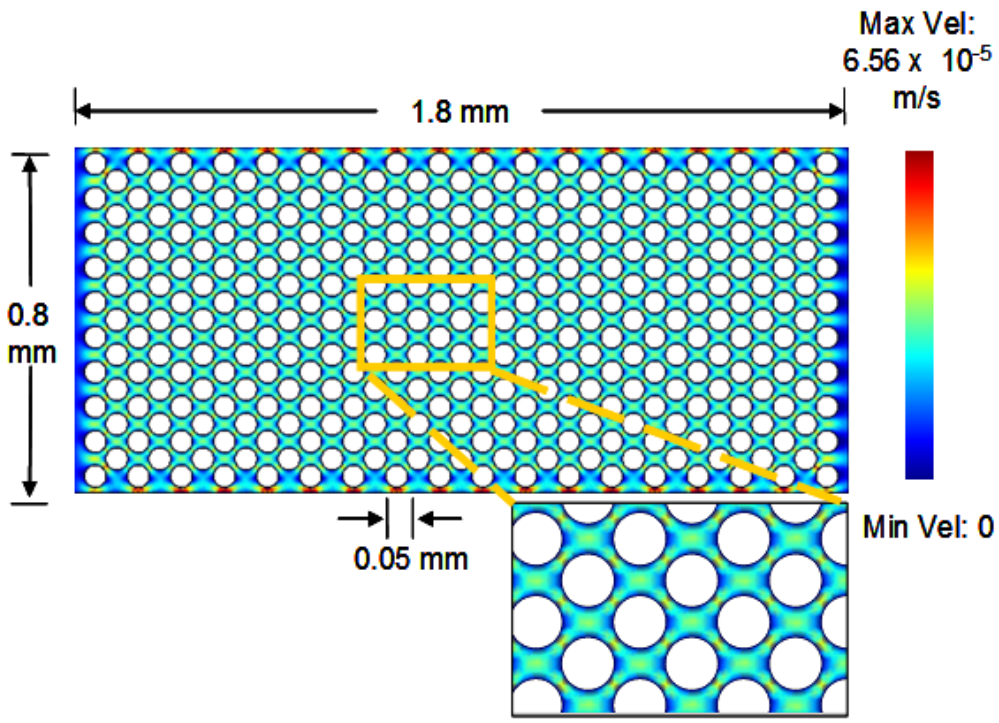

Figure 2.1: Simulated velocity field for an ordered pack. The fluid velocity is large near the edge of the pack because of high local permeability. Inset: magnified view of the local velocity field inside the medium. The local velocity is higher at the pore throat than in the pore body.

Solving Convection-Diffusion Equation

Next, we study movement of a solute front through the defined pore geometry by solving the convection diffusion equation. The initial solute concentration is zero everywhere in the medium. We make a step change in solute concentration at the inlet face. The solute is assumed to be inert. To obtain solute concentration as a function of time and space, the convection-diffusion equation is solved in the flow domain. The convection-diffusion equation needs two parameters – fluid velocity and a diffusion coefficient. The fluid velocity is already obtained from the Navier-Stokes equation and the diffusion coefficient is supplied as an input.

The solute travels with the local fluid velocity and diffusion moves it from regions of high to low concentrations. The effect of various factors on solute transport and mixing can be directly visualized from the concentration profile in the flow domain.

2.4 COMMENT ON SOLUTE BREAKTHROUGH CURVES

Core scale mixing (cup-mixed solute concentration histories typically measured in experiments) is the velocity weighted average solute concentration at the outlet face. We can sample small lengths of the outlet and obtain local solute breakthrough curves (from which local dispersion can be quantified) corresponding to each sample length. If solute transport in the medium is a Fickian process, there would not be any significant variation in solute concentration in the transverse direction. The core scale averaged solute concentration history would be Gaussian. The local solute concentration histories would also be Gaussian and very similar to the core scale averaged solute concentration history. In case of a correlated heterogeneity in the medium, the core scale averaged solute concentration history would be non-Gaussian and local solute concentration histories will be different from core-scale averaged concentration history. Thus comparing local and the core scale averaged solute concentration curves gives us information about the nature transport process taking place in the medium. We study how the pore structure and diffusion affect this process.

2.5 BASIC MECHANISM OF LOCAL MIXING

In order to understand the mixing mechanisms at the pore scale, we first focus on the movement of a solute slug past a single sand grain. Because of velocity gradients the

solute front stretches. This increases the contact area between high and low solute concentration regions and enhances the effect of diffusion (Figure 2.2). When the slug encounters an impervious sand grain, it splits around it. Depending on the local pore geometry, the two filaments of the split front may either rejoin or get further subdivided and join with filaments split across other grains. In either case, splitting of the solute slug further increases the contact area between regions of high and low solute concentrations. Now diffusion becomes a much more effective mixing mechanism as compared to what it is in a static state. After rejoining the segments of a solute front segment, there is a concentration gap developed between the two segments of the split front. Diffusion tends to wipe out this gap by moving solute from the regions of high to low concentration. If diffusion is effective enough, the two filaments do not remain separated.

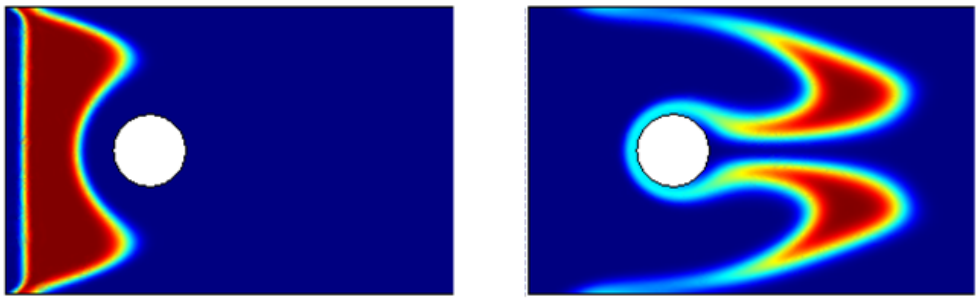

Figure 2.2: Stretching and splitting of a solute slug around an impervious disk. Because of the increase in contact area between regions of high and low solute concentrations diffusion becomes an effective mixing mechanism.

Next, we present results of simulation studies carried out for various pore geometries and diffusion coefficients.

2.6 SIMULATIONS ON AN ORDERED PACK

A step-change miscible displacement simulation was carried out in a two dimensional medium with an ordered arrangement of holes (staggered array of disks). The velocity field is uniform inside the medium on average (Figure 2.1). However, near the edge of the medium because of the local permeability heterogeneity the fluid velocity is higher.

We monitor movement of the solute front as it moves through the pore space. Figure 2.3 shows solute concentration profile for a diffusion coefficient of $10^{-11}\ m^2/\ s$. The solute front splits across sand grains and the filaments of the split solute front rejoin because of symmetry of the velocity field. If we magnify the solute concentration profile, we can see solute front stretching and splitting around sand grains and diffusion wiping out the concentration discontinuity between the split filaments of the solute front. In this case diffusion is not large enough to completely eliminate the gap between two split filaments.

The outlet of the medium is sampled with a number of smaller intervals as indicated in Figure 2.3 (a). Velocity weighted solute concentration is obtained for each portion and compared with the core scale solute breakthrough curve (Figure 2.3(b)). The local solute breakthrough curves are symmetric about the center, i.e. the local breakthrough curves at the same distance from center coincide with each other. The medium does not have any correlated heterogeneity except at the edges where fluid finds

straight uninterrupted path from the inlet to the outlet. The local solute breakthrough curves near the edge are distinctly different from those at the inner part of the medium. Because of the higher velocity solute in this region breaks through earlier and because of a wider distribution of travel times, it has a larger variance. All other local concentration curves are very similar to the core scale concentration curve. Since the portion affected by the wall is small, it has little impact on the core scale concentration except at earlier time intervals.

If the diffusion coefficient is increased to $10^{-10}\ m^2/s$, the local mixing increases as shown in the magnified view of concentration profile in the Figure 2.4. Moreover, the effect of local heterogeneity near the wall on local dispersion is reduced (Figure 2.4(a)) because diffusion causes solute in the high velocity region to move to other regions of lower velocity (but lower solute concentration). This causes decorrelation of solute particle velocities in the channel near the boundary and solute transport becomes closer to Fickian. Decorrelation is essential for a solute transport process to become Fickian. Local solute breakthrough curves move closer to the core scale averaged curve (Figure 2.4(b)). If diffusion is increased further and the process becomes diffusion dominated, all the local and core scale mixing curves collapse into one and solute transport becomes completely Fickian.

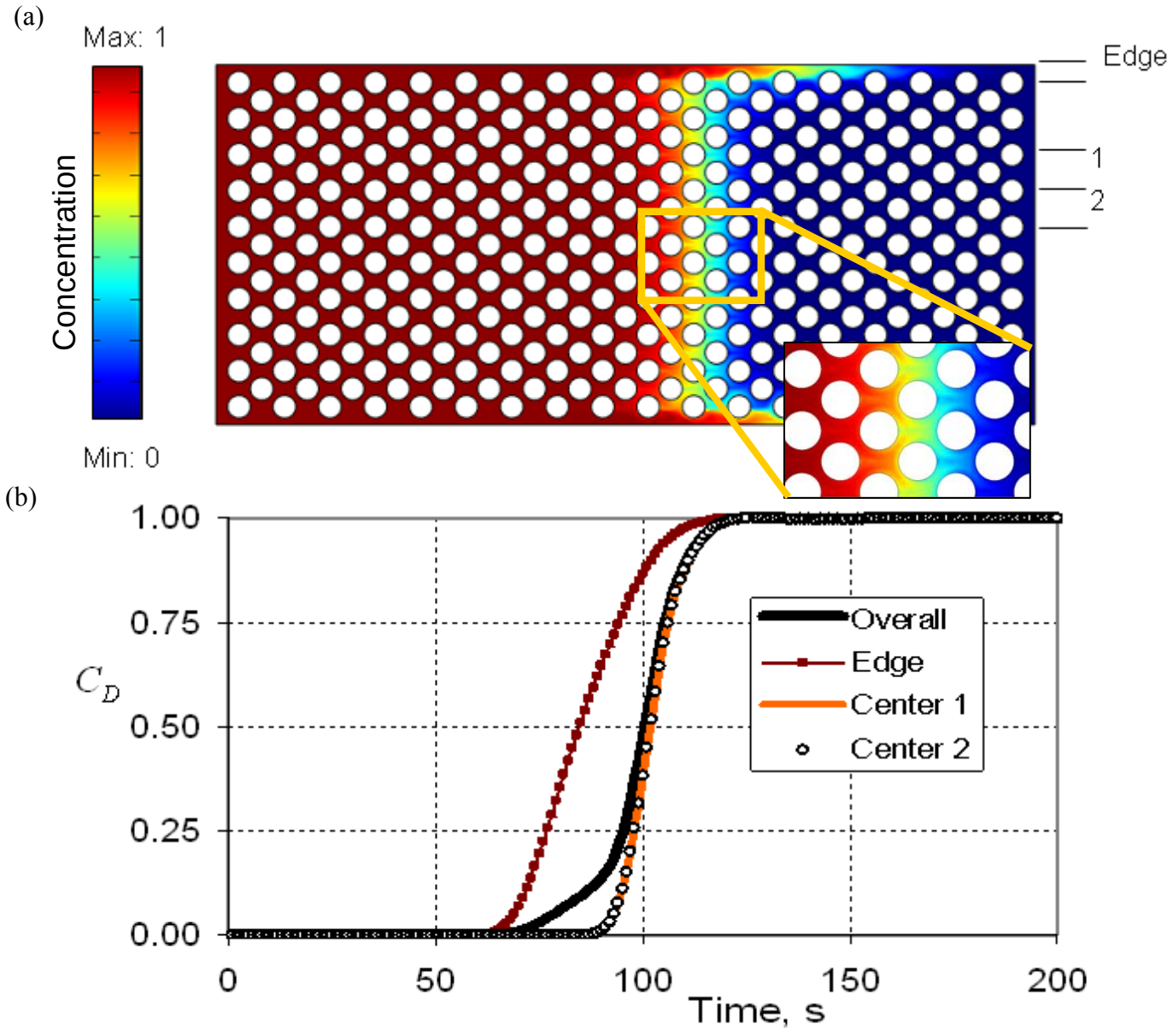

Figure 2. 3: (a) Simulated concentration profile (at t = 60 s) and (b) local dispersion at the indicated sections for $D_o = 10^{-11}\ m^2/s$. The local dispersion near the edge is higher because of permeability heterogeneity near the edge. Inset: Magnified view of local solute concentration. The effect of stream splitting, rejoining and resulting transverse concentration variation in the pore can be seen.

(a)

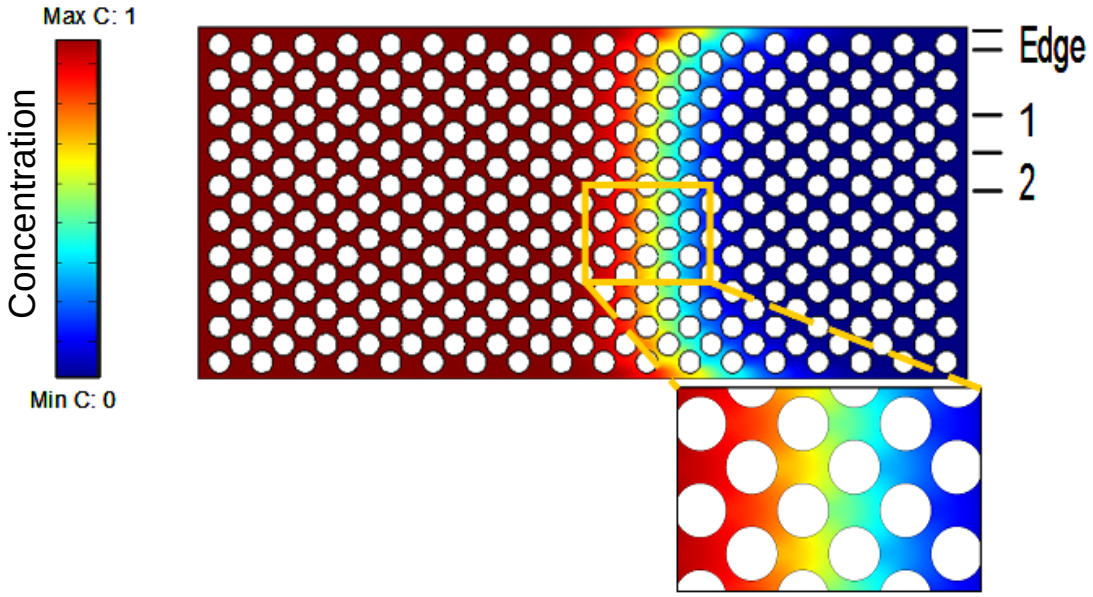

(b)

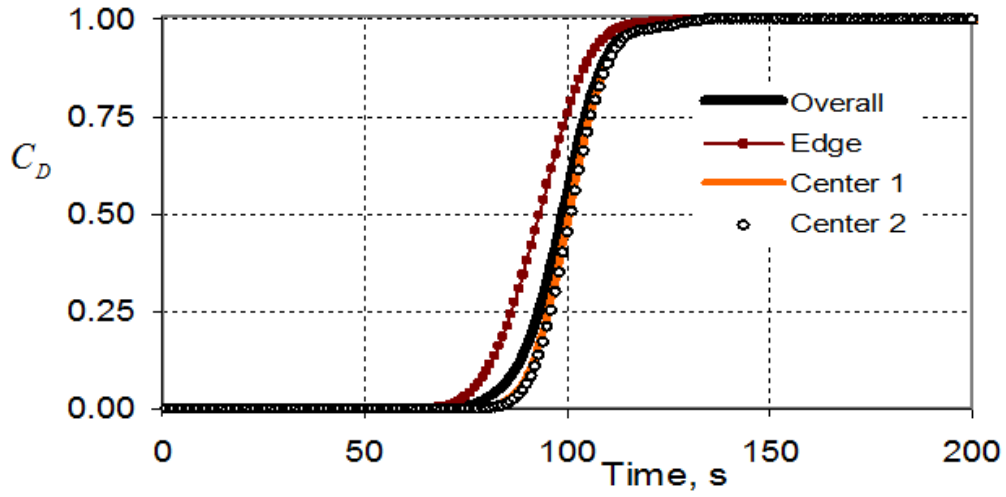

Figure 2.4: (a) Simulated concentration profile (at t = 60 s) and (b) local dispersion at the indicated sections for $D_o = 10^{-10}\ m^2/s$. Diffusion enhances local mixing and reduces the effect of permeability heterogeneity on local dispersion. Inset: magnified view of local concentration profile. Diffusion eliminates the transverse variation in local concentration caused because of splitting and rejoining of streams and homogenizes solute concentration inside a pore body.

2.7 SIMULATIONS ON A DISORDERED PACK

To examine the relationship between local and core scale dispersions for a more general case, simulation studies were carried out in a disordered medium with a correlated heterogeneity. Now local velocities vary widely from point to point (Figure 2.5) and the solute front moves unevenly. It spreads more in the correlated regions of high velocity and solute transport is non-Fickian. The mixing mechanism is still the same as described previously. In the magnified solute concentration profile we can see splitting of the solute front around sand grains and diffusion homogenizing solute concentration and causing mixing.

Here also, local solute breakthrough curves are compared with core scale mixing curve (Figure 2.6 (a,b)) for $D_o = 10^{-11}\ m^2/s$. In this case, the amount of local dispersion differs for each section because of differences in the local pore morphology. The transport process is not Fickian and local solute breakthrough curves are different from core scale mixing (dispersion), the latter being the average of all the local solute breakthrough curves. If diffusion is increased to $10^{-9}\ m^2/s$ (Figure 2.7 (a,b)), the amount of local mixing increases and also the solute is spread more in the transverse direction to the regions having low solute concentration. This reduces effect of correlated heterogeneity since diffusion is a random process. In this case, diffusion has to be very large to eliminate effects of the correlated pore structure and make the transport process Fickian. If diffusion is very large and the transport process becomes diffusion dominated, solute transport becomes Fickian and all local and core scale dispersion curves coincide into one.

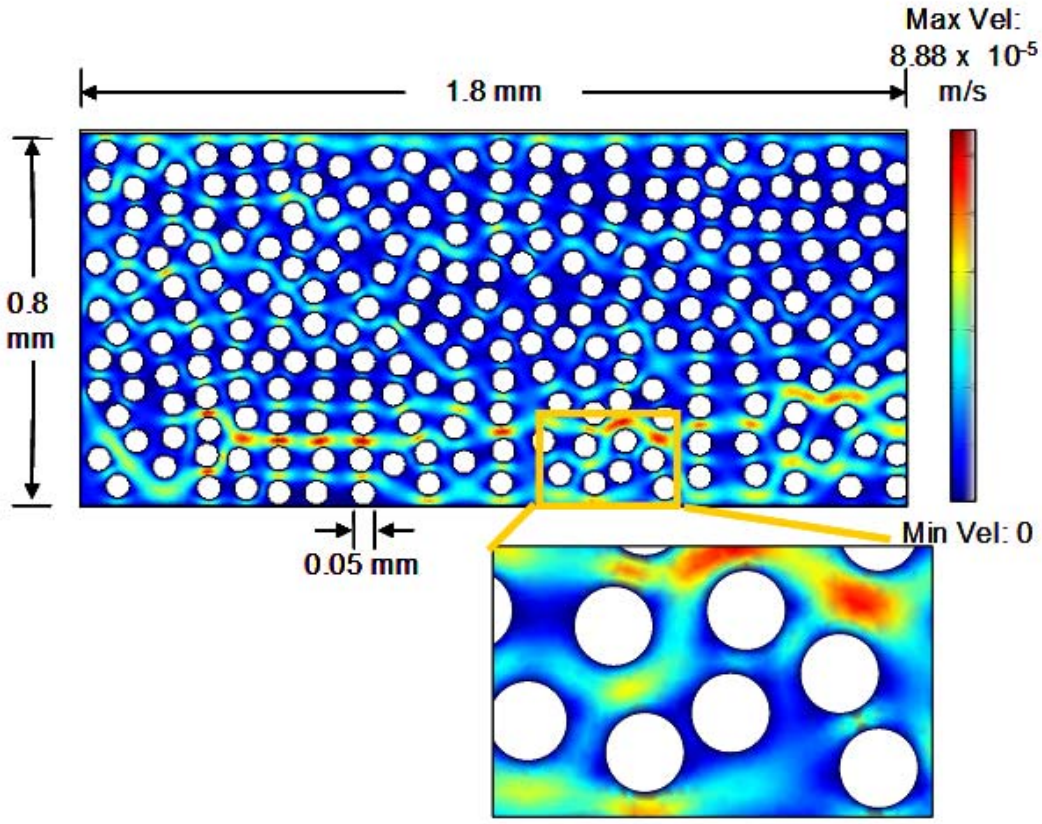

Figure 2.5: Simulated velocity profile for a disordered pack. In this case, the local velocity varies widely from point to point. Inset: magnified view of a portion of the local velocity field.

(a)

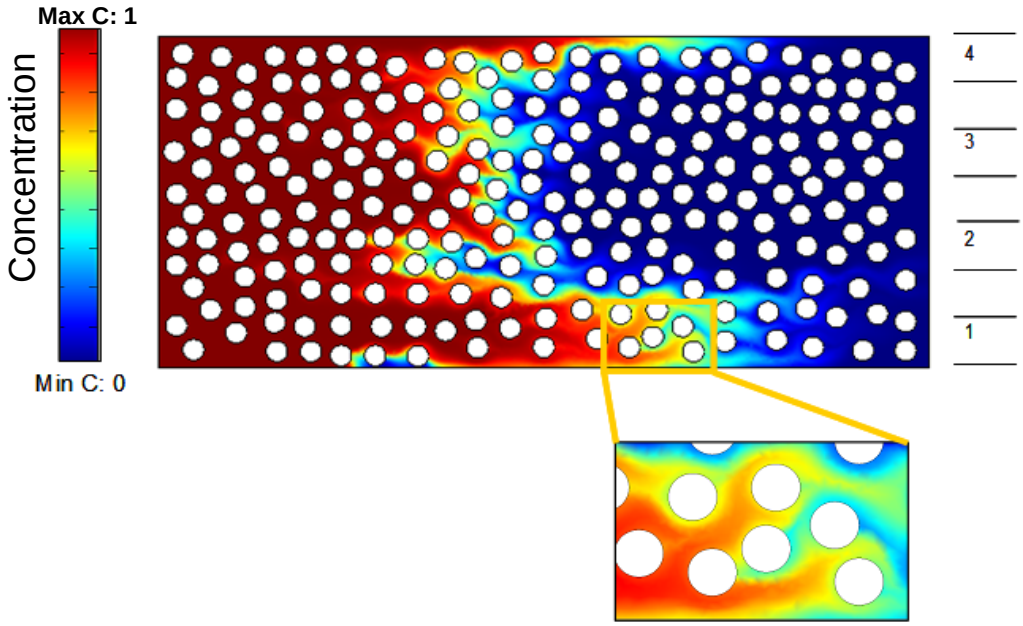

(b)

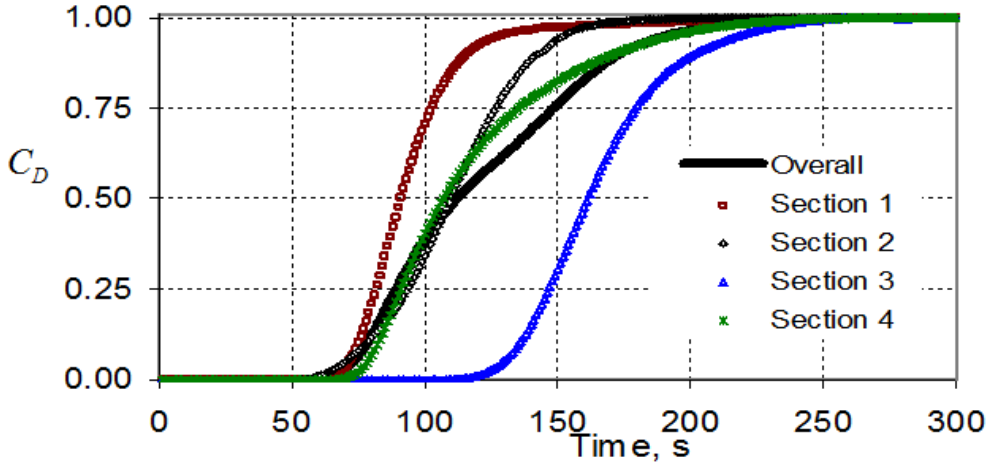

Figure 2.6: (a) Solute concentration profile and (b) local dispersion at the indicated sections for $D_o = 10^{-11}\ m^2/\ s$. Local dispersion varies significantly with position. Inset: magnified view of local concentration profile. The streams splitting, rejoining and diffusion homogenizing local concentration can be seen.

(a)

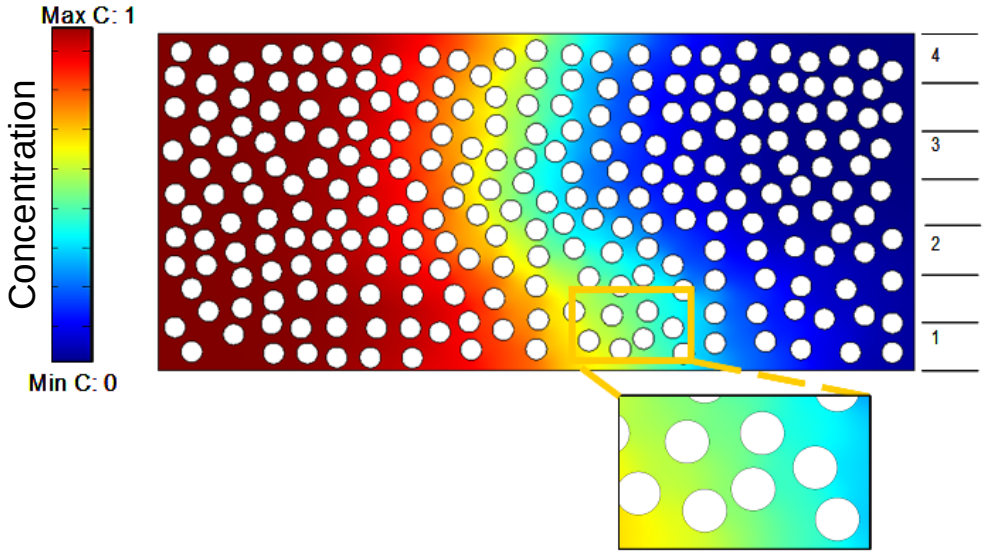

(b)

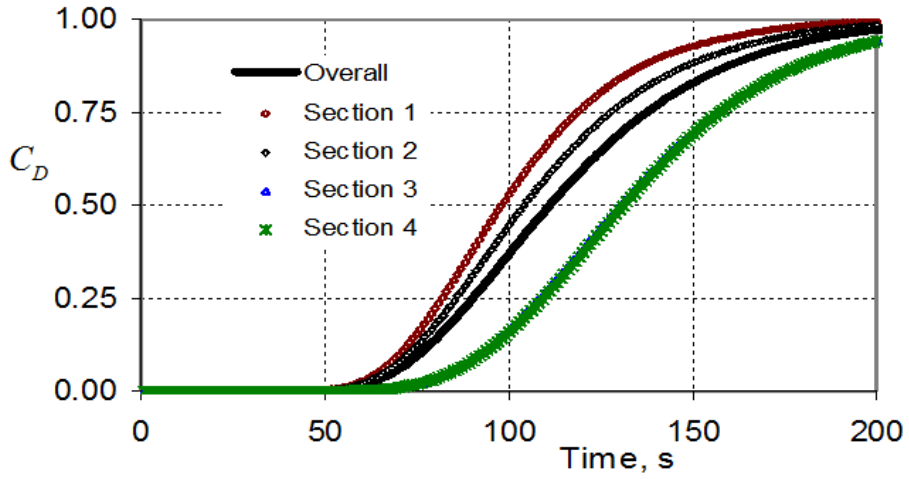

Figure 2.7: (a) Solute concentration profile and (b) local dispersion at the indicated sections for $D_o = 10^{-9}\ m^2/s$. Diffusion enhances local mixing and reduces the effect of permeability heterogeneity on local mixing. Inset: magnified view of local concentration profile. Diffusion eliminates the radial variation in local concentration caused because of splitting and rejoining of streams and homogenizes solute concentration inside a pore body.

2.8 EFFECT OF PECLET NUMBER ON MIXING: SIMULATIONS ON A REGULAR PACK

A series of solute slug tests are carried out to examine the effect of flow rates and diffusion coefficients on local mixing. In this case, a solute slug (0.228 pore volume) is injected into the medium where injection of solute slug is followed by injection of water. It is easier to visualize local mixing in the case of slug injection since in this case mixing takes place at the front as well as rear end of the slug. The convection diffusion equation is solved as before to determine the solute concentration distribution as a function of time. For comparison, all concentration profiles have been shown at a dimensionless time of $t_D = 0.684$. Here t_D is the dimensionless time defined as $t_D = v.t/L$, where v is average interstitial velocity, t is time and L is the length of the medium.

Pore scale Peclet number, vD_p / D_o , where v is the average interstitial fluid velocity, D_p the particle diameter and D_o the diffusion coefficient, is a measure of the time available for diffusion to homogenize the solute concentration in the pore space (Perkins and Johnston, 1963). Simulations have been run for local Peclet numbers of 1, 10, 100 and 1000. Each pore scale Peclet number, vD_p / D_o is obtained by two methods (i) changing the diffusion coefficient keeping velocity constant and (ii) changing velocity keeping the diffusion coefficient constant. The results showed identical concentration profiles as long as vD_p / D_o remains the same, regardless of the individual values of v or D_o.

Figure 2.8 compares concentration profiles at $t_D = 0.684$. It clearly shows that as the value of the pore scale Peclet number vD_p / D_o increases; the mixing inside the pore body becomes more and more incomplete. For small local Peclet number, the solute

particles spend enough time in the pore space to allow homogenization of the mixture by diffusion. For vD_p / D_o=1, flow is in the diffusion-dominated regime. The solute is well mixed inside the pore body. For vD_p / D_o=10 also there is no significant difference in solute concentration inside a pore body. For vD_p / D_o=100 we get an indication of ineffective local mixing as we can see discontinuity in solute concentration inside a pore body. For vD_p / D_o=1000 we find a clear indication of incomplete local mixing. For the given fluid velocity, diffusion does not have enough time to homogenize solute concentration inside the pore body.

These results are consistent with that predicted by Aris and Amundson (1957). Based on mixing cell theory (Deans, 1962) they show that for pore scale Peclet numbers between 4 and 50, solute particles spend enough time inside a pore to allow homogenization of solute concentration inside the pore body. For pore scale Peclet numbers smaller than 4, the process is dominated by diffusion and for Peclet numbers greater than 50, there is incomplete local mixing.

The FEMLAB simulations become numerically unstable for larger values of local Peclet number. Still, the trend clearly shows that if there were no diffusion at all, the solute particles would travel along individual streamlines and no local mixing will take place (Figure 1.3) and it will be a case of purely convective spreading.

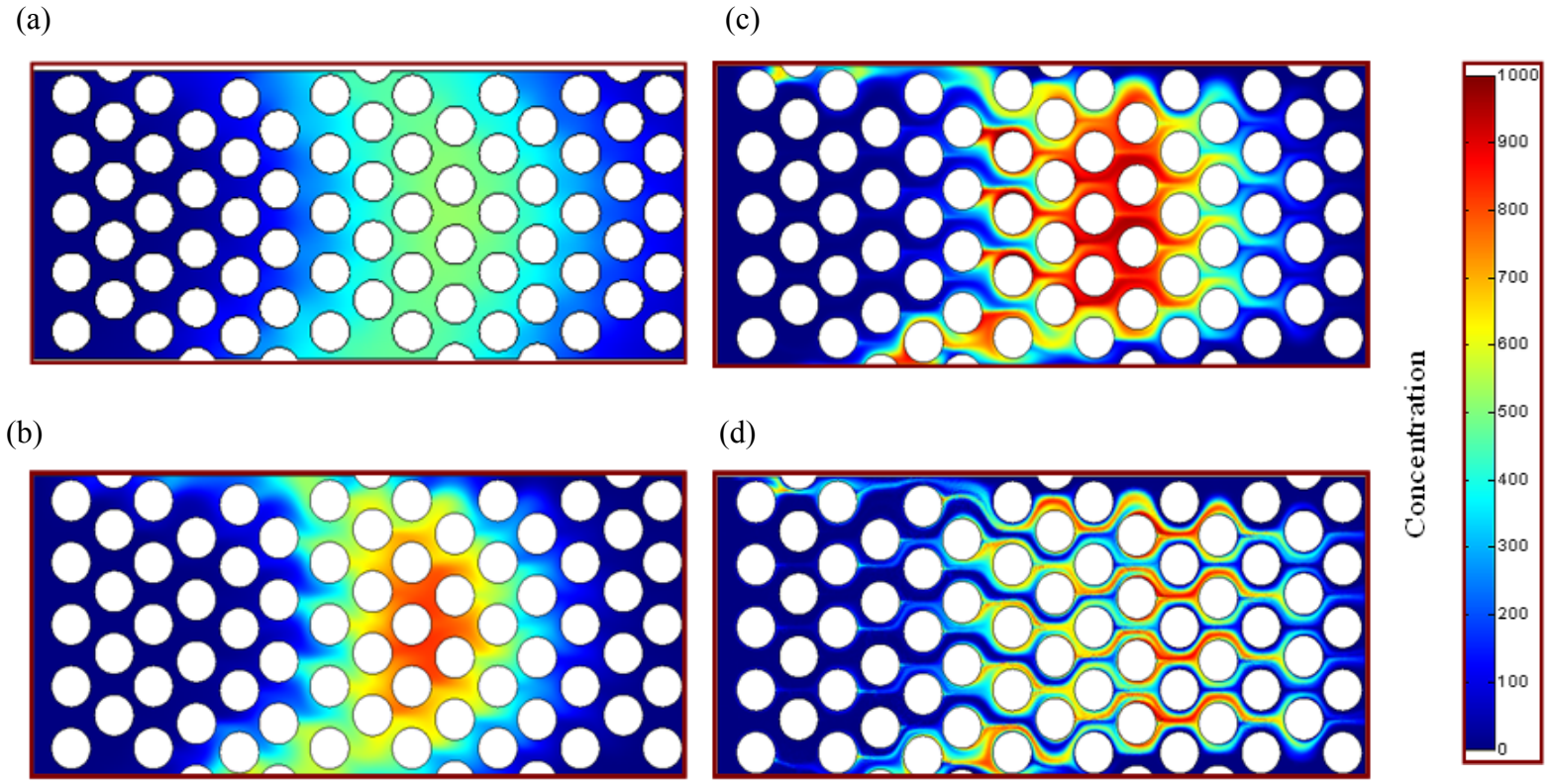

Figure 2.8: Concentration profiles for slug injection at $t_D = 0.684$ (*a*) $vD_p/D_o = 1$ (*b*) $vD_p/D_o = 10$ (*c*) $vD_p/D_o = 100$ (*d*) $vD_p/D_o = 1000$. There is a complete local mixing for smaller values of local Peclet number, vD_p/D_o. Local mixing becomes increasingly more incomplete as the local Peclet number increases.

2.9 CONCLUSIONS

- Because of converging-diverging flow around sand grains a solute slug stretches, splits and rejoins. This process increases by many times the surface area available for diffusion between injected and initially resident fluids and enables diffusion to be an effective mixing mechanism. Similar results are also reported by Garmeh et al. (2007).
- In the absence of a correlated heterogeneity in the medium, local and core scale averaged solute breakthrough curves are same and the transport process is Fickian.
- In case of correlated heterogeneity in the medium, local and core scale averaged solute breakthrough curves are different and the transport process is non-Fickian. For higher diffusion, the effect of correlated heterogeneity on the transport process is reduced and the process becomes closer to Fickian.
- At low pore scale Peclet numbers, diffusion is able to homogenize solute concentration inside each pore.
- In limit of very large fluid velocity (or no diffusion) local mixing tends to zero.

REFERENCES

1. Aris, R. and Amundson, N.R.: "Some remarks on longitudinal mixing or diffusion in fixed beds", AIChE Journal (Jun. 1957).
2. Auset, M. and Keller, A.A.: "Pore scale processes that control dispersion of colloids in saturated porous media", Water Resources Research, Volume 40 (2004).

3. Buyuktas, D. and Wallender, W.W.: “Dispersion in spatially periodic porous media”, Heat and Mass Transfer, Volume 40, 261-270 (2004).
4. Deans, H.A.: “A mathematical model for dispersion in the direction of flow in porous media”, SPE Journal (Mar. 1962).
5. FEMLAB Chemical Engineering Module Users Guide (Oct. 2004).
6. Garmeh, G., Johns R. T. and Lake, L. W.: “Pore scale simulation of dispersion in porous media”, SPE 110228 presented at SPE ATCE held at Anaheim, California, (Nov. 2007).
7. Graton, L. C. and Fraser, H. J.: “Systematic packing of spheres”, Journal of Geology (Nov-Dec. 1935).
8. Greenkorn, R.A. and Kesseler, D.P.: “Dispersion in heterogeneous nonuniform anisotropic porous media”, Industrial and Engineering Chemistry, 61, 33, (1969).
9. Jha, R. K.: *Pore Level Investigation of Dispersivity*, MS Thesis, The University of Texas at Austin, (May, 2005).
10. Perkins, T. K. and Johnston, O. C.: “A Review of Diffusion and Dispersion in Porous Media”**,** SPE 480, SPE Journal, 3(3), 70-84 (Mar., 1963).

Chapter 3: Flow Reversal and Mixing

3.1 INTRODUCTION

Core-scale averaged ("cup-mixed") solute concentration histories fail to differentiate between convective spreading and mixing (dilution). The dispersion coefficient obtained from an averaged concentration history has the contributions of convective spreading and diffusion lumped together. Transmission displacement experiments carried out on core samples do not give any information about the mechanism of solute transport and mixing within the medium.

Convective spreading (Figure 1.3) implies that if the direction of flow is reversed the solute particles would retrace their paths to the origin and the injected slug will be received back at the inlet without any dissipation. The convective spreading of solute particles would thus be *reversible*. Reversibility has been demonstrated for slow, laminar flow of viscous liquids between disordered arrays of cylinders (Hiby, 1962), flow between concentric cylinders (Taylor, 1972) and in the Couette viscometer (Heller, 1960).

However, *echo dispersion* (Hulin and Plona, 1989) experiments on homogeneous core samples, in which the direction of flow is reversed after the solute has penetrated into the medium (but not exited) to a pre determined distance, show dispersion to be *irreversible*. The solute continues to disperse (and mix) as the fluid moves back toward the original inlet. Dispersivities obtained from such flow reversal experiments on

homogeneous core samples in the lab (Rigord et al., 1990) and from single well tracer tests in the field (Mahadevan et al., 2003) are as large as the corresponding transmission values. On the other hand, echo dispersion experiments on layered media show largely reversible dispersion (Hulin and Plona, 1989; Rigord et al., 1990a; Rigord et al., 1990b). Thus, comparing the transmission and echo dispersions gives information about heterogeneities of the medium and helps ascertain the nature of the dispersion mechanism (what fraction of dispersion arises because of convective spreading and what because of local mixing). The irreversibility of solute dispersion (in homogeneous media) is contrary to the convective spreading hypothesis and indicates that there is local mixing taking place. The fraction of irreversibility of dispersion depends on the degree of local mixing taking place. Local mixing is essentially caused by diffusion and therefore, irreversible (Jha et al.,2006).

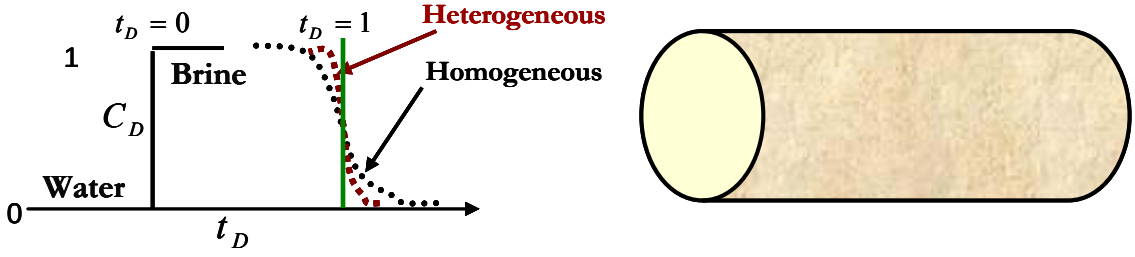

Figure 3.1: Echo dispersion experiment. Echo dispersion (indicated by dotted curves) is the same as the transmission dispersion in a homogeneous medium and smaller than the transmission dispersion in a heterogeneous medium.

Flow reversal provides insights about mixing mechanisms in flow through porous media. We carry out pore scale simulation studies with flow reversal. The direction of flow is reversed before solute exits the medium. The simulation studies are carried out for several diffusion coefficients, penetration depths and for several flow geometries. The

simulation studies presented in this chapter further illustrate the mechanisms of mixing and explain the origin of irreversibility of dispersion. We also explain several experimental observations on flow reversal tests found in the literature.

3.2 METHOD

Method used is the same as that described in the previous chapter. We used a multi-physics modelling software FEMLAB to solve simultaneously the Navier-Stokes and convection diffusion equations directly for the given flow geometry. This approach allows investigation of solute transport and mixing from first principles without making assumptions about macroscopic dispersive models for mixing (Jha et al., 2006).

The direction of flow is reversed before any solute particle could exit the medium. Here we make an assumption that upon flow reversal solute particles attain the steady state velocity immediately in the backward direction. It is a reasonable assumption for the slow velocity in our simulations. In reality, because of slower velocity during transient state there will be more time for diffusion to cause mixing. Therefore, by making an assumption of instantaneous achievement of the steady state we under-predict mixing slightly. Since our conclusions are qualitative in nature and not quantitative, we neglect this effect.

We visualize the interplay of convective spreading and diffusion and calculate core-scale average mixing (dispersion) for forward as well as backward flows. First, we carried out pore-scale simulations for miscible flow in several simple two-dimensional (2D) flow geometries to understand the mechanisms of local mixing and the factors influencing it. Then we use these insights to investigate the effect of flow reversal on

mixing in more realistic models of porous media. In this chapter we explain the results of those simulation studies and discuss the origin of irreversibility of dispersion.

3.3 MIXING MECHANISMS AND EFFECT OF FLOW REVERSAL ON MIXING

We have carried out FEMLAB simulations in two-dimensional porous media consisting of a rectangular plate with circular holes in it (Jha et al., 2006). The holes represent the sand grains and the fluid can flow through the pore space between them. The grain diameter is taken as 100 microns (unless shown otherwise). The size of the flow domain is 1800×800 micrometers. In each case, a solute slug is injected into the medium at a small velocity of 10^{-5} *m/s* for 20 seconds (which corresponds to 0.1 PV, approximately). The outlet face of the medium is maintained at atmospheric pressure. All other boundaries including the sand grain boundaries are of "no-slip" kind. The steady state velocity at each point inside the medium is obtained by solving the Navier-Stokes equation. The Reynolds number is very low in these simulations (Re ≈ 10^{-3}) and inertial effects may be neglected. The solute concentration as a function of time and space is then determined by solving the convection-diffusion equation. This equation uses the computed velocities at each point and an input diffusion coefficient of $D_o = 10^{-11}$ m^2/s. When the slug reaches the center of the medium the direction of flow is reversed. Solute concentration profiles at a short distance from the inlet can be compared during forward and during backward flow to investigate the degree of irreversibility of mixing. We also compare averaged solute concentration histories in forward (without reversal) and backward directions. Since flow was reversed from the center of the medium, the solute slug spends the same time in the medium whether flowing forward or backward. If

dispersion is completely irreversible, i.e., the change in direction of flow does not make any difference to dispersion, the forward and backward concentration histories would be identical.

First we study the mixing mechanism and the effect of flow reversal on dispersion in simple flow geometries to illustrate the principles and then advance to more realistic models of porous media. The results of simulation studies on simple models are presented below.

(i) Plug Flow in a Channel (Figure 3.2) - In this case, the fluid velocity is uniform throughout the cross-sectional area of the medium. There is no local velocity gradient and convection plays no role in dispersion. There is no stretching or splitting of the solute slug. Dispersion is caused solely by diffusion. Mixing and dispersion are the same in this case. Upon flow reversal, the slug encounters exactly the same conditions and behaves exactly same way while moving backward that it would have done had it continued to move forward. Therefore, flow reversal has no effect on dispersion and dispersion is completely irreversible. This is also indicated by identical forward and backward concentration histories. Local mixing, as evidenced by concentration transition zones at the front and back of the slug, is small.

(ii) Parabolic Flow in a Channel (Figure 3.3) - In this case the fluid velocity is maximal at the center of the medium and zero at the walls. Because of velocity gradients the solute-front stretches (there is no splitting of the slug) and the contact area between large and small solute concentrations increases (Taylor, 1953; Aris, 1959). Therefore, more local mixing takes place compared to case (i). However, convective spreading is much

larger than local mixing. Upon flow reversal, the convective spreading cancels and dispersion is largely reversible (except for small local mixing caused as in case (i)).

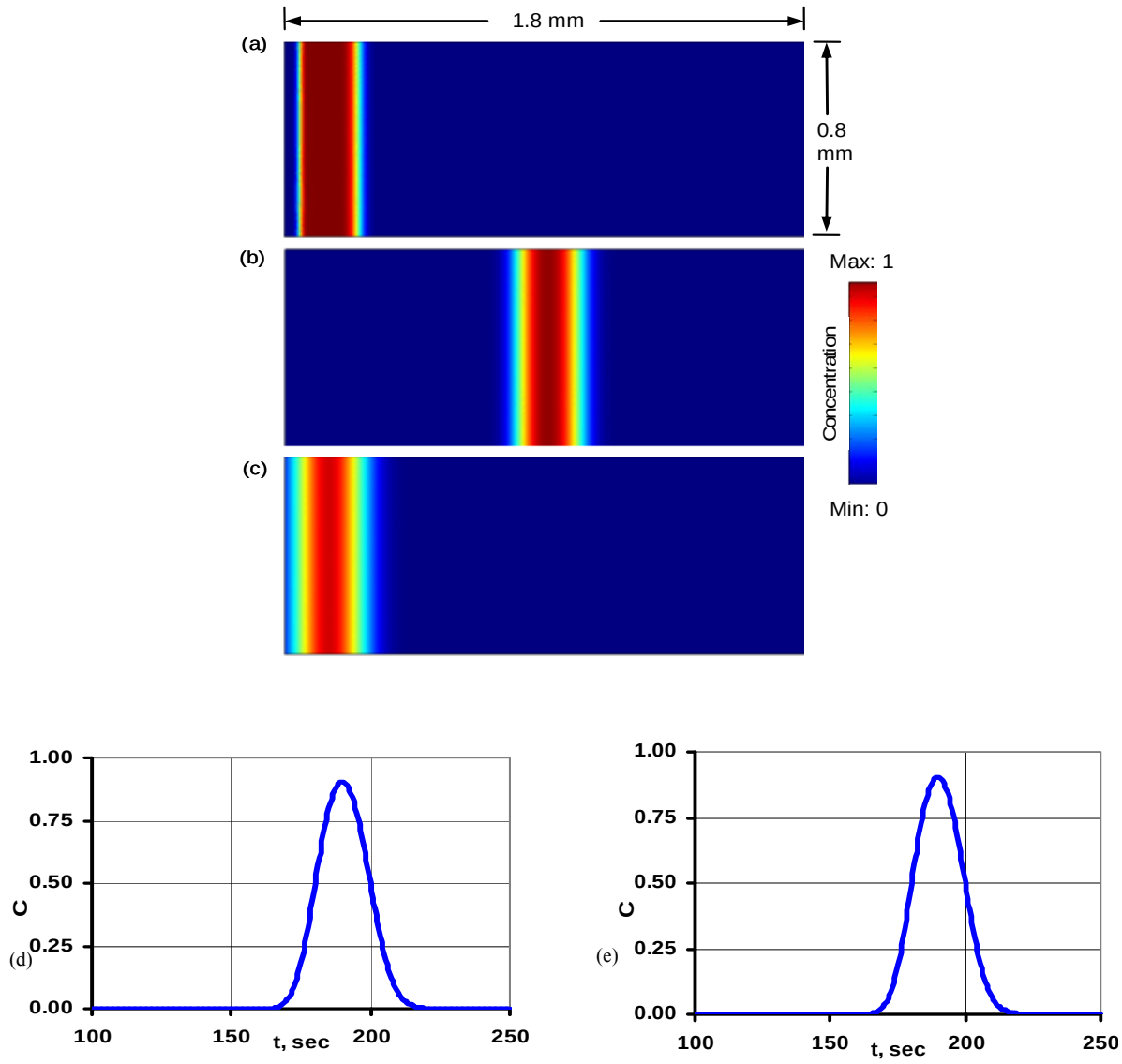

Figure 3.2: Solute concentration profiles for a plug flow of a solute slug (a) five seconds after injection, (b) at the time of flow reversal and (c) five seconds before exit. The solute slug is injected for 20 seconds. The velocity across the whole cross-section is constant at 10^{-5} *m/s*. Dispersion is caused by diffusion alone. Upon flow reversal the slug behaves exactly the same way it would have done had it continued moving forward. Dispersion is same as mixing and therefore, irreversible. (d) Forward solute concentration history and (e) backward solute concentration history are identical. (1 PV ≈ 200 s).

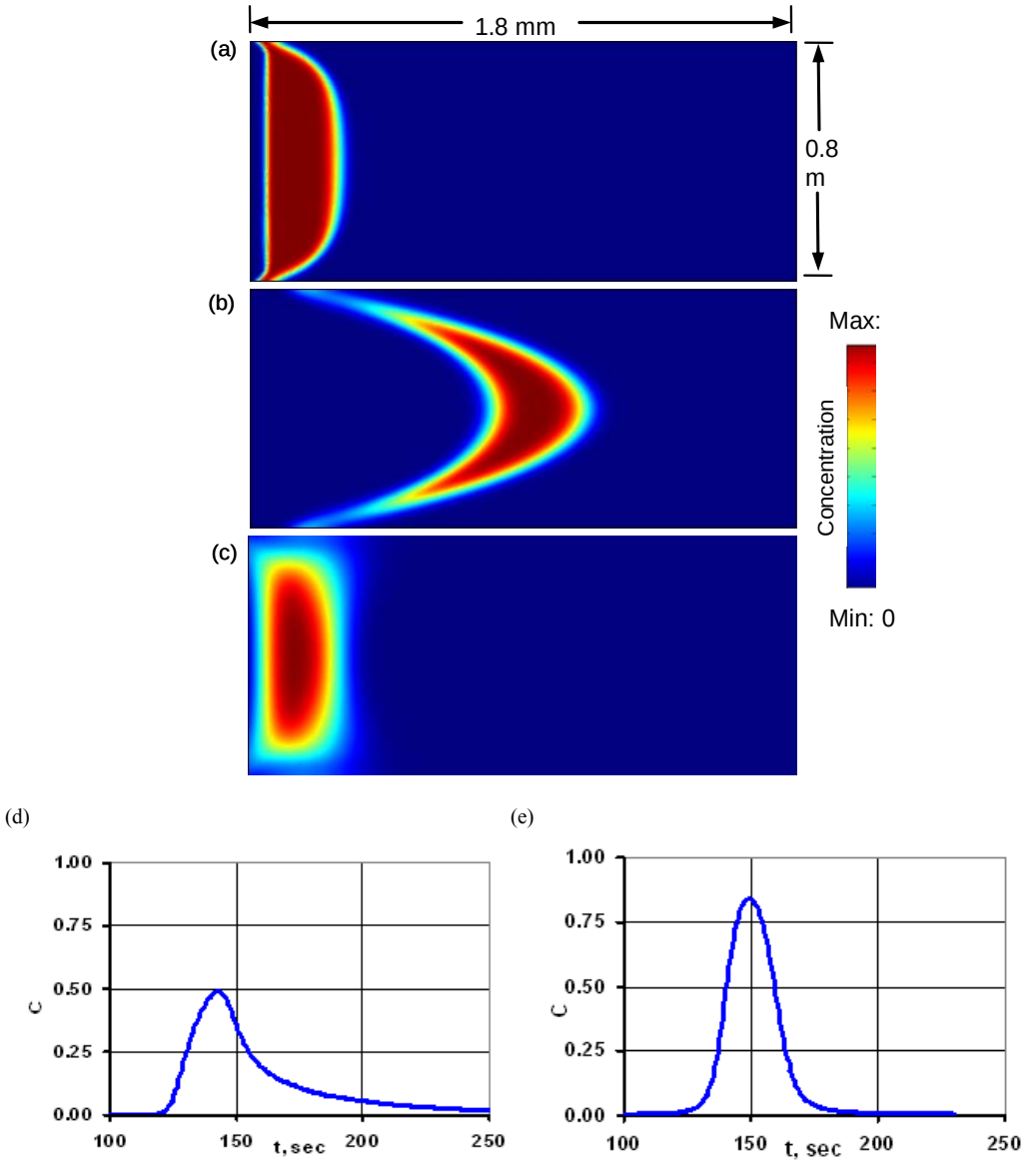

Figure 3.3: Solute concentration profiles for a slug with parabolic velocity (a) five seconds after injection, (b) at the time of flow reversal and (c) five seconds before exit. Stretching of solute front enhances mixing due to diffusion. However, convective spreading dominates mixing caused by diffusion. Upon flow reversal the convective mixing cancels and dispersion is largely reversible. A large difference in (d) forward solute concentration history and (e) backward solute concentration history also suggests largely reversible dispersion is occurring. (1 PV ≈ 200 s).

Reversibility of mixing is also evident from differences in the solute concentration histories in the forward and backward directions.

(iii) Flow around a Grain (Figure 3.4) - Here the solute slug encounters an obstruction in the form of a sand grain. The grain being impervious and having no-slip boundaries, the solute front splits around the sand grain and then rejoins. Because splitting increases the contact area between large and small solute concentrations, mixing by diffusion is enhanced. Upon flow reversal, even though convective spreading vanishes, the local mixing is large as compared to that in Figures 3.1 and 3.2. Dispersion is not as reversible as in case (ii).

Experiments and simulations in a similar flow geometry show that the solute transport is slightly irreversible even with a very small diffusion coefficient (Flekkoy et al., 1995,1996). However, this irreversibility is insignificant for the low Reynolds number ($Re \approx 10^{-3}$) in our simulations and not considered.

(iv) Flow around Three Grains (Figure 3.5) - More grains cause more stretching, splitting and rejoining of the solute slug. This results in enhanced local mixing (Muzzio et al., 1992). Greater local mixing yields greater irreversibility of dispersion.

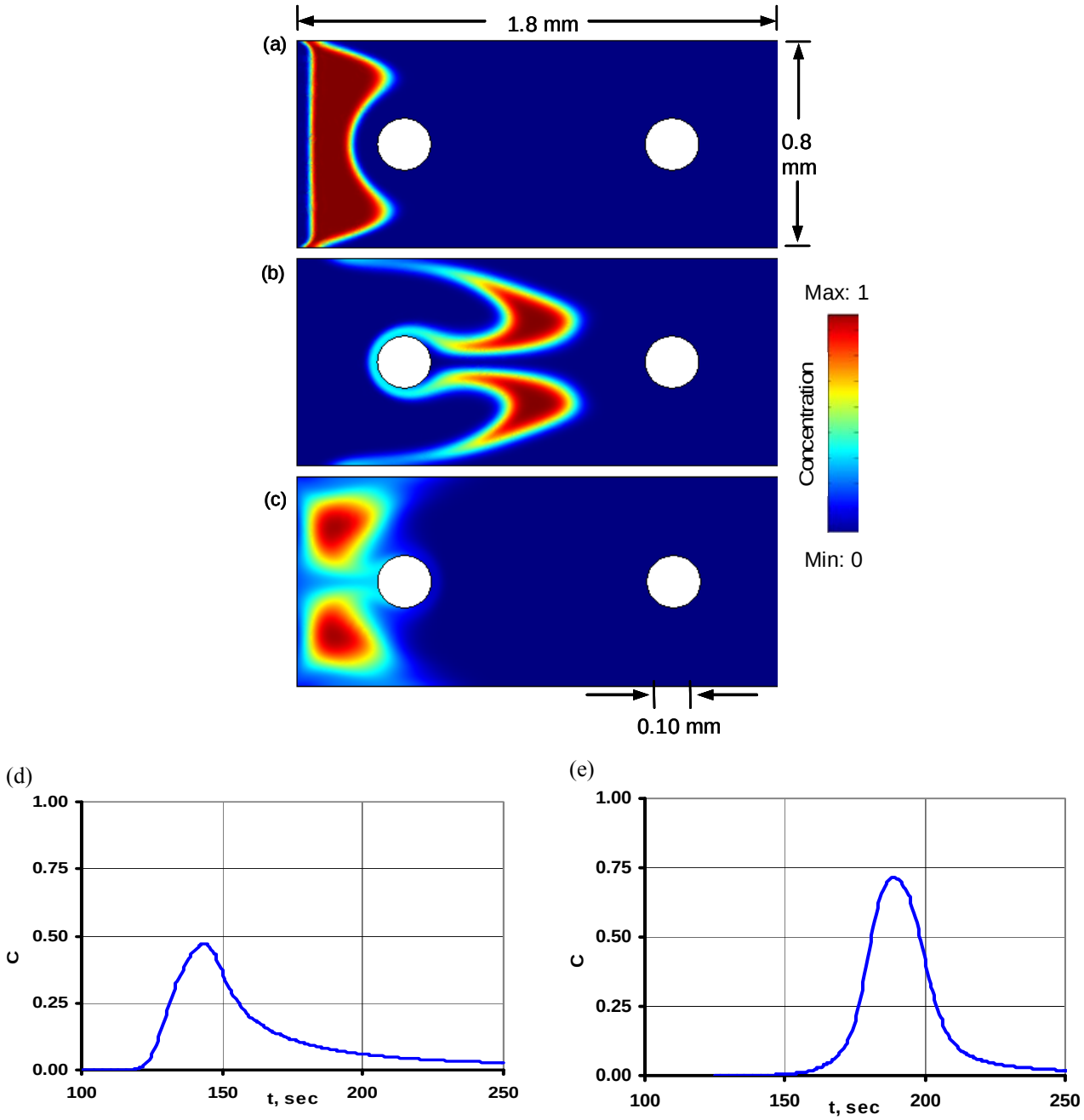

Figure 3.5: Solute concentration profiles for solute slug flowing around a sand grain (a) five seconds after injection, (b) at the time of flow reversal and (c) five seconds before exit. Splitting around sand grain increases area for diffusion and enhances local mixing. (d) Forward concentration history and (e) backward concentration history. (1 PV ≈ 200 s).

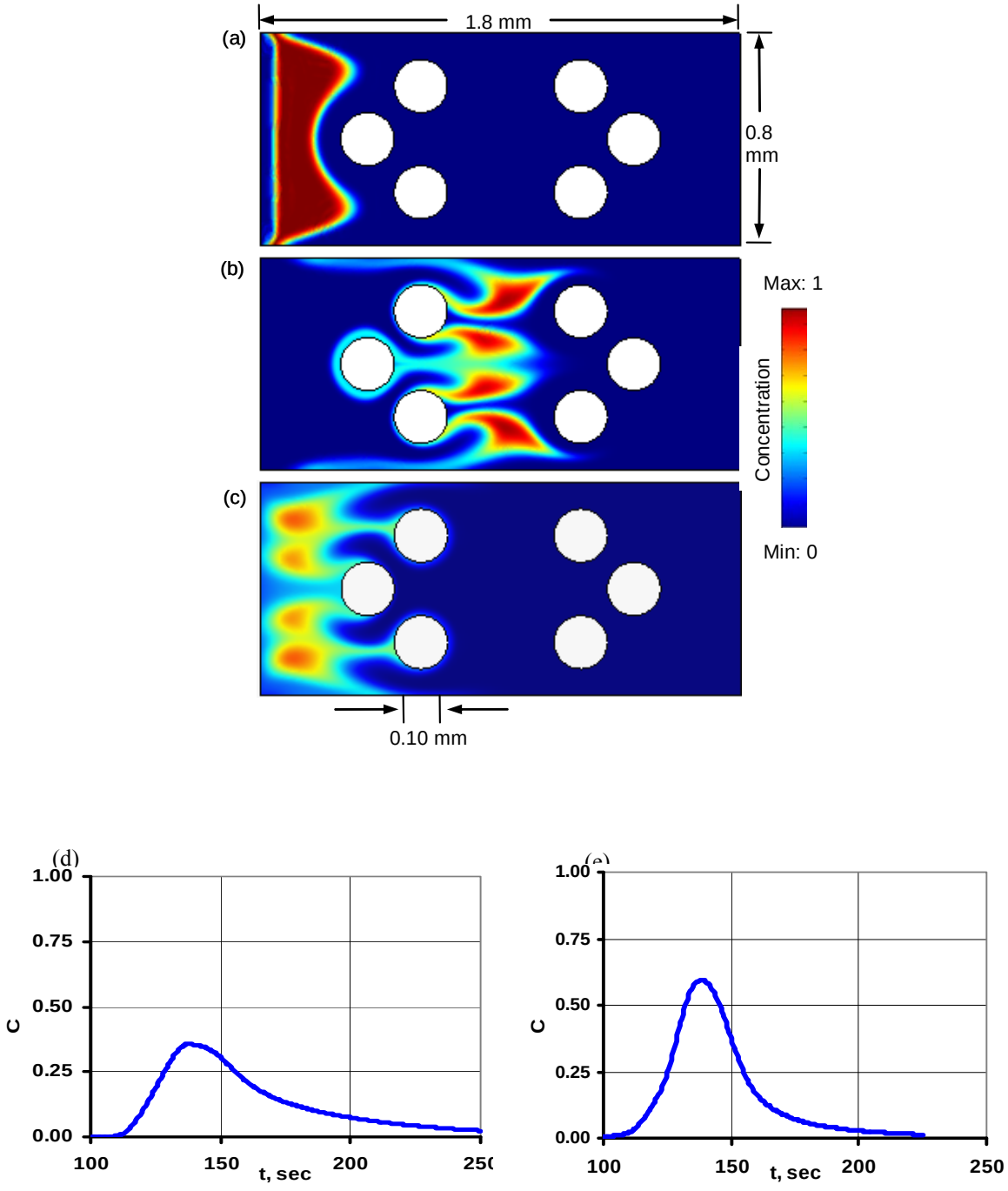

Figure 3.6: Solute concentration profiles for flow of solute slug around three grains (a) five seconds after injection, (b) at the time of flow reversal and (c) five seconds before exit. More grains correspond to more splitting of solute slug and hence enhanced local mixing and more irreversibility of dispersion. (d) Forward concentration history and (e) backward concentration history. (1 PV ≈ 200 s).

3.4 DISCUSSION ON LOCAL MIXING MECHANISM

A comparison of the effluent concentration histories during backward flow at the original inlet (which becomes the outlet during backward flow) for all the previous cases is shown in Figure 3.6 for $D_o = 10^{-11}\ m^2/s$. These histories are velocity weighted average solute concentrations at the outlet face (original inlet). The input concentration and slug size is same in all the cases. If mixing were completely reversible, the effluent concentration history in each case would be the same, which in turn would be the same as the input concentration history. The deviation of the effluent history from the input history indicates the degree of irreversibility of dispersion resulting from the local mixing. In the examples presented here, a longer area of contact between large and small solute concentrations allows more local mixing to occur during the same interval of time. The greater the local mixing, the greater is the extent of irreversibility of dispersion.

The rate of diffusion affects the local mixing significantly. Figure 3.7 compares the effluent concentration histories for the same cases for a smaller diffusion coefficient $D_o = 10^{-12}\ m^2/s$. Reducing the diffusion coefficient has reduced the local mixing and all the curves shift towards the input concentration. In the limit of zero diffusion all the effluent concentration histories will coincide with the input concentration. On the other hand, if we increase the diffusion coefficient to $10^{-10}\ m^2/s$, more local mixing will result (Figure 3.8). Dispersion is irreversible in all the cases and all of the curves are nearly the same.

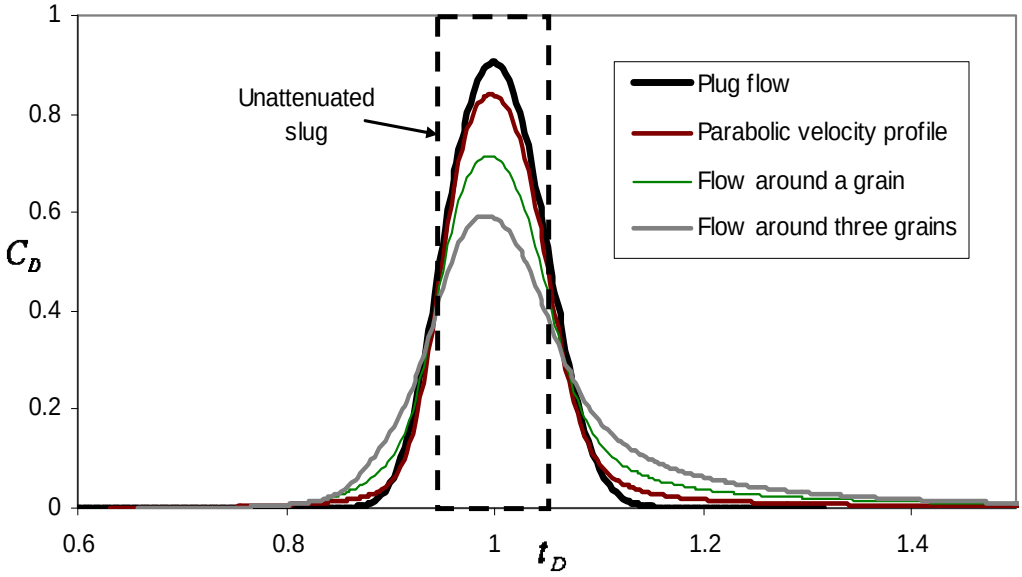

Figure 3.6: Comparison of backward solute concentration histories at the original inlet ($D_o = 10^{-11}\ m^2/s$) after flow reversal. The falling peak of concentration indicates more local mixing.

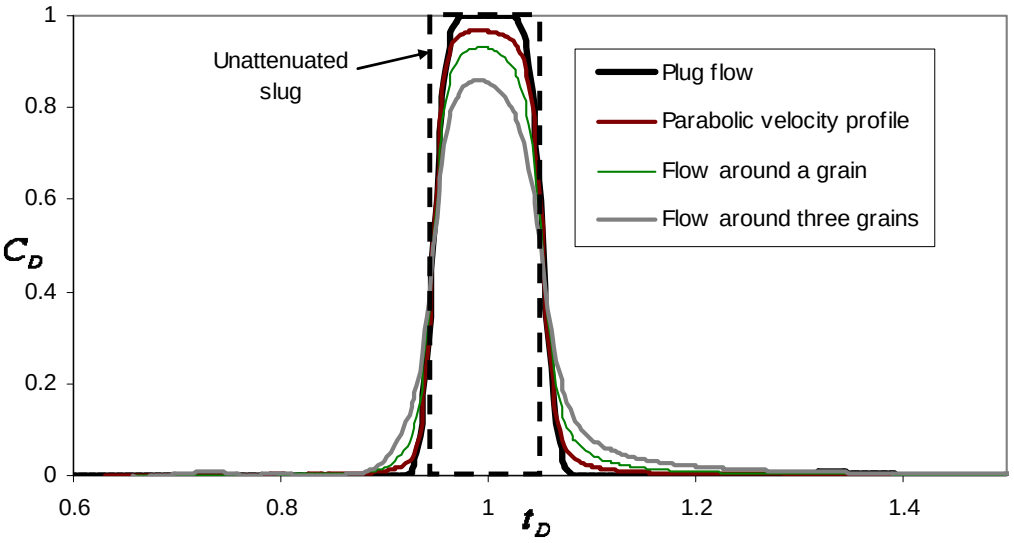

Figure 3.7: Comparison of backward solute concentration histories with a smaller diffusion coefficient ($D_o = 10^{-12}\ m^2/s$). Less diffusion causes greater reversibility of dispersion.

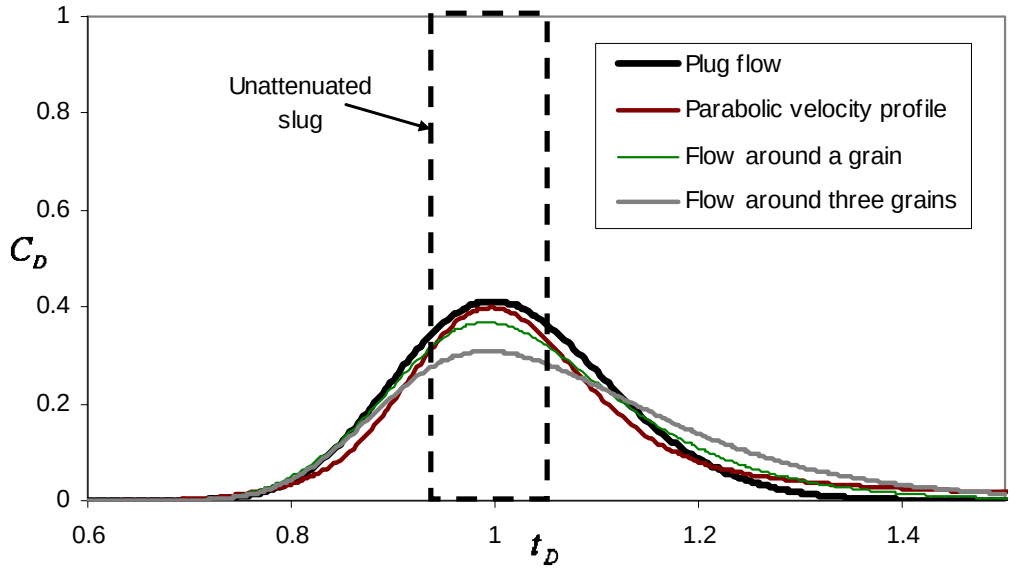

Figure 3.8: Comparison of backward solute concentration histories with larger diffusion coefficient ($D_o = 10^{-10}\ m^2/s$). Because of irreversibility of mixing, all the curves look the same.

3.5 FLOW REVERSIBILITY SIMULATIONS IN A DISORDERED PACK (WITH A CORRELATED HETEROGENEITY)

We test these insights gained from simulations in the simple pore geometries by conducting flow reversal studies in a disordered arrangement of disks (Figure 3.9). Even though this model of porous media is two dimensional and has an unrealistically large porosity, it does capture the basic physics of the process and allows qualitative comparisons with experimental observations.

The dimensions of the flow domain and flow conditions are the same as described for previous cases. The only difference is that now the medium has many disks representing sand grains and the diameter of the disks are half of that used previously.

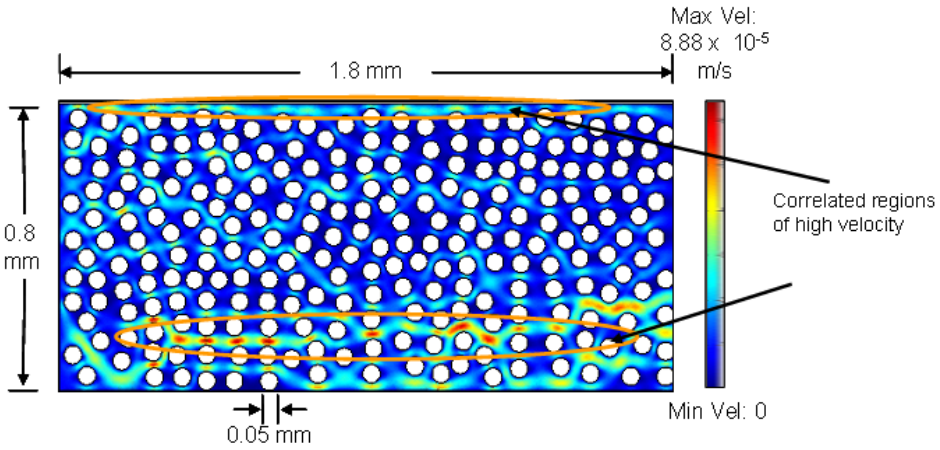

Figure 3.9: Velocity profile in a disordered pack. The pack has correlated regions of high velocity because of inhomogeneity of packing.

The velocity inside the medium varies widely both in the longitudinal as well as the lateral direction. The medium has correlated regions of high velocity as shown in Figure 3.9. Therefore, the solute slug does not move uniformly throughout the cross-section of the medium. It spreads more in the correlated regions having high velocity (Figure 3.10 (a), (b)). The differential movement of different parts of the solute slug across the cross section grows with time and distance traveled. If the slug keeps on moving in the forward direction and effluent concentration is monitored at the outlet, it would not satisfy the 1D convection-diffusion equation (in other words, concentration history curve is non-Fickian). However, if the flow direction is reversed and effluent concentration history is monitored at the original inlet, the backward or echo dispersion curve becomes Fickian because the convective spreading cancels upon flow reversal (Flekkoy et al., 1996) (Figure 3.11). Cancellation of convective spreading is also evident if we compare solute concentration profiles at the same distance from the inlet in forward and backward flow (Figure 3.10). The two profiles look similar in shape. However, the

backward profile is more dispersed because of irreversible local mixing and resulting reduction in solute concentration. This illustrates cancellation of convective spreading on flow reversal.

If the diffusion coefficient is increased, the solute spreads more in the lateral direction due to diffusion and greater local mixing takes place. Diffusion causes decorrrelation of solute velocity. The effect of convective spreading is reduced (Jha et al., 2006) and the forward concentration history becomes closer to Fickian. Because of higher diffusion, the degree of irreversibility of dispersion increases and forward and backward concentration histories become similar (Figure 3.12).

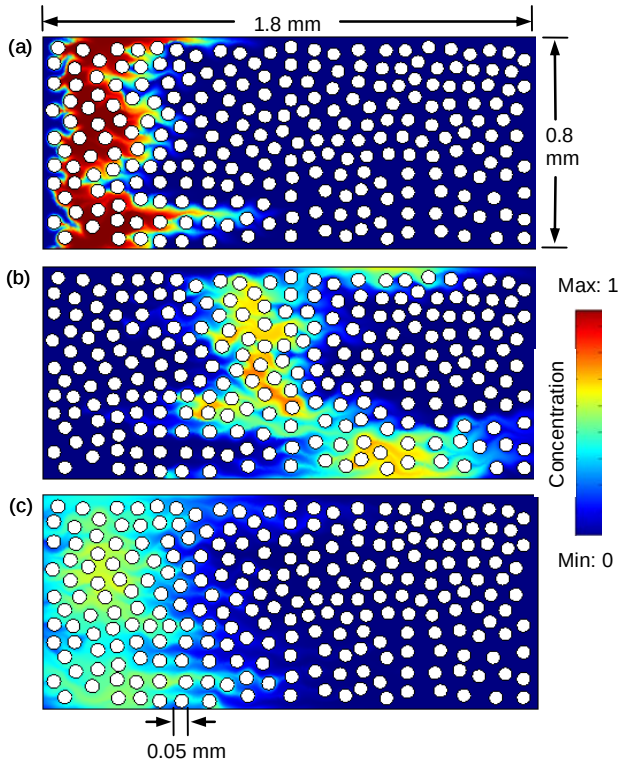

Figure 3.10: Solute concentration profiles for a slug in an irregular arrangement of disks (a) five seconds after injection, (b) at the time of flow reversal and (c) five seconds before exit. Similarity in shapes of concentration profiles in parts (a) and (c) indicate cancellation of convective spreading. (1 PV ≈ 110 s).

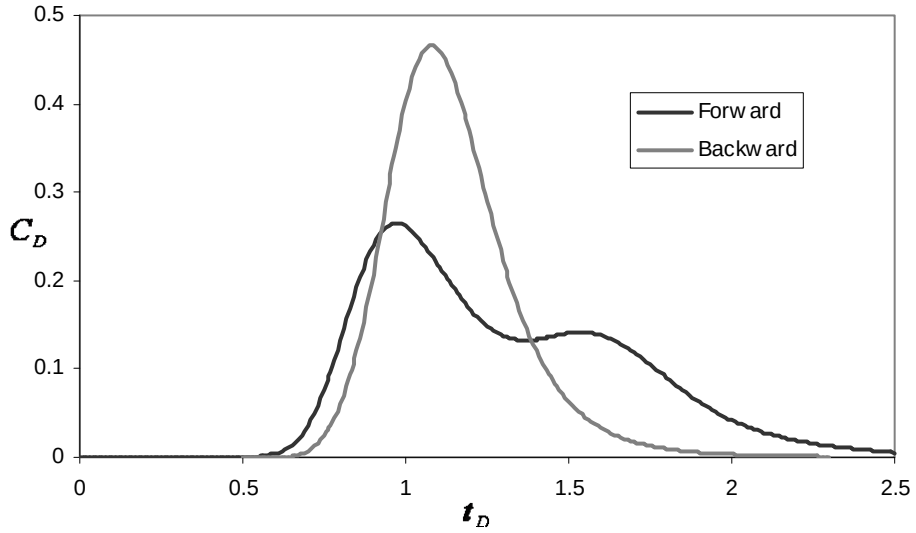

Figure 3.11: Comparison of solute concentration histories for a slug in a medium with irregular packing (D_o = 10^{-11} m^2/s). Forward curve (at original outlet) is non-Gaussian because of the heterogeneous nature of the medium. The backward curve (at original inlet) on the other hand is Gaussian as it results from local mixing.

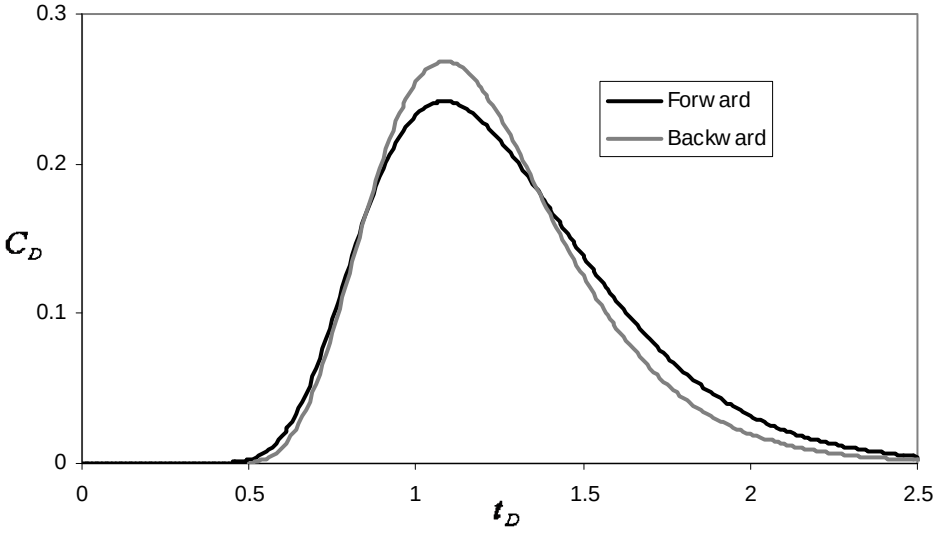

Figure 3.12: Comparison of solute concentration histories for a slug in a medium with irregular packing (D_o = 10^{-9} m^2/s). Higher diffusion coefficient reduces effect of inhomogeneity on mixing. For a diffusion dominated processes the forward and backward dispersions are the same.

3.6 EFFECT OF DEPTH OF PENETRATION ON IRREVERSIBILITY OF MIXING

In this section we present results of reversing flow of a solute front from several depths of penetration. Flow was reversed after injecting solute for 25, 50, 75 and 150 seconds respectively. The mean positions of solute fronts at the time of flow reversal is shown in Figure 3.13.

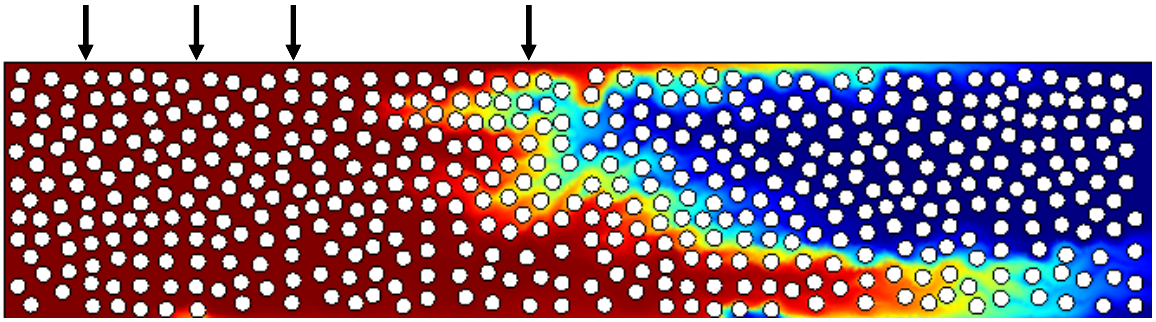

Figure 3.13: Continuous solute injection in a long core. The flow was reversed from four different depths of penetration shown by the four arrows.

We compare the solute concentration histories in forward and backward direction for all the cases (Figure 3.14). The forward concentration history is non-Gaussian because of local heterogeneities in the medium. However, the backward concentration history shows dispersion and that is Gaussian in each case. As the depth of penetration increases, diffusion gets more time to cause mixing. Therefore, there is greater mixing and greater irreversibility of dispersion corresponding to greater depth of penetration.

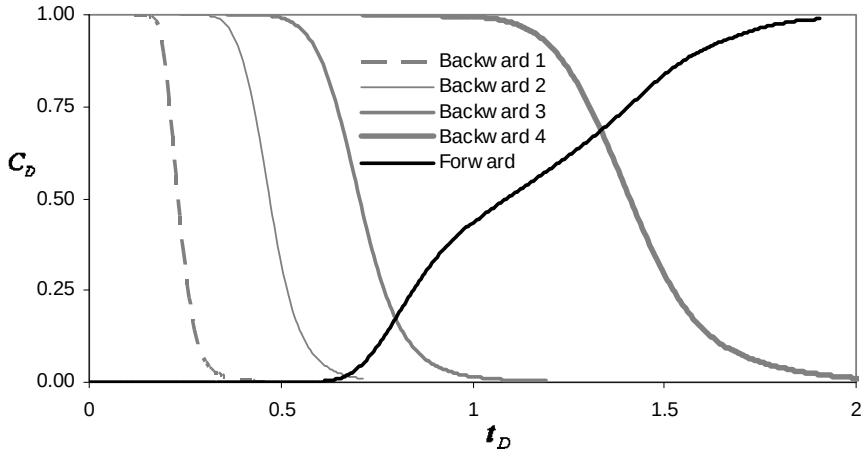

Figure 3.14: Comparison of backward concentration histories from different penetration depths with the forward concentration history. Forward curve is non-Gaussian. Backward curves are Gaussian. Greater depth of penetration corresponds to greater local mixing and more irreversibility of dispersion.

3.7 FLOW REVERSIBILITY SIMULATIONS IN AN ORDERED PACK

Flow reversal simulations were also carried out for a regular arrangement of disks. In this case the local velocity does not vary widely from point to point (except at the edges) and even a small diffusion is able to eliminate concentration discontinuities in a pore and homogenize solute concentration in the transverse direction. The solute slug appears to move like a plug. The effect of convection, splitting and rejoining around sand grains is to enhance the effective diffusion coefficient and mixing during flow is "diffusion-like". It is analogous to case (i) (plug flow) but with a larger dispersion (effective diffusion) coefficient. Upon flow reversal, the slug behaves exactly same way while flowing backward that it would have done while flowing forward. Therefore flow reversal has no effect on dispersion and dispersion is completely irreversible (Hulin and Plona, 1989; Rigord et al., 1990) (Figure 3.15, 3.16).

For zero diffusion, we would expect no local mixing (except for that arising from the numerical dispersion) and hence solute transport would be reversible. Simulations for small diffusion coefficient tend to be numerically unstable. Since increasing the velocity has the same effect on local mixing as reducing the diffusion coefficient, we simulated the process for a diffusion coefficient 20 times smaller and twice the velocity. This has the same effect on local mixing as reducing diffusion coefficient by a factor of forty. The results show partial reversibility of mixing for this increased Peclet number (Figure 3.17). If there is no diffusion at all the solute particles will move along individual streamlines. Upon flow reversal they would retrace their path to origin and dispersion will be reversible.

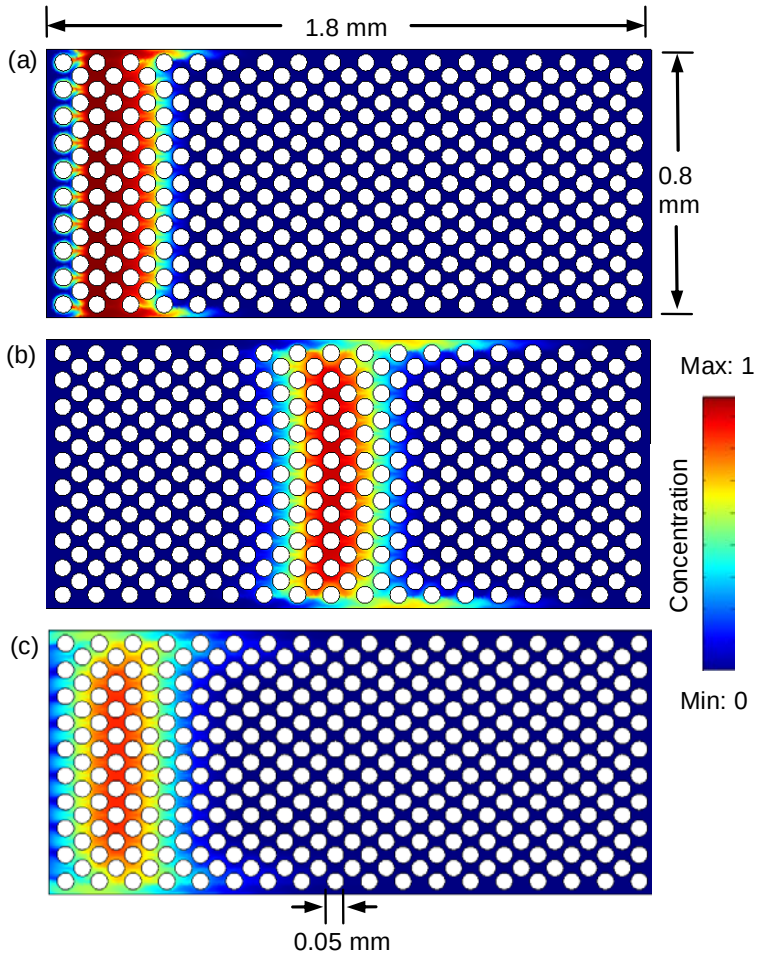

Figure 3.15: Solute concentration profiles for a slug in regular arrangement of disks (a) five seconds after injection, (b) at the time of flow reversal and (c) five seconds before exit. This process is diffusion-like. The role of solute front-splitting and rejoining is to enhance the effective diffusion coefficient. The slug behaves the same way on its way back as it would have done while flowing forward. Dispersion is completely irreversible. For a uniform medium a very small diffusion coefficient is able to homogenize solute concentration in transverse direction and dispersion is dominated by local mixing. (1 PV $\approx$ 110 s).

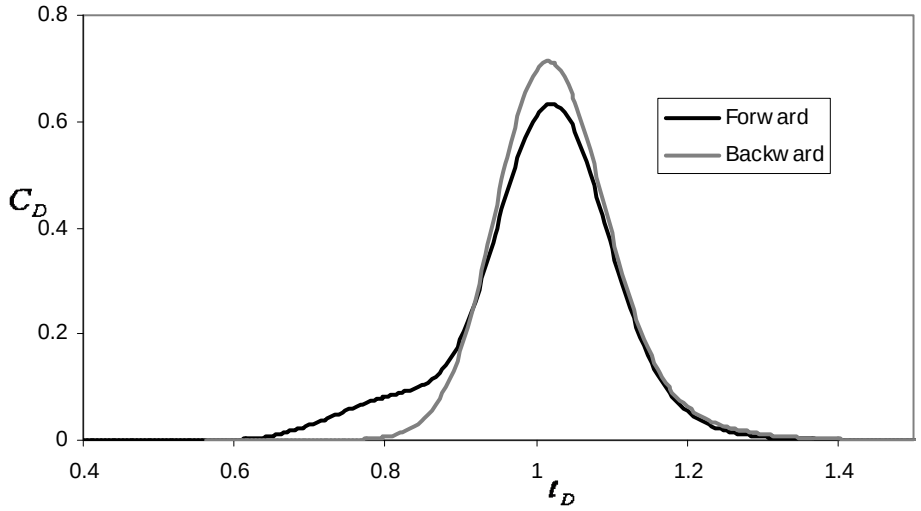

Figure 3.16: Forward and backward solute concentration histories for flow in a uniform pack ($D_o = 10^{-11}\ m^2/s$). Dispersion is irreversible.

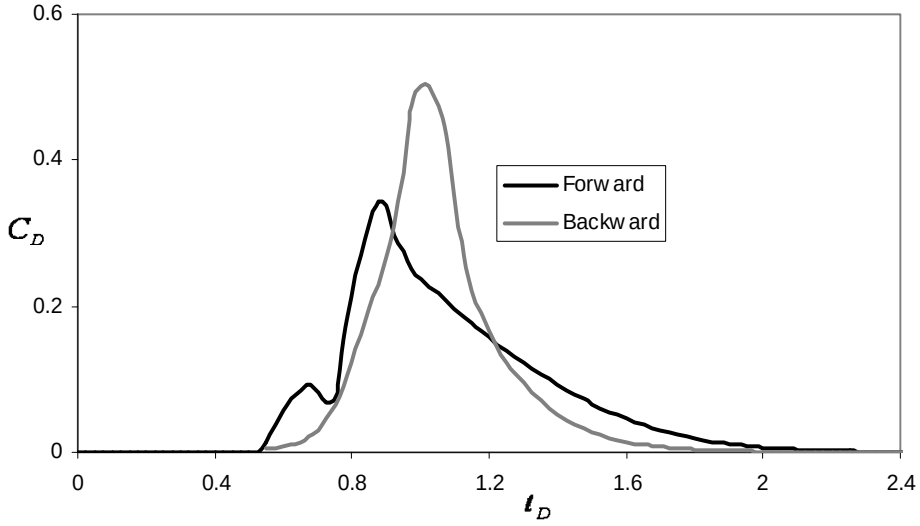

Figure 3.17: Solute concentration histories for flow in a uniform pack at forty times smaller effective diffusion coefficient. The backward curve shows partial reversibility of dispersion.

3.8 FLOW REVERSIBILITY SIMULATIONS IN A DISORDERED PACK WITHOUT CORRELATED HETEROGENEITY

We show in Chapter 7 that an ordered pack is not a proper model of realistic porous media as it does not model the velocity dependence of dispersion coefficient correctly. A random array of disks without any correlated heterogeneity is a much more representative model.

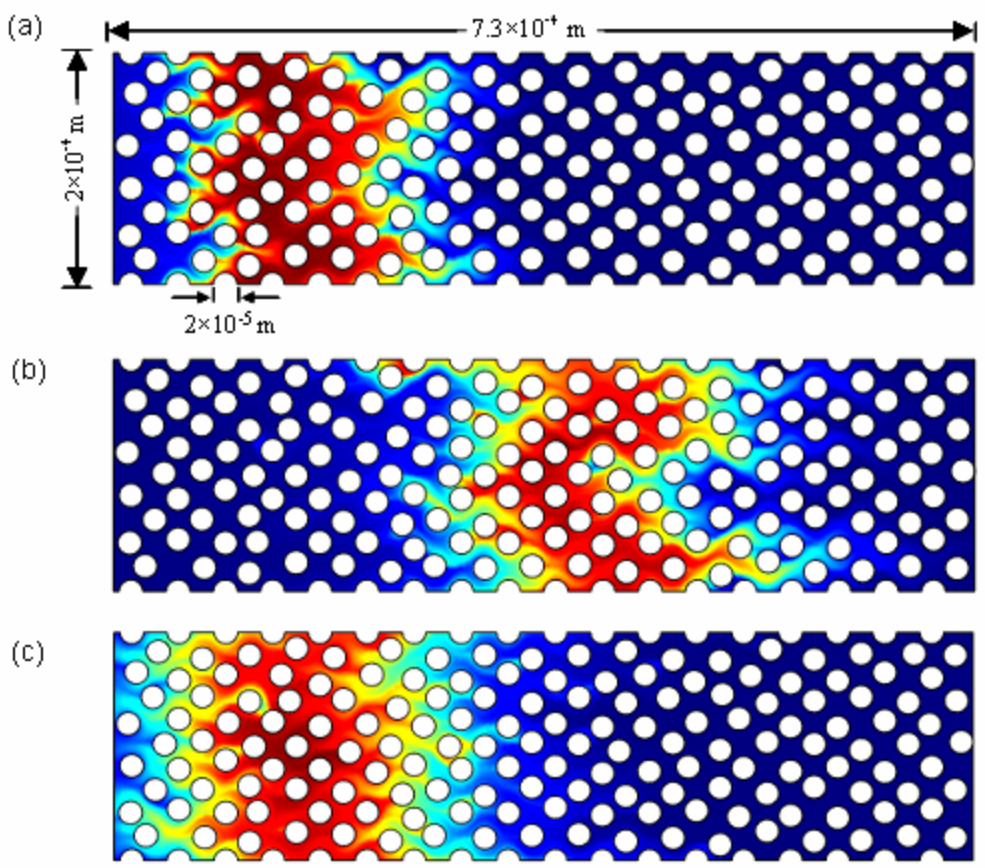

Figure 3.18: Solute concentration profiles for a slug in a random arrangement of disks (a) five seconds after injection, (b) at the time of flow reversal and (c) five seconds before exit. The mixing mechanism is same as that in case of ordered arrangement of disks. The role of solute front-splitting, rejoining and local mixing enhances the effective diffusion coefficient. The slug behaves the same way on its way back as it would have done while flowing forward. Dispersion is irreversible. For a random medium without correlated heterogeneity a very small diffusion coefficient is able to homogenize solute concentration in the transverse direction.

In this case, the solute slug distorts due to local velocity gradients but then recovers its shape on average (Figure 3.18). This is different from a medium with correlated heterogeneity where the distortion of the slug shape continues as shown in Figure 3.10.

Mixing in this case is similar to that in an ordered array of disks. Variations in local velocity are not very large. Even a small diffusion is able to eliminate transverse concentration discontinuities in a pore. The solute slug appears to move like a plug. The effect of convection, splitting and rejoining around sand grains is to enhance the effective diffusion coefficient and mixing during flow is "diffusion-like".

The forward solute concentration history is Gaussian in this case. Flow reversal does not have much impact on mixing and mixing is irreversible even for small diffusion coefficient of D_o=10^{-12} m^2/s.

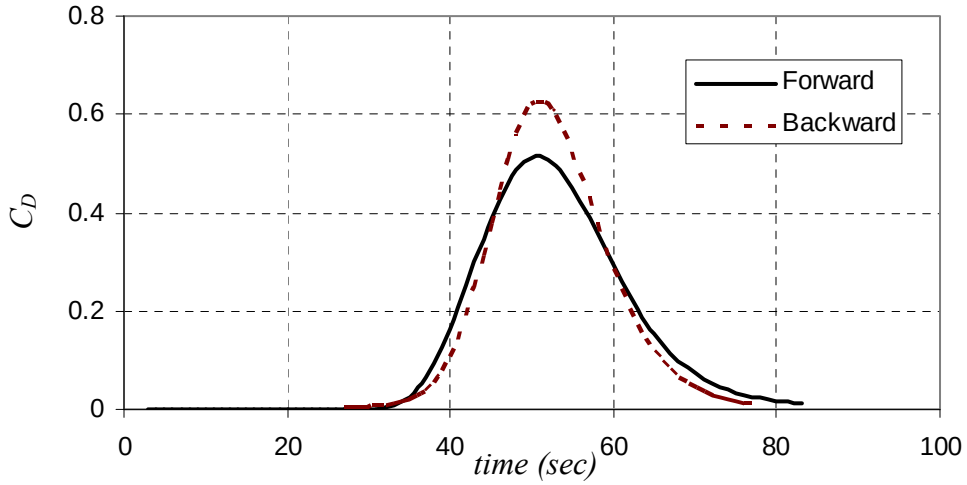

Figure 3.19: Forward and backward solute concentration histories for flow in a random pack (D_o = 10^{-12} m^2/s). Dispersion is irreversible.

3.9 COMMENT ON FLOW REVERSAL STUDIES AT FIELD SCALE

Velocity gradients in pore space and splitting of solute front around sand grains significantly enhance mixing by increasing the surface area available for diffusion. This local mixing, caused by diffusion, is irreversible. Echo dispersion which approaches zero in absence of diffusion, becomes non zero (and much larger than diffusion) when effect of diffusion is included. We show that even a small amount of diffusion is enough to cause irreversibility of mixing. Although seemingly small, diffusion can homogenize concentrations in pore space and cause mixing (dilution) of the solute slug.

As shown by Mahadevan et al. (2003) and John et al. (2008) echo dispersion at field scale is of the same order of magnitude as the forward dispersion. Mixing in pore space causes irreversibility of mixing even at the field scale. Thus it is important to include the effect of diffusion when analyzing miscible displacements in porous media.

3.10 CONCLUSIONS

- The dispersion coefficients obtained from transmission dispersion experiments have effects of convective spreading and diffusion lumped together. Flow reversal tests (echo dispersion) discriminate between convective spreading and local mixing ("true" mixing). Echo dispersion for the former case approaches zero and in the latter case equals the transmission dispersion. Fraction of irreversibility of dispersion indicates the degree of local mixing.

- Pore scale simulations show that mixing caused by diffusion is enhanced by the local velocity gradients induced by the grain arrangement and because of splitting of the solute front along sand grains.
- Purely convective spreading in absence of diffusion is reversible. It is the local mixing caused by diffusion that makes dispersion in porous media irreversible. Diffusion is the fundamental mechanism of local ("true") mixing at pore scale.
- In ordered arrangement of disks with no significant variation in flow velocity, a small amount of diffusion is enough to eliminate transverse differences in solute concentration and cause effective local mixing. Role of convection is to enhance effective diffusion coefficient. Dispersion is same as local mixing and therefore completely irreversible.
- In heterogeneous media local heterogeneity can cause wide variations in flow velocity. Convective spreading dominates solute transport and therefore dispersion is only partially irreversible. High diffusion is required to make the dispersion irreversible.

3.11 LIMITATIONS

Femlab simulations even though very insightful, suffer from the following limitations:

(i) two dimensional

(ii) unrealistically high porosity

(iii) does not run in absence of diffusion

(iv) can be compared with experimental results only qualitatively and not quantitatively

Therefore, we use solute particle tracking in a dense, random packing of spheres to explain core scale mixing quantitatively.

REFERENCES

1. Aris, R.: "Dispersion of a solute by diffusion, convection, and exchange between phases." Proc. Roy. Soc. (London) A252: 538-50, (1959).
2. FEMLAB Chemical Engineering Module Users Guide , (Oct. 2004).
3. Flekkoy, E.G., Oxaal, U., Feder, J. and Jossang, T.: "Hydrodynamic dispersion at stagnant points: simulations and experiments", Physics Review E, Volume 52, Number 5, (Nov. 1995).
4. Flekkoy, E.G., Rage, T., Oxaal, U. and Feder, J.: "Hydrodynamic irreversibility in creeping flow", Physical Review Letters, Volume 77, Number 20, (Nov. 1996).
5. Heller, J. P.: "An Unmixing Demonstration", American J Phys, 28 (4), 348-353, (1960).
6. Hiby, J. W. "Longitudinal and transverse mixing during single-phase flow through granular beds." Symposium on the interaction between fluids and particles, Institute of Chemical Engineers, London, (1962).
7. Hulin, J. P. and T. J. Plona: "Echo tracer dispersion in porous media." Physics of Fluids A: Fluid Dynamics 1(8): 1341-7, (1989).

8. Jha, R.K., Bryant, S.L., Lake, L.W. and John, A.: "Investigation of pore-scale (local) mixing**",** paper SPE - 99782 presented at SPE Improved Oil Recovery Symposium, Tulsa, Oklahoma, (Apr. 2006).
9. John, A. K., Lake, L. W., Bryant, S. L. and Jennings, J. W.: "Investigation of field scale dispersion", paper SPE - 113429 presented at SPE Improved Oil Recovery Symposium, Tulsa, Oklahoma, (Apr. 2008).
10. Mahadevan, J., Lake, L. W. and Johns, R. T.: "Estimation of true dispersivity in field-scale permeable media**",** SPE Journal, (Sep. 2003).
11. Muzzio, F.J., Swanson, P.D. and Ottino, J.M.: "Mixing distributions produced by multiplicative stretching in chaotic flows", International Journal of Bifurcation and Chaos, Volume 2, Number 1 37-50, (1992).
12. Rigord, P., Calvo, A. and Hulin, J.P.: "Transition to irreversibility for the dispersion of a tracer in porous media", Physics of Fluids, 681 (May 1990).
13. Rigord, P., Leroy, C., Charlaix, E., Baudet, C., Guyon, E. and Hulin, J.P.: "Reversible and irreversible tracer dispersion in porous media", Journal of Physics, Condens. Matter 2, (1990) , SA437-SA442.
14. Taylor, G.:"Dispersion of soluble matter in solvent flowing slowly through a tube." Proc. Roy. Soc. (London) A219: 186-203. (1953).
15. Taylor, G.I. : "*Low Reynolds Number Flows",* The National Committee for Fluid Mechanics Films. Released by Encyclopedia Britannica Educational Corp., Chicago, IL, (1972).

Chapter 4: Preparing a Physically Representative Network Model

4.1 INTRODUCTION

Direct numerical simulation for solving flow and transport through porous media is limited to very small model sizes because of intensive computational requirements. Moreover, we never have details of pore geometry at larger length scales. Therefore, for modeling flow at larger length scales a continuum approach is used where the microscopic behavior (pore-scale details) is not resolved and the fluid and matrix properties are averaged over a certain volume. The properties are assumed to be constant over this volume.

Continuum scale parameters strongly depend on the pore-scale physics. Pore-network modeling is an important tool that provides a link between continuum scale properties of a porous medium and pore scale physics. Network models are computationally much less demanding as compared to direct numerical simulation. To create a network, the pore space is discretized into an interconnected set of pores (nodes) and pore throats (bonds). By assigning hydraulic conductivities to pore throats, the flow problem can be viewed as a resistor network problem. A mass conservation equation is written for each pore in the network. It produces a set of linear equations that can be solved for hydraulic potential at individual pores. Using potential gradients across a bond and its hydraulic conductivity, the flow rate in each bond can be calculated. Thus, solving

the Navier-Stokes equation is replaced by solving a simple mass balance equation. Single-phase flow and solute transport problems can be modeled efficiently using networks of tens of thousands of pores.

Similarly, solving the convection-diffusion equation can be replaced by tracing the movement of a swarm of solute particles through a pore network. Movement of solute particles is divided into several time steps of equal duration. During each time step, the particle moves with the velocity existing at that location and then makes a random diffusive jump. By tracing paths of a swarm of particles through a network of thousands of pores, we can quantify dispersion from spatial and temporal particle statistics.

Continuum scale properties are governed by pore scale geometry and topology. However, it is very difficult to explicitly capture all the details of pore geometry. Therefore, most of the network models have to make some simplifying assumptions (Acharya et al., 2007, Bijeljic et al., 2004, Bruderer et al. 2001) such as (i) bond radii are picked randomly from an assumed distribution, (ii) all bonds have the same length, (iii) pores have some characteristic shape (e.g., circular or square cross section), and (iv) the network lattice is regular.

Most of these assumptions are found to be invalid in a dense random packing of spheres. The first geometrically characterized random packing was studied by Finney (1970). Flow path lengths calculated in a Finney pack are found to be almost uniformly distributed between zero and 0.8 sphere radii, with a few path lengths exceeding 1.0 sphere radii (Bryant et al., 1993). The assumption of a regular lattice is also invalid, since Mellor (1989) showed that the topology of the pore space network in the Finney pack is completely disordered. There has been found to be significant correlation in pore sizes,

which has an important influence on macroscopic properties of the medium. The decorrelated network (with properties randomly redistributed from the Finney pack) had permeability 78% larger than that of the original network. Neglecting correlation may fail to account for physically significant features of porous media (Bryant et al., 1993). Since dispersivity is strongly affected by correlation of pore size, it is important to test whether the assumptions of classical network models are adequate for studies of dispersion. The hypothesis of this work is that accounting for the structure of porous media more realistically will better explain core-scale mixing behavior quantitatively.

We prepared a physically representative network model of a dense random packing of spheres. It explicitly accounts for the connection of a pore with its unique set of neighbors. This model preserves the geometry and topology of the pore space as well as spatial correlation in flow properties. By tracing paths of a swarm of solute particles through this network we can evaluate mixing properties of the medium and compare results quantitatively with the experimental data reported in the literature quantitatively. Moreover, because the physically representative network is constructed entirely from a knowledge of the sphere locations, it contains no adjustable parameters. Thus if its predictions of dispersivity agree with experiments, then we have some confidence that the relevant physical phenomena have been captured.

This chapter describes a methodology to prepare a physically representative network model for a dense random packing of spheres. It also discusses an algorithm for obtaining flow rate in each bond by solving mass balance equation at each pore.

4.2 DESCRIPTION OF DENSE RANDOM PACKING OF SPHERES

A dense random packing of mono-disperse spheres is a simple yet realistic model of an unconsolidated well-sorted sand. We have spatial coordinates of a computer generated dense random packing of 5000 spheres from Thane (2006a). It is similar to the Finney pack except that it is cubic in shape whereas the Finney Pack is spherical. Therefore, we can impose linear flow in the Thane pack whereas the Finney pack is better suited for modeling spherical flow. The radius and the spatial coordinates of the center of each sphere are known. This completely specifies the geometry of the medium and completely determines the micro-structure of the medium. From this data we extract a network model that replicates the pore space preserving its geometry, topology and spatial correlation in flow properties.

The Thane pack is periodic and thus can be used as a building block to create an arbitrarily long pack of spheres. The spheres on the lower face of the pack fit exactly on the upper face. Therefore, we can stack packs of 5000 spheres one above another and create an infinitely long porous medium. Keeping computational limitations in mind, we stacked two packs of 5000 spheres above one another and created a porous medium consisting of 10000 spheres (Figure 4.1). It allows sufficient travel length for solute particles inside the medium to get representative travel time statistics and quantify dispersion.

The medium is about 34 sphere diameters long in the z-direction and 17 sphere diameters long in x as well as y direction. The radius of each sphere is 2.1918 (arbitrary units). In all the tables we show the coordinates in the arbitrary units (in which radius of each sphere is 2.1918) form for convenience of presentation. For having realistic pore

sizes in the network, the radius of the sphere is taken as 2.1918 x 10^{-4} m for calculation of flow and transport through the medium. The porosity of the pack is 36%.

4.3 DISCRETIZING THE PORE SPACE

The pore space in a pack of spheres can be hydraulically approximated as a network where the pore space is discretized into pore bodies (nodes) and pore throats (bonds). The network model consists of pores or void spaces connected by narrower constrictions or throats. Delaunay tessellation is an unambiguous way of dividing the sphere packing into cells called Delaunay cells. Delaunay tessellation groups together sets of four nearest spheres and thus a Delaunay cell in three dimensions is a tetrahedron (Figure 4.2). Each edge of the Delaunay cell (tetrahedron) represents the distance between two adjacent sphere centers.

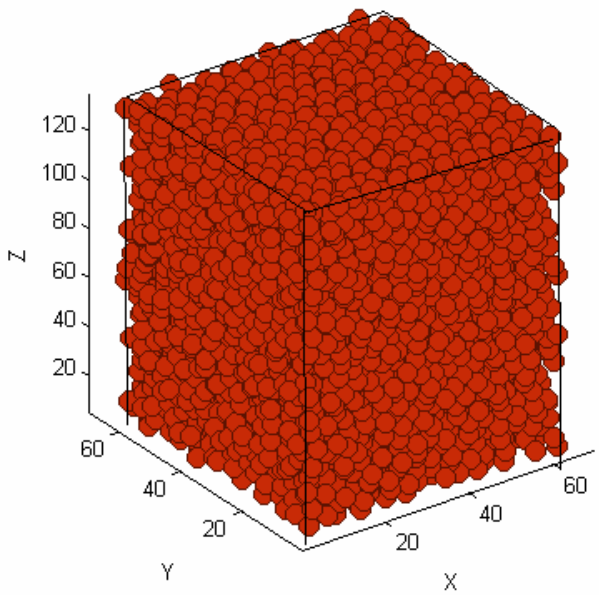

Figure 4.1: A dense random packing of 10000 spheres, formed by stacking two copies of a periodic packing of 5000 spheres.

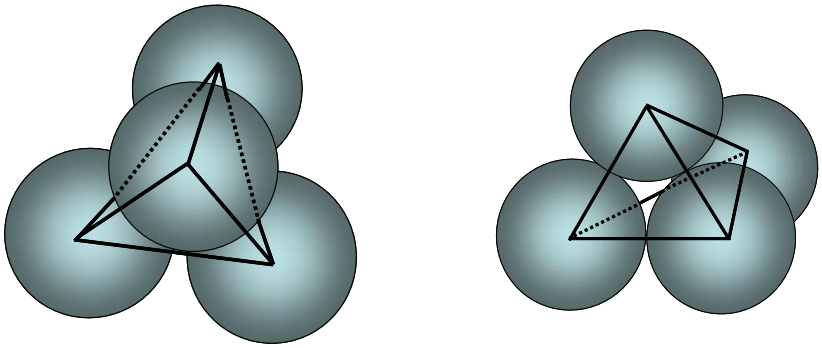

Figure 4.2: Delaunay tessellation grouping together four nearest neighboring spheres. The vertices of the tetrahedra correspond to the centers of the spheres.

The vertices of the Delaunay cells lie at sphere centers, while the interior of the cell encloses a region of void space. Each cell face is a plane of maximum constriction or maximum curvature of pore space and thus represents a narrow entrance to the wider void inside the cell. We may identify the pores with the interior of the Delaunay cells and the throats with the faces – each cell represents a pore and each cell face is a throat. Since each cell is a tetrahedron, every pore has four throats leading from it – the coordination number of the network is 4.

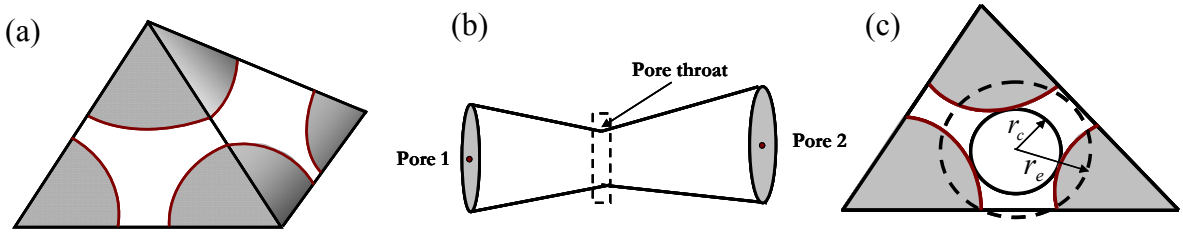

Figure 4.3: (a) A Delaunay cell having sand grains and void space. The body of the cell can be visualized as pore body. (b) A converging-diverging path connecting two neighboring pores. (c) The faces are the areas of narrowest constriction (throats) that connect the cell to neighboring cells. r_c is the radius of the largest circle that can fit in the constriction. r_e is the radius of the circle having same area as that of the void space. Arithmetic average of r_c and r_e is a good estimate of the equivalent radius of the bond that describes its hydraulic conductivity.

The built-in Matlab function *delaunay3* was used to group spheres into Delaunay cells. We specify center-coordinates of each sphere in the pack. The function reads a $3 \times n$ input matrix representing the centre coordinates of n spheres. It assigns an index to each sphere 1, 2,…, n. After grouping together the nearest neighbors, it returns a four column output matrix with each row corresponding to the indices of the spheres forming the four vertices a Delaunay cell.

Upon tessellation of a pack of 10000 spheres, we get 60680 Delaunay cells. This tessellation does not account for periodicity of the packs. Thus at the pack boundaries we get unrealistically low number of cell faces there. Therefore, we remove one layer of spheres and tessellated cells from each of the six faces of the pack. This leaves us with 34627 cells. Every cell is assigned an index.

Each Delaunay cell contains one pore body and four throats through which it is connected to its four neighbors. For preparing a physically representative network model, we need to evaluate hydraulic conductances of each bond connecting every pore with its unique set of four neighbors. First we group together the neighbors of a cell and then determine hydraulic conductances of the bonds connecting them.

4.4 GROUPING TOGETHER NEIGHBORS OF A CELL

Each Delaunay cell shares one face with each of its four neighbors. The algorithm for grouping together neighbors of a cell is illustrated below. Tables 4.1 through 4.6 illustrate the process with example calculations. For simplicity example calculations have been shown for cells 21-46 only.

1. After Delaunay tessellation in MATLAB, we get the indices of spheres forming that cell. Table 4.1 shows sphere indices forming cells 21 through 46 and the center-coordinates of those spheres. The center of the cell is taken as its geometric center, i.e. the arithmetic average of the four vertices of the tetrahedron (or the centers of the four spheres forming the cell). It ensures that center of the cell lies inside the cell.

2. Next, we group together the indices of spheres forming the four faces of all the cells. The sphere numbers of each face are sorted in ascending order (Table 4.2).

3. We put the sphere indices forming the faces of all the cells one below each another along with the cell number they belong to (Table 4.3)

4. Then we sort the columns vertically by the sphere indices (data in Table 4.3 is sorted by second column followed by third and fourth columns in ascending order). All the faces shared by two cells get aligned one below another. This is illustrated in Table 4.4 where the neighbors are grouped together and highlighted. For example, cells 45 and 46 are neighbors sharing a face formed by sphere numbers 802, 846 and 2066. Similarly, cells 44 and 46 are neighbors sharing a face formed by sphere numbers 846, 2066 and 4935.

Cell No.	Sphere Nos.				Coordinates, Sphere 1			Coordinates, Sphere 2			Coordinates, Sphere 3			Coordinates, Sphere 4			Center of the Cell		
21	4475	4284	4295	1855	58.8968	60.1982	48.7674	63.3824	60.1309	45.4674	61.4016	64.1981	47.2438	63.1137	60.0094	49.9500	61.6986	61.1342	47.8572
22	4475	951	4295	1855	58.8968	60.1982	48.7674	61.0699	63.5341	51.6083	61.4016	64.1981	47.2438	63.1137	60.0094	49.9500	61.1205	61.9850	49.3924
23	4475	951	1855	4140	58.8968	60.1982	48.7674	61.0699	63.5341	51.6083	63.1137	60.0094	49.9500	58.9248	58.4544	52.7891	60.5013	60.5490	50.7787
24	1015	1938	1916	3529	40.0078	47.3861	25.9855	37.1108	47.0927	22.7087	38.4993	51.3750	24.0672	35.9140	48.8492	26.5477	37.8830	48.6758	24.8273
25	3348	3408	4541	2543	49.9068	57.2081	44.4218	47.6752	56.0868	48.0244	46.7562	53.2780	44.1383	50.6454	53.3138	46.3799	48.7459	54.9717	45.7411
26	1545	4475	4284	4295	59.2911	61.4302	44.5789	58.8968	60.1982	48.7674	63.3824	60.1309	45.4674	61.4016	64.1981	47.2438	60.7430	61.4894	46.5144
27	1105	3348	4392	4356	53.6319	57.7872	42.1847	49.9068	57.2081	44.4218	50.6578	56.9867	39.0654	50.0324	60.5320	41.5666	51.0572	58.1285	41.8096
28	4847	3223	4599	3814	5.1223	58.9058	13.2178	9.4427	58.5490	12.5673	6.8702	60.1253	9.3871	5.3431	63.3889	11.8838	6.6946	60.2423	11.7640
29	4847	3524	3223	3814	5.1223	58.9058	13.2178	6.9725	60.6938	16.7669	9.4427	58.5490	12.5673	5.3431	63.3889	11.8838	6.7201	60.3844	13.6090
30	4847	4956	3524	3223	5.1223	58.9058	13.2178	5.2216	55.8463	16.3556	6.9725	60.6938	16.7669	9.4427	58.5490	12.5673	6.6898	58.4987	14.7269
31	1101	1721	2367	2472	28.4364	56.9203	19.5019	26.0112	58.1434	23.0599	28.1707	61.6319	21.5160	25.5012	62.1745	17.8517	27.0299	59.7175	20.4824
32	1101	1721	3241	2472	28.4364	56.9203	19.5019	26.0112	58.1434	23.0599	24.0790	56.4411	19.5122	25.5012	62.1745	17.8517	26.0070	58.4198	19.9814
33	1101	115	2367	2472	28.4364	56.9203	19.5019	30.2549	60.5363	17.8185	28.1707	61.6319	21.5160	25.5012	62.1745	17.8517	28.0908	60.3158	19.1720
34	8559	8942	9976	8999	22.3729	43.2860	110.5373	17.5739	44.3264	110.2853	20.2445	44.1850	106.8120	20.6058	47.0736	111.8592	20.1993	44.7178	109.8735
35	8862	5847	7598	5512	32.9081	28.4639	125.5690	36.8658	29.6644	127.0221	35.5847	26.8476	122.4966	36.4578	25.6002	128.6135	35.4541	27.6440	125.9253
36	5526	6268	8198	7524	17.0050	37.6766	114.8654	18.7597	37.0508	110.1613	21.1891	36.4128	114.5300	19.2270	40.8243	112.3427	19.0452	37.9911	112.9749
37	5371	8645	8112	8410	32.1148	8.7880	99.6509	35.7803	6.4327	100.1340	35.1923	6.8195	94.9626	35.8422	10.1234	97.7695	34.7324	8.0409	98.1293
38	9234	9978	7346	5470	29.2640	11.4041	108.8408	24.9213	15.5656	108.6216	27.5003	14.0737	111.8373	29.0151	15.4031	107.0625	27.6752	14.1116	109.0906
39	5069	9234	7346	5470	31.4966	15.4621	110.6758	29.2640	11.4041	108.8408	27.5003	14.0737	111.8373	29.0151	15.4031	107.0625	29.3190	14.0858	109.6041
40	9450	9978	7346	5470	27.8805	18.2624	110.4068	24.9213	15.5656	108.6216	27.5003	14.0737	111.8373	29.0151	15.4031	107.0625	27.3293	15.8262	109.4821
41	9450	5069	7346	5470	27.8805	18.2624	110.4068	31.4966	15.4621	110.6758	27.5003	14.0737	111.8373	29.0151	15.4031	107.0625	28.9731	15.8003	109.9956
42	9221	6055	5802	5770	37.6659	13.2657	114.4375	34.4763	10.4312	115.4417	37.6796	7.6261	116.4841	37.7709	9.3751	112.3937	36.8982	10.1745	114.6893
43	9221	6055	5770	5261	37.6659	13.2657	114.4375	34.4763	10.4312	115.4417	37.7709	9.3751	112.3937	34.5153	12.3871	111.5188	36.1071	11.3648	113.4479
44	846	4935	1988	2066	37.0447	11.2256	48.9042	36.7220	7.2608	50.7462	39.1029	10.8371	52.7551	40.7624	8.4165	49.4988	38.4080	9.4350	50.4761
45	802	846	2172	2066	37.6796	7.6261	46.4841	37.0447	11.2256	48.9042	40.8862	10.4936	45.6404	40.7624	8.4165	49.4988	39.0932	9.4405	47.6319
46	802	846	4935	2066	37.6796	7.6261	46.4841	37.0447	11.2256	48.9042	36.7220	7.2608	50.7462	40.7624	8.4165	49.4988	38.0522	8.6323	48.9083

Table 4.1: Sphere indices forming a cell and coordinates of sphere centers. Radius of spheres = 2.1918.

Cell No.	Cell Spheres				Face 1			Face 2			Face 3			Face 4		
21	4475	4284	4295	1855	4284	4295	4475	1855	4284	4475	1855	4295	4475	1855	4284	4295
22	4475	951	4295	1855	951	4295	4475	951	1855	4475	1855	4295	4475	951	1855	4295
23	4475	951	1855	4140	951	1855	4475	951	4140	4475	1855	4140	4475	951	1855	4140
24	1015	1938	1916	3529	1015	1916	1938	1015	1938	3529	1015	1916	3529	1916	1938	3529
25	3348	3408	4541	2543	3348	3408	4541	2543	3348	3408	2543	3348	4541	2543	3408	4541
26	1545	4475	4284	4295	1545	4284	4475	1545	4295	4475	1545	4284	4295	4284	4295	4475
27	1105	3348	4392	4356	1105	3348	4392	1105	3348	4356	1105	4356	4392	3348	4356	4392
28	4847	3223	4599	3814	3223	4599	4847	3223	3814	4847	3814	4599	4847	3223	3814	4599
29	4847	3524	3223	3814	3223	3524	4847	3524	3814	4847	3223	3814	4847	3223	3524	3814
30	4847	4956	3524	3223	3524	4847	4956	3223	4847	4956	3223	3524	4847	3223	3524	4956
31	1101	1721	2367	2472	1101	1721	2367	1101	1721	2472	1101	2367	2472	1721	2367	2472
32	1101	1721	3241	2472	1101	1721	3241	1101	1721	2472	1101	2472	3241	1721	2472	3241
33	1101	115	2367	2472	115	1101	2367	115	1101	2472	1101	2367	2472	115	2367	2472
34	8559	8942	9976	8999	8559	8942	9976	8559	8942	8999	8559	8999	9976	8942	8999	9976
35	8862	5847	7598	5512	5847	7598	8862	5512	5847	8862	5512	7598	8862	5512	5847	7598
36	5526	6268	8198	7524	5526	6268	8198	5526	6268	7524	5526	7524	8198	6268	7524	8198
37	5371	8645	8112	8410	5371	8112	8645	5371	8410	8645	5371	8112	8410	8112	8410	8645
38	9234	9978	7346	5470	7346	9234	9978	5470	9234	9978	5470	7346	9234	5470	7346	9978
39	5069	9234	7346	5470	5069	7346	9234	5069	5470	9234	5069	5470	7346	5470	7346	9234
40	9450	9978	7346	5470	7346	9450	9978	5470	9450	9978	5470	7346	9450	5470	7346	9978
41	9450	5069	7346	5470	5069	7346	9450	5069	5470	9450	5470	7346	9450	5069	5470	7346
42	9221	6055	5802	5770	5802	6055	9221	5770	6055	9221	5770	5802	9221	5770	5802	6055
43	9221	6055	5770	5261	5770	6055	9221	5261	6055	9221	5261	5770	9221	5261	5770	6055
44	846	4935	1988	2066	846	1988	4935	846	2066	4935	846	1988	2066	1988	2066	4935
45	802	846	2172	2066	802	846	2172	802	846	2066	802	2066	2172	846	2066	2172
46	802	846	4935	2066	802	846	4935	802	846	2066	802	2066	4935	846	2066	4935

Table 4.2: Sphere indices forming the four faces of a cell. The sphere indices for a face are sorted in ascending order.

Cell No.	Spheres of Face			Cell No.	Spheres of Face			Cell No.	Spheres of Face		
21	4284	4295	4475	29	3223	3524	3814	38	5470	7346	9234
21	1855	4284	4475	30	3524	4847	4956	38	5470	7346	9978
21	1855	4295	4475	30	3223	4847	4956	39	5069	7346	9234
21	1855	4284	4295	30	3223	3524	4847	39	5069	5470	9234
22	951	4295	4475	30	3223	3524	4956	39	5069	5470	7346
22	951	1855	4475	31	1101	1721	2367	39	5470	7346	9234
22	1855	4295	4475	31	1101	1721	2472	40	7346	9450	9978
22	951	1855	4295	31	1101	2367	2472	40	5470	9450	9978
23	951	1855	4475	31	1721	2367	2472	40	5470	7346	9450
23	951	4140	4475	32	1101	1721	3241	40	5470	7346	9978
23	1855	4140	4475	32	1101	1721	2472	41	5069	7346	9450
23	951	1855	4140	32	1101	2472	3241	41	5069	5470	9450
24	1015	1916	1938	32	1721	2472	3241	41	5470	7346	9450
24	1015	1938	3529	33	115	1101	2367	41	5069	5470	7346
24	1015	1916	3529	33	115	1101	2472	42	5802	6055	9221
24	1916	1938	3529	33	1101	2367	2472	42	5770	6055	9221
25	3348	3408	4541	33	115	2367	2472	42	5770	5802	9221
25	2543	3348	3408	34	8559	8942	9976	42	5770	5802	6055
25	2543	3348	4541	34	8559	8942	8999	43	5770	6055	9221
25	2543	3408	4541	34	8559	8999	9976	43	5261	6055	9221
26	1545	4284	4475	34	8942	8999	9976	43	5261	5770	9221
26	1545	4295	4475	35	5847	7598	8862	43	5261	5770	6055
26	1545	4284	4295	35	5512	5847	8862	44	846	1988	4935
26	4284	4295	4475	35	5512	7598	8862	44	846	2066	4935
27	1105	3348	4392	35	5512	5847	7598	44	846	1988	2066
27	1105	3348	4356	36	5526	6268	8198	44	1988	2066	4935
27	1105	4356	4392	36	5526	6268	7524	45	802	846	2172
27	3348	4356	4392	36	5526	7524	8198	45	802	846	2066
28	3223	4599	4847	36	6268	7524	8198	45	802	2066	2172
28	3223	3814	4847	37	5371	8112	8645	45	846	2066	2172
28	3814	4599	4847	37	5371	8410	8645	46	802	846	4935
28	3223	3814	4599	37	5371	8112	8410	46	802	846	2066
29	3223	3524	4847	37	8112	8410	8645	46	802	2066	4935
29	3524	3814	4847	38	7346	9234	9978	46	846	2066	4935
29	3223	3814	4847	38	5470	9234	9978				

Table 4.3: Sphere indices forming the four faces of a cell put one below another along with the cell number.

Cell No.	Spheres of Face			Cell No.	Spheres of Face			Cell No.	Spheres of Face		
33	115	1101	2367	26	1545	4295	4475	43	5261	5770	6055
33	115	1101	2472	31	1721	2367	2472	43	5261	5770	9221
33	115	2367	2472	32	1721	2472	3241	43	5261	6055	9221
45	802	846	2066	23	1855	4140	4475	37	5371	8112	8410
46	802	846	2066	21	1855	4284	4295	37	5371	8112	8645
45	802	846	2172	21	1855	4284	4475	37	5371	8410	8645
46	802	846	4935	21	1855	4295	4475	38	5470	7346	9234
45	802	2066	2172	22	1855	4295	4475	39	5470	7346	9234
46	802	2066	4935	24	1916	1938	3529	40	5470	7346	9450
44	846	1988	2066	44	1988	2066	4935	41	5470	7346	9450
44	846	1988	4935	25	2543	3348	3408	38	5470	7346	9978
45	846	2066	2172	25	2543	3348	4541	40	5470	7346	9978
44	846	2066	4935	25	2543	3408	4541	38	5470	9234	9978
46	846	2066	4935	29	3223	3524	3814	40	5470	9450	9978
23	951	1855	4140	29	3223	3524	4847	35	5512	5847	7598
22	951	1855	4295	30	3223	3524	4847	35	5512	5847	8862
22	951	1855	4475	30	3223	3524	4956	35	5512	7598	8862
23	951	1855	4475	28	3223	3814	4599	36	5526	6268	7524
23	951	4140	4475	28	3223	3814	4847	36	5526	6268	8198
22	951	4295	4475	29	3223	3814	4847	36	5526	7524	8198
24	1015	1916	1938	28	3223	4599	4847	42	5770	5802	6055
24	1015	1916	3529	30	3223	4847	4956	42	5770	5802	9221
24	1015	1938	3529	25	3348	3408	4541	42	5770	6055	9221
31	1101	1721	2367	27	3348	4356	4392	43	5770	6055	9221
31	1101	1721	2472	29	3524	3814	4847	42	5802	6055	9221
32	1101	1721	2472	30	3524	4847	4956	35	5847	7598	8862
32	1101	1721	3241	28	3814	4599	4847	36	6268	7524	8198
31	1101	2367	2472	21	4284	4295	4475	38	7346	9234	9978
33	1101	2367	2472	26	4284	4295	4475	40	7346	9450	9978
32	1101	2472	3241	39	5069	5470	7346	37	8112	8410	8645
27	1105	3348	4356	41	5069	5470	7346	34	8559	8942	8999
27	1105	3348	4392	39	5069	5470	9234	34	8559	8942	9976
27	1105	4356	4392	41	5069	5470	9450	34	8559	8999	9976
26	1545	4284	4295	39	5069	7346	9234	34	8942	8999	9976
26	1545	4284	4475	41	5069	7346	9450				

Table 4.4: Sphere indices vertically sorted in ascending order. The neighbors sharing a face (highlighted) are lined up one below another.

4.5 CALCULATING BOND CONDUCTANCE CONNECTING TWO NEIGHBORS

Approximate single phase flow properties of a bond connecting two neighboring pores can be calculated using an approach suggested by Bryant et al. (1993).

The converging-diverging flow path between two pores may be represented by an equivalent cylinder of radius r_{eff} that has the same conductivity as the actual path. The conductivity of the converging diverging flow path is dominated by the narrowest constriction along the path, which occurs at the face shared by the cells. As illustrated in the Figure 4.3 r_c is the largest circle that can be inscribed in the narrowest constriction (cell face). The figure also shows r_e, the radius of the circle having the same area as the narrowest constriction. r_c underestimates the equivalent tube radius since it does not consider the entire cross sectional area available for flow. On the other hand, r_e is an overestimate, since for a fixed area a circle is the most efficient cross section for fluid flow. It is found that the average of r_c and r_e, $r_{eff} = (r_e + r_c)/2$, is a good estimate of the effective radius (Bryant et al., 1993).

The conductivity of the bond connecting two neighboring pores can then be determined by

$$g = \frac{\pi r_{eff}^{4}}{8\mu l},$$

where μ is the fluid viscosity and *l* is the distance between two pore (cell) centers.

Calculation of Throat Radius, r_c

To calculate the radius of the largest inscribed circle in the pore throat, first we find the center of the face (the point equidistant from all the vertices of the face or circum-center of the throat).

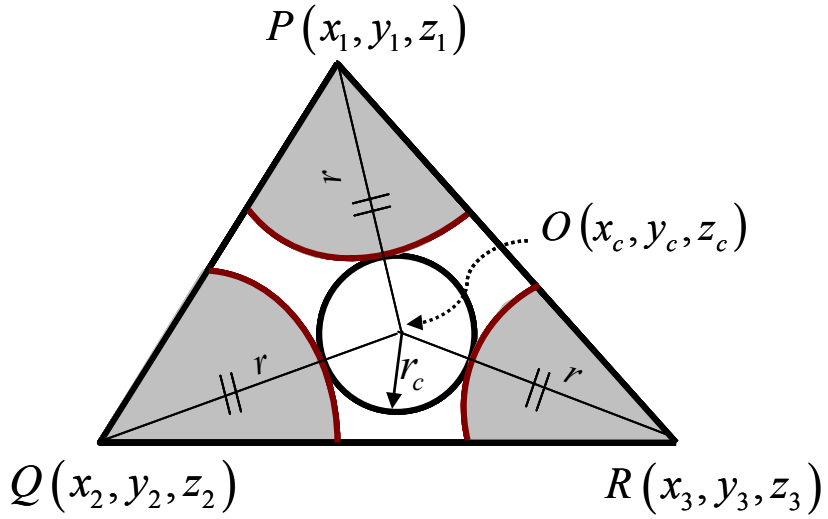

Figure 4.4: Throat radius on a face of a Delaunay cell.

Let *O* denote the circum center of the face. *P, Q* and *R* are the three vertices of the triangle. If *r* be the circum radius of the triangle,

$OP = OQ = OR = r$.

We need to find the coordinates of the circum-center $O(x_c, y_c, z_c)$. We need three equations to find the three unknowns.

The first equation comes from the fact that *OP=OQ*.

$$(x_1 - x_c)^2 + (y_1 - y_c)^2 + (z_1 - z_c)^2 = (x_2 - x_c)^2 + (y_2 - y_c)^2 + (z_2 - z_c)^2 .$$

Expanding and simplifying,

$$\begin{aligned} x_1^2 + x_c^2 - 2x_1x_c \quad & \quad x_2^2 + x_c^2 - 2x_2x_c \\ + y_1^2 + y_c^2 - 2y_1y_c \quad & = \quad + y_2^2 + y_c^2 - 2y_2y_c \\ + z_1^2 + z_c^2 - 2z_1z_c \quad & \quad + z_2^2 + z_c^2 - 2z_2z_c \,. \end{aligned}$$

Rearranging,

$$(x_1 - x_2)x_c + (y_1 - y_2)y_c + (z_1 - z_2)z_c = \frac{1}{2}\left[\left(x_1^2 - x_2^2\right) + \left(y_1^2 - y_2^2\right) + \left(z_1^2 - z_2^2\right)\right] \text{ --------(4.5.1).}$$

Similarly using *OQ=OR* we obtain the second equation,

$$(x_2 - x_3)x_c + (y_2 - y_3)y_c + (z_2 - z_3)z_c = \frac{1}{2}\left[\left(x_2^2 - x_3^2\right) + \left(y_2^2 - y_3^2\right) + \left(z_2^2 - z_3^2\right)\right] \text{ --------(4.5.2).}$$

However, we cannot use *OR=OP* to obtain the third equation as this will not be independent of the first two equations.

We use the equation of the plane of the face to find the third equation. The standard equation of a plane in 3 D space is

$Ax + By + Cz = D$.

The vector *(A, B, C)* is a normal to the plane. For a plane passing through the points (x_1, y_1, z_1), (x_2, y_2, z_2) and (x_3, y_3, z_3)

$$A = \begin{vmatrix} 1 & y_1 & z_1 \\ 1 & y_2 & z_2 \\ 1 & y_3 & z_3 \end{vmatrix} \qquad B = \begin{vmatrix} x_1 & 1 & z_1 \\ x_2 & 1 & z_2 \\ x_3 & 1 & z_3 \end{vmatrix} \qquad C = \begin{vmatrix} x_1 & y_1 & 1 \\ x_2 & y_2 & 1 \\ x_3 & y_3 & 1 \end{vmatrix} \quad \text{and } D = \begin{vmatrix} x_1 & y_1 & z_1 \\ x_2 & y_2 & z_2 \\ x_3 & y_3 & z_3 \end{vmatrix}.$$

Since this plane passes through the point $O(x_c, y_c, z_c)$, we have

$Ax_c + By_c + Cz_c = D$ --------(4.5.3).

Arranging the three equations 4.5.1-4.5.3 in matrix form,

$$\begin{bmatrix} (x_1 - x_2) & (y_1 - y_2) & (z_1 - z_2) \\ (x_2 - x_3) & (y_2 - y_3) & (z_2 - z_3) \\ A & B & C \end{bmatrix} \begin{bmatrix} x_c \\ y_c \\ z_c \end{bmatrix} = \begin{bmatrix} \frac{1}{2}\left\{\left(x_1^2 - x_2^2\right) + \left(y_1^2 - y_2^2\right) + \left(z_1^2 - z_2^2\right)\right\} \\ \frac{1}{2}\left\{\left(x_2^2 - x_3^2\right) + \left(y_2^2 - y_3^2\right) + \left(z_2^2 - z_3^2\right)\right\} \\ D \end{bmatrix}.$$

Solving this matrix we get the coordinates of the circum-center. Circum-radius of the face

$$r = \sqrt{(x_1 - x_c)^2 + (y_1 - y_c)^2 + (z_1 - z_c)^2}\ .$$

The radius of the largest circle to fit in the throat

$r_c = r - R_{sph}$, where R_{sph} is the radius of spheres.

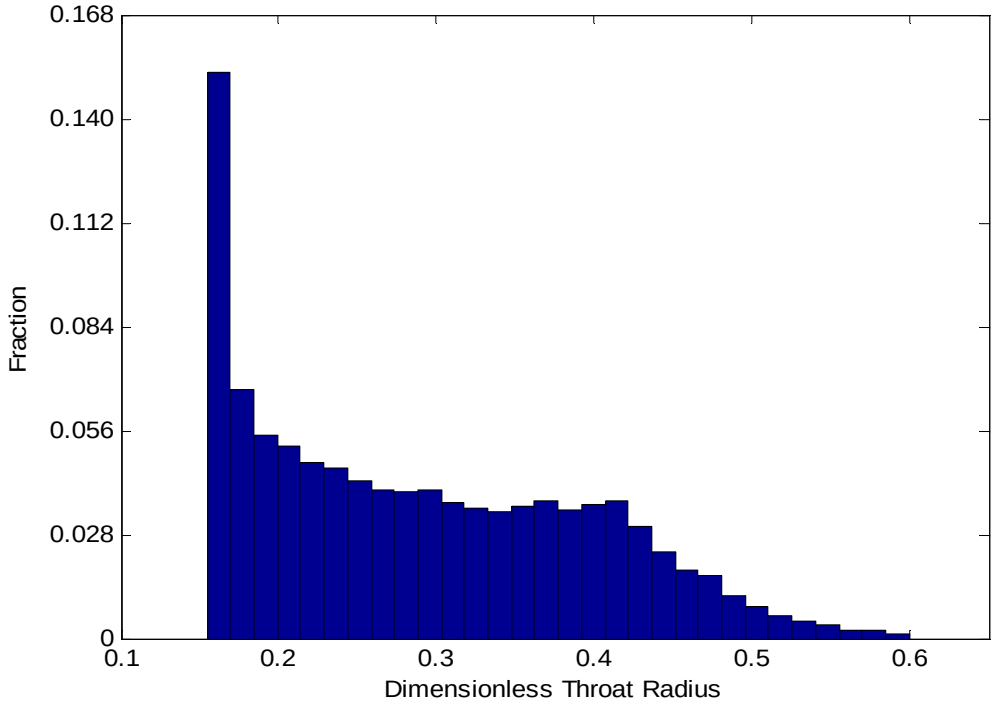

Figure 4.5: Histogram of throat radii in a sphere pack.

Figure 4.5 shows distribution of throat radii in the network. All throat radii have been normalized by the sphere radius. We can see a large number of throats having radius close to 0.15 sphere radius. This is expected to happen when three spheres are in contact with each other.

Calculation of Void Radius, r_e

r_e is radius of the circle having area equal to that of void space on the face

$r_e = \sqrt{A_{void} / \pi}$.

We calculate the lengths of the three sides of the triangular face:

$$p = \sqrt{(x_2 - x_3)^2 + (y_2 - y_3)^2 + (z_2 - z_3)^2}$$

$$q = \sqrt{(x_3 - x_1)^2 + (y_3 - y_1)^2 + (z_3 - z_1)^2}$$

$$r' = \sqrt{(x_1 - x_2)^2 + (y_1 - y_2)^2 + (z_1 - z_2)^2} .$$

The half perimeter of the triangle

$$s = \frac{p + q + r'}{2}$$

and area of the triangular face

$A_{face} = \sqrt{s(s-p)(s-q)(s-r')}$.

Area of the void open to fluid flow in the face

$A_{void} = A_{face} - Area\ occupied\ by\ solid$.

The areas occupied by solid in a face are circular sections. The area occupied by solid will be the sum of the areas of the three circular sections occupied by the three spheres.

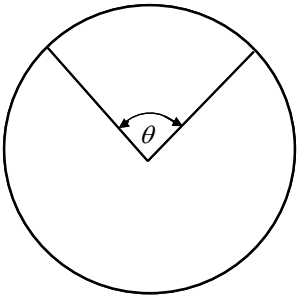

Area of a section of a circle = $\frac{1}{2}R^2\theta$.

Total area occupied by the three grains = $\frac{1}{2}R^2(\theta_1+\theta_2+\theta_3)$

where θ_1, θ_2 and θ_3 are the vertex angles of the triangle. Since

$\theta_1+\theta_2+\theta_3=\pi$,

total area occupied by the three grains $=\frac{1}{2}\pi R_{sph}^2$.

$A_{void}=A_{face}-\frac{1}{2}\pi R_{sph}^2$.

Equivalent radius of curvature

$r_e=\sqrt{A_{void}/\pi}$.

Equivalent radius of the bond connecting two neighbors

$r_{eff}=\frac{r_e+r_c}{2}$.

Distribution of effective bond radii over the network is shown in Figure 4.6.

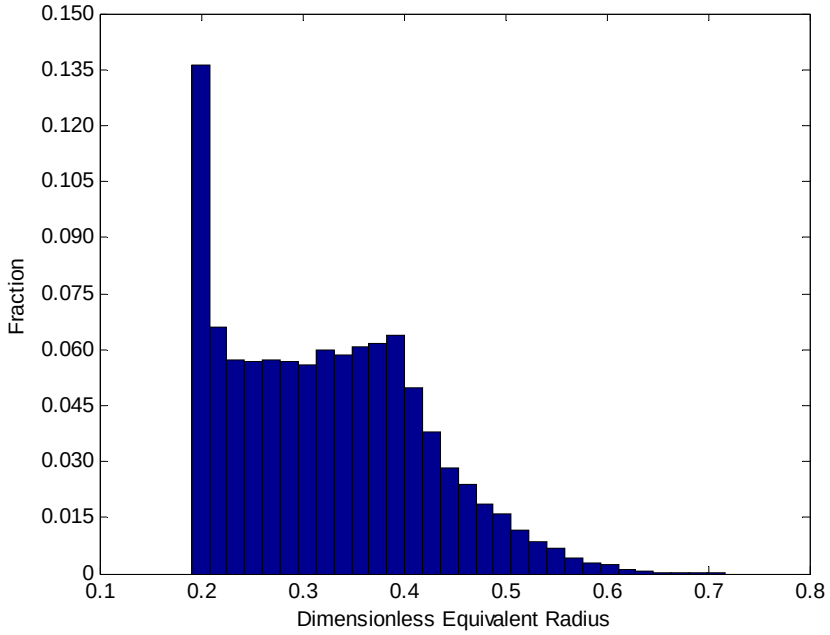

Figure 4.6: Histogram of equivalent bond radii in a sphere pack.

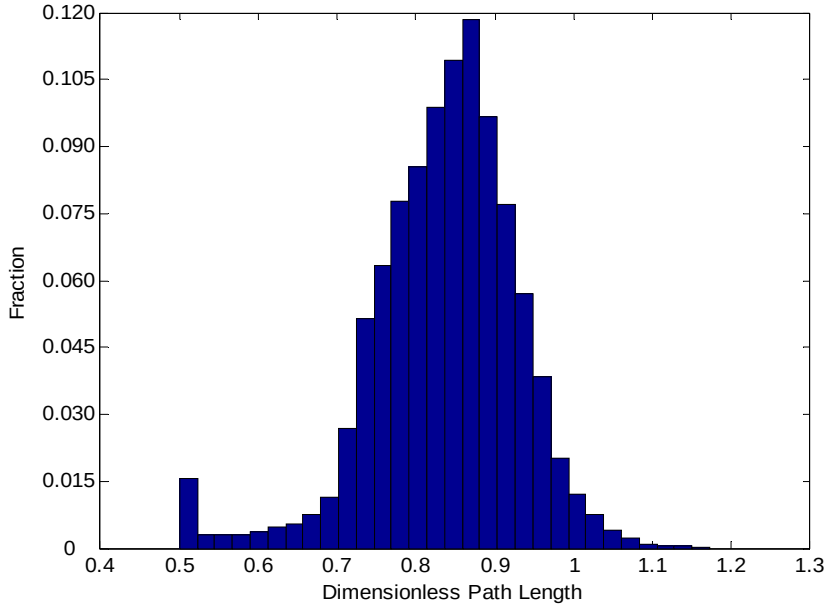

Figure 4.7: Histogram of path lengths in a sphere pack.

Figure 4.7 shows distribution of path lengths in the network. It is seen that most of the path lengths range between 0.7 and 1 sphere radius.

After finding equivalent bond radii and bond lengths, bond conductivity can be calculated using $g = \frac{\pi r_{eff}^4}{8 \mu l}$ where l is the distance between two pores.

Table 4.5 shows calculation of bond conductance connecting two neighbors. The table shows the sphere coordinates in dimensionless form. However, the conductance is shown in SI units of $m^3/s/Pa$. We have to apply a unit conversion factor of 10^{-9} to the dimensionless conductance to get the corresponding value in SI units. The viscosity of the fluid is taken as 1 *cp* or 10^{-3} *Pa-s*.

Cell No.	Coordinates, Sphere 1			Coordinates, Sphere 2			Coordinates, Sphere 3			rc	re	Req	Cell Center			l	g, m3/s/Pa
33	30.2549	60.5363	17.8185	28.4364	56.9203	19.5019	28.1707	61.6319	21.5160	0.5113	0.7076	0.6095	28.0908	60.3158	19.1720		
33	30.2549	60.5363	17.8185	28.4364	56.9203	19.5019	25.5012	62.1745	17.8517	0.9536	1.0383	0.9960	28.0908	60.3158	19.1720		
33	30.2549	60.5363	17.8185	28.1707	61.6319	21.5160	25.5012	62.1745	17.8517	0.5135	0.7473	0.6304	28.0908	60.3158	19.1720		
45	37.6796	7.6261	46.4841	37.0447	11.2256	48.9042	40.7624	8.4165	49.4988	0.4041	0.6043	0.5042	39.0932	9.4405	47.6319	1.8347	1.383E-11
46	37.6796	7.6261	46.4841	37.0447	11.2256	48.9042	40.7624	8.4165	49.4988	0.4041	0.6043	0.5042	38.0522	8.6323	48.9083		
45	37.6796	7.6261	46.4841	37.0447	11.2256	48.9042	40.8862	10.4936	45.6404	0.5011	0.7003	0.6007	39.0932	9.4405	47.6319		
46	37.6796	7.6261	46.4841	37.0447	11.2256	48.9042	36.7220	7.2608	50.7462	0.3391	0.4966	0.4179	38.0522	8.6323	48.9083		
45	37.6796	7.6261	46.4841	40.7624	8.4165	49.4988	40.8862	10.4936	45.6404	0.3391	0.4967	0.4179	39.0932	9.4405	47.6319		
46	37.6796	7.6261	46.4841	40.7624	8.4165	49.4988	36.7220	7.2608	50.7462	0.3391	0.4966	0.4179	38.0522	8.6323	48.9083		
44	37.0447	11.2256	48.9042	39.1029	10.8371	52.7551	40.7624	8.4165	49.4988	0.4041	0.6043	0.5042	38.4080	9.4350	50.4761		
44	37.0447	11.2256	48.9042	39.1029	10.8371	52.7551	36.7220	7.2608	50.7462	0.4143	0.6173	0.5158	38.4080	9.4350	50.4761		
45	37.0447	11.2256	48.9042	40.7624	8.4165	49.4988	40.8862	10.4936	45.6404	0.5524	0.7998	0.6761	39.0932	9.4405	47.6319		
44	37.0447	11.2256	48.9042	40.7624	8.4165	49.4988	36.7220	7.2608	50.7462	0.4041	0.6043	0.5042	38.4080	9.4350	50.4761	1.7969	1.412E-11
46	37.0447	11.2256	48.9042	40.7624	8.4165	49.4988	36.7220	7.2608	50.7462	0.4041	0.6043	0.5042	38.0522	8.6323	48.9083		
23	61.0699	63.5341	51.6083	63.1137	60.0094	49.9500	58.9248	58.4544	52.7891	0.8000	1.0445	0.9223	60.5013	60.5490	50.7787		
22	61.0699	63.5341	51.6083	63.1137	60.0094	49.9500	61.4016	64.1981	47.2438	0.5596	0.7535	0.6566	61.1205	61.9850	49.3924		
22	61.0699	63.5341	51.6083	63.1137	60.0094	49.9500	58.8968	60.1982	48.7674	0.4517	0.6612	0.5565	61.1205	61.9850	49.3924	2.0898	1.802E-11
23	61.0699	63.5341	51.6083	63.1137	60.0094	49.9500	58.8968	60.1982	48.7674	0.4517	0.6612	0.5565	60.5013	60.5490	50.7787		
23	61.0699	63.5341	51.6083	58.9248	58.4544	52.7891	58.8968	60.1982	48.7674	0.7318	0.9428	0.8373	60.5013	60.5490	50.7787		
22	61.0699	63.5341	51.6083	61.4016	64.1981	47.2438	58.8968	60.1982	48.7674	0.5651	0.8353	0.7002	61.1205	61.9850	49.3924		
24	40.0078	47.3861	25.9855	38.4993	51.3750	24.0672	37.1108	47.0927	22.7087	0.4604	0.7001	0.5803	37.8830	48.6758	24.8273		
24	40.0078	47.3861	25.9855	38.4993	51.3750	24.0672	35.9140	48.8492	26.5477	0.3994	0.5980	0.4987	37.8830	48.6758	24.8273		
24	40.0078	47.3861	25.9855	37.1108	47.0927	22.7087	35.9140	48.8492	26.5477	0.3399	0.4984	0.4192	37.8830	48.6758	24.8273		
31	28.4364	56.9203	19.5019	26.0112	58.1434	23.0599	28.1707	61.6319	21.5160	0.5253	0.7394	0.6324	27.0299	59.7175	20.4824		
31	28.4364	56.9203	19.5019	26.0112	58.1434	23.0599	25.5012	62.1745	17.8517	1.2432	1.3685	1.3059	27.0299	59.7175	20.4824	1.7267	6.613E-10
32	28.4364	56.9203	19.5019	26.0112	58.1434	23.0599	25.5012	62.1745	17.8517	1.2432	1.3685	1.3059	26.0070	58.4198	19.9814		

Table 4.5.1: Calculation of conductance of bonds connecting two cells.

Cell No.	Coordinate, Sphere 1			Coordinate, Sphere 2			Coordinate, Sphere 3			rc	re	Req	Cell Center			l	g, m3/s/Pa
32	28.4364	56.9203	19.5019	26.0112	58.1434	23.0599	24.0790	56.4411	19.5122	0.3573	0.5323	0.4448	26.0070	58.4198	19.9814		
31	28.4364	56.9203	19.5019	28.1707	61.6319	21.5160	25.5012	62.1745	17.8517	0.9778	1.1263	1.0521	27.0299	59.7175	20.4824	1.7890	2.689E-10
33	28.4364	56.9203	19.5019	28.1707	61.6319	21.5160	25.5012	62.1745	17.8517	0.9778	1.1263	1.0521	28.0908	60.3158	19.1720		
32	28.4364	56.9203	19.5019	25.5012	62.1745	17.8517	24.0790	56.4411	19.5122	1.1176	1.2785	1.1981	26.0070	58.4198	19.9814		
27	53.6319	57.7872	42.1847	49.9068	57.2081	44.4218	50.0324	60.5320	41.5666	0.3763	0.5643	0.4703	51.0572	58.1285	41.8096		
27	53.6319	57.7872	42.1847	49.9068	57.2081	44.4218	50.6578	56.9867	39.0654	0.5946	0.7542	0.6744	51.0572	58.1285	41.8096		
27	53.6319	57.7872	42.1847	50.0324	60.5320	41.5666	50.6578	56.9867	39.0654	0.3762	0.5643	0.4703	51.0572	58.1285	41.8096		
26	59.2911	61.4302	44.5789	63.3824	60.1309	45.4674	61.4016	64.1981	47.2438	0.4417	0.6482	0.5450	60.7430	61.4894	46.5144		
26	59.2911	61.4302	44.5789	63.3824	60.1309	45.4674	58.8968	60.1982	48.7674	0.6461	0.7739	0.7100	60.7430	61.4894	46.5144		
26	59.2911	61.4302	44.5789	61.4016	64.1981	47.2438	58.8968	60.1982	48.7674	0.4661	0.6718	0.5690	60.7430	61.4894	46.5144		
31	26.0112	58.1434	23.0599	28.1707	61.6319	21.5160	25.5012	62.1745	17.8517	1.1243	0.8780	1.0012	27.0299	59.7175	20.4824		
32	26.0112	58.1434	23.0599	25.5012	62.1745	17.8517	24.0790	56.4411	19.5122	1.2158	1.3220	1.2689	26.0070	58.4198	19.9814		
23	63.1137	60.0094	49.9500	58.9248	58.4544	52.7891	58.8968	60.1982	48.7674	0.5579	0.7363	0.6471	60.5013	60.5490	50.7787		
21	63.1137	60.0094	49.9500	63.3824	60.1309	45.4674	61.4016	64.1981	47.2438	0.6416	0.9117	0.7767	61.6986	61.1341	47.8572		
21	63.1137	60.0094	49.9500	63.3824	60.1309	45.4674	58.8968	60.1982	48.7674	0.6580	0.8126	0.7353	61.6986	61.1341	47.8572		
21	63.1137	60.0094	49.9500	61.4016	64.1981	47.2438	58.8968	60.1982	48.7674	0.6437	0.9027	0.7732	61.6986	61.1341	47.8572	1.8480	7.595E-11
22	63.1137	60.0094	49.9500	61.4016	64.1981	47.2438	58.8968	60.1982	48.7674	0.6437	0.9027	0.7732	61.1205	61.9850	49.3924		
24	38.4993	51.3750	24.0672	37.1108	47.0927	22.7087	35.9140	48.8492	26.5477	0.4059	0.6074	0.5067	37.8830	48.6758	24.8273		
44	39.1029	10.8371	52.7551	40.7624	8.4165	49.4988	36.7220	7.2608	50.7462	0.4143	0.6173	0.5158	38.4080	9.4350	50.4761		
25	50.6454	53.3138	46.3799	49.9068	57.2081	44.4218	47.6752	56.0868	48.0244	0.3463	0.5114	0.4289	48.7459	54.9717	45.7411		
25	50.6454	53.3138	46.3799	49.9068	57.2081	44.4218	46.7562	53.2780	44.1383	0.5107	0.7391	0.6249	48.7459	54.9717	45.7411		
25	50.6454	53.3138	46.3799	47.6752	56.0868	48.0244	46.7562	53.2780	44.1383	0.4649	0.6897	0.5773	48.7459	54.9717	45.7411		
29	9.4427	58.5490	12.5673	6.9725	60.6938	16.7669	5.3431	63.3889	11.8838	1.2079	1.4890	1.3485	6.7201	60.3844	13.6090		
29	9.4427	58.5490	12.5673	6.9725	60.6938	16.7669	5.1223	58.9058	13.2178	0.5667	0.7410	0.6539	6.7201	60.3844	13.6090	2.1924	3.274E-11
30	9.4427	58.5490	12.5673	6.9725	60.6938	16.7669	5.1223	58.9058	13.2178	0.5667	0.7410	0.6539	6.6898	58.4987	14.7269		
30	9.4427	58.5490	12.5673	6.9725	60.6938	16.7669	5.2216	55.8463	16.3556	1.0838	1.3413	1.2126	6.6898	58.4987	14.7269		

Table 4.5.2: Calculation of conductance of bonds connecting two cells.

Cell No.	Coordinate, Sphere 1			Coordinate, Sphere 2			Coordinate, Sphere 3			rc	re	Req	Cell Center			l	g, m3/s/Pa
28	9.4427	58.5490	12.5673	5.3431	63.3889	11.8838	6.8702	60.1253	9.3871	1.0035	0.8069	0.9052	6.6946	60.2423	11.7640		
28	9.4427	58.5490	12.5673	5.3431	63.3889	11.8838	5.1223	58.9058	13.2178	0.9982	0.9299	0.9641	6.6946	60.2423	11.7640	1.8506	1.833E-10
29	9.4427	58.5490	12.5673	5.3431	63.3889	11.8838	5.1223	58.9058	13.2178	0.9982	0.9299	0.9641	6.7201	60.3844	13.6090		
28	9.4427	58.5490	12.5673	6.8702	60.1253	9.3871	5.1223	58.9058	13.2178	0.3391	0.4966	0.4179	6.6946	60.2423	11.7640		
30	9.4427	58.5490	12.5673	5.1223	58.9058	13.2178	5.2216	55.8463	16.3556	0.9507	0.8095	0.8801	6.6898	58.4987	14.7269		
25	49.9068	57.2081	44.4218	47.6752	56.0868	48.0244	46.7562	53.2780	44.1383	0.5755	0.8384	0.7070	48.7459	54.9717	45.7411		
27	49.9068	57.2081	44.4218	50.0324	60.5320	41.5666	50.6578	56.9867	39.0654	0.5946	0.7542	0.6744	51.0572	58.1285	41.8096		
29	6.9725	60.6938	16.7669	5.3431	63.3889	11.8838	5.1223	58.9058	13.2178	0.7616	0.9010	0.8313	6.7201	60.3844	13.6090		
30	6.9725	60.6938	16.7669	5.1223	58.9058	13.2178	5.2216	55.8463	16.3556	0.5222	0.7150	0.6186	6.6898	58.4987	14.7269		
28	5.3431	63.3889	11.8838	6.8702	60.1253	9.3871	5.1223	58.9058	13.2178	0.4008	0.6000	0.5004	6.6946	60.2423	11.7640		
21	63.3824	60.1309	45.4674	61.4016	64.1981	47.2438	58.8968	60.1982	48.7674	0.7890	1.0870	0.9380	61.6986	61.1341	47.8572	1.6860	1.803E-10
26	63.3824	60.1309	45.4674	61.4016	64.1981	47.2438	58.8968	60.1982	48.7674	0.7890	1.0870	0.9380	60.7430	61.4894	46.5144		
39	31.4966	15.4621	110.6758	29.0151	15.4031	107.0625	27.5003	14.0737	111.8373	0.5262	0.7185	0.6224	29.3190	14.0858	109.6041	1.7923	3.287E-11
41	31.4966	15.4621	110.6758	29.0151	15.4031	107.0625	27.5003	14.0737	111.8373	0.5262	0.7185	0.6224	28.9731	15.8003	109.9956		
39	31.4966	15.4621	110.6758	29.0151	15.4031	107.0625	29.2640	11.4041	108.8408	0.4719	0.6769	0.5744	29.3190	14.0858	109.6041		
41	31.4966	15.4621	110.6758	29.0151	15.4031	107.0625	27.8805	18.2624	110.4068	0.4094	0.6244	0.5169	28.9731	15.8003	109.9956		
39	31.4966	15.4621	110.6758	27.5003	14.0737	111.8373	29.2640	11.4041	108.8408	0.4724	0.6781	0.5753	29.3190	14.0858	109.6041		
41	31.4966	15.4621	110.6758	27.5003	14.0737	111.8373	27.8805	18.2624	110.4068	0.3905	0.5914	0.4910	28.9731	15.8003	109.9956		
43	34.5153	12.3871	111.5188	37.7709	9.3751	112.3937	34.4763	10.4312	115.4417	0.4108	0.6259	0.5184	36.1071	11.3648	113.4479		
43	34.5153	12.3871	111.5188	37.7709	9.3751	112.3937	37.6659	13.2657	114.4375	0.3686	0.5528	0.4607	36.1071	11.3648	113.4479		
43	34.5153	12.3871	111.5188	34.4763	10.4312	115.4417	37.6659	13.2657	114.4375	0.3391	0.4967	0.4179	36.1071	11.3648	113.4479		
37	32.1148	8.7880	99.6509	35.1923	6.8195	94.9626	35.8422	10.1234	97.7695	0.7897	0.8040	0.7969	34.7324	8.0409	98.1292		
37	32.1148	8.7880	99.6509	35.1923	6.8195	94.9626	35.7803	6.4327	100.1340	0.8720	1.0630	0.9675	34.7324	8.0409	98.1292		
37	32.1148	8.7880	99.6509	35.8422	10.1234	97.7695	35.7803	6.4327	100.1340	0.3391	0.4966	0.4179	34.7324	8.0409	98.1292		
38	29.0151	15.4031	107.0625	27.5003	14.0737	111.8373	29.2640	11.4041	108.8408	0.5257	0.7173	0.6215	27.6752	14.1116	109.0906	1.7223	3.402E-11
39	29.0151	15.4031	107.0625	27.5003	14.0737	111.8373	29.2640	11.4041	108.8408	0.5257	0.7173	0.6215	29.3190	14.0858	109.6041		

Table 4.5.3: Calculation of conductance of bonds connecting two cells.

Cell No.	Coordinate, Sphere 1			Coordinate, Sphere 2			Coordinate, Sphere 3			rc	re	Req	Cell Center			l	g, m3/s/Pa
40	29.0151	15.4031	107.0625	27.5003	14.0737	111.8373	27.8805	18.2624	110.4068	0.5584	0.7907	0.6746	27.3293	15.8262	109.4821	1.7223	4.721E-11
41	29.0151	15.4031	107.0625	27.5003	14.0737	111.8373	27.8805	18.2624	110.4068	0.5584	0.7907	0.6746	28.9731	15.8003	109.9956		
38	29.0151	15.4031	107.0625	27.5003	14.0737	111.8373	24.9213	15.5656	108.6216	0.5257	0.7173	0.6215	27.6752	14.1116	109.0906	1.7924	3.269E-11
40	29.0151	15.4031	107.0625	27.5003	14.0737	111.8373	24.9213	15.5656	108.6216	0.5257	0.7173	0.6215	27.3293	15.8262	109.4821		
38	29.0151	15.4031	107.0625	29.2640	11.4041	108.8408	24.9213	15.5656	108.6216	0.8225	0.8071	0.8148	27.6752	14.1116	109.0906		
40	29.0151	15.4031	107.0625	27.8805	18.2624	110.4068	24.9213	15.5656	108.6216	0.3711	0.5561	0.4636	27.3293	15.8262	109.4821		
35	36.4578	25.6002	128.6135	36.8658	29.6644	127.0221	35.5847	26.8476	122.4966	1.0239	1.1606	1.0923	35.4541	27.6440	125.9253		
35	36.4578	25.6002	128.6135	36.8658	29.6644	127.0221	32.9081	28.4639	125.5690	0.6173	0.7636	0.6905	35.4541	27.6440	125.9253		
35	36.4578	25.6002	128.6135	35.5847	26.8476	122.4966	32.9081	28.4639	125.5690	1.0241	1.1608	1.0925	35.4541	27.6440	125.9253		
36	17.0050	37.6766	114.8654	18.7597	37.0508	110.1613	19.2270	40.8243	112.3427	0.5280	0.7659	0.6470	19.0452	37.9911	112.9749		
36	17.0050	37.6766	114.8654	18.7597	37.0508	110.1613	21.1891	36.4128	114.5300	0.6107	0.8784	0.7446	19.0452	37.9911	112.9749		
36	17.0050	37.6766	114.8654	19.2270	40.8243	112.3427	21.1891	36.4128	114.5300	0.5914	0.8109	0.7012	19.0452	37.9911	112.9749		
42	37.7709	9.3751	112.3937	37.6796	7.6261	116.4841	34.4763	10.4312	115.4417	0.3973	0.6018	0.4996	36.8982	10.1745	114.6892		
42	37.7709	9.3751	112.3937	37.6796	7.6261	116.4841	37.6659	13.2657	114.4375	0.8176	0.8374	0.8275	36.8982	10.1745	114.6892		
42	37.7709	9.3751	112.3937	34.4763	10.4312	115.4417	37.6659	13.2657	114.4375	0.3874	0.5826	0.4850	36.8982	10.1745	114.6892	1.8930	1.148E-11
43	37.7709	9.3751	112.3937	34.4763	10.4312	115.4417	37.6659	13.2657	114.4375	0.3874	0.5826	0.4850	36.1071	11.3648	113.4479		
42	37.6796	7.6261	116.4841	34.4763	10.4312	115.4417	37.6659	13.2657	114.4375	0.8140	0.8064	0.8102	36.8982	10.1745	114.6892		
35	36.8658	29.6644	127.0221	35.5847	26.8476	122.4966	32.9081	28.4639	125.5690	0.6169	0.7634	0.6902	35.4541	27.6440	125.9253		
36	18.7597	37.0508	110.1613	19.2270	40.8243	112.3427	21.1891	36.4128	114.5300	0.6656	0.9268	0.7962	19.0452	37.9911	112.9749		
38	27.5003	14.0737	111.8373	29.2640	11.4041	108.8408	24.9213	15.5656	108.6216	0.8226	0.8071	0.8149	27.6752	14.1116	109.0906		
40	27.5003	14.0737	111.8373	27.8805	18.2624	110.4068	24.9213	15.5656	108.6216	0.3506	0.5198	0.4352	27.3293	15.8262	109.4821		
37	35.1923	6.8195	94.9626	35.8422	10.1234	97.7695	35.7803	6.4327	100.1340	0.5360	0.7237	0.6299	34.7324	8.0409	98.1292		
34	22.3729	43.2860	110.5373	17.5739	44.3264	110.2853	20.6058	47.0736	111.8592	0.4555	0.6620	0.5588	20.1993	44.7178	109.8735		
34	22.3729	43.2860	110.5373	17.5739	44.3264	110.2853	20.2445	44.1850	106.8120	0.4555	0.6619	0.5587	20.1993	44.7178	109.8735		
34	22.3729	43.2860	110.5373	20.6058	47.0736	111.8592	20.2445	44.1850	106.8120	0.7415	0.7972	0.7694	20.1993	44.7178	109.8735		
34	17.5739	44.3264	110.2853	20.6058	47.0736	111.8592	20.2445	44.1850	106.8120	0.7415	0.7972	0.7694	20.1993	44.7178	109.8735		

Table 4.5.4: Calculation of conductance of bonds connecting two cells.

Cell No.	Neighboring Cell Numbers				Conductances, m3/s/Pa			
21	509	22	26		6.302E-11	7.596E-11	1.803E-10	0
22	99	23	21		5.243E-11	1.801E-11	7.596E-11	0
23	22	600	81	5	1.801E-11	1.046E-10	3.582E-11	1.673E-10
24	203	3170	1574	2565	2.264E-11	1.335E-11	6.103E-12	1.242E-11
25	617	2586	840	2153	6.914E-12	3.239E-11	2.302E-11	5.195E-11
26	224	508	98	21	1.654E-11	5.477E-11	2.026E-11	1.803E-10
27	5765	2592	88	206	1.011E-11	4.729E-11	9.985E-12	4.714E-11
28	301	29	476		1.637E-10	1.833E-10	6.217E-12	0
29	298	30	28		8.062E-10	3.274E-11	1.833E-10	0
30	262	258	29		5.041E-10	1.315E-10	3.274E-11	0
31	1007	32	33	3	3.117E-11	6.614E-10	2.689E-10	2.219E-10
32	279	1039	31	2	6.447E-12	4.247E-10	6.614E-10	5.726E-10
33	1009	284	3379	31	2.689E-11	2.031E-10	3.106E-11	2.689E-10
34	8105	1216	3709	3702	1.852E-11	1.902E-11	9.203E-11	9.232E-11
35	323	321	3976	8115	3.280E-10	4.514E-11	2.930E-10	4.310E-11
36	8109	16068	333	1220	3.693E-11	6.450E-11	5.159E-11	9.065E-11
37	336	343	16647		9.152E-11	1.962E-10	5.358E-12	0
38	39	40	16445	16440	3.401E-11	3.269E-11	1.394E-10	1.128E-10
39	41	1314	1334	38	3.287E-11	2.118E-11	2.201E-11	3.401E-11
40	41	3627	1286	38	4.721E-11	9.067E-12	6.949E-12	3.269E-11
41	8452	1272	39	40	1.485E-11	1.206E-11	3.287E-11	4.721E-11
42	1345	353	3932	43	1.311E-11	1.148E-10	9.942E-11	1.148E-11
43	1349	9282	352	42	1.520E-11	9.293E-12	6.264E-12	1.148E-11
44	364	9650	46		1.363E-11	1.429E-11	1.412E-11	0
45	46	256	2450	361	1.383E-11	2.670E-11	5.923E-12	4.714E-11
46	4301	45	44		6.163E-12	1.383E-11	1.412E-11	0

Table 4.6: Neighbors of a cell grouped together and the corresponding bond conductances. Cells with only three neighbors are located at an outer boundary of the network.

After finding conductances of faces for all the cells as illustrated in Table 4.5, we can group together the neighboring cells of all the cells. Table 4.6 shows all the neighbors for cells 21-46 and conductance of the bonds connecting them to those neighbors.

Cells at the boundaries have less than four neighbors. Cell faces at the side boundaries of the sphere pack are assigned zero conductivity. Faces at the inlet or outlet of the column are assigned high conductivities.

We have a total of 34627 cells. Therefore, we have 34627×4 faces. We found 67005 pairs of shared faces (which are formed by same spheres and these faces connect two neighboring cells). Remaining 4498 faces are at the boundaries. These faces do not have any neighbor. Depending on their location, they will be treated as a no-flow boundary or as an exit or entrance throat.

4.6 SOLVING FOR POTENTIALS IN THE NETWORK

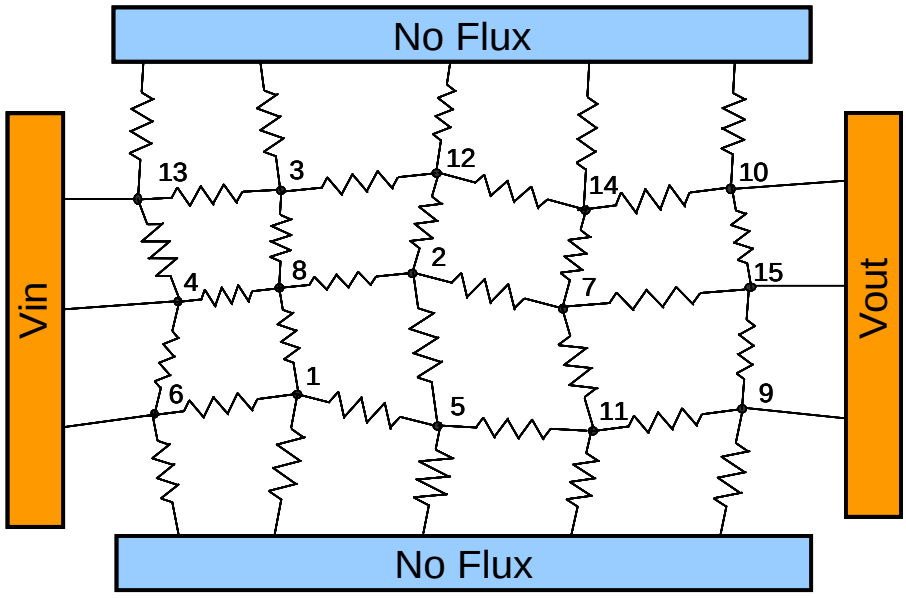

Figure 4.7: Schematic diagram for a network of resistors. The numbers indicate the junction number.

Pore network model can be viewed as a resistor network problem. The side boundaries of the network are insulated. Inlet and outlet potentials are specified. If conductance of each resistor in the network is known, current balance equation can be written at each junction. This gives a set of linear equations which can be solved for potential at each junction. Then flow through each resistor can be easily calculated.

A schematic network model is shown in Figure 4.7. It is unstructured and neighboring junctions (equivalently nodes) are not in any particular order. For simplicity, we illustrate the network flow calculations on this schematic model rather than on the actual network which is too large to show conveniently.

Let i denote a particular node and N_1, N_2, N_3 and N_4 its four neighbors. Let g_{i,N_1}, g_{i,N_2}, g_{i,N_3} and g_{i,N_4} denote the conductance of the bonds joining the node with its four neighbors. Let V_i denote potential at the node i and V_{N_1}, V_{N_2}, V_{N_3} and V_{N_4} the potentials of the four neighbors respectively. Let q_{i,N_1}, q_{i,N_2}, q_{i,N_3} and q_{i,N_4} denote flow coming to the node i from its four neighbors, respectively:

$$q_{i,N_1} = g_{i,N_1}(V_i - V_{N_1}),$$

$$q_{i,N_2} = g_{i,N_2}(V_i - V_{N_2}),$$

$$q_{i,N_3} = g_{i,N_3}(V_i - V_{N_3}),$$

$$q_{i,N_4} = g_{i,N_4}(V_i - V_{N_4}).$$

From mass conservation,

$$q_{i,N_1} + q_{i,N_2} + q_{i,N_3} + q_{i,N_4} = 0.$$

$$g_{i,N_1}\left(V_i - V_{N_1}\right) + g_{i,N_2}\left(V_i - V_{N_2}\right) + g_{i,N_3}\left(V_i - V_{N_3}\right) + g_{i,N_4}\left(V_i - V_{N_4}\right) = 0 .$$

$$\left(g_{i,N_1} + g_{i,N_2} + g_{i,N_3} + g_{i,N_4}\right)V_i - g_{i,N_1}V_{N_1} - g_{i,N_2}V_{N_2} - g_{i,N_3}V_{N_3} - g_{i,N_4}V_{N_4} = 0 .$$

$$\left(\sum_{k=1}^{4} g_{i,N_k}\right)V_i - \sum_{k=1}^{4} g_{i,N_k}V_{N_k} = 0$$

where N_k represents the k[th] neighbor of the node i.

Potentials at the inlet and outlet faces are known from boundary conditions.

$V_m = V_{in} \quad \forall$ *cell m at inlet* (taken as 100005 Pa).

$V_p = V_{out} \quad \forall$ *cell p at outlet* (taken as 100000 Pa).

The side walls of the sphere pack are sealed. There is no flow across these walls. Therefore, bonds connecting the nodes to the side walls have zero conductances. We arrange mass conservation equation at each node in form of a matrix. The matrix for the schematic network is shown below in Figure 4.8. We may write the equation as *conductance* . *V* = *RHS* .

$$
\begin{pmatrix}
\sum g_{1,N_k} & 0 & 0 & 0 & -g_{1,5} & -g_{1,6} & 0 & -g_{1,8} & 0 & 0 & 0 & 0 & 0 & 0 & 0 \\
0 & \sum g_{2,N_k} & 0 & 0 & -g_{2,5} & 0 & -g_{2,7} & -g_{2,8} & 0 & 0 & 0 & -g_{2,12} & 0 & 0 & 0 \\
0 & 0 & \sum g_{3,N_k} & 0 & 0 & 0 & 0 & -g_{3,8} & 0 & 0 & 0 & -g_{3,12} & -g_{3,13} & 0 & 0 \\
0 & 0 & 0 & 1 & 0 & 0 & 0 & 0 & 0 & 0 & 0 & 0 & 0 & 0 & 0 \\
-g_{5,1} & -g_{5,2} & 0 & 0 & \sum g_{5,N_k} & 0 & 0 & 0 & 0 & 0 & -g_{5,11} & 0 & 0 & 0 & 0 \\
0 & 0 & 0 & 0 & 0 & 1 & 0 & 0 & 0 & 0 & 0 & 0 & 0 & 0 & 0 \\
0 & -g_{7,2} & 0 & 0 & 0 & 0 & \sum g_{7,N_k} & 0 & 0 & 0 & -g_{7,11} & 0 & 0 & -g_{7,14} & -g_{7,15} \\
-g_{8,1} & -g_{8,2} & -g_{8,3} & -g_{8,4} & 0 & 0 & 0 & \sum g_{8,N_k} & 0 & 0 & 0 & 0 & 0 & 0 & 0 \\
0 & 0 & 0 & 0 & 0 & 0 & 0 & 0 & 1 & 0 & 0 & 0 & 0 & 0 & 0 \\
0 & 0 & 0 & 0 & 0 & 0 & 0 & 0 & 0 & 1 & 0 & 0 & 0 & 0 & 0 \\
0 & 0 & 0 & 0 & -g_{11,5} & 0 & -g_{11,7} & 0 & -g_{11,9} & 0 & \sum g_{11,N_k} & 0 & 0 & 0 & 0 \\
0 & -g_{12,2} & -g_{12,3} & -g_{12,4} & 0 & 0 & 0 & 0 & 0 & 0 & 0 & \sum g_{12,N_k} & 0 & 0 & 0 \\
0 & 0 & 0 & 0 & 0 & 0 & 0 & 0 & 0 & 0 & 0 & 0 & 1 & 0 & 0 \\
0 & 0 & 0 & 0 & 0 & 0 & -g_{14,7} & 0 & 0 & -g_{14,10} & 0 & -g_{14,12} & 0 & \sum g_{14,N_k} & 0 \\
0 & 0 & 0 & 0 & 0 & 0 & 0 & 0 & 0 & 0 & 0 & 0 & 0 & 0 & 1
\end{pmatrix}
\begin{pmatrix} V_1 \\ V_2 \\ V_3 \\ V_4 \\ V_5 \\ V_6 \\ V_7 \\ V_8 \\ V_9 \\ V_{10} \\ V_{11} \\ V_{12} \\ V_{13} \\ V_{14} \\ V_{15} \end{pmatrix}
=
\begin{pmatrix} 0 \\ 0 \\ 0 \\ V_{in} \\ 0 \\ V_{in} \\ 0 \\ 0 \\ V_{out} \\ V_{out} \\ 0 \\ 0 \\ V_{in} \\ 0 \\ V_{out} \end{pmatrix}
$$

Conductance V *RHS*

Figure 4.8: System of linear equations for determining node potentials.

Cell 1	Cell 2	Cond.		Cell 1	Cell 2	Cond.
1	5	$g_{1,5}$		8	1	$g_{8,1}$
1	6	$g_{1,6}$		8	2	$g_{8,2}$
1	8	$g_{1,8}$		8	3	$g_{8,3}$
2	5	$g_{2,5}$		8	4	$g_{8,4}$
2	7	$g_{2,7}$		9	11	$g_{9,11}$
2	8	$g_{2,8}$		9	15	$g_{9,15}$
2	12	$g_{2,12}$		10	14	$g_{10,14}$
3	8	$g_{3,8}$		10	15	$g_{10,15}$
3	12	$g_{3,12}$		11	5	$g_{11,5}$
3	13	$g_{3,13}$		11	7	$g_{11,7}$
4	6	$g_{4,6}$		11	9	$g_{11,9}$
4	8	$g_{4,8}$		12	2	$g_{12,2}$
4	13	$g_{4,13}$		12	3	$g_{12,3}$
5	1	$g_{5,1}$		12	14	$g_{12,14}$
5	2	$g_{5,2}$		13	3	$g_{13,3}$
5	11	$g_{5,11}$		13	4	$g_{13,4}$
6	1	$g_{6,1}$		14	7	$g_{14,7}$
6	4	$g_{6,4}$		14	10	$g_{14,10}$
7	2	$g_{7,2}$		14	12	$g_{14,12}$
7	11	$g_{7,11}$		15	7	$g_{15,7}$
7	14	$g_{7,14}$		15	9	$g_{15,9}$
7	15	$g_{7,15}$		15	10	$g_{15,10}$

Table 4.7: Bond conductances for the schematic network.

Algorithm

1. Read the neighboring cell indices and the conductance connecting those neighbors. An example is shown in the table 4.7. The first two columns show the neighboring cells indices and the third one shows the conductance connecting those two neighbors.
2. The conductance matrix is a sparse matrix as apparent from Figure 4.8. Sparsity of the matrix will increase with the network size. We used *spconvert* command in MATLAB to store conductances efficiently as a matrix having conductance values in the row number (first neighbor) and column number (second neighbor). All these elements are multiplied by -1.
3. The main diagonal of the matrix is the sum of all conductances in that row.
4. All the elements in rows corresponding to inlet or outlet cells are zero, except the main diagonal element which has a value of 1.
5. All the elements on the right hand side (RHS) are zero except those corresponding to the inlet or outlet cells. Incoming potential, V_{in} is assigned to elements corresponding to the inlet cells and outgoing potential, V_{out} to the elements corresponding to the out-flowing cells.
6. We can solve for potentials directly in MATLAB using *V=conductance\RHS*.

Material balance error is calculated at each node to evaluate accuracy of results. The maximum material balance error is within acceptable limits. Figure 4.9 shows potentials obtained at each pore in the pack.

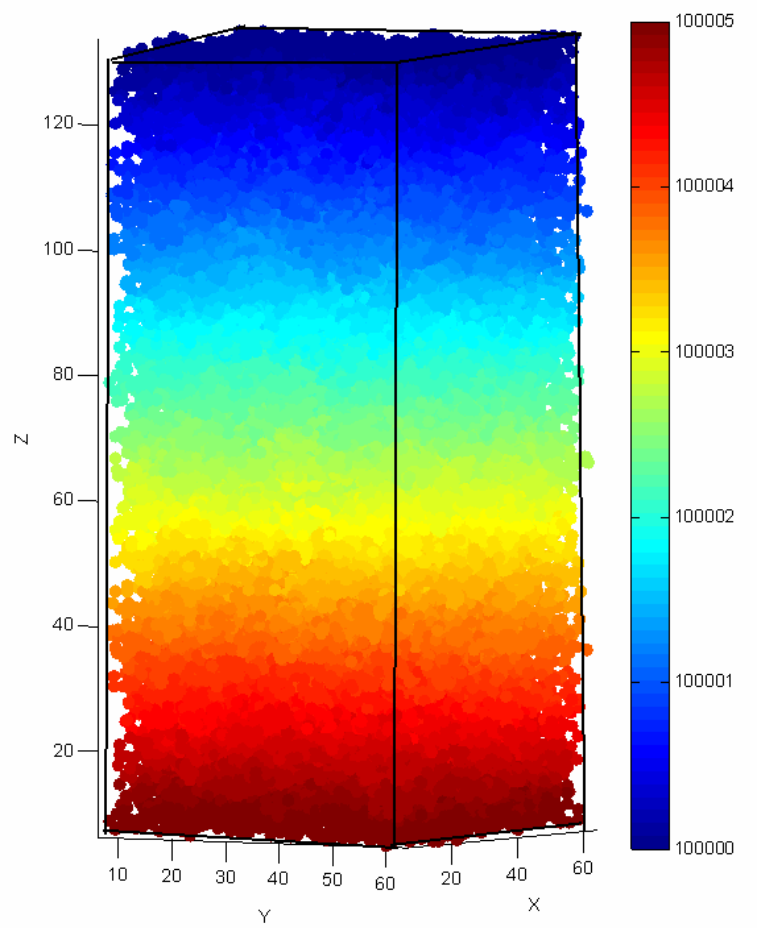

Figure 4.9: Potential at each pore in the network for steady-state single-phase flow in the z direction, with no-flow boundaries on the x and y faces.

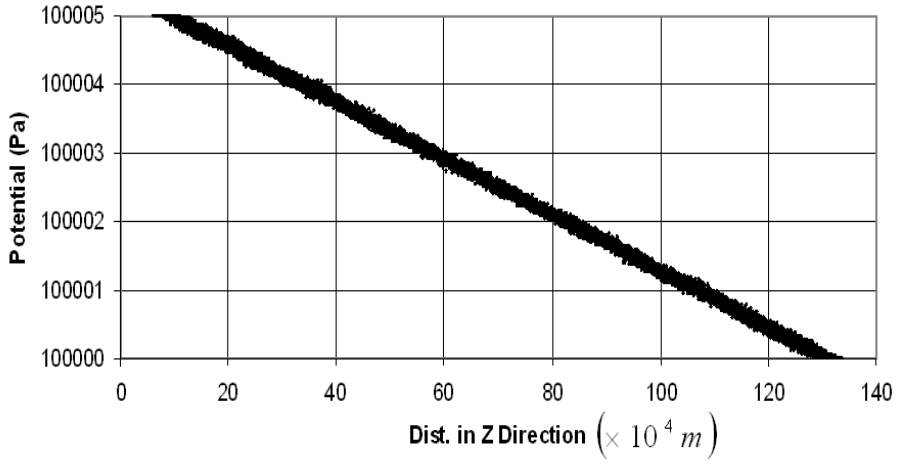

Figure 4.10: Potential variation in the longitudinal direction. Potential declines linearly from inlet to outlet of the medium. Small variations occur within a plane of constant z because of local variations of pore throat size.

Figure 4.10 plots conductance in the longitudinal direction. We can see the potential decreases almost linearly from inlet to outlet. There is very little scatter in potential at a given cross section.

Total flow going into the network = 818.2252×10^{-12} m^3/s.

Cross-section area of the medium = $58.5\times58.5\times10^{-8}$ m^2.

Length of the medium = 0.0135 m.

This corresponds to a permeability of 64.55 D.

The permeability for this pack expected from correlations is $2.72\times10^{-3}\times (R_{sph})^2$ = 130.67 D (Bryant et al., 1993).

The estimated permeability is about half of the expected value for the given pack of spheres. This difference comes because of the bond length used. We are using the natural definition of the bond length as the distance between the geometric centers of the two cells. However, this definition overestimates the distances traversed by elements of fluid in the void space. Assuming that a flow path extends all the way to the centre of a cell means that the four flow paths entering any cell overlap each other in the vicinity of the cell centre. Therefore, resistance to flow in the overlapping region near cell centers is counted twice.

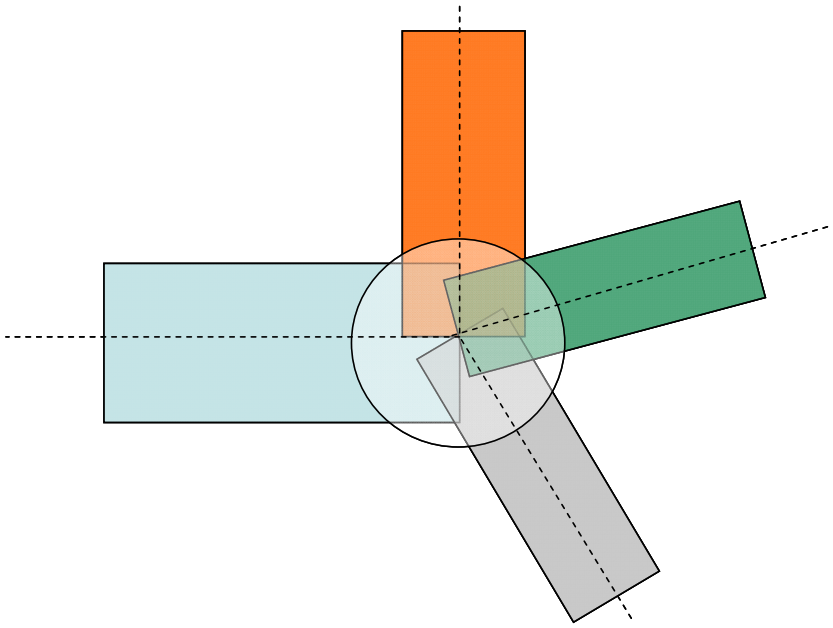

Figure 4.11: Removing overlapping of bonds near a pore body. A sphere can be placed at the cell center. The momentum loss in the sphere is ignored.

To eliminate this multiple counting of momentum loss in a bond, we can shorten the lengths of the flow paths. We can place a sphere at the center of the pore so that bonds terminate at the sphere surface rather than extending to the center of the pore (Bryant et al., 1993). The radius of the sphere is determined by trial and error so that overlapping of bonds is removed. The momentum loss in the sphere is neglected.

We calculated the radii of spheres to be placed at each pore to eliminate overlapping of bonds.

Average bond length = 3.71 units (sphere radius = 2.1918 units)

Average radius of overlap removing sphere = 1.01 units

Total fraction of bond length removed = 1.01×2/3.71 = 0.54.

After removing overlapped bond lengths, the calculated permeability of the pack agrees quantitatively with the experimental data.

This also has implications in calculation of pore scale Peclet number $v D_p / D_o$. Overlapping bonds imply that diffusion has to cause mixing in the overlapping region twice. We need to correct for this by reducing bond lengths. Therefore, pore scale Peclet number is taken as $0.46 v D_p / D_o$.

It should be noted, however, that reduction of bond length it is not a fitting parameter to match the experimental data. Removing overlapping of bonds is based on physics of the process.

4.7 EFFECT OF SPATIAL CORRELATIONS IN PORE STRUCTURE

To examine the influence of spatial correlation of the throat radii, we carry out a numerical experiment. We redistribute bond radii randomly over the entire network. The distribution of bond radii is still the same as that shown in Figure 4.6. The bond lengths are not changed and therefore, the geometry of the medium is still the same. For the same pressure drop across the network we get a higher flow rate in the network.

Total flow in the randomized network = 1107×10^{-12} m^3/s.

It corresponds to a permeability of 87.3 D (without removing overlap in bonds). Thus, we get 35% higher permeability in the network just by redistributing the bond radii. It signifies the importance of accounting for spatial correlation in flow properties in a physically representative network model.

4.8 SUMMARY

We developed a physically representative network model for a three dimensional random packing of spheres. It preserves the geometry, topology and spatial correlation in flow properties. We grouped together neighbors of each cell and calculated conductance of the bonds connecting the neighboring cells. We used mass balance at each pore to obtain flow rate through each bond for the applied potential gradient across the network. After removing overlapping of bonds near pore centers, the calculated permeability agrees quantitatively with the experimental data. The permeability of the network with bond radii randomly distributed over the network is 35% higher than that of the actual network.

REFERENCES

1. Acharya, R. C., van Dijke, M. I. J., Sorbie, K. S., Van der Zee, S. E. A. T. M. and Leijnse, A.: "Quantification of dispersion by upscaling Brownian motion of tracer displacement in a 3D pore-scale network model", Advances in Water Resources, 30 (2), 199 – 213, (2007).
2. Bijeljic, B., Muggeridge, A. H. and Blunt, M. J.: "Pore-scale modeling of longitudinal dispersion", Water Resources Research, Vol. 40, W11501 (2004).
3. Bruderer, C. and Y. Bernabe: "Network modeling of dispersion: Transition from Taylor dispersion in homogeneous networks to mechanical dispersion in very heterogeneous ones", Water Resources Research 37(4): 897-908 (2001).
4. Bryant, S. L., King, P. R. and Mellor, D. W.: "Network model evaluation of permeability and spatial correlation in a real random sphere packing", Transport in Porous Media, 11, 53-70, (1993).
5. Bryant, S. L. and Blunt, M.: "Prediction of relative permeability in simple porous media", Physical Review A, 46 (4), (Aug. 1992).

6. Finney, J.: “Random packings and the structure of simple liquids. I. The geometry of random close Packing”, Proc. Roy. Soc. 319A, 479 494, (1970).
7. Mellor, D. W.: “*Random close packing (RCP) of equal spheres: structure and implications for use as a model porous medium*”, PhD dissertation, Dept. of Earth Sciences, Open University, (1989).
8. Thane, C.: Personal communication (2006).
9. Thene, C.: *Geometry and Topology of Model Sediments and Their Influence on Sediment Properties*, M.S. Thesis, The University of Texas at Austin (2006).

Chapter 5: Deterministic Rules for Tracking Solute Particle through a Physically Representative Network Model

5.1 INTRODUCTION

We prepared a physically representative network model for a dense random packing of spheres. The flow rate in bonds was calculated using mass conservation equation at each pore. Thus in a network model solving the Navier-Stokes equation is replaced by solving a simple set of mass balance equations.

Similarly, solving convection diffusion equation can be replaced by tracking paths of a swarm of solute particles through the network. Dispersion can be quantified from spatial and temporal statistics of solute particles.

One of the most common simplifying assumptions made in particle tracking studies through a network model is probabilistic choice of out-flowing bond at pore junctions. A solute particle arrives at a pore junction and is assigned to a new out-flowing bond randomly with a flow rate weighted probability. We show in the next chapter that a probabilistic choice of out-flowing node is not realistic as it makes dispersion an irreversible process even in the absence of diffusion. Moreover, it ignores spatial correlations in flow properties at pore junctions which is one of the key features of physically representative network models.

Therefore, we developed deterministic rules for tracking solute particles through the network. The rules closely follow the patterns followed by streamlines. The path of solute particle is completely known in the absence of diffusion.

This chapter describes the deterministic rules developed for tracking solute particles in the absence of diffusion. Then the algorithm to simulate solute transport with diffusion in a capillary tube is described. The algorithm is validated by comparing the simulated results with Taylor's theory and experiments. Finally, the complete algorithm for tracking particle movement through the network with convection and diffusion is described.

5.2 DETERMINISTIC RULES FOR CHOOSING AN OUT-FLOWING BOND

The essence of the problem is local to individual pores. A particle enters the pore through one throat, and it leaves the pore through another throat. The task is to develop a rule for calculating which throat will be the exit. This could be done, for example, by solving the Navier-Stokes equation and mapping streamlines between the entrance and the exit throats. Here we describe a much simpler and computationally tractable approach that uses the network model flow calculation. This approach will differ in detail from full streamline simulation. However the essential feature of the streamlines for this application is that they provide a deterministic rule for calculating exit throats. The method described below also has this feature.

We have approximated the converging-diverging flow path connecting two pore bodies with an equivalent cylindrical bond. Therefore, at the center of a pore body we have four intersecting bonds that connect a pore to its four neighbors (Figure 5.1). We trace movement of solute particles through this local network of intersecting bonds. However, we neglect momentum loss and mixing in the overlapping region as described in the previous chapter.

We make some simplifying assumptions to track solute particle path in a network of three dimensional, randomly oriented bonds. We note that there are few flow configurations feasible at a pore junction. One reason is that all pores have four throats in the physically representative networks used here.

We first number the bonds according to their flow rates. We assign positive sign for inflow and negative sign for outflow. Then we sort the flow rates in descending order along with their sign. Thus the first bond is the one carrying maximum inflow and fourth one is carrying maximum outflow.

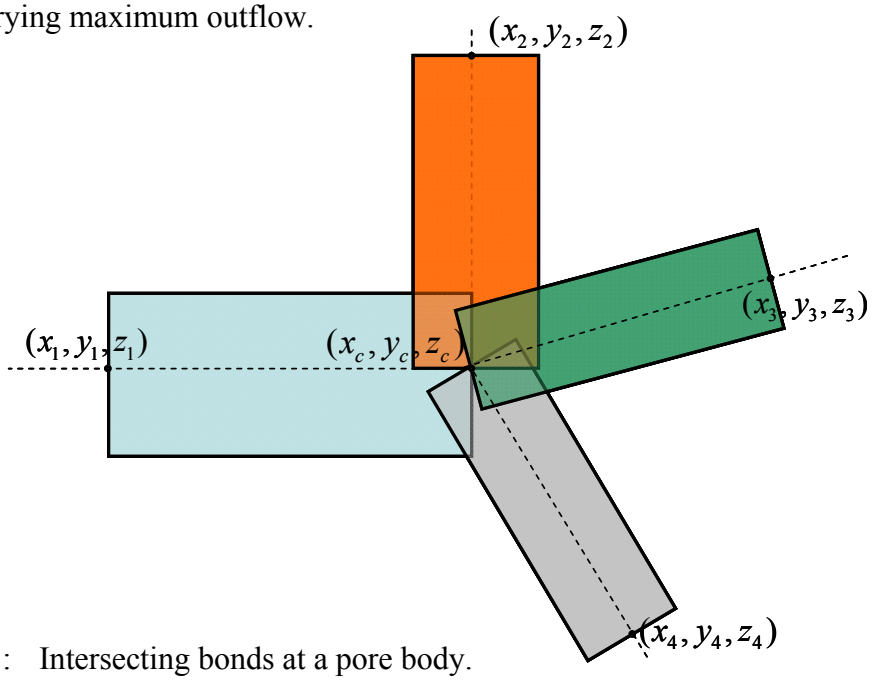

Figure 5.1: Intersecting bonds at a pore body.

We identify six possible flow configurations at a pore junction. In each case we calculate some reference points that serve as guiding points to map the exact position of solute particle on the out-flowing bond. For ease of illustration and for calculating the reference points, we displace all the bonds along their axes by equal distance. The displacement should be enough to remove overlap between the bonds. After identifying flow configuration and calculating reference points, all the bonds are moved back to their original locations (Figure 5.2).

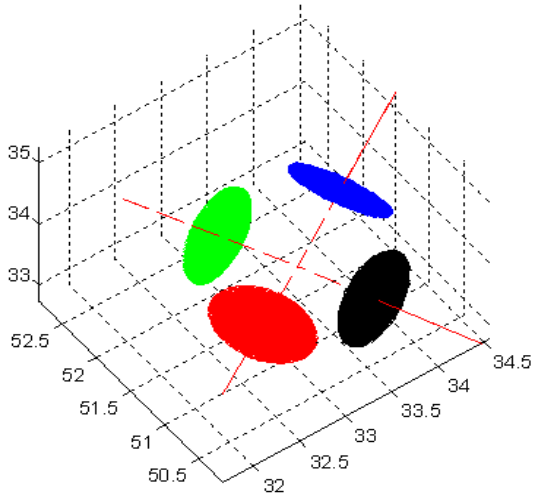

Figure 5.2: Faces of four bonds at a pore junction. They are displaced along their bond axes for finding flow configuration and calculating reference points and then moved back to their original location.

Next the six possible flow configurations at a pore junction are described.

Configuration 1: One bond flowing in, three flowing out

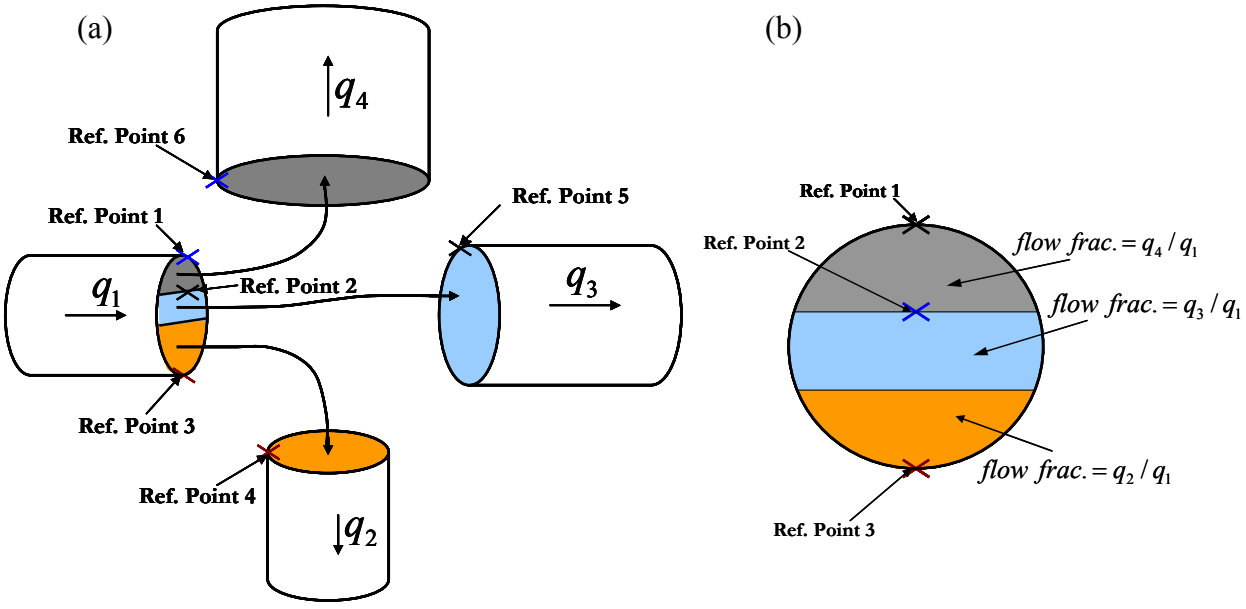

Figure 5.3: (a) Flow configuration with one in-flowing and three out-flowing bonds. The in-flowing stream splits into three segments. (b) Face of the in-flowing bond.

In this case one in-flowing bond feeds all the out-flowing bonds. Therefore, the incoming stream splits into three segments based on the flow rates of the three out-flowing bonds.

We calculate the distances of the face centers of all the out-flowing bonds from the face center of the in-flowing bond. The closest bond will have the biggest influence on flow. For example, in Figure 5.3 the fourth bond is the closest to the in-flowing bond. First, we find (numerically) the pair of points on the first and fourth bond faces that are closest to each other. These are reference points (reference point 1 on bond 1 and reference point 6 on bond 4). A solute particle exiting bond 1 at reference point 1 will enter bond 4 at reference point 6. These reference points also guide the mapping of the other points.

Starting with reference point 1, we mark a segment of the in-flowing bond that has the same flow rate as the out-flowing bond 4 (shown with grey color in Figure 5.3). In other words, we mark a segment that carries a fraction q_4 / q_1 of inflow (Figure 5.3 (b)). A solute particle exiting bond 1 from this segment will enter bond 4.

For the example shown in Figure 5.3, the third bond is the farthest bond. Since streamlines cannot cross, the farthest bond receives flow from the middle segment of the in-flowing bond.

Reference point 2 on the in-flowing face is taken as point where the line joining reference point 1 to the center of the face intersects the boundary of segment 1. Starting with reference point 2, we mark the middle segment of the in flowing bond that has the same flow rate as that in the out-flowing bond 3. In other words, we mark the middle segment of the bond that carries a flow fraction q_3 / q_1 of the incoming flow. Corresponding reference point on the out-flowing bond 3 is the point that is closest to reference point 2. This is marked as reference point 5 on bond 3. A solute particle exiting bond 1 at reference point 2 will enter bond 3 at reference point 5. In general, any point

exiting bond 1 in the middle segment (shown with blue color in Figure 5.3) will enter bond 3. Reference points serve as guides to mark the exact location of entrance.

Solute particle exiting bond 1 on the remaining third segment of the in-flowing bond (shown with orange color in Figure 5.3) will enter the second bond. The reference point on the in-flowing segment, reference point 3 is the diametrically opposite point of reference point 1. The corresponding reference point on the third bond, reference point 4 is the point on the face of the bond that is closest to reference point 3.

Method to mark a segment of a circle carrying a fraction f of total flow is described in the appendix A1-A3.

Configuration 2: Three bonds flowing in, one flowing out

This configuration is exactly opposite of the configuration 1. Three in-flowing bonds feed to one out-flowing bond. Therefore, the out-flowing stream consists of three segments, each segment receiving flow from one of the in-flowing bonds. The procedure described for connecting segments and calculating reference points in configuration 1 is applicable in this case also.

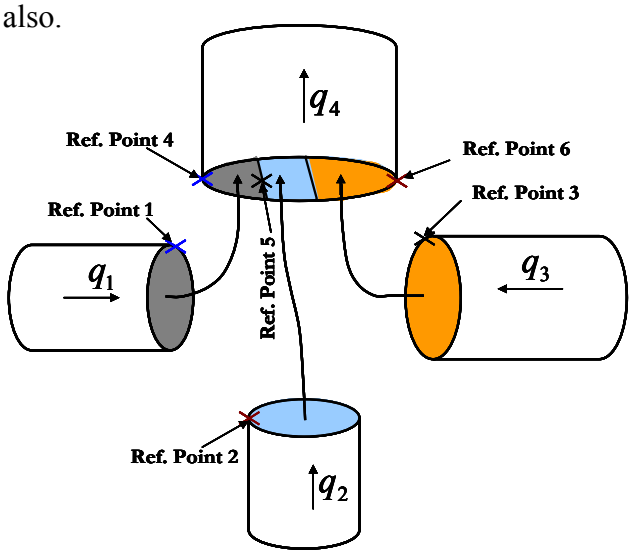

Figure 5.4: Flow configuration with three in-flowing and one out-flowing bonds. The out-flowing stream consists of flow from all the three in-flowing streams.

There are more than one possible flow configurations when we have two in-flowing and two out-flowing bonds at a pore junction. From mass balance we know that $q_1 + q_2 + q_3 + q_4 = 0$. Since flow rates have been sorted in ascending order with positive sign indicating inflow and negative sign indicating outflow, we have $abs(q_1) + abs(q_2) = abs(q_3) + abs(q_4)$.

Configuration 3: Third bond farthest from the first bond and flow rate in first bond is smaller than that in the fourth bond

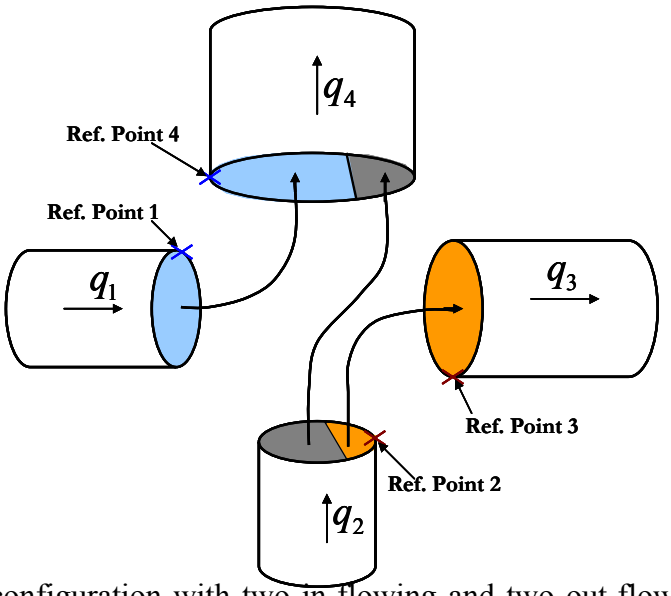

Figure 5.5: Flow configuration with two in-flowing and two out-flowing bonds. Third bond is the farthest from bond 1 and flow in bond 4 is greater than that in bond 1.

Since $abs(q_1) < abs(q_4)$, the fourth bond has to receive flow from both the in-flowing bonds. Since some streamlines move from bond 2 to bond 4 and streamlines cannot cross, no streamline can move from bond 1 to bond 3. Therefore, bond 3 will get all its flow from bond 2 and all of flow from bond 1 will go to bond 4.

Considering bonds 1 and 4, reference points are determined (numerically) as the pair of points closest to each other. On bond 4, starting with reference point 4 (as shown in Figure 4), we mark a segment that carries a fraction q_1/q_4 of outflow in bond 4 (filled

with blue color in Figure 5.5). This segment receives flow from bond 1. The other segment (shown with grey color) receives flow for bond 2.

Similarly on bonds 2 and 3, reference points are calculated as the pair of points closest to each other. On bond 2, starting with reference point 2, we mark a segment that carries a fraction q_3/q_2 of inflow in bond 2 (filled with orange color in Figure 4). This segment feeds to bond 3. The other segment (shown with grey color) feeds to bond 4.

Thus we know a solute particle exiting a bond in a particular segment will exit which segment of which bond. Exact location of exit point is decided based on its relative location from reference point as described later.

Method to mark a segment of a bond carrying a given fraction f if flow is shown in the appendix A1-A3.

Configuration 4: Third bond farthest from the first bond and flow in first bond is greater than that in the fourth bond

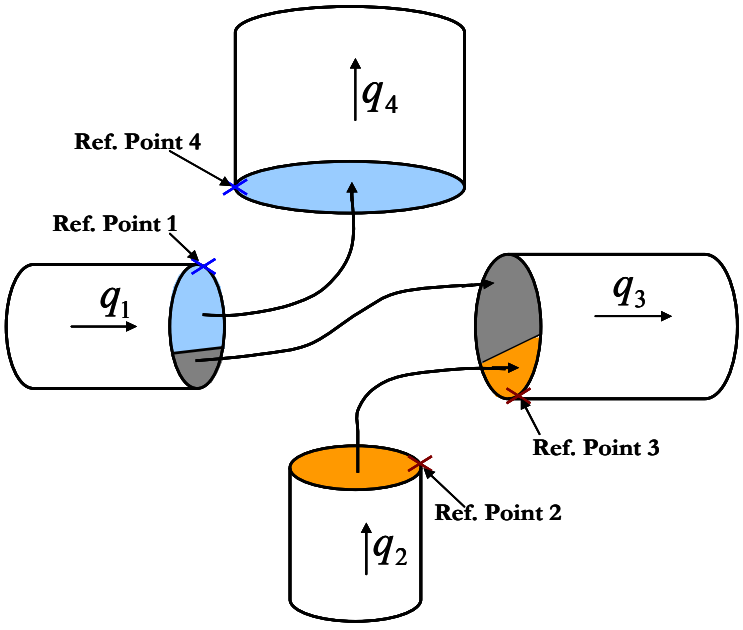

Figure 5.6: Flow configuration with two in-flowing and two out-flowing bonds. Third bond is the farthest from bond 1 and flow in bond 4 is smaller than that in bond 1.

It is similar to the configuration 3, except that in this case $abs(q_1) > abs(q_4)$ and therefore for mass balance, $abs(q_3) > abs(q_2)$. In this case the fourth bond receives all its flow from bond 1 and all of the second bond's flow enters the third bond. The first bond feeds to both the out-flowing bonds. Calculations of reference points and flow segments are similar to that described for configuration 3.

Configuration 5: Fourth bond is the farthest

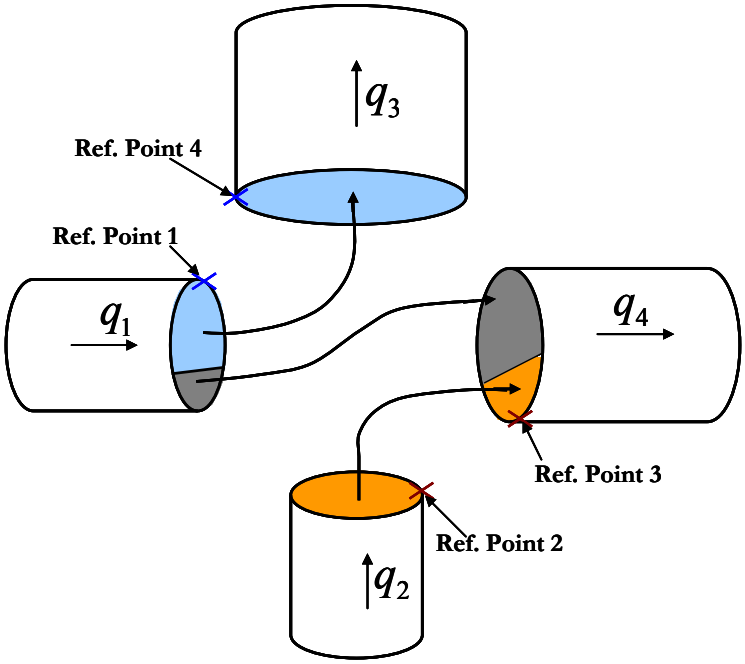

Figure 5.7: Flow configuration with two in-flowing and two out-flowing bonds. The fourth bond is farthest from bond 1.

This configuration is similar to the configurations 3 and 4. In this case the fourth bond (carrying the maximum outflow) is also the farthest from the first bond. Since, $abs(q_4) > abs(q_2)$, the fourth bond receives flow from both the inflowing bonds. Since

streamlines cannot cross, flow from the second bond cannot enter the third bond. Hence, all the flow from the second bond enters the fourth bond. Also the third bond receives all its flow from the first bond.

As evident from Figure 5.7, bond 1 feeds to both the out-flowing bonds and bond 4 receives flow from both the in flowing bonds. The procedure for calculating reference points and marking flow segments is the same as described previously.

Configuration 6: The second bond is the farthest

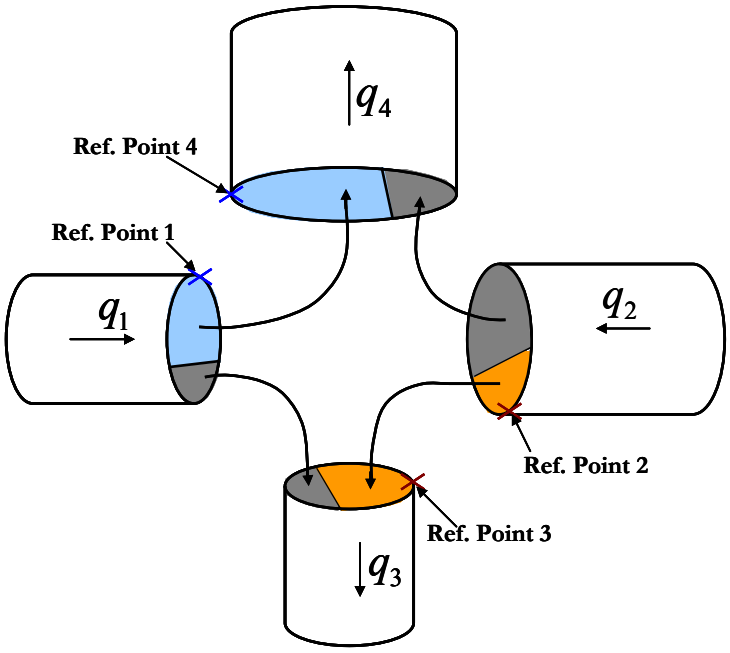

Figure 5.8: Flow configuration with two in-flowing and two out-flowing bonds. The second bond is the farthest from bond 1. In this configuration, both the in-flowing bonds feed both the out-flowing ones.

In this configuration the farthest bond is in-flowing. Or in other words, the second bond is the farthest. In this case, both the inflowing bonds will feed to both the out-flowing ones as shown in Figure 5.8. Each in-flowing stream splits into two segments, in

proportion to the flow rates of the out-flowing bonds. For example, the first segment of bond 1 (shown with blue color in Figure 5.8) carries a fraction $f = q_4/(q_3+q_4)$ of total flow. Flow segments and reference points are calculated as described previously.

This kind of flow configuration is unphysical in structured network with all the bonds having equal length (Bruderer and Bernabe, 2001). However, it can occur in the unstructured, physically representative network model we are using.

5.3 MAPPING AN INCOMING POINT TO AN OUT-FLOWING BOND

After deciding the in-flowing and out-flowing segments of the bonds, we have to map the incoming point to a corresponding point on the out-flowing section. In-flowing and out-flowing segments are arbitrary sections of a circle. We impose geometric rules that are physically reasonable: (i) the reference point on the in-flowing segment will connect to the corresponding reference point on the out-flowing segment and (ii) the center of the in-flowing segment connects to the center of the out-flowing segment. We take the center of the circular section as its geometric center (or the center of gravity). We call the vector joining the reference point to the center of the segment the "reference vector". We mark reference vectors on incoming as well as outgoing segments.

In a polar coordinate system, two parameters are sufficient to describe the outgoing point: (i) the angle the position vector of the outgoing point (here defined with reference to the center of the segment) makes with the reference vector and (ii) its relative radial distance from the center (defined as the distance of the point from the center normalized by the distance to the boundary in that direction). We impose another geometric rule: these parameters for the outgoing point have the same value as that for the incoming point. Therefore, we evaluate the angle θ, the position vector of incoming point makes with the reference vector on the in-flowing segment and relative radial

distance of the point from the boundary, *r/R*. Here *r* is the distance of the incoming point from the center and *R* is the distance from the center to the boundary of the segment. We place the outgoing point at the same θ and *r/R* on the outgoing section (Figure 5.9). It is important to note that this rule provides a deterministic, one-to-one mapping between exit points and entrance points. This means that if the direction of flow were reversed, a particle would travel through exactly the same sequence of pores and throats in the network, in reverse order.

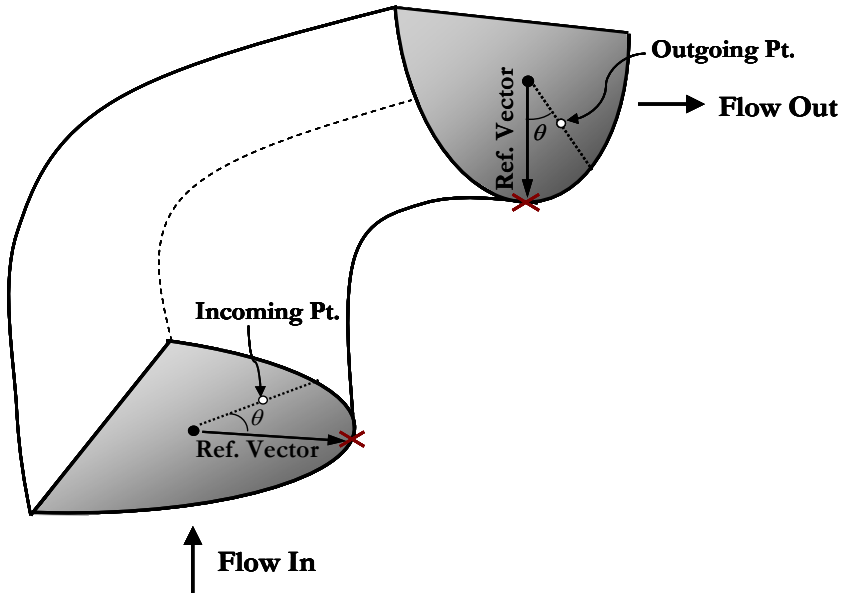

Figure 5.9: Marking the outgoing point based on reference angle and relative radial distance of the incoming point.

The procedure for calculating the relative distance of solute particles to the boundary is described in the appendix A4.

For simplifying calculations, we rotate the incoming and outgoing segments to the x-y plane (with normal to the plane pointing in the positive z-direction). We also shift the planes so that centers of both the segments lie at the origin. Now we have to work in two-dimensions only (Figure 5.10). After marking the outgoing point on the horizontal outgoing segment, it is rotated back to its original direction and shifted to its original position.

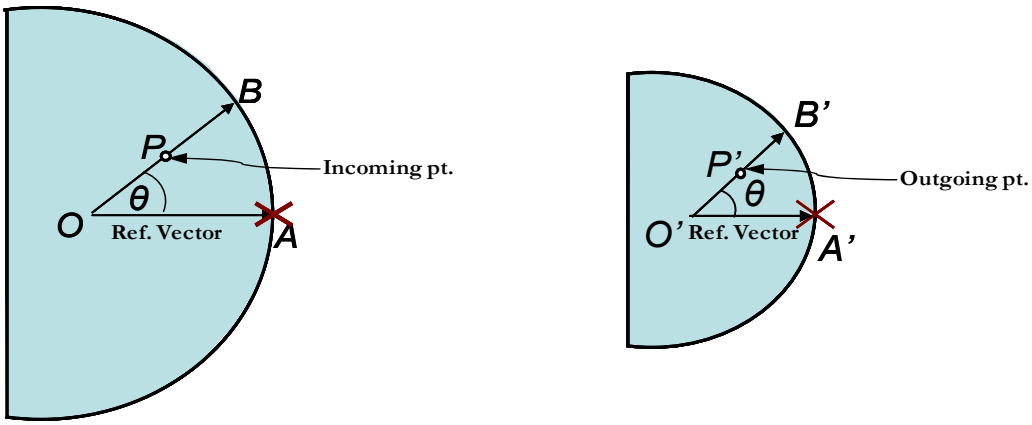

Figure 5.10: Marking the outgoing point on a horizontal segment.

The method to rotate a point in any plane to a horizontal plane and vice versa is described in the appendix A5.

5.4 PARTICLE MOVEMENT IN THE NETWORK

Within a bond a solute particle moves parallel to the bond axis. After reaching the outlet face of the bond, the particle immediately jumps to the inlet face of the next bond as per the deterministic rules described above and continues its motion to the next pore junction. This causes a little discontinuity in the path of the particle because of overlap in the region near the pore body. However, intersecting bonds are a way to model flow from one pore to another. Discontinuities are small as compared to the path length. Moreover,

the effect of discontinuities accumulated over several pores tends to get cancelled. Thus the particle statistics is not affected by these discontinuities. This is illustrated in the next chapter.

Because of deterministic rules, a solute particle retraces its path when the direction of flow is reversed. Therefore, flow and particle transport are reversible in the absence of diffusion (Figure 5.11).

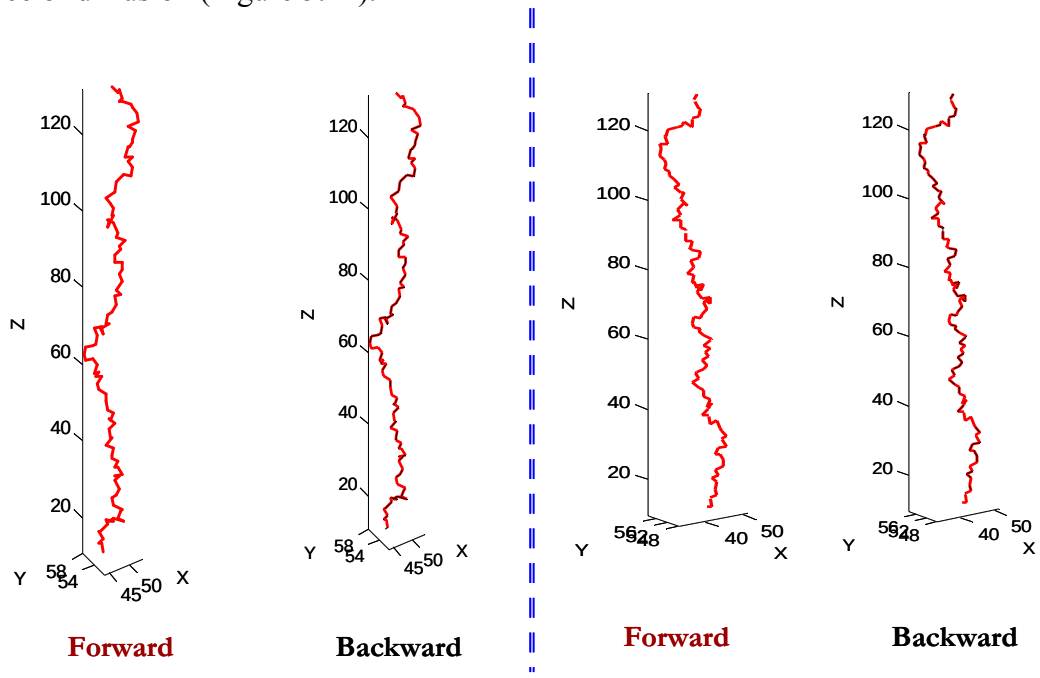

Figure 5.11: Forward and backward paths of two solute particles in the network. The solute particles retrace their path in the absence of diffusion.

5.5 PARTICLE TRACKING IN A TUBE WITH CONVECTION AND DIFFUSION

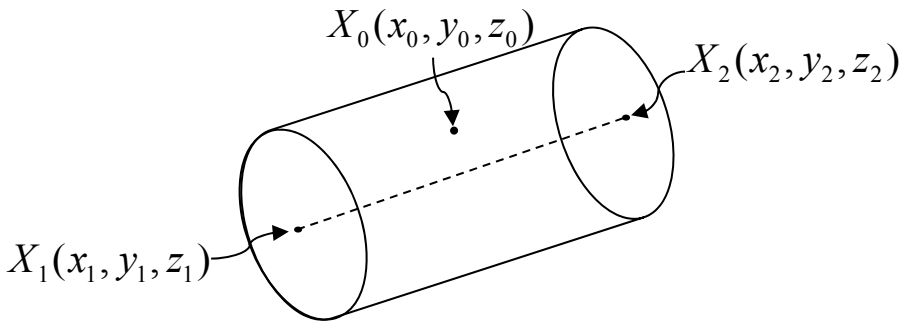

Figure 5.12: Movement of a solute particle in a randomly oriented tube.

For tracing particle's motion with convection and diffusion, its motion is divided into several time steps of equal duration dt. The particle first moves due to convection and then instantaneously makes a diffusive jump. We could move the particle due to convection and diffusion together. However, that is computationally expensive and does not have any significant advantage over separate steps (Bijeljic et al., 2004).

We consider movement of a particle through a tube of radius *R*. The axial points of the tube are $X_1(x_1, y_1, z_1)$ and $X_2(x_2, y_2, z_2)$ at the inlet and exit pores respectively (Figure 5.12). Length of the tube is given by

$$l = \sqrt{(x_2 - x_1)^2 + (y_2 - y_1)^2 + (z_2 - z_1)^2}\ .$$

For parabolic velocity profile in the tube (as in Taylor's problem), the velocity is dependent only on the radial position of the solute particle within the tube. We consider a solute particle at arbitrary location $X_0(x_0, y_0, z_0)$ within the tube. Radial distance of the particle from axis of the tube is given by

$$\vec{r} = \frac{\left|(X_2 - X_1) \times (X_1 - X_0)\right|}{\left|(X_2 - X_1)\right|}.$$

For a parabolic velocity profile in the tube

$$v(r) = 2\overline{v}\left(1 - \frac{r^2}{R^2}\right)$$

where $\overline{v} = q / \pi R^2$ is the average flow velocity through the tube.

Unit vector in the axial direction of the tube is

$$\hat{a} = \frac{(x_2 - x_1)\vec{i} + (y_2 - y_1)\vec{j} + (z_2 - z_1)\vec{k}}{l}.$$

Convective displacement during time interval *dt*

$$\vec{dX}_{con} = v \times \hat{a} \times dt \quad \text{…….. (5.6.1).}$$

In the diffusive step, particle moves in a random direction defined by the coordinates of a spherical coordinate system $\left(r_{diff}, \varphi, \theta\right)$ where φ and θ are randomly chosen angles and r_{diff} is the magnitude of the diffusive jump (Bruderer and Bernabe, 2001):

$$r_{diff} = \sqrt{6 D_o dt}$$

where D_o is the diffusion coefficient.

The particle's diffusive displacement in a Cartesian coordinate system is given by (Bijeljic et al., 2004):

$$\Delta x = r_{diff} \cos\theta \sin\varphi,$$

$$\Delta y = r_{diff} \sin\theta \sin\varphi,$$

$$\Delta z = r_{diff} \cos\varphi.$$

Here θ is uniformly distributed between 0 and 2π and $\cos\varphi$ is uniformly distributed between 0 and π. For every time step we pick a value for θ and φ. θ is a random number between 0 and 2π. For generating φ, we pick a random number between -1 and 1 and take the inverse cosine (Bijeljic, 2007).

In vector form the diffusive jump is

$$\vec{dX}_{diff} = \Delta x \vec{i} + \Delta y \vec{i} + \Delta z \vec{i} \quad \text{…….. (5.6.2).}$$

Therefore, the new location of the particle after convective and diffusive steps is

$$\vec{X}_{new} = \vec{X}_0 + \vec{dX}_{con} + \vec{dX}_{diff} \quad \text{…….. (5.6.3).}$$

Particle displacement in the direction of axis of the tube

$$dl = \frac{(\vec{X}_{new} - \vec{X}_0).(\vec{X}_2 - \vec{X}_1)}{\left|\vec{X}_2 - \vec{X}_1\right|} \quad \ldots\ldots\ldots (5.6.4).$$

The process is repeated till total movement in the direction of tube becomes equal to the length of the tube.

Reflection from Tube Wall

If during any time step, the particle hits the wall of the tube, it is reflected back into the tube (Figure 5.13).

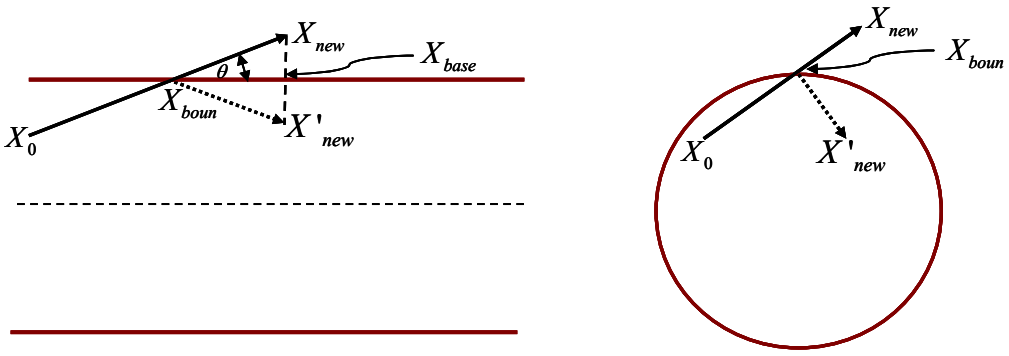

Figure 5.13: Solute particle reflecting at tube wall.

If the particle is not reflected back into the tube, it would cross the tube and its radial distance from the axis of the tube would be greater than the radius of the tube. Let X_{boun} be the point where the particle path crosses the tube wall. X_{boun} will lie on the line joining X_0 and X_{new}:

$X_{boun} = X_0 + t(X_{new} - X_0)$ …….. (5.6.5),

where *t* is a parameter.

Radial distance of X_{boun} would be equal to the radius of the tube *R*

$$\vec{R} = \frac{\left|(X_2 - X_1) \times (X_1 - X_{boun})\right|}{\left|(X_2 - X_1)\right|} \quad \ldots\ldots\ldots (5.6.6).$$

Using equations (5.6.5) and (5.6.6), we can determine *t*.

We denote

$$\vec{X}_{out} = \vec{X}_{new} - \vec{X}_{boun} \quad \ldots\ldots\ldots (5.6.7).$$

Projection of this vector in the direction of the tube is given by

$$pp = \frac{\vec{X}_{out} . (\vec{X}_2 - \vec{X}_1)}{l} \quad \ldots\ldots\ldots (5.6.8)$$

Angle made by the particle path with the axis of the tube is given by

$$\theta = \frac{\vec{X}_{out} . (\vec{X}_2 - \vec{X}_1)}{l \left| \vec{X}_{out} \right|} \quad \ldots\ldots\ldots (5.6.9).$$

Component of the outward vector in the perpendicular direction is given by

$$pn = \left| \vec{X}_{out} \right| \sin\theta \quad \ldots\ldots\ldots (5.6.10).$$

$$\vec{X}_{base} = \vec{X}_{boun} + pp \frac{\left(\vec{X}_2 - \vec{X}_1 \right)}{l} \quad \ldots\ldots\ldots (5.6.11).$$

Unit normal vector

$$\vec{X}_{norm} = \frac{\vec{X}_{base} - \vec{X}_{new}}{\left| \vec{X}_{base} - \vec{X}_{new} \right|} \quad \ldots\ldots\ldots (5.6.12),$$

$$\vec{X}'_{new} = \vec{X}_{base} + pn \times \vec{X}_{norm} \quad \ldots\ldots\ldots (5.6.13).$$

This is the position after reflection from the tube wall. In some cases multiple reflections may be required in a single time step to get the particle inside the tube.

We trace the particle with convection and diffusion till it exits the tube. The last time step may need truncation (if the particle exits the tube) to find the total residence time inside the tube.

5.7 VALIDATION OF PARTICLE TRACKING ALGORITHM

Taylor (1953) derived an expression for dispersion in flow through a capillary tube:

$$D_L = D_o + \frac{\bar{v}^2 R^2}{48 D_o}$$

where D_L = longitudinal dispersion coefficient, m^2/s

D_o = diffusion coefficient, m^2/s

$\bar{v}$ = average velocity, m/s and

R = radius of capillary, m.

For laminar flow of miscible fluids through a capillary tube, the dispersion coefficient is proportional to the square of velocity. Taylor validated his theory with experiments. Table 5.1 shows the details of two of his experiments.

Table 5.1: Comparison of simulated dispersion in a capillary tube with Taylor's experiments

	$l\,(m)$	$\bar{v}\,(m/s)$	$Pe_L = \frac{\bar{v}\,l}{D_L}$, theory	Pe_L, simulated
Expt. 1	0.632	2.633×10^{-3}	145.16	150.51
Expt. 2	0.319	2.843×10^{-5}	4244.28*	4365.7

* In this case the diffusion term in dispersion coefficient is not negligible.

For both the experiments $D_o = 8\times10^{-10}\ m^2/s$ and $R = 2.52\times10^{-4}\ m$.

We simulate Taylor's experiments by tracking movement of a swarm of solute particles through a capillary tube. The dispersion coefficient is quantified from particle residence time statistics. As shown in Table 5.1, the simulated Peclet numbers are very close to the experimental values.

We also studied the effect of varying fluid velocity on dispersion through a capillary tube. Figure 5.14 shows the comparison of simulated dispersion with that predicted by Taylor's theory. Again, we find a very close match for the simulated and theoretically predicted values. This validates our particle tracking algorithm in a capillary tube.

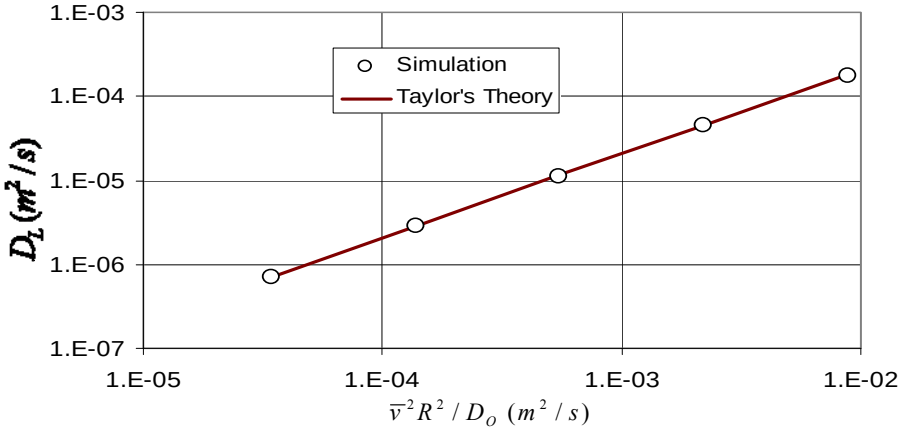

Figure 5.14: Comparison of simulated dispersion in a capillary tube with Taylor's theory.

5.8 ALGORITHM FOR TRACKING PARTICLE THROUGH THE NETWORK

As described, we developed deterministic rules for deciding exit point of a solute particle at a pore junction. In this section we describe an algorithm for tracking a solute particle's path through a physically representative network.

1. Flow configuration and reference points are calculated for all 34627 pores of the network and stored. Changing potential gradient across the network changes flow rates in each bond proportionately. Therefore, flow configuration and reference points remain unchanged. Storing this information eliminates the need to recalculate these data every time and saves computational resources.
2. The starting position of a swarm of 15000 particles at the inlet face of the network is decided in advance. The number of particles entering an inlet bond is proportional to its flow rate. The particles are distributed uniformly in each bond.
3. We track one particle at a time. Particle moves with convective and diffusive steps through a bond till it reaches a pore junction. At a pore body (bond junction) its position is mapped to an out-flowing bond based on the arrival position of the particle and the flow configuration of the pore. The particle instantaneously jumps to an out-flowing bond based on the deterministic rules described earlier in the chapter. Residence time of the particle in each bond is noted.

   A solute particle can move out of a bond through the inlet face because of diffusion. We continue its motion through convective and diffusive steps till it finally reaches the outlet face of the bond and subsequently mapped to the next bond.

   We used same rules for particle tracking for all the Peclet numbers. Particle's position on outlet bond is decided based on relative flow rates

and flow configuration. This rule is strictly valid when solute transport is dominated by convection. A better rule to decide the out-flowing bond in the diffusion dominated regime ($Pe < 4$) should be based on cross sectional areas of bonds rather than their flow rates. This is suggested as a future modification of the tracking algorithm.

4. The particle continues it movement through bonds till it reaches the outlet of the network. The dispersion coefficient can be quantified from residence time distribution. Particle positions are also scanned at regular time intervals. Dispersion coefficient can also be quantified from spatial statistics. Results of particle tracking through the network are described in the next chapter.

5.8 SUMMARY

We developed rules to track a particle's path through a physically representative network. Within a bond a solute particle moves parallel to the axis of the bond. When the particle reaches a pore junction, its position on the out-flowing bond is decided based on deterministic rules. Then particle continues its motion in the next bond. This algorithm completely determines the particle path in absence of diffusion.

Then algorithm to simulate solute transport with diffusion in a capillary tube is described. The algorithm is validated by comparing the simulated results with Taylor's theory and experiments. Finally, complete algorithm for tracking particle movement through the network with convection and diffusion is described.

REFERENCES

1. Acharya, R. C., van Dijke, M. I. J., Sorbie, K. S., Van der Zee, S. E. A. T. M. and Leijnse, A.: "Quantification of dispersion by upscaling Brownian motion of tracer displacement in a 3D pore-scale network model", Advances in Water Resources, 30 (2), 199 – 213, (2007).
2. Bijeljic, B., Muggeridge, A. H. and Blunt, M. J.: "Pore-scale modeling of longitudinal dispersion", Water Resources Research, Vol. 40, W11501 (2004).
3. Bijeljic, B.:Personal Communication (2007).
4. Bruderer, C. and Y. Bernabe: "Network modeling of dispersion: Transition from Taylor dispersion in homogeneous networks to mechanical dispersion in very heterogeneous ones", Water Resources Research 37(4): 897-908 (2001).
5. Taylor, G.: "Dispersion of soluble matter in solvent flowing slowly through a tube", Proc. R. Soc. London, Ser. A, 219, 186-203 (1953).

Chapter 6: Quantitative Investigation of Dispersion in a Dense, Random Packing of Spheres

6.1 INTRODUCTION

Solute transport through porous media can be interpreted in terms of streamlines. Solute particles travel along streamlines and make random jumps across streamlines to emulate diffusion. We prepared a physically representative network model of a three dimensional random packing of spheres. We monitor movement of a swarm of solute particles as it moves through the network. We developed deterministic rules to trace a solute particle's path from an inlet to a pore to an outlet of pore. We can therefore trace a particle's path across the entire network. Because the rules are deterministic, the paths of solute particles are completely known in absence of diffusion. This allows us to investigate convective spreading explicitly in realistic pore space geometry. To the best of our knowledge, it has not been reported before.

Next, diffusion is superimposed and movement of solute particles due to combined effects of convection and diffusion is monitored. Dispersion is quantified from spatial and temporal statistics of solute particles. Then the effect of diffusion on dispersion is investigated. This chapter presents the results of network model calculations to simulate solute transport. We study interaction between diffusion and convective spreading and explain the origin of power law dependence of the dispersion coefficient on the pore scale Peclet number. We also study effect of flow reversal on mixing in the sphere pack. All our results are supported by theoretical and experimental results found in the literature. The prediction from the physically representative network model contains

no adjustable parameters. So the agreement with the measurements indicates that the model captures the essential physics.

6.2 CONVECTIVE SPREADING AS A DIFFUSIVE PROCESS

Dispersion in porous media results from a combination of convective spreading and molecular diffusion. Convective spreading (mechanical dispersion) is considered to be "diffusion –like"; a statistically random process (Bear, 1972).

Pore scale features (variations in geometry and topology) play an important role in determining dispersive properties of a porous medium (Sahimi et al., 1986). We monitor movement of solute particles through a physically representative network model of pore space which preserves the geometry and topology of an actual granular material. Solute front moving through the pore space splits at each pore junction due to pore morphology and the fluid dynamics. Therefore, solute particles starting very close to each other travel together, entering and leaving pores through the same throats for a few pores. Eventually they fall on the opposite sides of the split stream and they exit through different throats. Subsequently those particles take different paths and their movements become independent of each other. They are unlikely to come together again.

Figure 6.1 shows paths of five different neighboring pairs of particles starting close to each other. They travel together through some number of pores and then get split, taking two different exits from a pore. The number of pores entered before splitting depends on the initial location of particles and local pore geometry. The split is due only to the flow field; even arbitrarily close particles will be on streamlines that eventually follow different exits out of a pore. Once the paths split, particles' movements can be considered independent of each other. This is convective spreading.

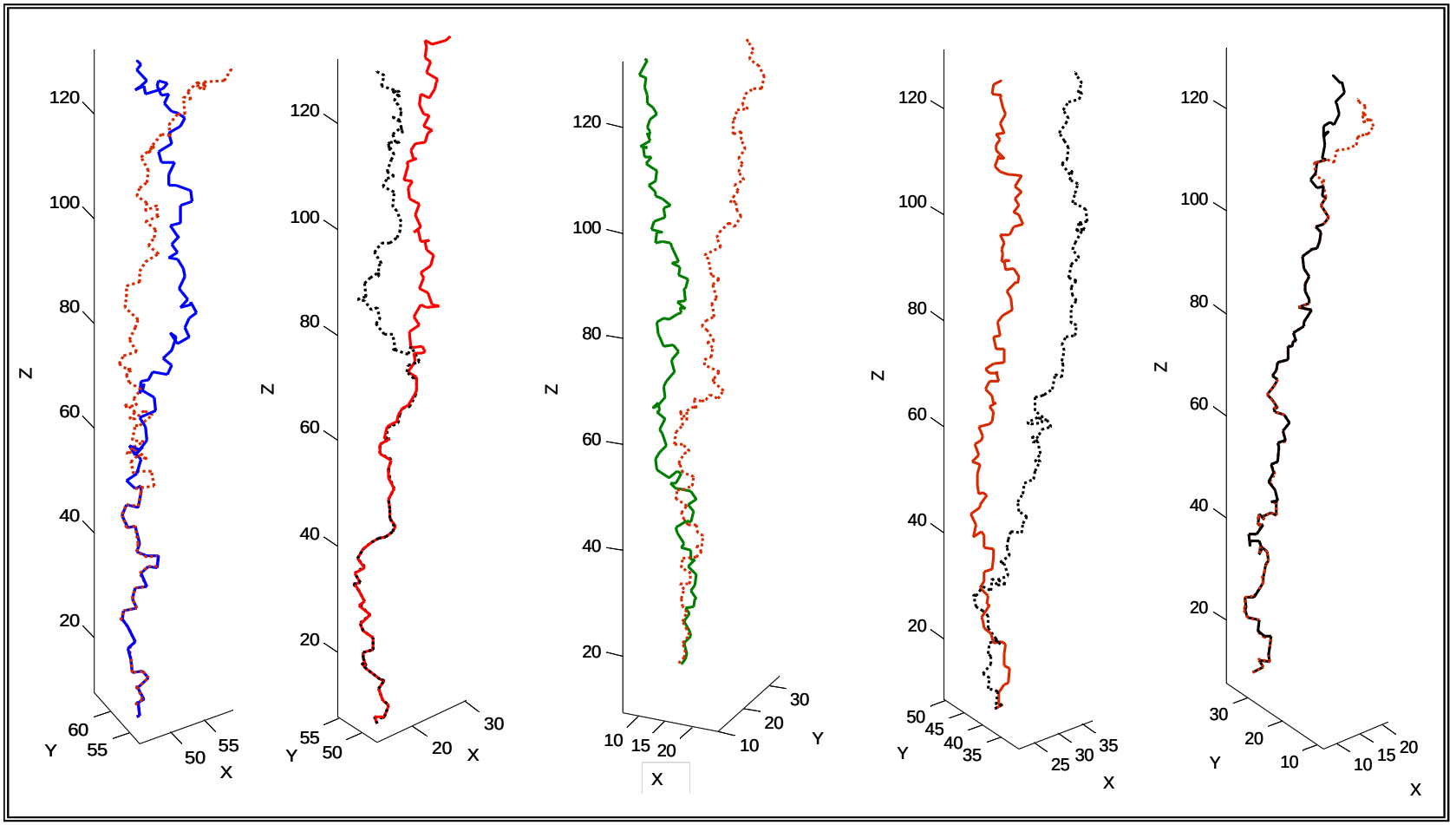

Figure 6.1: Paths of five different pairs of neighboring particles with no diffusion. Particles split their paths after traveling together for a few pores.

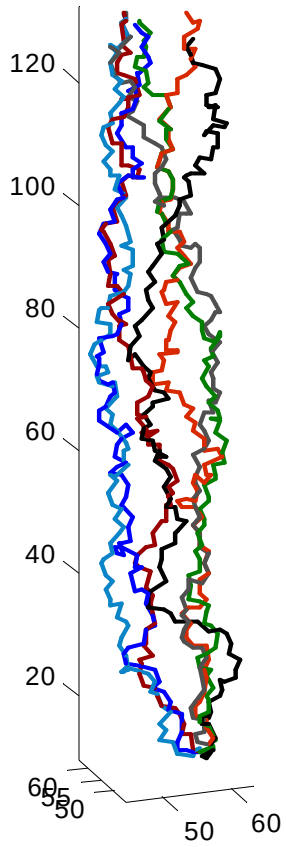

Figure 6.2: Paths of several particles starting at different positions in the same pore. Particles paths are independent of each other. If each convective step is independent and has the same global statistics, solute particle displacements will be normally distributed.

Figure 6.2 shows paths of several solute particles starting at the same inlet pore. A particle's movement gets decorrelated with other particles very quickly because of frequent splitting of flow passages – every pore has two or three exits. The randomness of convective spreading in porous medium is inherent in the morphology of the pore space (Sahimi et al., 1986).

The sufficient conditions that convective spreading due to splitting at pore bodies (bond junctions) can be treated like diffusion in a continuum transport equation can be stated in terms of the central limit theorem (Chandrashekhar, 1943; Sahimi et al., 1986).

The central limit theorem (CLT) states that the sum of a large number of independent and identically distributed random variables will be approximately normally distributed if the random variables have a finite variance (Bear, 1972). A particle's total displacement is the sum of its displacements over previous steps. After a particle's velocity over successive steps becomes decorrelated, it can sample velocities randomly from the global velocity distribution (ergodic hypothesis). Therefore, after a few steps the spatial distribution of particle positions is expected to be normal (Gaussian) as per the central limit theorem.

Cenedese et al. (1996) and Moroni et al. (2001) show by three-dimensional particle tracking velocimetry (3D-PTV) experiments in bead packs that velocity components quickly become decorrelated. Correlation lengths are of the same order as the grain dimensions, and an exponential correlation law seems to model their behavior correctly. Longitudinal dispersion goes Fickian after the solute front has traversed five to six pore diameters (Manz et al., 1999). The experiments are not diffusion free, however.

6.3 PARTICLE TRACKING IN A PHYSICALLY REPRESENTATIVE NETWORK MODEL WITH PLUG FLOW IN BONDS (WITHOUT DIFFUSION)

We track movements of a swarm of 15000 particles through a physically representative network model for a three dimensional, dense, random packing of spheres. A plug flow velocity profile is assumed in each bond of the network. In the absence of diffusion a solute particle enters a bond at the inlet face and moves parallel to the axis of the bond to its outlet. At the outlet face of the bond its position is mapped to the next bond depending on the radial position of the particle, local pore geometry and the flow configuration. The particle continues its motion in the next bond. The particle tracking algorithm was described in detail in the previous chapter.

Figure 6.3 shows a histogram of velocities in bonds. There are a large number of bonds having low velocities. These bonds are mainly located at the no-flow faces (side boundaries) of the network. These are also some bonds approximately perpendicular to the flow direction. There is negligible potential gradient across the two ends of such bonds and flow velocity is very low.

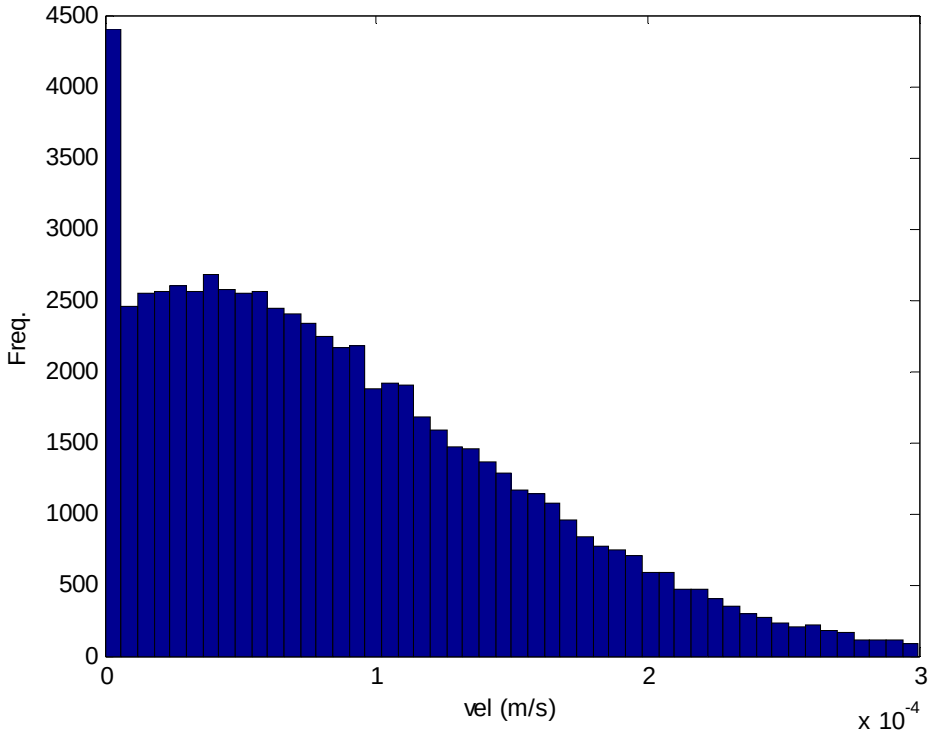

Figure 6.3: Mean flow velocity distribution in bonds. There are many bonds perpendicular to the flow direction that have small velocity.

Paths of a swarm of 15000 particles are traced from inlet to the outlet of the network. Particles at the inlet face of the network are distributed to the inlet bonds proportional to the flow rates in those bonds. In any inlet bond the particles are uniformly distributed over the cross-section of that bond. The particles move through the network

following the rules described in Chapter 5 for determining the exit path from each pore. Their spatial positions are scanned at regular time intervals. Time spent by each particle inside the medium is also recorded.

Figure 6.4 shows a cumulative distribution function (cdf) plot of residence times of solute particles (thick curve). The figure also shows cumulative distribution function plots of solute particles arriving at some outlet pores individually. Each (thin) curve shows residence time distribution of particles arriving at a particular outlet pore. The thick curve represents core scale averaged solute concentration history whereas the thin curves show pore scale averaged solute concentration histories for several different pores.

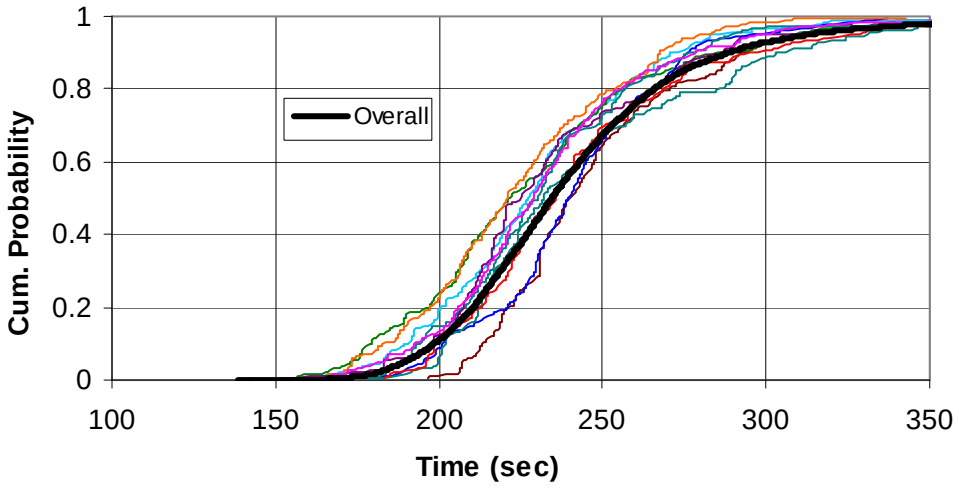

Figure 6.4: Comparison of core-scale averaged (thick curve) and pore-scale averaged (thin curves) solute concentration histories in absence of diffusion.

All pore scale averaged and core scale averaged solute concentration curves are very similar to each other. The residence times are normally distributed (this is shown more explicitly in the next figure). It is because the solute particles move with independent convective steps. Even a single outlet pore receives solute particles that had independent histories at the time of arrival at the outlet. Similarity of pore scale averaged

and core scale averaged solute concentration histories was shown experimentally by Jha (2005).

Figure 6.5 shows a cumulative distribution function of distance traveled by solute particles.

Mean path length $L_t = 0.0207\ m$,

length of the medium, $L_e = 0.0124\ m$,

therefore, $\tau = L_t / L_e = 1.674$ …….. (6.1).

This value agrees well with that reported in the literature (Carman, 1937; Bear, 1972, Dullien, 1979). It shows that the effect of discontinuity in particle movement at a pore body (bond junction) is small compared to the path length. Moreover, the effect of discontinuities accumulated over several pores tends to cancel. Therefore, we get a value of tortuosity that is in good agreement with the results found in the literature. Thus the discontinuity of solute particle movement at pore bodies (bond junctions) does not affect the particle statistics.

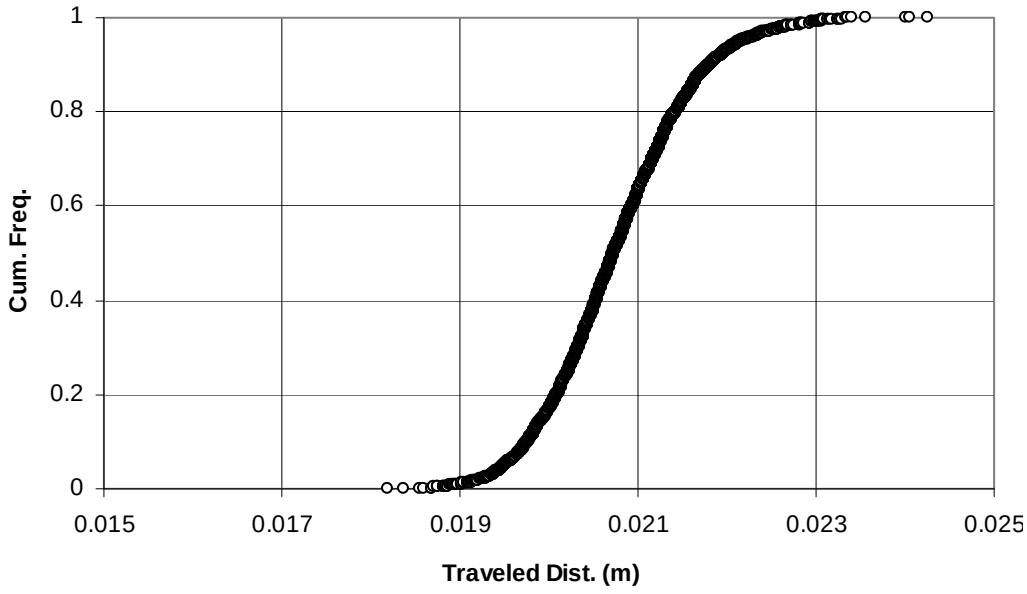

Figure 6.5: Cumulative distribution of path lengths of solute particles.

As evident from Figure 6.4, solute particles start exiting the medium at about 150 seconds. Particles positions within the medium are scanned at five different times: 25 s, 50 s, 100 s, 125 s and 150 s. The particle statistics is plotted in Figure 6.6. A probability distribution plot of particles' spatial positions is shown at each time. For comparison, a normally distributed probability distribution plot having the same mean and standard deviation as the actual data is also plotted in each case. The closeness of the two probability distributions shows how close the actual data is to being normally distributed.

The dispersion coefficient at those times is calculated using:

$$D_L = \frac{\sigma_z^2}{2t},$$

where σ_z^2 is the variance of solute particle positions in the z (longitudinal) direction at time t. The dispersion coefficient is also calculated using the particles' residence time statistics and using a solution to the one dimensional convection diffusion equation. It is observed that the dispersion coefficient calculated from spatial statistics increases with time (and travel distance) and finally converges to an asymptotic value (Figure 6.6 (f)). The asymptotic dispersion coefficient is very close to that obtained from temporal statistics in all the cases studied. For consistency, the dispersion coefficient obtained from temporal statistics is taken as the dispersion coefficient.

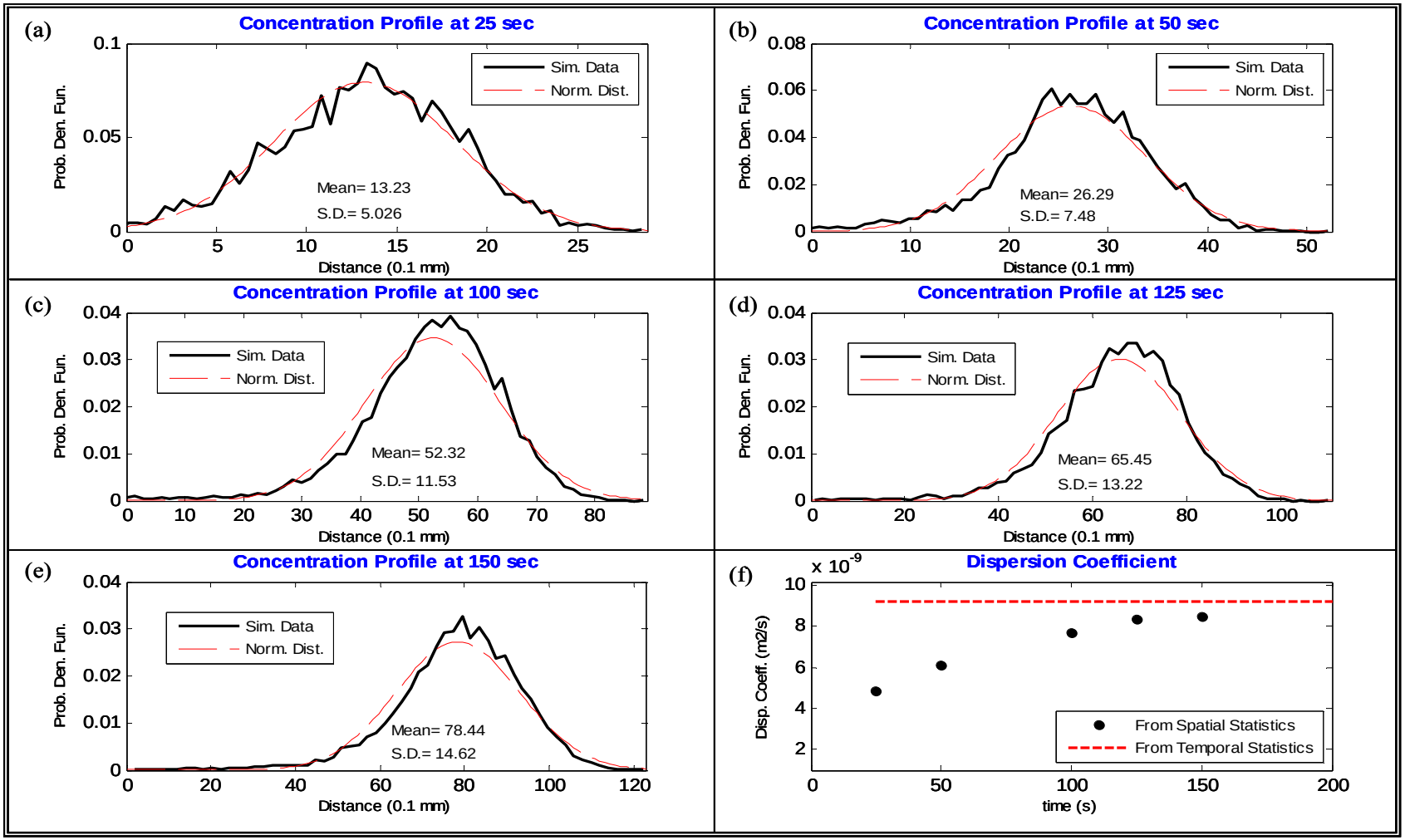

Figure 6.6: Figure 6.6: (a)-(e) Scanned spatial distribution of solute particles. Plug flow is assumed in the network bonds and $D_o = 0$ m^2/s. Normally distributed curves having same mean and standard deviation as the actual data are also shown for comparison. (f) Dispersion coefficient as evaluated from spatial and temporal statistics.

It can be seen that particles (equivalently solute concentration) are normally distributed at all the times. The particle velocities become decorrelated very quickly and particle displacements tend to a normal distribution as expected from the central limit theorem.

The approach to convergence of the dispersion coefficient to an asymptotic value is governed by correlation in the local pore structure. After sufficient time that the asymptotic value of the dispersion coefficient has been obtained, purely mechanical dispersion is Fickian. The asymptotic dispersion coefficient for purely mechanical dispersion is evaluated to be $9.25\times10^{-9}\ m^2/s$. The average interstitial fluid velocity in the network is $v = 5.12\times10^{-5}\, m/s$.

For length scales in the pre-asymptotic region, the averaged macro-scale version of Fick's law is not applicable. Koch and Brady (1987) developed a non-local transport theory for the description of solute transport in the pre-asymptotic region. It is beyond the scope of this dissertation.

6.4 EFFECT OF DIFFUSION ON PARTICLE STATISTICS

Next we study the influence of diffusion on particle statistics and the dispersion coefficients. A particle's movement inside a bond is divided into several time steps of equal length. In each time step, the particle moves due to convection parallel to the axis of the bond and then makes an instantaneous diffusive jump.

The time step should not be greater than that to make the diffusive jump magnitude larger than the bond diameter (Bruderer and Bernabe, 2001). The time step was taken to be one tenth of the value for average bond diameter to reduce numerical error. The algorithm for tracing particles was described in the previous chapter.

Figure 6.7 shows effect of diffusion on solute particle statistics. We can see that diffusion has a negligible impact on particle distribution for diffusion coefficients ranging from 0 to 10^{-9} m^2/s because diffusion is very small in magnitude compared to the mechanical dispersion. The dispersion coefficient remains constant in this range of diffusion coefficients (Figure 6.8). For higher diffusion coefficients the diffusion becomes significant in magnitude compared to the mechanical dispersion and therefore the spread of particles increases and this increases dispersion coefficient.

When diffusion is very small, transport is dominated by convection. However, at very low Peclet numbers when diffusion is large in magnitude, our flow rate weighted rule for deciding an out-flowing bond is not strictly applicable. Therefore, in this case the particle statistics starts deviating from normal distribution at longer times.

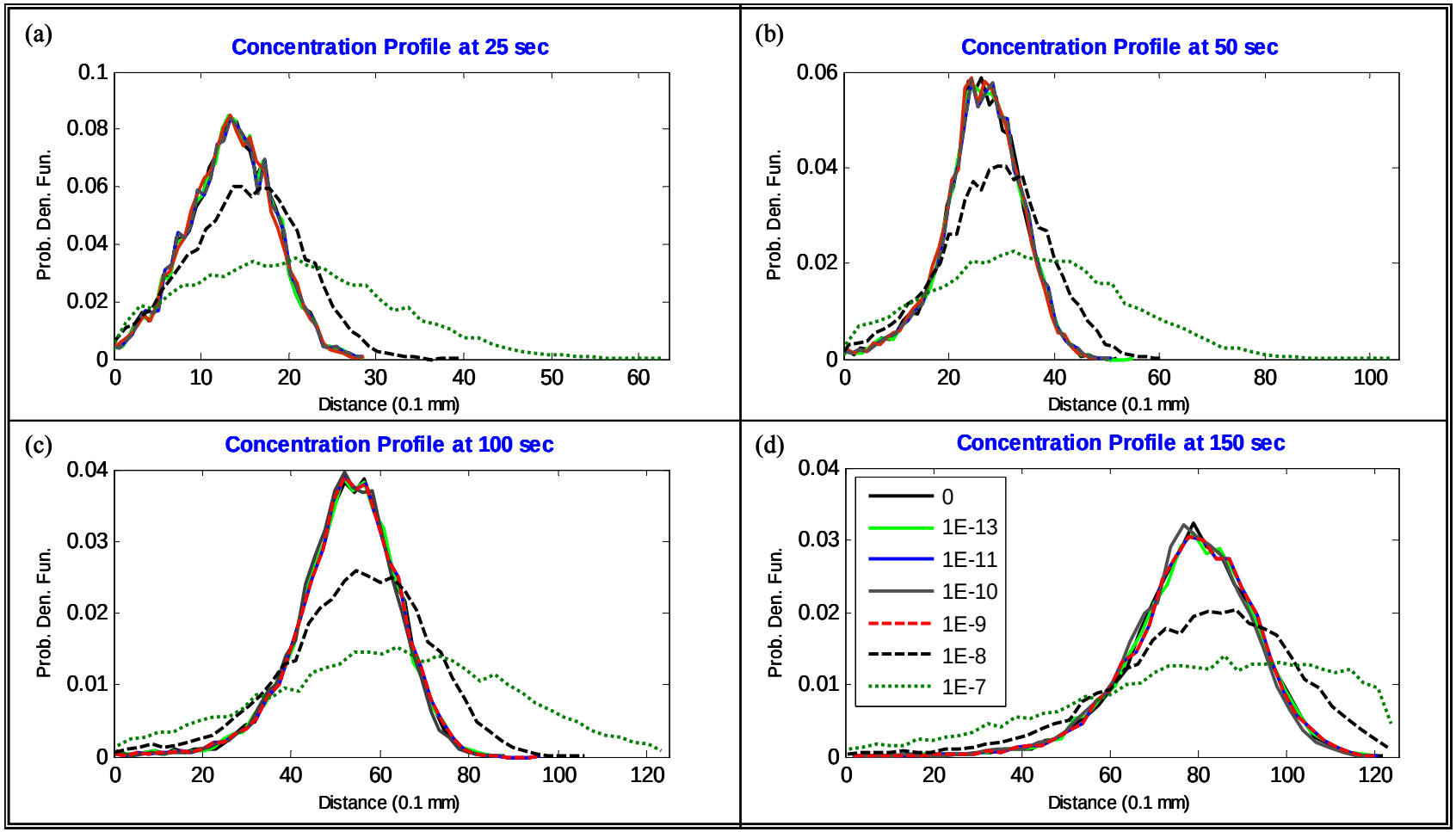

Figure 6.7: Effect of diffusion on spatial statistics of solute particles for the plug flow profile in bonds. Diffusion has negligible impact on the particle statistics unless its magnitude becomes significant compared to the mechanical dispersion. All diffusion coefficients shown in the legend are in m^2/s.

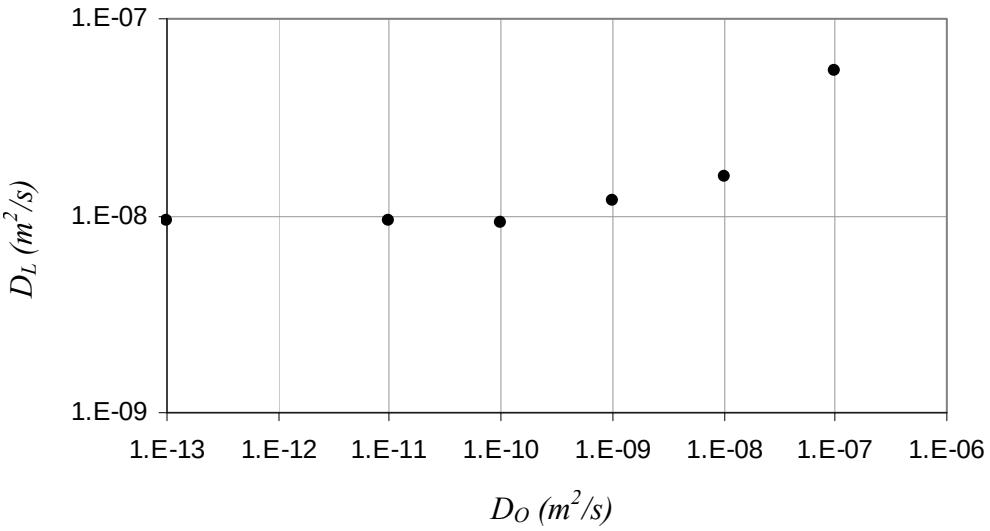

Figure 6.8: Variation of dispersion coefficient vs. diffusion coefficient for the plug flow velocity profile in bonds in a physically representative network. Dispersion coefficient does not change with diffusion unless diffusion becomes significant in magnitude compared to mechanical dispersion.

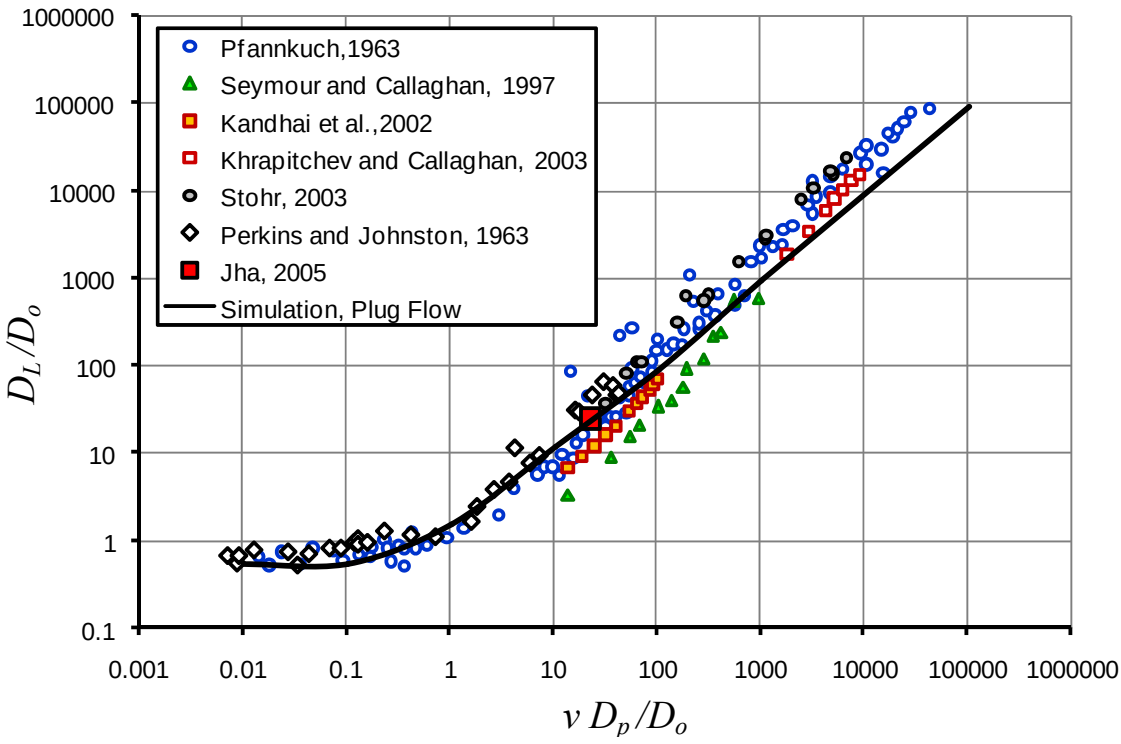

Figure 6.9: Comparison of simulated dimensionless dispersion coefficient with plug flow in bonds in a physically representative network of bead pack (bead radius = 2.1918×10^{-4} m) and experimental data in the literature.

Figure 6.9 shows that our a priori prediction of the dimensionless dispersion coefficient vs. pore scale Peclet number agrees closely with the experimental data from the literature. However, it does not get the scaling of dimensionless dispersion coefficient vs. pore scale Peclet number right for high Peclet numbers.

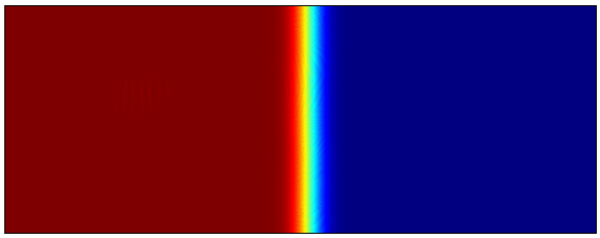

Figure 6.10: Effect of diffusion in case of plug flow in a bond. Diffusion acts independently of velocity.

The prediction shown in Figure 6.9 assumes plug flow within the network bonds. In the case of plug flow profile, there is no stretching of the solute front in the bonds. Therefore, velocity has no impact on diffusion (Figure 6.10). Diffusion acts independently of mechanical dispersion (convective spreading). Therefore, in this case the dispersion coefficient is just a sum of pure mechanical dispersion and diffusion. We get a linear dependence of dimensionless dispersion coefficient on pore scale Peclet number (for higher Peclet numbers) whereas the experimental data suggests a power law relationship between the two with the power law coefficient in the range of 1.1-1.3.

6.5 ANALYTICAL EXPRESSION FOR DISPERSION COEFFICIENT

We show a simple expression can accurately reproduce the simulation results. For network flow calculations we have:

Average interstitial fluid velocity $v = 5.12 \times 10^{-5} m/s$,

characteristic length $D_p = 2.06 \times 10^{-4} m$ and

tortuosity $\tau = 1.7$ (obtained in equation 6.1).

In the absence of molecular diffusion hydrodynamic dispersion is totally because of convective spreading (mechanical mixing) and we determined mechanical dispersion coefficient

$D_{mech} = 9.25 \times 10^{-9} m^2/s$.

Next we calculate the dispersion coefficient in the presence of diffusion for a broad range of Peclet numbers using the expression:

$D_L = \frac{D_o}{\tau} + D_{mech}$. This is applicable for plug flow in the bonds of a network.
Convective spreading increases linearly with the particle size and fluid velocity

$$\frac{D_{mech}}{v D_p} = \frac{9.25 \times 10^{-9}}{(5.12 \times 10^{-5}) \times (2.06 \times 10^{-4})} = 0.877.$$

We can generalize the results for arbitrary particle size and fluid velocities.

$D_{mech} = 0.877 v D_p$.

Therefore,

$$\frac{D_L}{D_o} = \frac{1}{\tau} + \frac{D_{mech}}{D_o},$$

$$\frac{D_L}{D_o} = \frac{1}{\tau} + 0.877 \frac{v D_p}{D_o}.$$

Using this expression we can calculate the dispersion coefficient for unconsolidated porous media for any arbitrary fluid velocity, particle diameter or Peclet number. It says that diffusion and convective spreading in porous media are additive for

plug flow profile in bonds. Their sum determines the dispersion coefficient. Figure 6.11 shows a match of the simulated results with the calculated ones. The two almost overlap with each other.

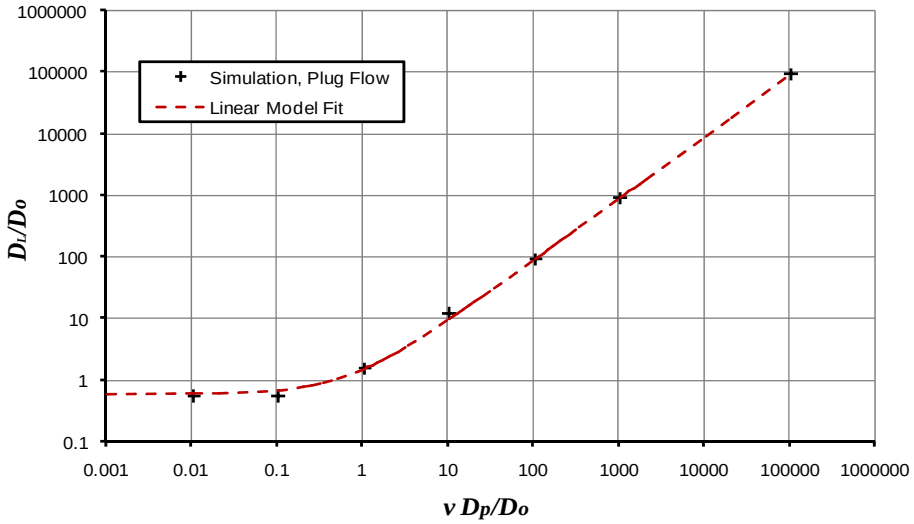

Figure 6.11: Comparison of simulated dispersion coefficient with plug flow in bonds and linear model fit. A close match between the two suggests that the simulated dispersion coefficient is the sum of convective spreading and diffusion.

6.6 PARTICLE TRACKING WITH A PROBABILISTIC CHOICE OF OUT-FLOWING BOND AT PORE BODIES

One of the most common simplifying assumptions made in the particle tracking studies through a network model is a probabilistic choice of the out-flowing bond at pore bodies (bond junctions). A solute particle arrives at a pore body and is assigned to a new bond randomly with a flow rate weighted probability (Bijeljic et al., 2004; Acharya et al., 2004).

Solute transport in the absence of diffusion is a reversible process (Jha et al., 2006). Figure 6.12 shows the effect of flow reversal on dispersion coefficients with a probabilistic sampling of the out-flowing bond with no diffusion. Paths of solute particles are reversed from three different times (equivalently, depths of penetration). It is

evident that with this approach the solute transport is irreversible even without an input diffusion. Backward (echo) dispersion coefficient increases with the depth of penetration of the solute front.

Because of probabilistic rules to randomly pick an out-flowing bond, a solute particle takes a backward path different from the one on which it had arrived. Probabilistic choice of an out-flowing bond at a pore junction introduces an artificial diffusion and makes the solute transport an irreversible process even in the absence of any input diffusion.

Figure 6.13 shows a comparison of dispersion coefficients (plug flow in bonds without diffusion) with probabilistic and deterministic choice of out-flowing bonds at pore junctions. In the probabilistic approach, dispersion does not change much with time (and distance traveled). This is because the probabilistic approach does not account for local correlation of the pore structure. The asymptotic dispersion coefficients with the probabilistic approach are smaller than that obtained with the deterministic approach for the same reason.

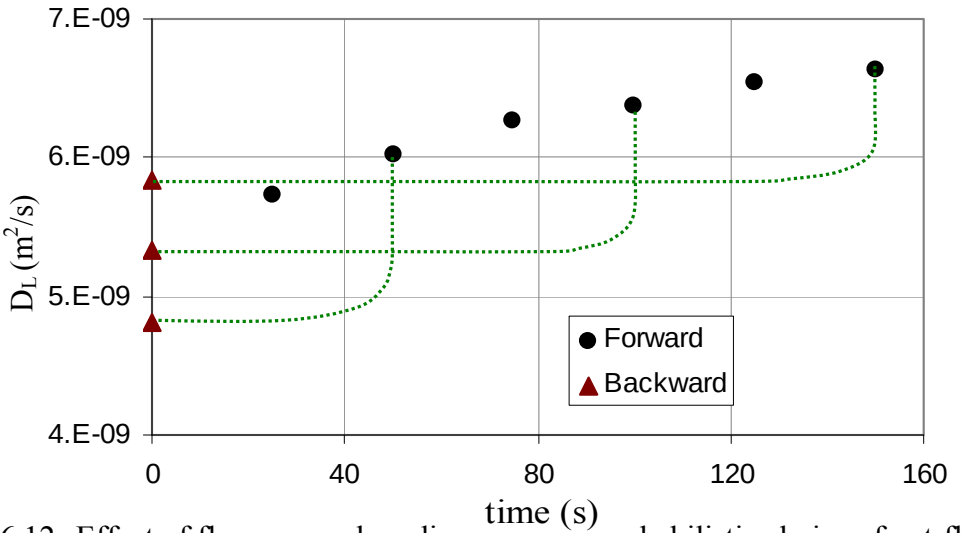

Figure 6.12: Effect of flow reversal on dispersion for probabilistic choice of out-flowing bond. Probabilistic rules introduce an artificial diffusion. Dispersion is an irreversible process even when input diffusion is zero.

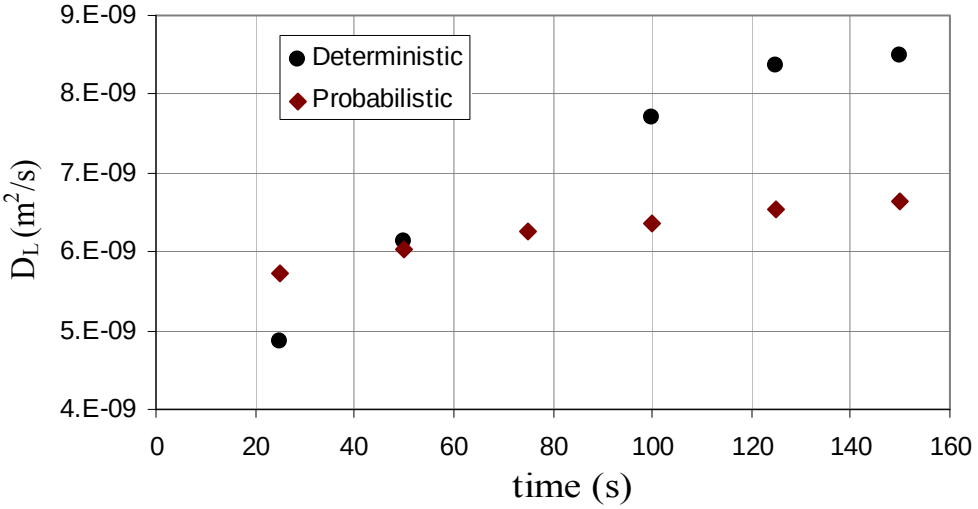

Figure 6.13: Comparison of dispersion without diffusion (assuming plug flow in bonds) with probabilistic and deterministic choice of out-flowing bonds at a pore junction.

This shows the importance of having deterministic rules for choosing an out-flowing bond at a pore body.

6.7 SIMULATION WITH A PARABOLIC VELOCITY PROFILE IN BONDS

A plug flow profile in the bonds creates a linear dependence between dispersion coefficient and the pore scale Peclet number. It is known from Taylor-Aris dispersion in straight capillary tubes that the combination between molecular diffusion and a cross sectional parabolic velocity profile results in a quadratic dependence of D_L on mean flow velocity. This suggests the possibility that in a porous medium the experimentally observed mild non-linear dependence of the longitudinal dispersion coefficient arises from a combination of mechanical dispersion and Taylor's dispersion in individual bonds (Sahimi et al., 1986).

The velocity gradient in a bond allows interaction between convection and diffusion. Now the solute front in the bond stretches as it travels and diffusion becomes a more effective mixing mechanism. Now velocity influences dispersion through a bond, and the dispersion coefficient will not simply be the summation of mechanical dispersion and diffusion.

To test this expectation, we carried out physically representative network simulation with a parabolic velocity profile in the network bonds. Because of the increased area of contact between regions of high and low solute concentrations, mixing inside the bonds is enhanced. This leads to a Taylor like dispersion in bonds.

Figure 6.14 shows a comparison of simulated dimensionless dispersion coefficients with the experimental data. We get an excellent match for the whole range of Peclet numbers. This is an a priori quantitative prediction of dispersion coefficients in a dense, random packing of spheres.

We conclude that the essential phenomena giving rise to hydrodynamic dispersion observed in porous media are (i) stream splitting of the solute front at every pore, thus causing independence of particle velocities purely by convection, (ii) a velocity gradient within throats and (iii) diffusion. Taylor's dispersion in a capillary tube accounts for only the second and third of these phenomena, yielding a quadratic dependence of dispersion on Peclet number. Plug flow in the bonds of a physically representative network accounts for the only the first and third phenomena, resulting in a linear dependence of dispersion upon Peclet number.

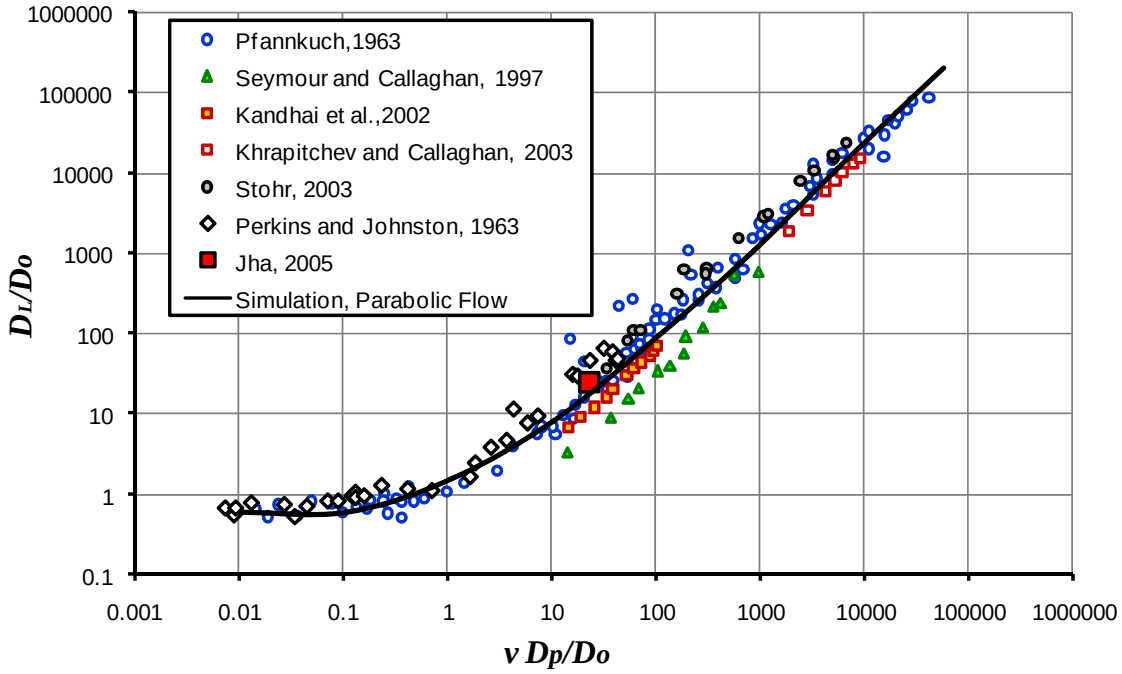

Figure 6.14: Comparison of simulated dimensionless dispersion coefficient with parabolic flow in bonds and the literature experimental data. The simulated data matches quantitatively with the experimental data for all range of Peclet numbers.

From curve fitting, we get

$$\frac{D_L}{D_o} = \frac{1}{\tau} + 0.282\left(\frac{v\,D_p}{D_o}\right)^{1.229} .$$

We get a power law coefficient of 1.229. Figure 6.15 shows a match of simulated data with the power law relationship.

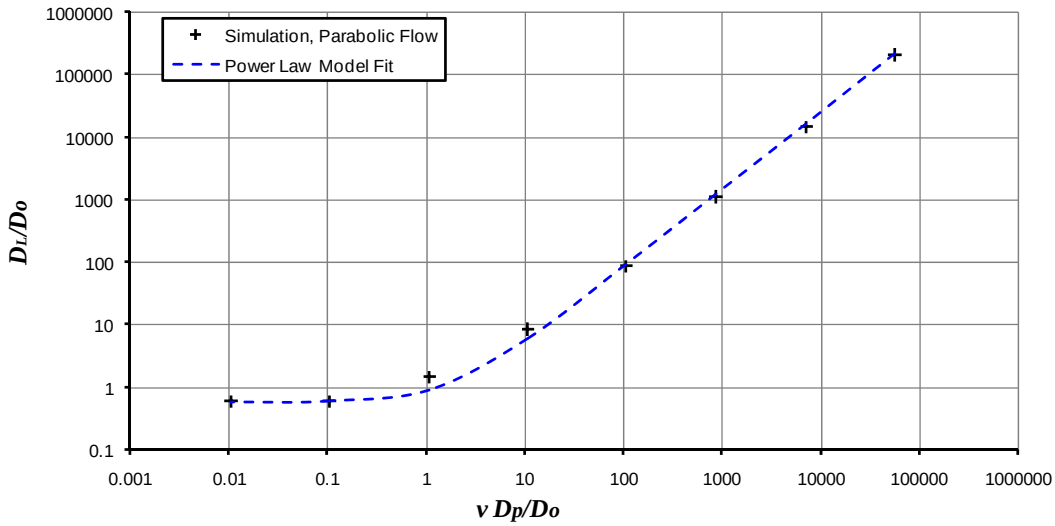

Figure 6.15: Comparison of the simulated dispersion coefficients using a parabolic velocity profile in bonds with a power law model fit.

6.8 CONVECTIVE SPREADING WITH PARABOLIC VELOCITY PROFILE IN BONDS

We investigate the interaction of convection and dispersion more closely. Figure 6.16 shows particle statistics for parabolic flow through the network with no diffusion. We can see two peaks in the probability distribution function. The first peak at smaller displacement corresponds to fluid particles located in the slower zone near the wall of the bonds. At longer distances, a second peak appears in the distribution. The second peak corresponds to particles which have traveled a sufficiently large distance to have left the flow channel where they were initially (Lebon et al., 1997). These particles have experienced a wide range of flow velocities and at longer times, the second peak is closer to normal distribution. However, the first peak persists at the longest time observed.

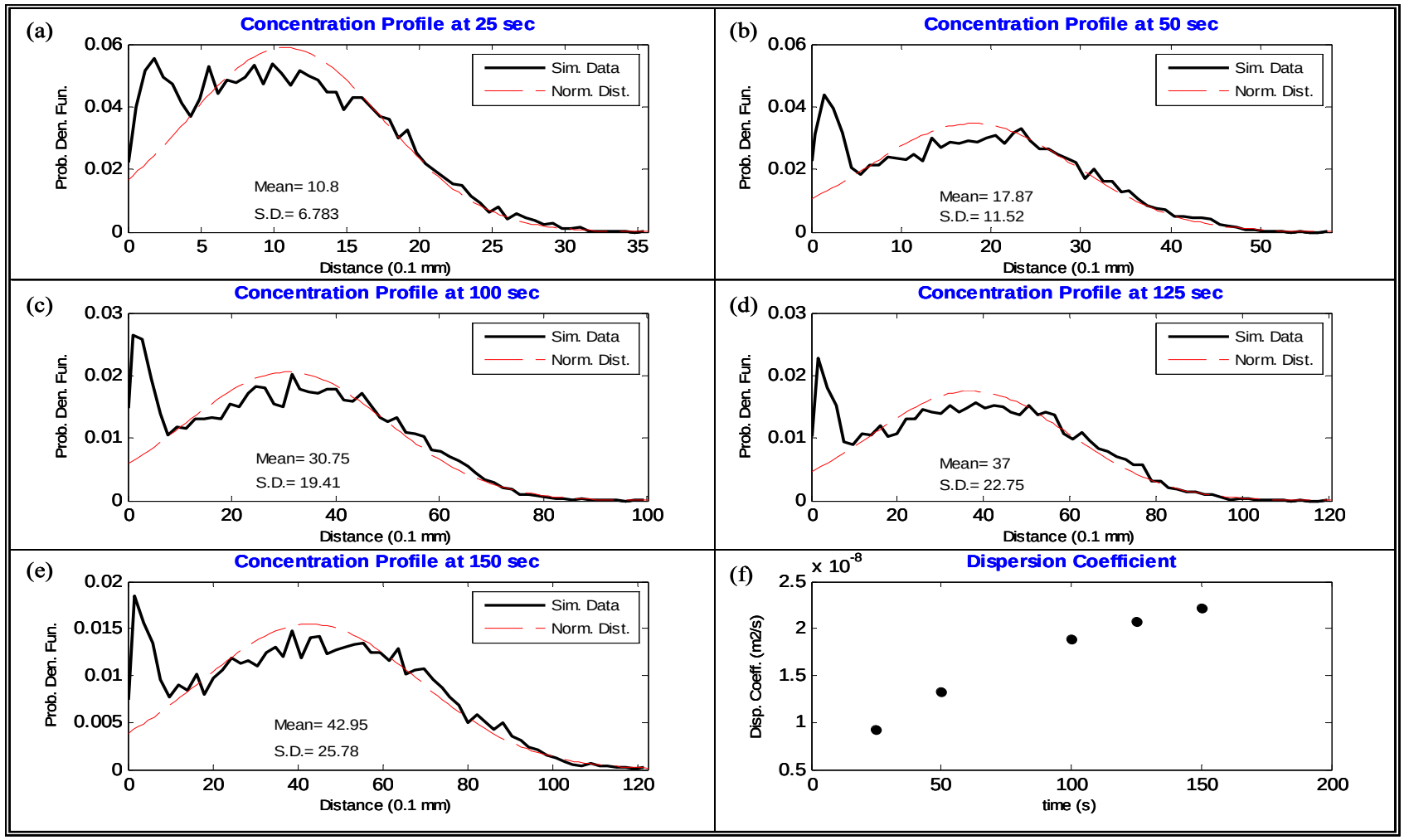

Figure 6.16: (a)-(e) Spatial distribution of solute particles. Parabolic flow is assumed in the network bonds and $D_o = 0\ m^2/s$. The first peak in the distribution corresponds to particles in the slow velocity regions near the pore walls. Other particles that are free to move form a second peak. Dispersion is not Fickian in this case. (f) Dispersion coefficient as evaluated from spatial statistics.

It may be argued that the dispersion coefficient is converging to an asymptotic value. However, as clear from concentration profiles the transport process is not Fickian. An arbitrary stochastic velocity field does not necessarily lead to a Fickian mechanical dispersion. Since the velocity field contains regions of zero velocity, solute particles in these regions can reach the rest of the pore space by convection alone. Particles in these regions cannot have any random velocity from the velocity distribution. Therefore, the central limit theorem is not applicable and dispersion coefficient is not defined. The effect of diffusion must be considered for the transport process to become Fickian even in the limit of high Peclet numbers (Koch and Brady, 1985).

Saffman (1959) modeled the microstructure of a porous medium as a network of capillary tubes with random orientation. At high Peclet numbers and at very long times, Saffman found that the dispersion never becomes truly mechanical. The dispersion coefficient grows as *Pe ln (Pe)*. The logarithmic dependence results from the zero velocity of fluid at capillary walls. The time required for a tracer particle to leave a capillary would become infinite as its distance from the walls goes to zero, if molecular diffusion does not allow the tracer to escape the region of low velocity near the wall.

Because network flow is a linear process, when the overall pressure drop is changed the pressure difference between the extremities of each bond of the network changes in proportion and so also do all the velocities, flow rates and transit times. Hence the ratio between flow rates in different bonds that connect to the same node remain unchanged and therefore the mapping rule at the pore junction remains unchanged when the average velocity changes. Consequently the dispersion coefficients are proportional to the mean velocity. Therefore, in the absence of diffusion (or negligible diffusion), the mechanical dispersion scales linearly with velocity (Sahimi et al., 1986).

6.9 EFFECT OF DIFFUSION ON PARTICLE STATISTICS

Figures 6.17-23 show the effect of increasing diffusion on particle statistics for a physically representative network with parabolic velocity profile in the bonds. Even a vanishingly small amount of diffusion of 10^{-13} m^2/s starts moving solute particles from low velocity regions near the wall to high velocity regions. After moving out of this zone, solute particles can sample all the regions of the pore space because of convection. We see that the first peak corresponding to particles in the slow moving region near pore walls starts falling down and almost disappears at 150 seconds. We get a normal distribution of solute particle positions. When diffusion is increased to 10^{-12} m^2/s the first peak completely disappears at 100 seconds and we get a normal distribution of particle positions. With increasing diffusion coefficient the first peak disappears quickly. With time for any given diffusion coefficient the relative area of the first peak decreases while the second one gets bigger.

This is similar to what Lebon et al. (1997) showed experimentally. They studied dispersion at short times using a PFG-NMR technique. At short times, the local displacement was found to be proportional to the local velocity component along the magnetic field gradient. At mean displacements larger than 5 bead diameters, the displacement distribution was found to be Gaussian. At intermediate displacements, this distribution displayed two peaks.

At very high diffusion coefficients (10^{-7} m^2/s) our velocity weighted rule for deciding an out-flowing bond is not appropriate as described in the case of plug flow. Therefore, we see a deviation from a normal distribution in particle statistics at longer times.

Figure 6.24 shows a comparison of the solute concentration profiles for diffusion coefficients ranging from zero to 10^{-7} m^2/s. For zero diffusion there is a wide range of

particle positions because of a velocity gradient in the bonds. As diffusion is increased solute particles move in the radial direction in the bonds and effect of velocity gradient in bonds is reduced. This reduces the spread in solute particle positions and therefore dispersion coefficient is reduced. This trend continues with increasing diffusion and reverses when magnitude of diffusion coefficient becomes large as compared to the mechanical dispersion. As shown in Figure 6.25, the dispersion coefficient vs. diffusion coefficient plot goes through a minimum (Jha et al., 2008).

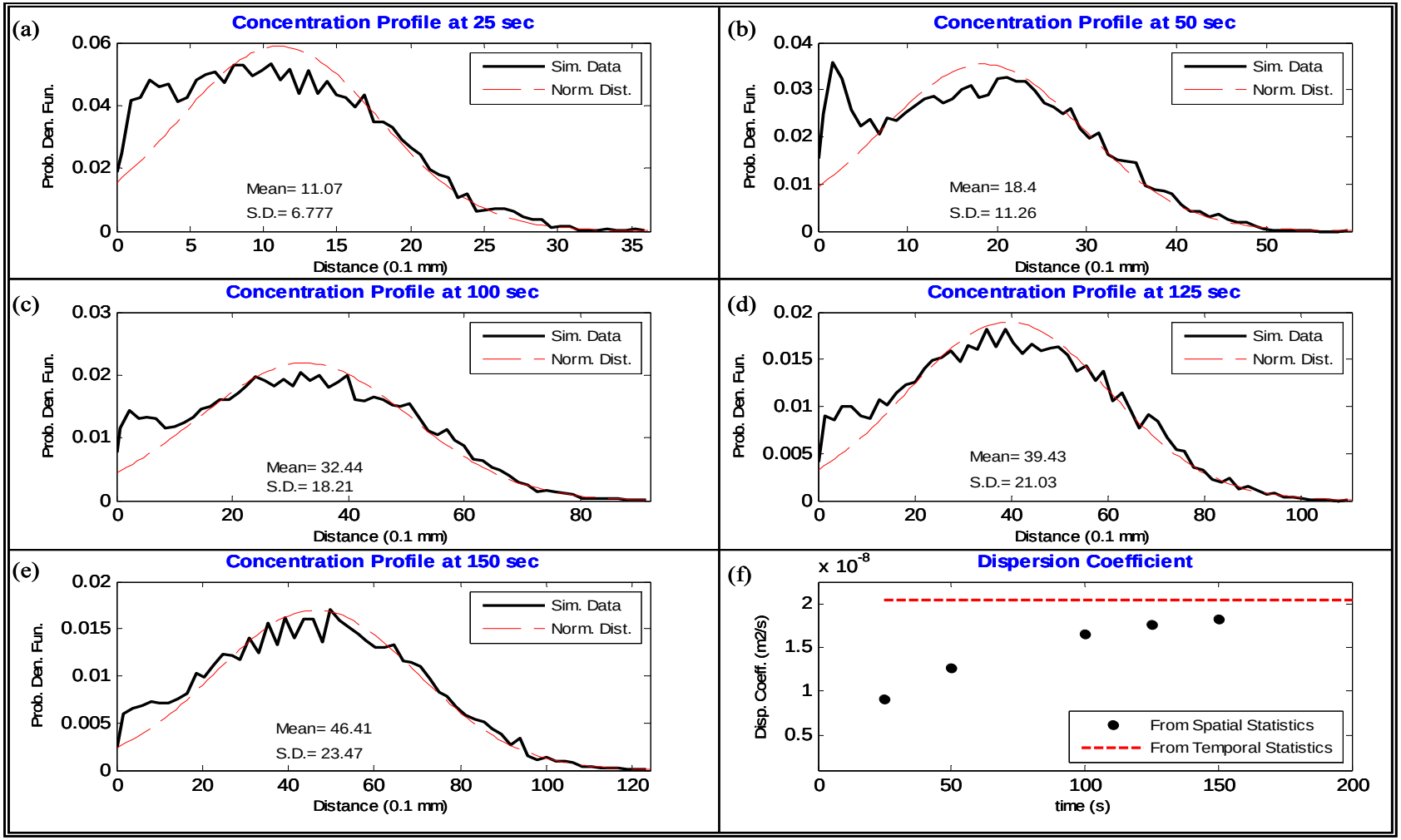

Figure 6.17: (a)-(e) Scanned spatial distribution of solute particles. Parabolic flow is assumed in the network bonds and $D_o = 10^{-13}$ m^2/s. The first peak which corresponds to particles in the slow velocity regions near the pore walls starts falling because of diffusion. Dispersion becomes Fickian at large times. (f) Dispersion coefficient as evaluated from spatial statistics.

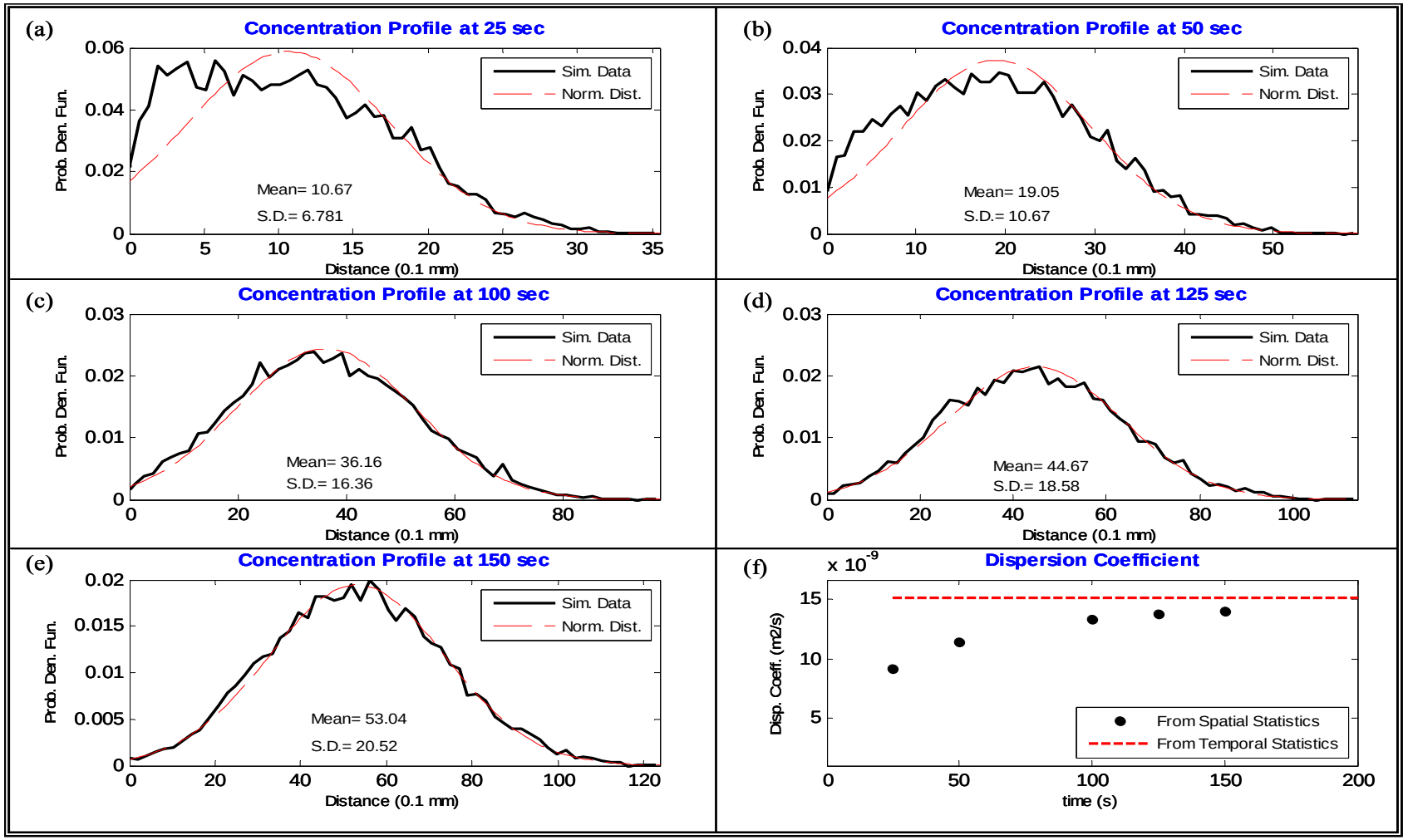

Figure 6.18: (a)-(e) Scanned spatial distribution of solute particles. Parabolic flow is assumed in network bonds and $D_o = 10^{-12}\ m^2/s$. The first peak corresponding to particles in the slow velocity regions near the pore walls disappears quicker for larger diffusion. (f) Dispersion coefficient as evaluated from spatial statistics.

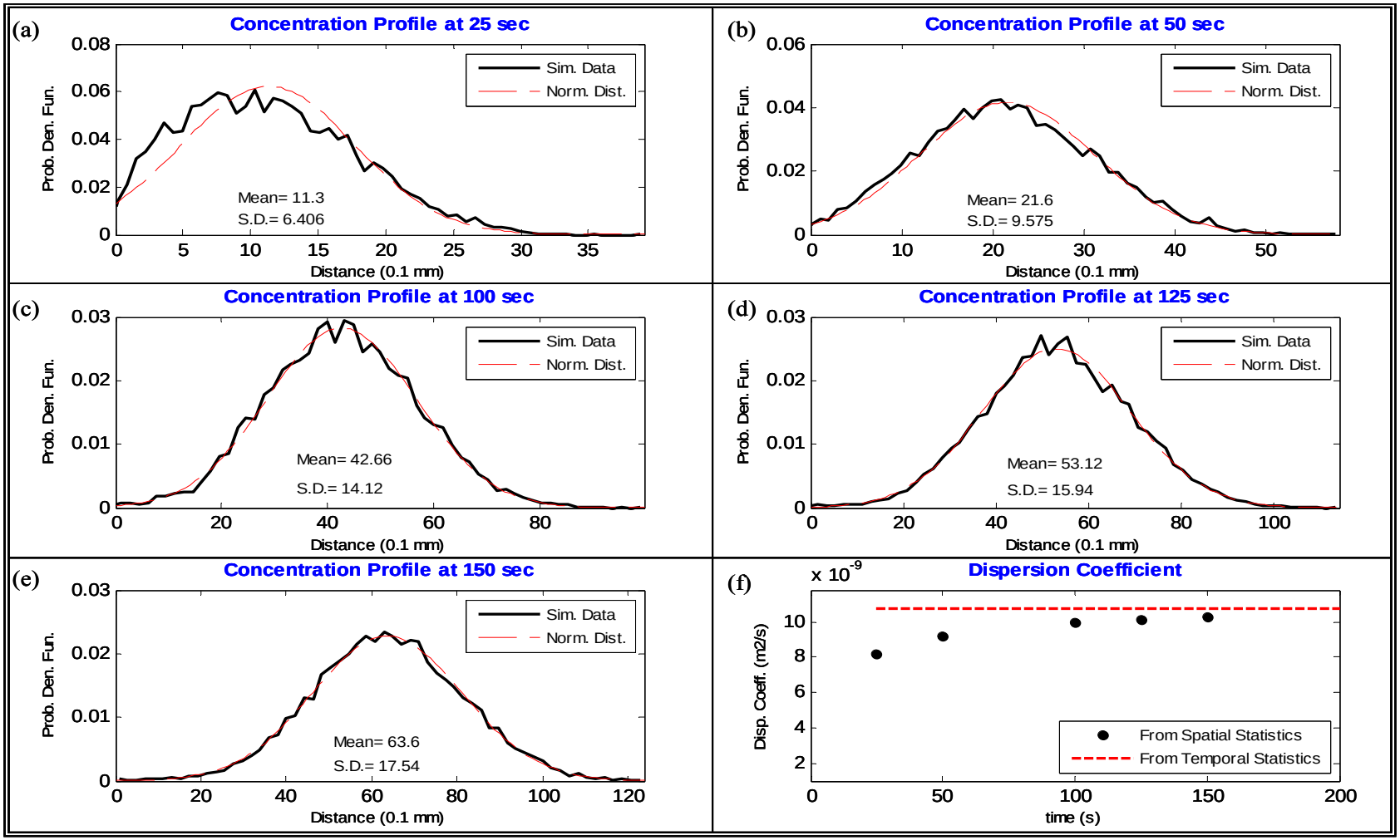

Figure 6.19: (a)-(e) Scanned spatial distribution of solute particles. Parabolic flow is assumed in network bonds and $D_o = 10^{-11}\ m^2/s$. The first peak corresponding to particles in the slow velocity regions near the pore walls disappears quicker for larger diffusion. (f) Dispersion coefficient as evaluated from spatial statistics.

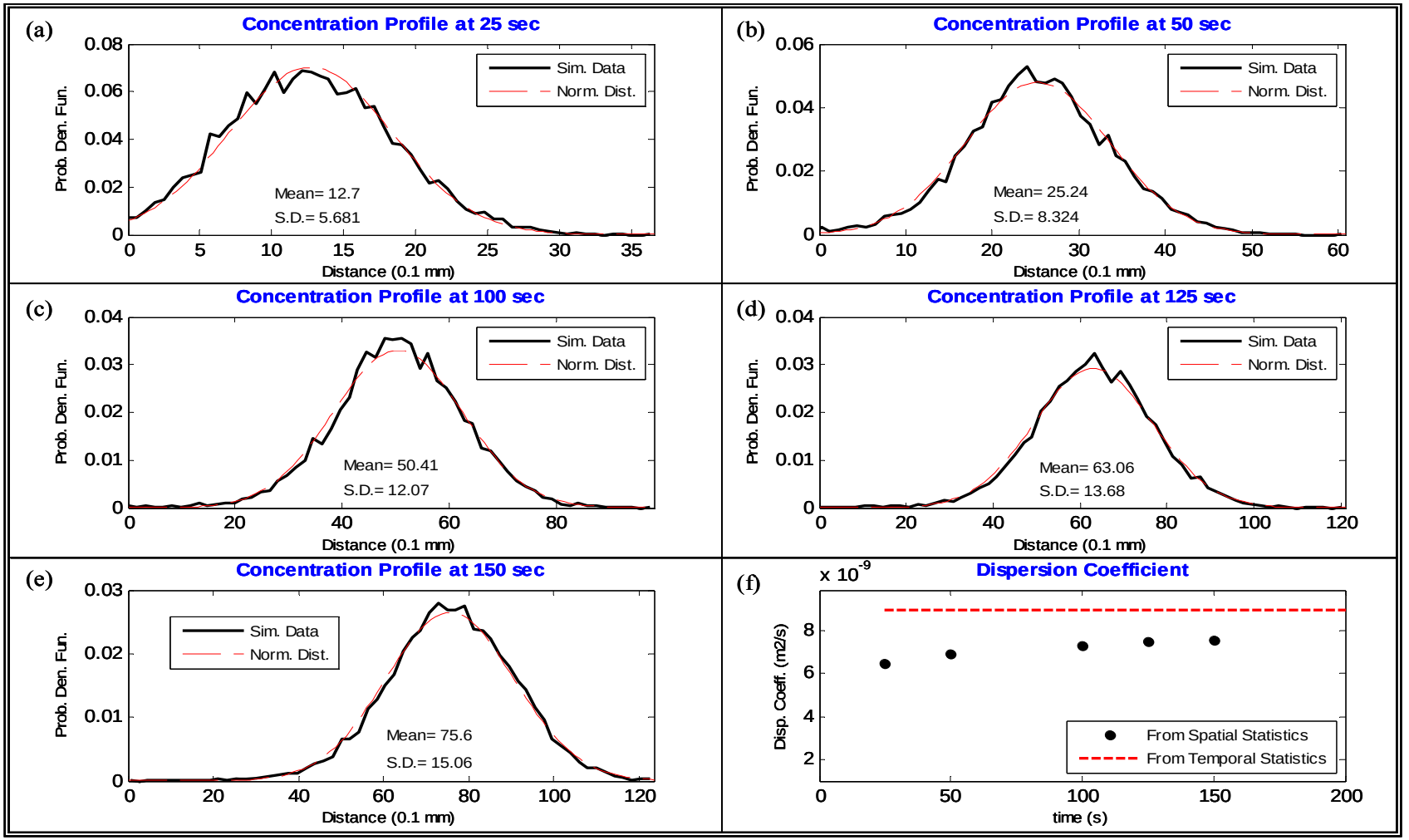

Figure 6.20: (a)-(e) Scanned spatial distribution of solute particles. Parabolic flow is assumed in the network bonds and $D_o = 10^{-10}$ m^2/s. (f) Dispersion coefficient as evaluated from spatial statistics.

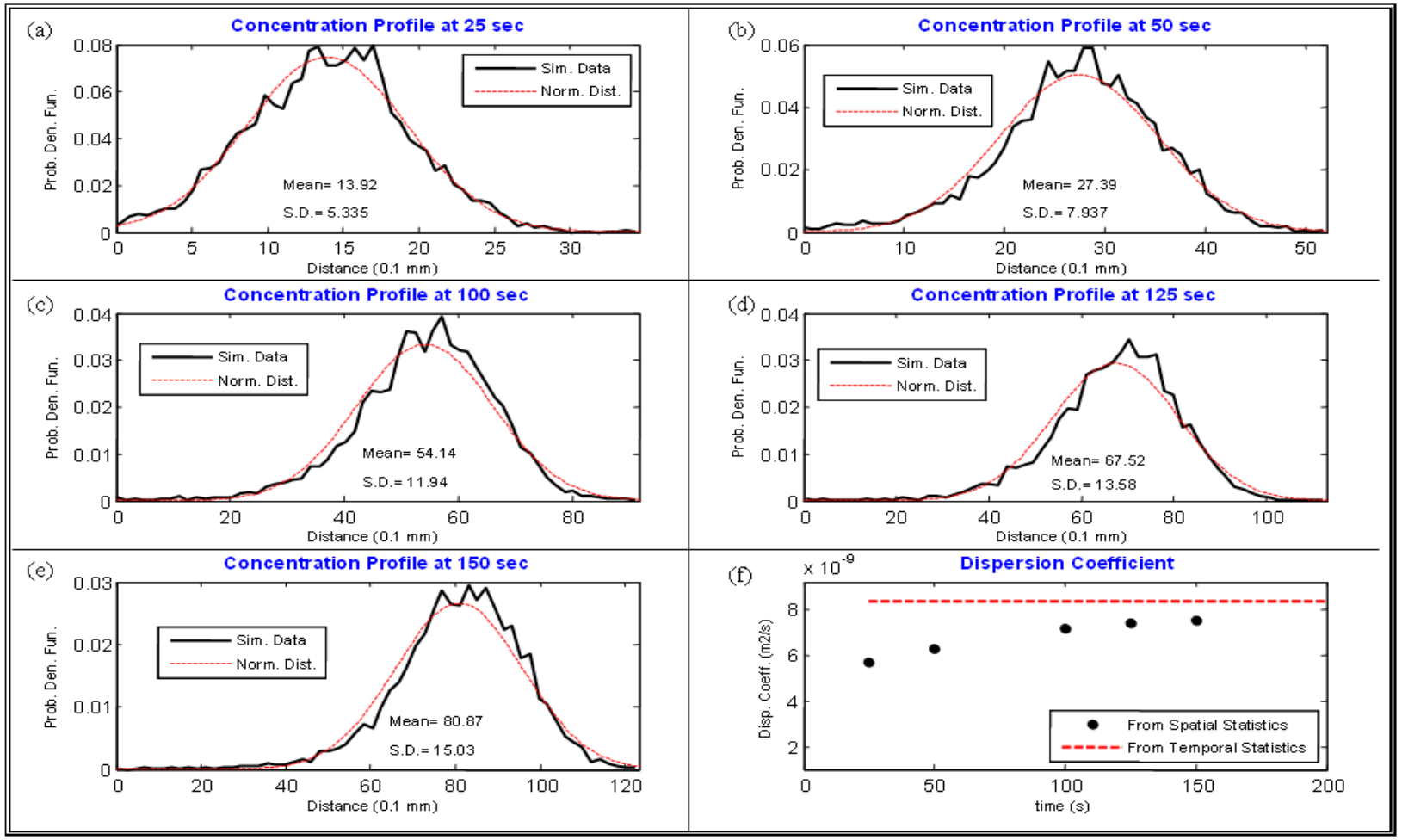

Figure 6.21: (a)-(e) Scanned spatial distribution of solute particles. Parabolic flow is assumed in network bonds and $D_o = 10^{-9}\ m^2/s$. (f) Dispersion coefficient as evaluated from spatial statistics.

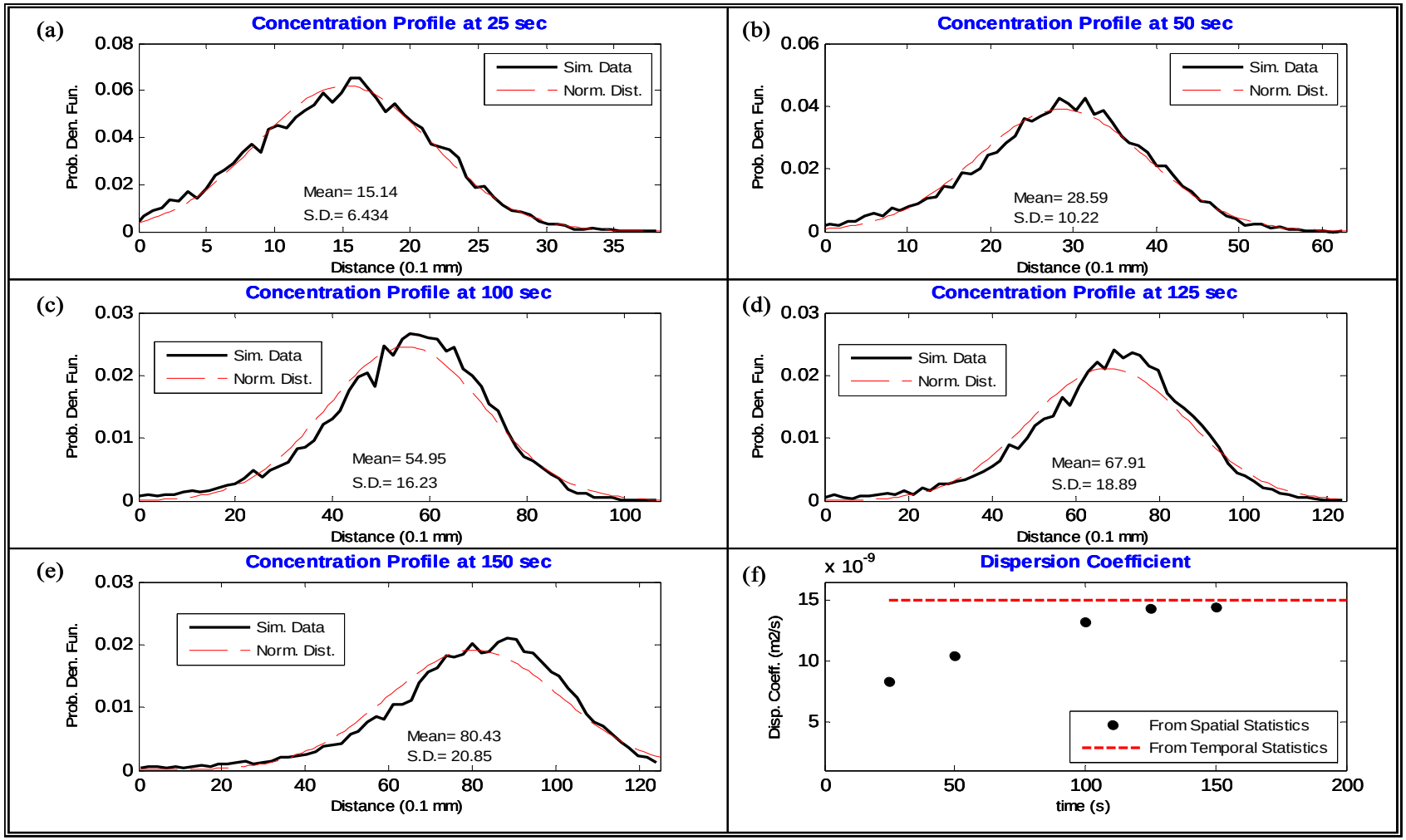

Figure 6.22: (a)-(e) Scanned spatial distribution of solute particles. Parabolic flow is assumed in network bonds and $D_o = 10^{-8}\ m^2/s$. (f) Dispersion coefficient as evaluated from spatial statistics.

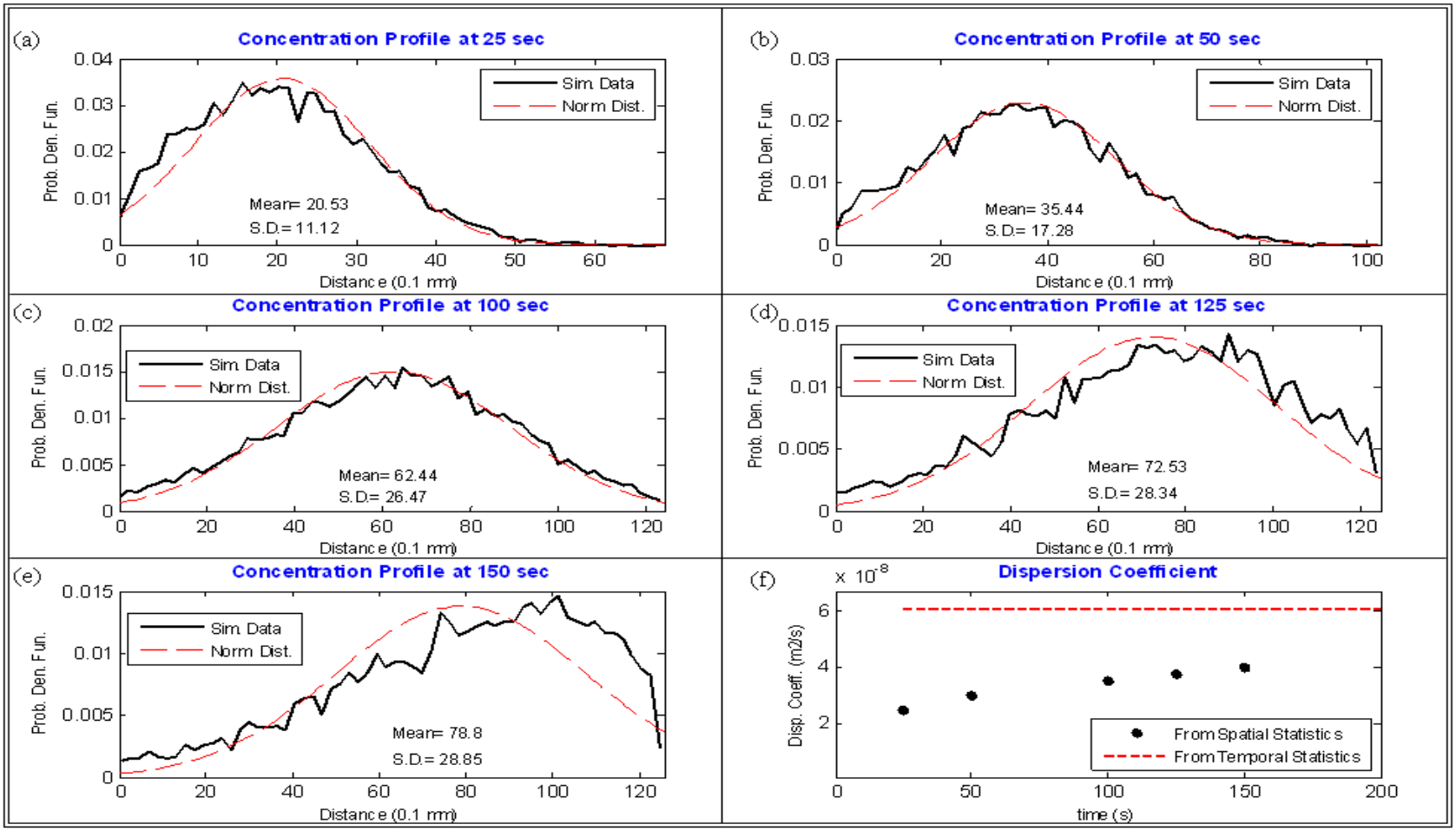

Figure 6.23: (a)-(e) Scanned spatial distribution of solute particles. Parabolic flow is assumed in network bonds and $D_o = 10^{-7}\ m^2/s$. At high diffusion coefficient, some solute particles enter bonds with low velocities and get stuck there for long times. Particle distribution starts deviating from normal at longer times. (f) Dispersion coefficient as evaluated from spatial statistics.

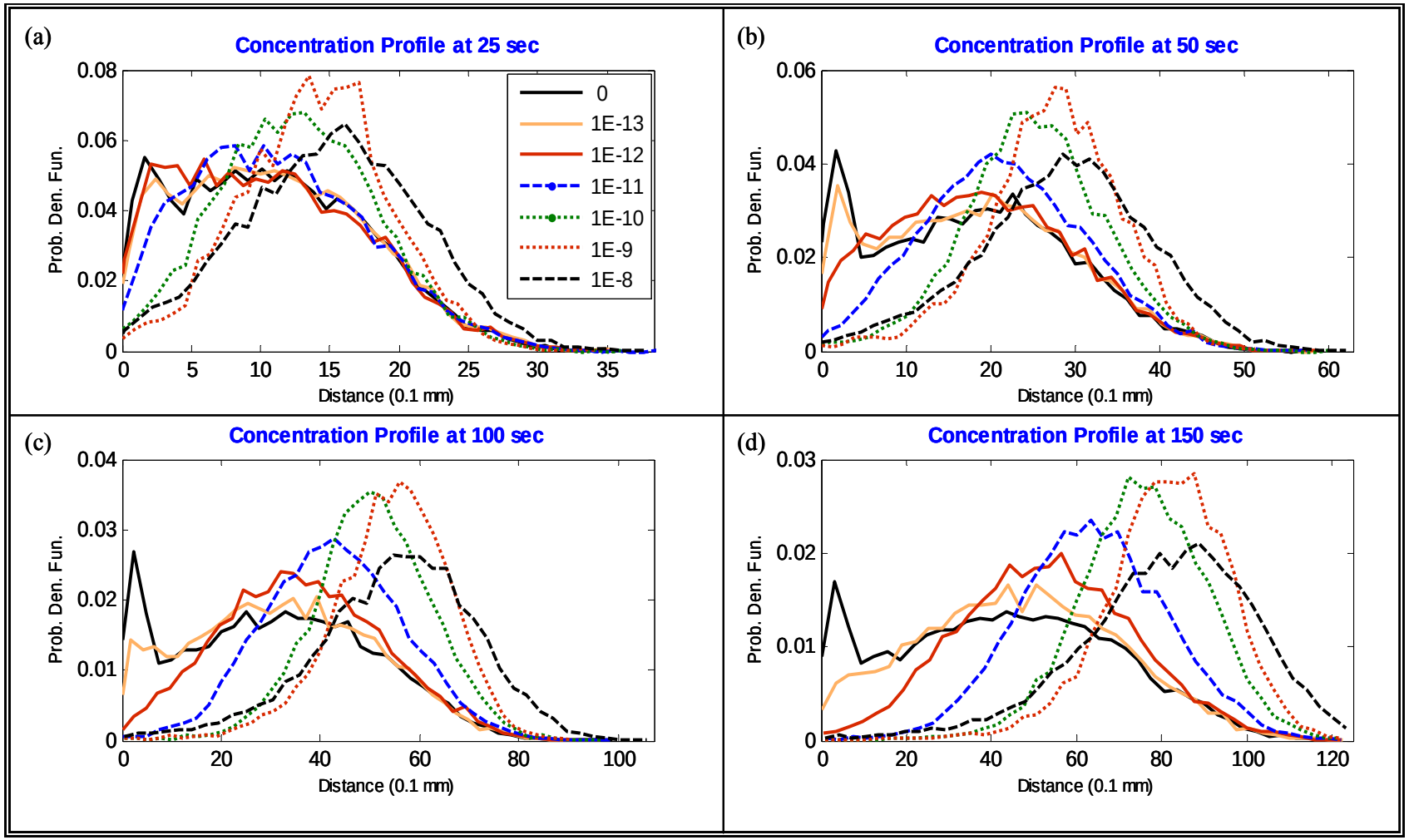

Figure 6.24: Effect of diffusion on spatial statistics of solute particles for parabolic velocity profile in bonds.

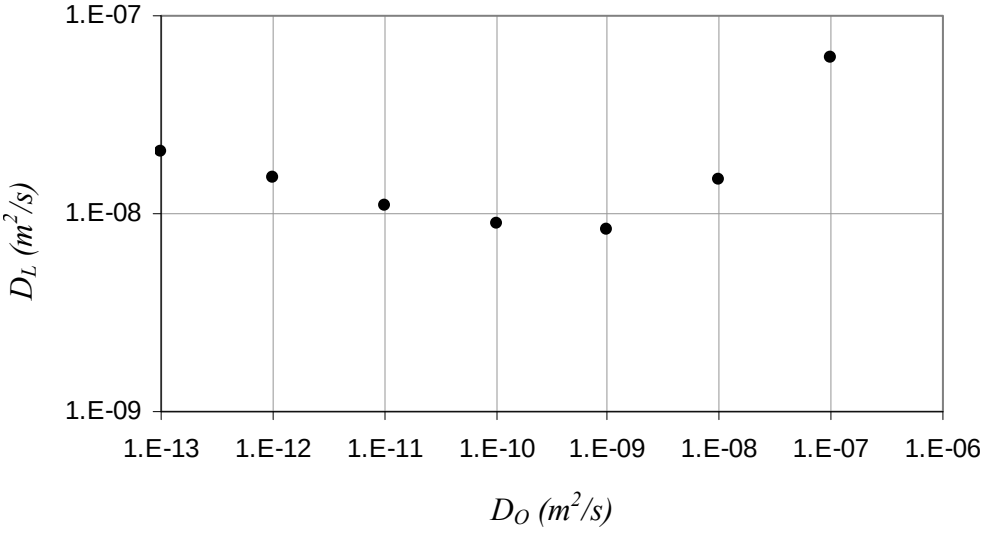

Figure 6.25: Variation of asymptotic dispersion coefficient vs. diffusion coefficient for parabolic velocity profile in bonds. Dispersion coefficient decreases with diffusion unless diffusion becomes significant in magnitude as compared to mechanical dispersion.

6.10 DISCUSSION

Dispersion in porous media results from an interaction between mechanical dispersion and diffusion. Purely mechanical dispersion that occurs at high Peclet numbers due to a stochastic velocity field alone grows like *Pe*. However, the purely mechanical analysis is not valid in the region of zero velocity.

The region of zero velocity near the bed particles gives rise to non-mechanical dispersion mechanisms that dominate the longitudinal diffusivity at high Peclet numbers. Non-mechanical dispersion arises when a solute molecule cannot sample all points within the pore space by convection alone. Non-mechanical dispersion arises from a diffusive boundary layer near the solid surfaces and from regions of closed streamlines

respectively and they grow as *Pe ln (Pe)* and Pe^2 respectively (Koch and Brady, 1985). The solute can escape the region of closed streamlines or the particle surface by molecular diffusion only.

A plug flow velocity profile does not have regions of zero velocity. Therefore, non-mechanical dispersion is absent and dispersion scales linearly with *Pe*. However, in the case of parabolic velocity profiles in network bonds there are regions of no-flow velocity near pore-walls. Therefore, we get a non-mechanical dispersion which becomes important at high Peclet numbers and results in a mild non-linear dependence of the dispersion coefficient on Peclet number.

In random bead packs a single, deterministic, streamline encounters a wide range of velocities. Here diffusion is important to transport solute particles from regions near the walls. Subsequently, mechanical mixing can ensure that a solute particle's displacements are independent, identically distributed and random. Mechanical mixing is the main mixing mechanism and we get a mild non-linear dependence of D_L on *Pe* (Duplay and Sen, 2004).

This is not the case in flow in a capillary tube or periodic porous media where mechanical mixing is absent and diffusion is solely responsible for ensuring that a solute particle encounters a wide range of velocities and D_L scales with Pe^2. We investigate this in more detail in the next chapter.

6.11 FLOW REVERSAL STUDIES

We carried out-flow reversal studies in the physically representative network. The direction of flow is reversed just before any solute particle could exit the medium.

The following figures show the results of reversing the direction of fluid flow for two different diffusion coefficients. In each case, the direction of flow is reversed from three different times.

For small diffusion of 10^{-13} m^2/s the flow is largely reversible for small times of reversal (or equivalently, depths of penetration). For larger depths of penetration mixing due to diffusion is increased and the flow becomes more irreversible. However, for this small diffusion, mixing is not completely reversible even for the largest depth of penetration investigated (Figure 6.26).

When diffusion is increased, mixing is enhanced and even from smaller depth of penetration we get greater irreversibility (Jha et al., 2006). For a diffusion of 10^{-10} m^2/s mixing becomes completely irreversible when flow is reversed at 150 s (Figure 6.27).

The mechanism and irreversibility of mixing has been already explained in the third chapter.

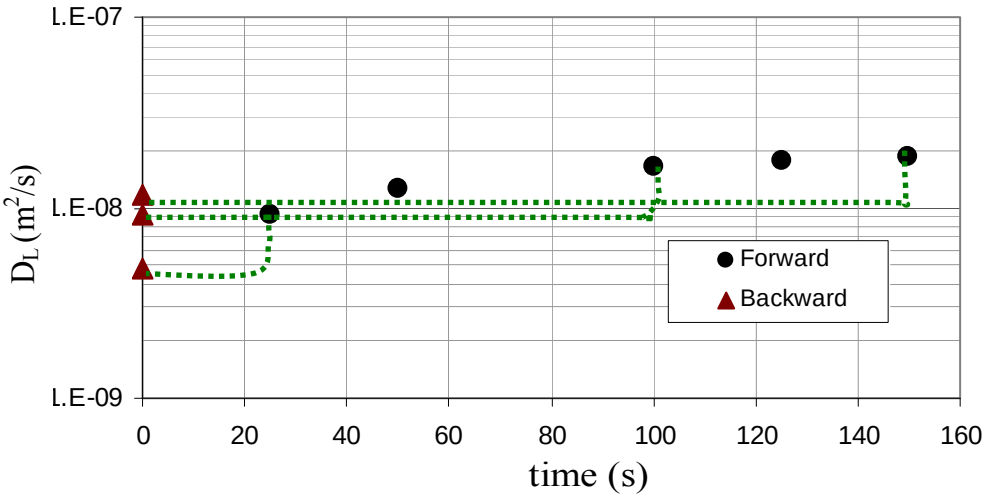

Figure 6.26: Effect of flow reversal on dispersion for D_o=10^{-13} m^2/s. Irreversibility of dispersion increases with residence time in the medium.

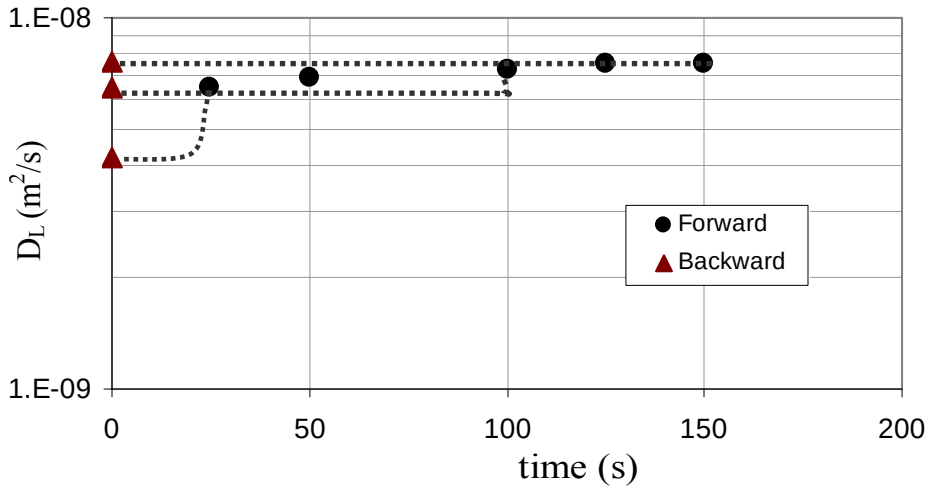

Figure 6.27: Effect of flow reversal on dispersion for $D_o=10^{-10}$ m^2/s. Greater diffusion enhances mixing and results in greater irreversibility of dispersion.

SUMMARY AND CONCLUSIONS

We construct a pore-level model of single-phase solute transport that has three key features: (i) splitting of solute swarms at every pore body (ii) velocity gradient within pore throats and (iii) diffusion. Particle tracking produces the particle positions at every time from which statistics and subsequently dispersion can be inferred. The flow field is obtained from physically representative network model of a model sediment, a dense random packing of equal spheres. We introduce mechanistic (non-stochastic) rules to determine the bond through which a particle exits a pore. The rules are essentially geometric and depend on the network flow field (rates in individual bonds and the local configuration of inlet and outlet bonds at each pore body). They enable us to attribute the contribution of convective spreading to core-scale dispersion without requiring a detailed (sub-pore) solution of the flow field through the porous medium.

The simulations provide *a priori* (no adjustable parameters) predictions of dispersion coefficient as a function of pore scale Peclet number. The predicted trends match

quantitatively the experimental data found in the literature for a wide range of Peclet numbers, including the well known empirical observation that the scaling exponent has a value of about 1.2. The agreement indicates that the key features of our model correspond to the key physical phenomena causing dispersion in porous media.

The model permits rigorous attribution of the contribution of the phenomena individually, and of the interaction between combinations of phenomena. Fickian behavior of solute transport is asymptotically observed when solute particles' displacements are independent, identically distributed and random. In the limiting case of a plug-flow velocity profile in network bonds, Fickian behavior can occur without diffusion. However, this is entirely reversible. Convective spreading and diffusion act independently of each other and dispersion coefficient is the sum of the two. In the more realistic case of parabolic velocity profile in bonds, purely convective (i.e. no diffusion) spreading is not asymptotically Fickian. Diffusion is required to move solute particles from low velocity regions near pore walls. Subsequently, stream splitting is responsible for independent, random movement of solute particles and causing Fickian behavior.

In the absence of diffusion, convective spreading in porous media results in a linear dependence of D_L on Pe. Interaction between convective spreading and diffusion results in a weak non-linear dependence of D_L on Pe, in agreement with the experimental observations.

REFERENCES

1. Acharya, R. C., van Dijke, M. I. J., Sorbie, K. S., Van der Zee, S. E. A. T. M. and Leijnse, A.: "Quantification of dispersion by upscaling Brownian motion of tracer

displacement in a 3D pore-scale network model", Advances in Water Resources, 30 (2), 199 – 213, (2007).

2. Bear, Jacob: *Dynamics of Fluids in Porous Media*, Elsevier, New York (1972).
3. Bijeljic, B., Muggeridge, A. H. and Blunt, M. J.: "Pore-scale modeling of longitudinal dispersion", Water Resources Research, Vol. 40, W11501 (2004).
4. Bruderer, C. and Y. Bernabe: "Network modeling of dispersion: Transition from Taylor dispersion in homogeneous networks to mechanical dispersion in very heterogeneous ones", Water Resources Research 37(4): 897-908 (2001).
5. Carman, P. C.: "Fluid flow through a granular bed", Trans. Inst. Chem. Eng. London, 15, 150-156 (1937).
6. Cenedese, A. and Viotti, P.: "Lagrangian analysis of nonreactive pollutant dispersion in porous media by means of particle image velocimetry technique", Water Resources Research, 32 (8), 2329-2343, (Aug., 1996).
7. Chandrasekhar, S.: "Stochastic problems in physics and astronomy", Rev. Mod. Phys., 15, 1-89, (1943).
8. Dullien, F. A. L., Porous Media: "*Fluid Transport and Pore Structure*", Academic, San Diego, Calif, (1992).
9. Duplay, R. and Sen, P.N.: "Influence of local geometry and transition to dispersive regime by mechanical mixing in porous media", Physical Review E, 066309, (2004).
10. Frosch, G. P., Tillich, J. E., Haselmeier, R., Holz, M. and Althaus E.: "Probing the pore space of geothermal reservoir sandstones by nuclear magnetic resonance", Geothermics, 29(6), 671– 687 (2000).

11. Gist, G. A., Thompson, A. H., Katz, A. J. and Higgins R. L. :"Hydrodynamic dispersion and pore geometry in consolidated rock", Phys. Fluids A, 2(9), 1533–1544, (1990).
12. Jha, R. K.: *Pore Level Investigation of Dispersivity*, MS Thesis, The University of Texas at Austin, (May, 2005).
13. Jha, R.K., John, A. K., Bryant, S. L. and Lake L. W.: "Flow reversal and mixing", SPE 103054 presented at SPE ATCE held at San Antonio, Texas, (Sep. 2006). To be published in SPE Journal (Sep., 2008).
14. Jha, R.K., Bryant, S. L. and Lake L. W.: "Influence of local mixing on core scale mixing", SPE 115961 to be presented at SPE ATCE held at Denver, Colorado, (Sep. 2008).
15. Kandhai, D., Hlushkou, D., Hoekstra, A. G., Sloot, P. M. A.,. Van As, H. and Tallarek U.: "Influence of stagnant zones on transient and asymptotic dispersion in macroscopically homogeneous porous media", Phys. Rev. Lett., 88(23), (2002).
16. Khrapitchev, A. A. and Callaghan, P. T.: "Reversible and irreversible dispersion in a porous medium", Phys. Fluids, 15(9), 2649– 2660, (2003).
17. Koch, D. L. and Brady, J. F.: "Dispersion in fixed beds", J. Fluid Mech., 154, 399-427, (1985).
18. Koch, D. L. and Brady, J. F.: "A non-local description of advection-diffusion with application to dispersion in porous media", J. Fluid Mech., 180, 387-403, (1987).
19. Lebon, L., Leblond, J. and Hulin, J. P.: "Experimental measurement of dispersion processes at short times using a pulsed gradient NMR technique", Physics of Fluids, 9(3), 481-490, (Mar., 1997).

20. Legatski, M. W. and Katz, D. L.:" Dispersion coefficients for gases flowing in consolidated porous media", SPE Journal, 7, 43–53, (1967).

21. Manz, B., Alexander, P. and Gladden, L.F.: "Correlations between dispersion and structure in porous media probed by nuclear magnetic resonance", Physics of Fluids, 11(2), 259-267, (Feb., 1999).

22. Moroni, M. and Cushman, J. H.: "Three dimensional particle tracking velocimetry studies of the transition from pore dispersion to Fickian dispersion for homogeneous porous media", Water Resources Research, 37(4), 873-884, (Apr., 2001).

23. Perkins, T. K. and Johnston, O. C.: "A Review of Diffusion and Dispersion in Porous Media"**,** SPE 480, SPE Journal, 3(3), 70-84 (Mar., 1963).

24. Pfannkuch, H. O.: "Contribution a l' etude des deplacements de fluiedes miscibles dans un milieu poreux", Rev. Inst. Fr. Pet., 18, 215–270,(1963).

25. Saffman, P. G.: "A theory of dispersion in a porous medium", Journal of Fluid Mech., 6, 321-349, (1959).

26. Sahimi, M., Hughes, B.D., Scriven, L. E. and Davis, H. T.:" Dispersion in flow through porous media, I, One-phase flow, *Chem. Eng. Sci*., *41*, 2103–2122, (1986).

27. Seymour, J. D. and Callaghan, P. T.: Generalized approach to NMR analysis of flow and dispersion in porous media, AIChE J., 43, 2096, (1997).

28. Sto¨hr, M.: "*Analysis of flow and transport in refractive index matched porous media*", Ph.D. thesis, Univ. of Heidelberg, Heidelberg, Germany, (2003).

Chapter 7: Effect of Medium Geometry on Dispersion

7.1 INTRODUCTION

Convection through porous media can be thought of as random movement of solute particles caused by the pore geometry. Fickian behavior of the solute transport process is observed if solute particle's displacements are independent, identically distributed and random. Convective spreading (mechanical dispersion) caused by the pore structure scales with *Pe*.

In case of laminar flow in a capillary tube, convection does not cause any randomness in fluid motion. In this case the solute particles' displacements become decorrelated solely because of diffusion. Dispersion in a capillary tube scales with Pe^2.

Dispersion in porous media results from a balance between two mechanisms. Pore structure plays an important role in determining convective spreading through porous media and its interaction with diffusion. In this chapter we study the role of pore geometry on dispersion through direct numerical simulation using FEMLAB (now COMSOL).

7.2 DISPERSION IN SPATIALLY ORDERED POROUS MEDIA (STAGGERED SRRAY OF DISKS)

First we simulate solute flow and mixing in a spatially ordered porous medium (staggered array of disks). We solved Navier Stokes and convection-diffusion equations directly in surrogate pore space as described previously.

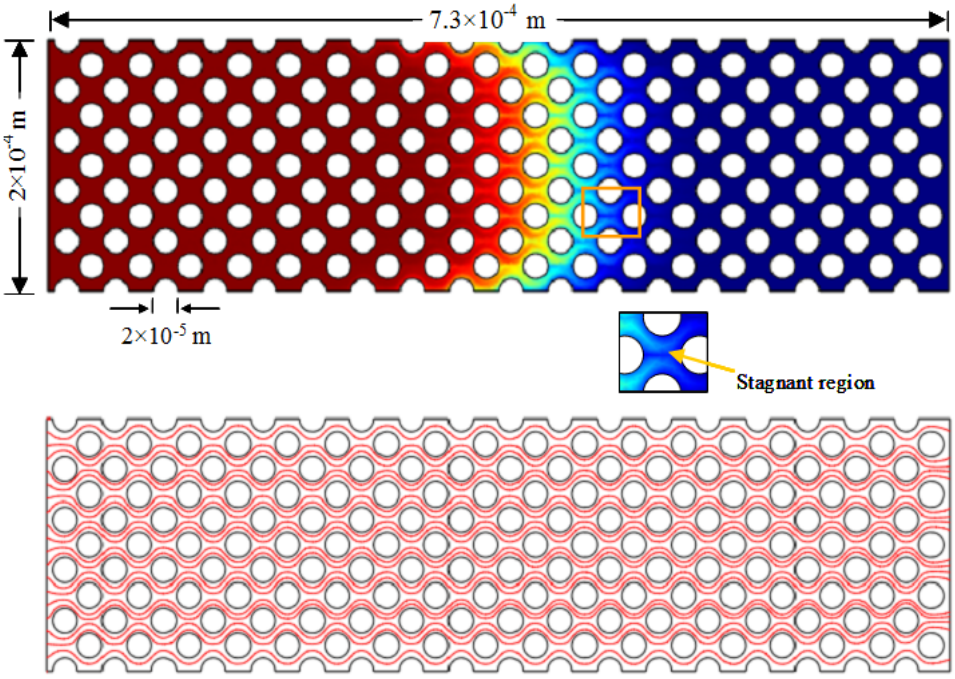

Figure 7.1: Solute concentration profile (upper) and streamlines (lower panel) in the flow domain in an ordered porous medium. Flow in this case is essentially unidirectional. Because of symmetry of the velocity field, there is a stagnant region of zero flow between the sand grains. Solute particles can enter this region only by diffusion.

Figure 7.1 shows the geometry of the flow domain. This flow geometry has been taken as the base case for the present study. Simulation in the same flow geometry was also reported by Garmeh et al. (2007). However, we present a different interpretation of

results based on the sensitivity studies that follow. Using the same flow geometry serves as a tool to cross-check results.

Figure 7.1 also shows streamlines in the velocity field (lower panel) and solute concentration profile (upper panel). As evident from the streamlines, the geometry of the medium does not cause any randomness in fluid motion. The flow is essentially unidirectional. Convection moves fluids in streamtubes that are sinusoidal in shape. The solute front undergoes a series of splitting and rejoining around sand grains. Because of symmetry of the velocity field there is a region of zero velocity between two sand grains in the longitudinal direction. Solute particles cannot reach this stagnant zone purely because of convection. This stagnant zone can be sampled by solute particles by diffusion only. Diffusion is responsible for homogenizing the solute concentration in the transverse direction. It is similar to mixing mechanism in a capillary tube.

Simulations were carried out for a range of pore scale Peclet numbers. The dispersion coefficients were calculated in each case by analyzing the solute concentration history using a solution to the one dimensional convection diffusion equation and shown in Figure 7.2. There is a power law dependence of the dispersion coefficient on the Peclet number. The power law coefficient is found to be 1.85, which suggests Taylor's mixing mechanism is dominant. This exponent is similar to that obtained by Hoagland et al. (1985) for a converging diverging (sinusoidal) tube.

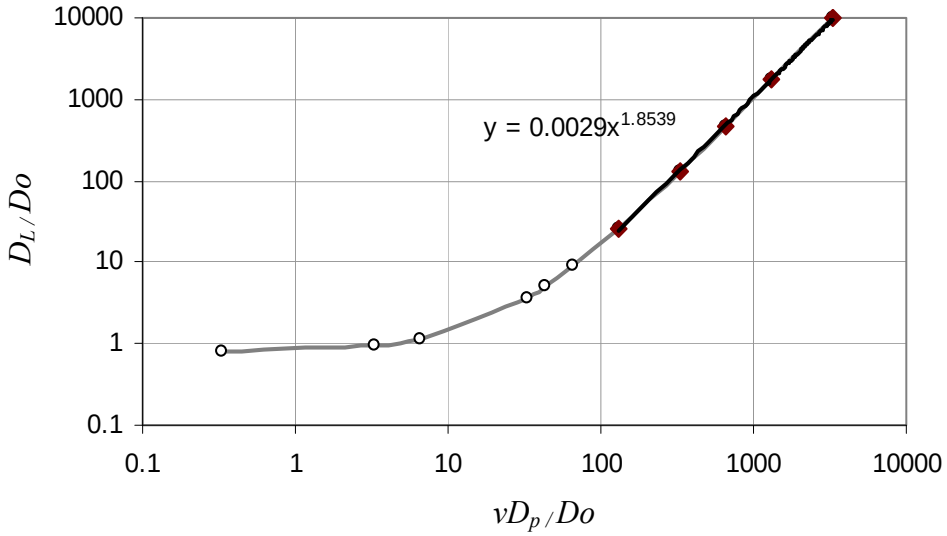

Figure 7.2: Dimensionless dispersion coefficient vs. pore scale Peclet number for an ordered porous medium of Figure 7.1. The open circles show all the data points, whereas the filled diamonds show data points corresponding to high *Pe*. The asymptotic exponent is close to two, suggesting a mixing mechanism similar to that in a capillary tube.

7.3 DISPERSION IN RANDOM POROUS MEDIA

The disks were moved randomly (random direction and small random distance). The porosity is still the same as the previous case but the geometry is changed. The random pore geometry makes the streamlines unstructured (Figure 7.3). Now the streamlines can carry the solute particles in the transverse direction by convection alone. The solute front need not rejoin after splitting at a sand grain. It may get sub divided further due to the random nature of the pore space. Solute particles can reach most of the flow domain by convection alone except the region near the wall of a grain. Dispersion in this case is dominated by mechanical dispersion and as shown in Figure 7.4 the power law exponent comes down to 1.19.

Salles et al. (1993) show that moving the grains in the longitudinal direction does not affect dispersion much. However, moving the grains in transverse direction changes the pore geometry and the shape of the streamlines. This changes the nature of dispersion in the porous medium.

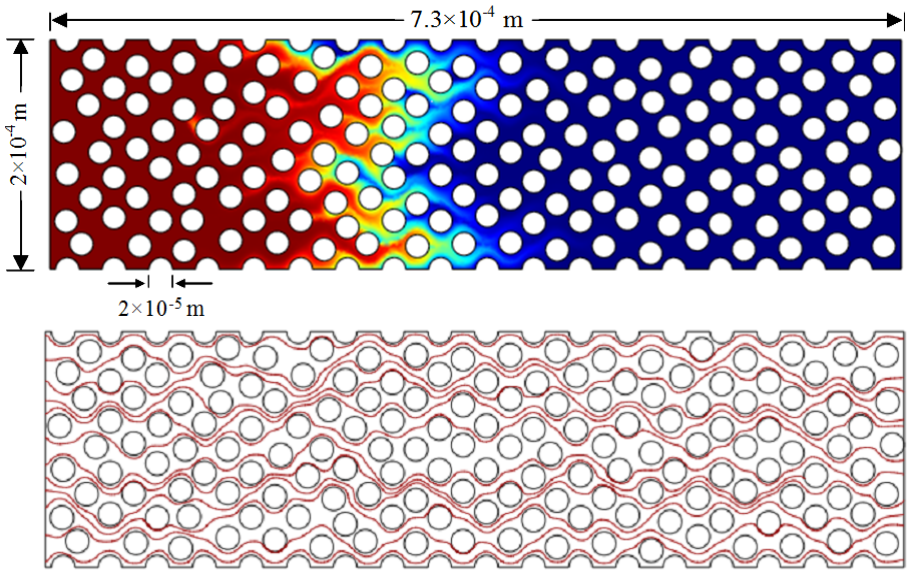

Figure 7.3: Solute concentration profile (upper panel) and streamlines in the flow domain (lower panel) in a random porous medium. Streamlines can carry solute particles in the transverse direction by convection alone. Diffusion is important in carrying solute particles from no-velocity regions near the pore walls.

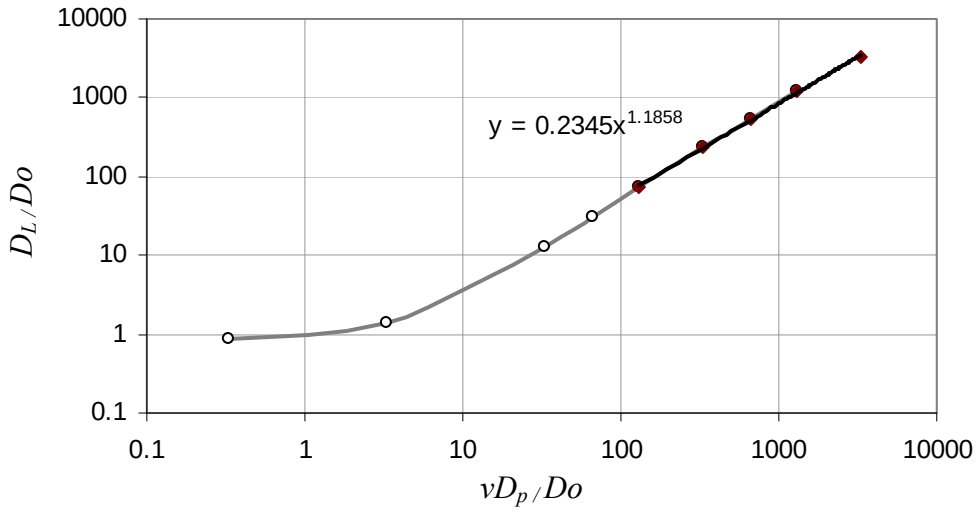

Figure 7.4: Dimensionless dispersion coefficient vs. pore scale Peclet number for the random porous medium of Figure 7.3. The exponent is close to unity, indicating that mechanical dispersion is the dominant dispersion mechanism.

7.4 DISCUSSION

Several theoretical considerations, experimental observations and network modeling studies reported in the literature suggest that the dispersion coefficient scales with Pe^2 in two or three dimensional ordered arrays and with Pe in random porous media.

Brenner (1980) developed a general theory for dispersion in ordered arrays (also called spatially periodic porous media) and showed that in the limit of long times the dispersion of a tracer particle is Fickian and found the power law coefficient, β characterizing the variation of dispersion coefficient with Pe to be close to 2.

Charette et al. (2007) show experimentally that in a tube filled with an ordered array of beads the dispersion coefficient scales with Pe^2, exactly like in an empty tube. With the same beads inside the same tube, but packed in a weakly disordered array,

dispersion is strongly reduced and β is reduced to 1.5. Similar observations have also been reported by Baudet et al. (1987). Eidsath et al. (1983) reported $\beta = 2$ in regular cubic packing of glass spheres and $\beta = 1.2$ for random packings.

Buyuktas and Wallender (2004) carried out two dimensional numerical simulation studies. They prepared a unit cell of few disks ordered in a square arrangement. They applied periodic boundary conditions to study dispersion in media of greater lengths. In the ordered (square) arrangement of disks the power law exponent, β was found to be 1.85 and it reduced to 1.36 when the disks were displaced to makes the cell geometry disordered.

Bruderer and Bernabe (2001) studied dispersion in a two dimensional square network of tubes with equal length. They show that the asymptotic dispersion coefficients increase with heterogeneity (variation in tube radii) for a given Peclet number. The power law coefficient, β decreases from 2 for a network of identical tubes to values slightly lower than 1.2 when coefficient of variation of tube radii exceeds 0.5. This shows a transition from Taylor's mechanism to a mechanical dispersion regime. The importance of mechanical dispersion increases with increasing level of heterogeneity, eventually obscuring the Taylor-Aris scaling law almost completely.

Dispersion coefficients at high Peclet numbers in random media are roughly proportional to vD_p. This suggests that at high *Pe* in a random medium, the dispersion mechanism depends only on the stochastic velocity field in the medium. In contrast, the random element introduced by molecular diffusion is required in the theory of dispersion in ordered porous media (at least for flow parallel to a line contained in the plane of

symmetry) in order that a solute particle should sample all points in the unit cell and in order that the dispersion be Fickian.

Randomness of the pore structure plays a key role in dispersion through porous media. Solute front splits across an impervious sand grain. In ordered porous media, the split filaments rejoin because of the symmetry of the velocity field. However, in random media the split filaments can get further subdivided and rejoin with filaments split across other grains. The tortuous nature of random medium is mainly responsible for this separation (Figure 6.1). On the other hand, in ordered porous media solute particle movement is not tortuous and diffusion is required for moving nearby solute particles apart and causing mixing.

A random array of disks with periodic boundary conditions as used by Buyuktas and Wallender (2004) can be considered an intermediate case between ordered and random porous media. The medium used by them preserves some spatial correlation in the pore structure due to the periodic boundary condition. Therefore, their value of β, 1.36 is a little on the higher side.

Diffusion plays similar role in ordered and disordered porous media. The non-mechanical dispersion mechanisms associated with the no-slip boundary of the fixed grains is qualitatively similar in ordered and disordered media. However, the dispersion that occurs due to fluid motion is qualitatively different in ordered and disordered porous media. In a disordered medium a solute particle's velocity becomes decorrelated with its initial position as the particle is convected through the random micro structure. In an ordered medium this mechanism is absent. The structure of the medium and, therefore, the velocity experienced by a solute traversing a streamline, remain correlated throughout

the pore space. Molecular diffusion must always be considered in order that the solute particle may forget its initial position. Thus, the mixing mechanism in ordered arrays is similar to the Taylor mechanism (Koch and Brady, (1985, 1989); Duplay and Sen (2004)).

7.5 EFFECT OF POROSITY ON DISPERSION

The porosity of the ordered porous medium (Figure 7.1) was reduced by increasing the grain diameters by 20%. This reduces the medium porosity from 60.5% to 43.2%. Figure 7.5 shows the variation of dispersion coefficients with Peclet numbers for the medium with reduced porosity. As evident from the figure, porosity does not have much impact on the power law coefficient, β. Increasing the grain size reduces the width of stream tubes, but does not change the flow geometry. The flow remains essentially unidirectional and there is no appreciable change in the power law coefficient.

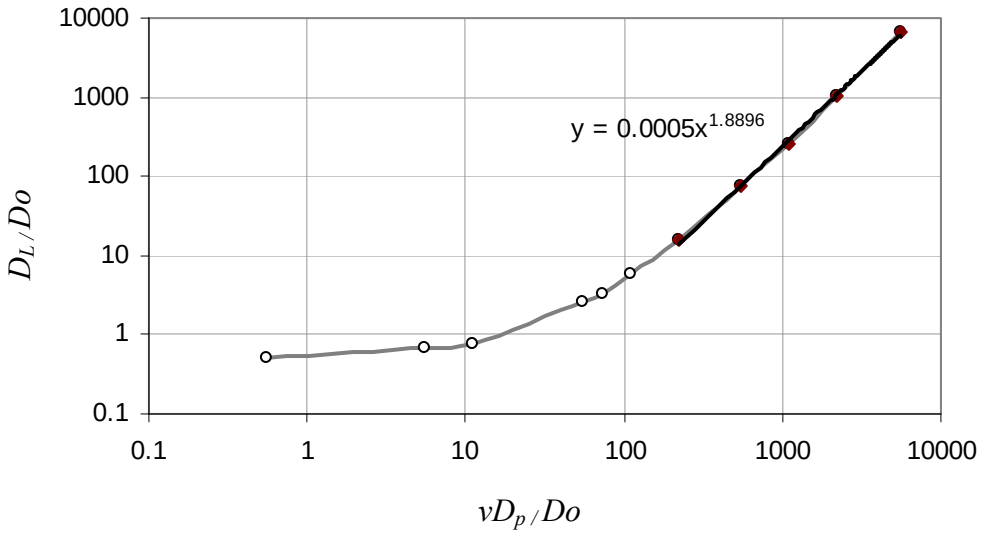

Figure 7.5: Dimensionless dispersion coefficient vs. pore scale Peclet number for an ordered porous medium with reduced porosity (43.5%). Porosity has small impact on mixing mechanism as long as flow geometry remains the same.

This is supported by results reported by Salles at al. (1993). They studied dispersion in a simple cubic array of spheres for various porosities ranging from 0.48 to 0.82. The longitudinal dispersion coefficient did not depend much on the porosity. They got the power law coefficient, β close to 2 for all the porosities.

Garmeh et al. (2007) changed the porosity of the ordered porous medium in a different way. They put some smaller disks in stagnant region of the pore space and the power law exponent fell to 1.6. The likely reason is that in this case diffusion has a smaller space to homogenize the solute concentration.

We studied the effect of changing porosity also in a random medium. We reduced the grain size by half. This increased the porosity of the medium to 90.2%. However, the geometry of the medium is random and it moves solute particles in the transverse direction by convection alone (Figure 7.6). As we see from the plot of normalized dispersion coefficient vs. pore scale Peclet number, the power law exponent is 1.12

(Figure 7.7). It has come down slightly. The likely reason for this is that because of reduced surface area of the grains, the boundary layer dispersion has gone down.

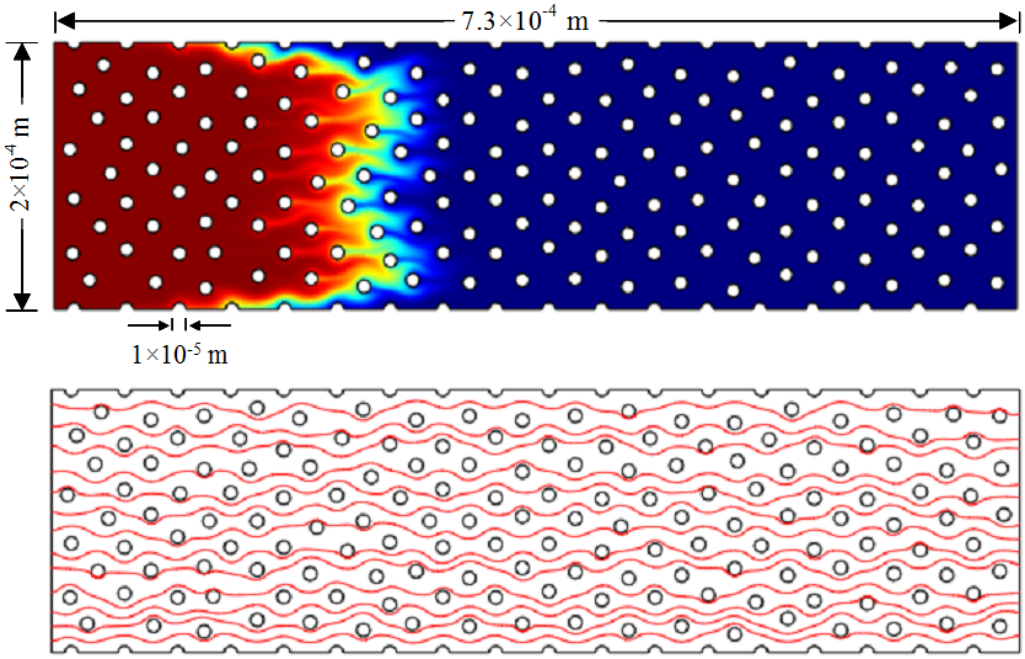

Figure 7.6: Solute concentration profile (upper panel) and streamlines (lower panel) in flow domain in a random porous medium with high porosity (90.2%). There is no change in flow geometry and therefore mixing mechanism does not change.

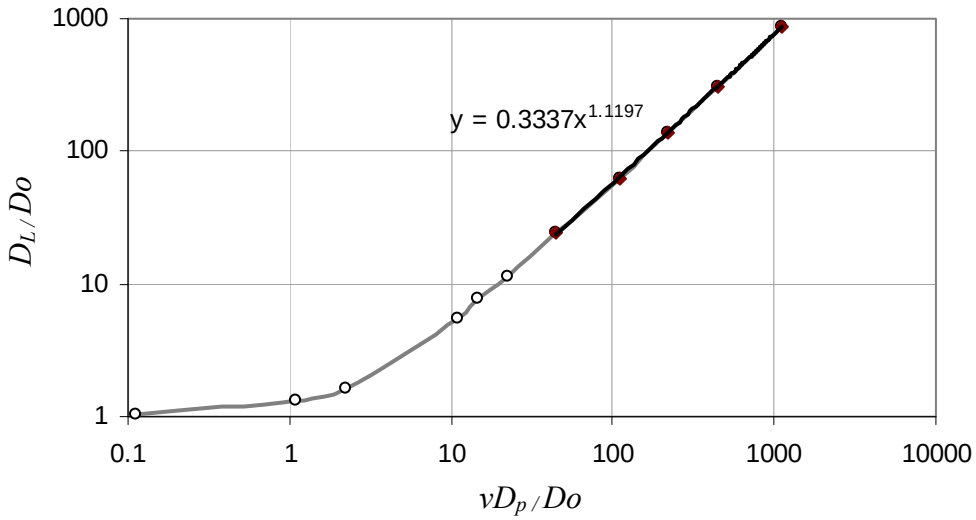

Figure 7.7: Dimensionless dispersion coefficient vs. pore scale Peclet number for a random porous medium with high porosity (90.2%) as shown in Figure 7.6. Porosity does not have any significant impact on mixing mechanism as long as flow geometry remains same.

7.6 CONCLUSIONS

In random bead packs, because of the random nature of the flow paths a single deterministic streamline encounters a range of velocities. Here even a very small diffusion can transport solute particles from the zero velocity region near the wall to the main flow stream. Subsequently, mechanical dispersion can take solute particles to different parts of the flow domain. One thus finds an asymptotic linear regime, due only to mechanical dispersion. Mechanical dispersion scales linearly with *Pe*, which implies that dispersion does *not* depend on diffusion. The role of diffusion in cutting down the residence time near pore walls results in the power law coefficient, β characterizing the variation of dispersion coefficient with *Pe* to be close to 1.2.

In contrast, the flow in ordered arrays is strongly correlated and diffusion is essential to move solute particles in the transverse direction, and in that direction cause decorrelation in solute particle displacements. Mixing in this case is similar to that in a capillary tube and dispersion scales with Pe^2.

The power law coefficient, β characterizing the variation of dispersion coefficient with Pe does not depend on porosity of the medium. As long as the geometry of the medium remains unchanged, there is no significant change in β.

REFERENCES:

1. Aris, R.: "On the dispersion of a solute in fluid flowing through a tube", Proc. R. Soc. London, Ser. A, 235, 67-77 (1956).
2. Baudet, C., Chertcoff, R. and Hulin, J.P.: "Effets de de´sordre de structure sur la dispersion d'un traceur dans un milieu poreux mode`le" *C. R. Acad. Sci*., Ser. II, *305*, 327–330, (1987).
3. Brenner, H.: "Dispersion resulting from flow through spatially periodic porous media", Phil. Trans. R. Soc. Lon., A, 297, 81-133, (1980).
4. Bruderer, C. and Y. Bernabe: "Network modeling of dispersion: Transition from Taylor dispersion in homogeneous networks to mechanical dispersion in very heterogeneous ones", Water Resources Research 37(4): 897-908 (2001).
5. Buyuktas, D. and Wallender, W. W.: "Dispersion in spatially periodic porous media", Heat and Mass Transfer, 40, 261-270 (2004).

6. Cherette, V. J., Evangelista E., Chertcoff R., Auradou, H., Hulin, J. P. and Ippolito, I.: “Influence of the disorder on solute dispersion in a flow channel”, Eur. Phys. J. Appl Phys., 39, 267-274, (2007).
7. Duplay, R. and Sen, P. N.: “Influence of local geometry and transition to dispersive regime by mechanical mixing in porous media”, Physical Review E, 70, 066309 (2004).
8. Eidsath, A., Carbonell, R. G., Whitkar, S. and Herrmann, L. R.: “Dispersion in pulsed systems, III, Comparison between theory and experiments for packed beds, Chem. Eng. Sci., 38, 1803-1816 (1983).
9. Garmeh, G., Johns R. T. and Lake, L. W.: “Pore scale simulation of dispersion in porous media”, SPE 110228 presented at SPE ATCE held at Anaheim, California, (Nov. 2007).
10. Hoagland, D. A. and Prud’homme R. K.: “Taylor-Aris dispersion arising from flow in a sinusoidal tube”, AIChE Journal, 31 (2), 2, 236-243, (1985).
11. Koch, D. L. and Brady, J. F.: “Dispersion in fixed beds”, J. Fluid Mech., 154, 399-427, (1985).
12. Koch, D.L., Cox, R.G., Brenner, H. And Brady J. F.: “The effect of order on dispersion in porous media”, J. Fluid Mech., 200, 173-188, (1989).
13. Salles J., Thovert, R., Delannay, R., Prevors, L., Auriault, J. L. and Adler, P. M.: “Taylor dispersion in porous media. Determination of the dispersion tensor”, Phys. Fluids A , 5 (10), 2348-2376, (Oct. 1993).
14. Taylor, G.: “Dispersion of soluble matter in solvent flowing slowly through a tube”, Proc. R. Soc. London, Ser. A, 219, 186-203 (1953).

Chapter 8: Summary, Conclusions and Future Work

8.1 SUMMARY AND CONCLUSIONS

Predictions of core scale dispersion in a physically representative network with velocity gradients in pore throats and diffusion agree with many experimental observations on cores, including the correct scaling of the power law exponent characterizing the dependence of dispersion coefficients on Peclet number. This is the first *a priori* prediction of this long standing observation. It provides confidence that the key mechanisms causing core scale dispersion have been identified.

Dispersion in porous media results from an interplay of molecular diffusion and convective spreading (mechanical dispersion). Molecular diffusion is a result of the random movement of solute particles that causes a net movement of solute particles from regions of high solute concentration to that of low solute concentration. Convective spreading in porous media arises because of variance in velocities and path lengths of solute particles traveling along different streamlines.

Velocity varies along a streamline because of differences in average velocities in different pore throats. There is also a difference in velocities along different streamlines due to velocity gradients in a pore throat and independent paths followed by the streamlines.

In the conventional Fickian representation of core scale mixing, convective spreading is considered to be “diffusion like”; a statistically random process. If the travel

time for a solute particle becomes much larger than the time interval during which successive velocities are still correlated, its total displacement may be considered as the sum of a large number of elementary displacements that are statistically independent. For such conditions, the probability distribution of the particles' total displacement should be normal according to the central limit theorem.

The randomness of dispersion is inherent in the morphology of the pore space. If we ignore velocity gradient in pores, a solute particle can encounter a wide range of velocities due to velocity differences in different pore throats. It leads to a Fickian behavior of purely convective spreading. In this case there is no concentration gradient in the transverse direction in a pore throat. Diffusion plays an additive role on longitudinal dispersion and there is a linear dependence of dispersion on *Pe* at high Peclet numbers where diffusion is negligible in magnitude compared to the convective spreading. It does not quite explain the power law dependence of dispersion on *Pe*.

If we consider the velocity gradients in pore throats then particles near the solid surface of sand grains have low velocity. Solute particles' velocities in this layer are not independent. These particles cannot sample all velocities because of convection alone and dispersion is non-Fickian in the absence of diffusion.

Diffusion is required to cause independence in velocities of these solute particles. Diffusion brings solute particles in the low velocity region to the main flow stream and subsequently dispersion becomes Fickian. In this case there is a concentration gradient in the transverse direction in pore throats. Diffusion decreases variations in the particle velocities in a pore throat and therefore dispersion is reduced. Dispersion reduces with increasing diffusion and results in a mild non-linear behavior of dispersion vs. *Pe*. For

low Peclet numbers, diffusion becomes very large compared to convective spreading and therefore the dispersion coefficients increase with increasing diffusion.

Pore structure plays an important role in causing randomness of particle velocities. If a medium has no correlated heterogeneity, correlated velocities exist only in a thin region near the solid particle surfaces. A small diffusion coefficient can easily make velocities independent by moving solute particles from these low velocity regions to the main flow stream and make the transport process Fickian. However, in a medium with correlated heterogeneity, velocities in that region are not independent and the transport is non-Fickian. A large amount of diffusion is required to move solute particles in the transverse direction and cause independence of solute particle movement.

In ordered porous media, convective displacements of solute particles are strongly correlated. Convective spreading is not random. Diffusion is solely responsible for moving solute particles in the transverse direction and cause independence of displacements. Mixing in this case is similar to that in a capillary tube and dispersion scales with Pe^2.

Diffusion, even though small in magnitude, plays a crucial role in causing mixing which is different from convective spreading. Flow reversal studies provide insights about mixing mechanisms in flow through porous media and differentiate between convective spreading and mixing. For purely convective transport, upon flow reversal solute particles retrace their path back to the inlet. Convective spreading cancels and echo dispersion is zero. Diffusion, even though small in magnitude, causes local mixing and makes dispersion in porous media irreversible. Local mixing is enhanced by velocity

gradients and splitting and rejoining of solute streams in pore throats. Echo dispersion in porous media is far greater than diffusion and as large as transmission dispersion.

8.2 FUTURE WORK

- Modify the particle tracking algorithm for low Peclet numbers. The choice of out-flowing bond at a pore body should be based on cross-sectional area of the bonds and not on their flow rates.
- Carry out network simulation studies in a larger network to confirm that the dispersion coefficients and fluid velocities have reached asymptotic limits.
- Investigate the effect of correlation in pore structure on distance traveled to converge to asymptotic dispersion coefficients.
- Investigate dispersion in cemented sphere packs where the throats are narrower and some of them may be even blocked.
- Investigate transverse dispersion.
- Investigate mixing in non-Newtonian fluids.
- Investigate dispersion for the multi-phase flow through the network.
- Investigate dispersion in a pack having non-uniform sphere diameters.

Appendix

A1. MARKING A SEGMENT OF A CIRCULAR TUBE CARRYING A KNOWN FRACTION OF TOTAL FLOW

(i) Plug Flow

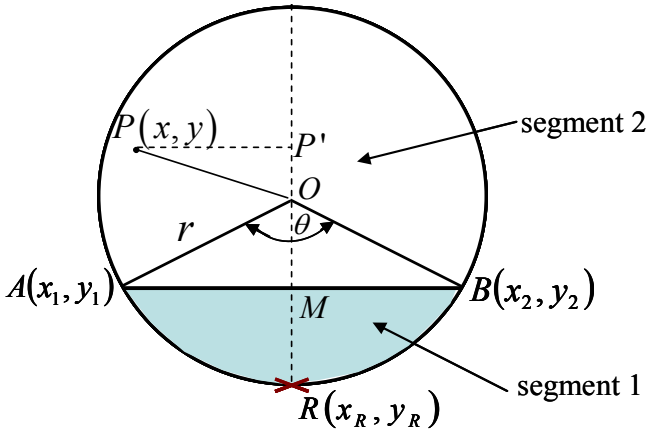

Figure A.1: Marking a segment of a circular tube carrying a known fraction of total flow.

We derive an analytical expression for marking a segment of a circular tube that carries a fraction *f* of total flow. The circular cross section is divided into two segments by line AB. We have to determine a solute particle exiting the in-flowing tube at a point *P(x,y)* falls on which segment as this will decide the choice of out-flowing tube.

For plug flow profile in the tube, the flow fraction carried a segment is same as its area fraction. The center of the circle lies at the origin, *O*. Let *f* be the fraction of flow that enters the tube closer to the reference point, *R*. Therefore, we have to mark a fraction *f* of the cross sectional area that is closer to the reference point. This is shown as the

shaded region in the Figure A1. The line segment AB marks the boundary of the shaded region. AB subtends an angle θ at the center.

Area of the shaded region is $\frac{1}{2}r^2(\theta - \sin\theta)$. Therefore,

$$f = \frac{\frac{1}{2}r^2(\theta - \sin\theta)}{\pi r^2} = \frac{1}{2\pi}(\theta - \sin\theta) \quad \text{…….. (A.1).}$$

We solve the above equation for θ using MATLAB's symbolic mathematics tools.

Next, we calculate the coordinates of points A and B. We calculate polar coordinates of the reference point. Polar angles for A and B

$\theta_A = \theta_R - \theta/2$, and

$\theta_B = \theta_R + \theta/2$.

Since both the points are at a distance *r* from the center, they can easily be converted to Cartesian coordinates (x_1, y_1) and (x_2, y_2).

We want to find whether point *P(x,y)* lies in region 1 or region 2.

Coordinates of *M*, mid-point of the line segment AB

$$(x_M, y_M) = \left(\frac{x_1 + x_2}{2}, \frac{y_1 + y_2}{2}\right) \quad .$$

$\left|\vec{RM}\right|$ is the depth of segment 1. OP' is projection of vector $\vec{OP}$ on to vector $\vec{RO}$.

$$OP' = \frac{\vec{OP}.\vec{RM}}{\left|\vec{RM}\right|} \text{ and}$$

$RP' = OP' + r$.

If $RP' \le \left| \vec{RM} \right|$ then the point *P* lies in the segment 1, else it lies in segment 2.

(ii) Parabolic Velocity Profile

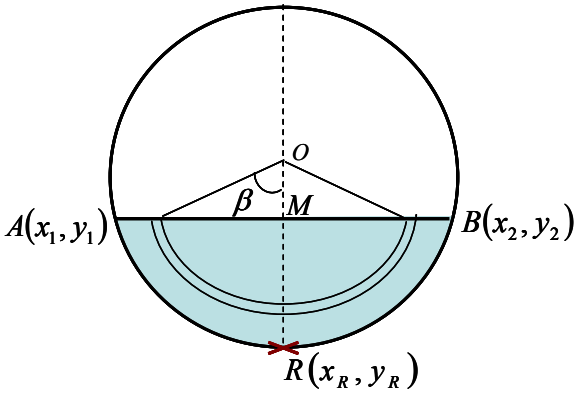

Figure A.2: Marking a segment of a circular tube carrying a known fraction of total flow wit parabolic velocity profile.

As before, we consider a line segment AB dividing the circular tube into two segments. The segment subtends an angle θ at the center.

In case of parabolic velocity profile in tubes, it is not possible to derive an analytical expression (similar to equation A.1) for the angle subtended flow at the center by a segment carrying a fraction *f* of total. Therefore, we solve this problem numerically. Let us denote $OM = x$. Therefore,

$MR = r - x$.

We divide the segment into a number of thin rings as shown in figure. Let radius of a ring be *r'* and its thickness *dr'*. Average radius of the ring $r_{avg} = r' + (dr'/2)$. Angle subtended by the ring at the center $\beta = \cos^{-1}(x / r_{avg})$.

Area of the ring $dA = 2 \times r_{avg} \times \beta \times dr'$.

Average flow velocity in the ring $v_r = 2\overline{v}\left(1 - \frac{r_{avg}^2}{r^2}\right)$, where $\overline{v}$ is the average flow velocity through the tube.

Flow rate in the ring $dq = v_r \times dA$.

By adding flow rates through all the rings numerically, we can calculate flow rate through the segment, *q*.

Fraction of flow rate carried out by the segment $f = q / \pi r^2 \overline{v}$.

By carrying out this calculation for several values of subtended angle θ, we can prepare a plot of θ vs. the fraction of flow rate carried out by the segment. Figure 3 shows the curve and compares it with the corresponding curve for plug flow. It is interesting to note that the two curves are very similar.

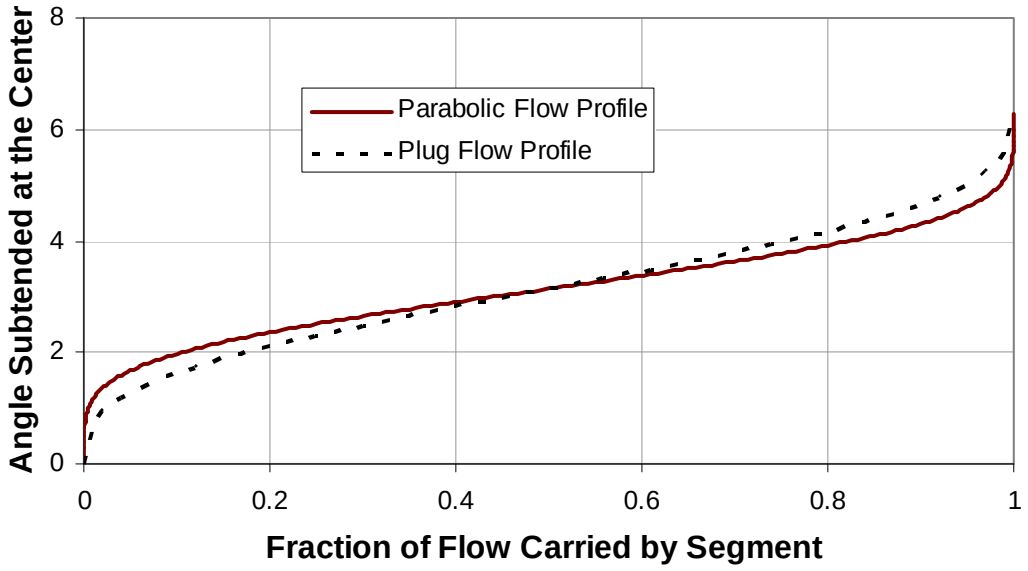

Figure A.3: Comparison of angles subtended at the center by a segment carrying a known fraction of total flow with plug flow and parabolic flow profiles.

After determining the value of θ from the chart, rest of the procedure is same for parabolic velocity profile and plug flow.

A2. DETERMINING GEOMETRIC CENTERS OF FLOW SEGMENTS

Next, we evaluate the coordinates of the geometric centers (center of gravity) of the two segments. The geometric centers of both the segments lie on the line joining the center of the circle to the reference point *R*.

The center of gravity of a segment of a circle lies on the bisector of the central angle and its distance from the center is

$$dist_{CG1} = \frac{4r\sin^3\left(\frac{\theta}{2}\right)}{3(\theta - \sin\theta)}.$$

Therefore, the distance of the second segment's center of gravity from the center is

$$dist_{CG2} = \frac{f \times dist_{CG1}}{1-f}.$$

Distance of mid-point M from the center

$$dist_M = \sqrt{x_M^2 + y_M^2}.$$

<u>If $f < 0.5$</u>

Coordinates of center of gravity of segment 1

$$CG1 = \frac{dist_{CG1}}{dist_M} \times (x_M, y_M).$$

Distance of CG2 from the mid point $dist_{M\_CG2} = dist_{CG2} + dist_M$.

Coordinates of center of gravity of the second segment

$$CG2 = \left(1 - \frac{dist_{M\_CG2}}{dist_M}\right) \times (x_M, y_M).$$

<u>If $f > 0.5$</u>

Distance of CG1 from the mid point $dist_{M\_CG1} = dist_{CG1} + dist_M$.

Coordinates of the two centers of gravity:

$$CG1 = \left(1 - \frac{dist_{M\_CG1}}{dist_M}\right) \times (x_M, y_M) \text{ and}$$

$$CG2 = \frac{dist_{CG2}}{dist_M} \times (x_M, y_M).$$

A3. MARKING SEGMENTS OF A CIRCULAR TUBE SPLITTING INTO THREE STREAMS

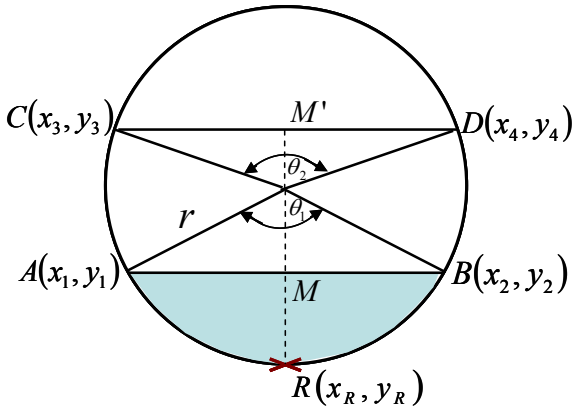

Figure A.4: Marking segments of a circular tube splitting into three streams.

Figure shows cross section of a tube splitting into three streams. Line segments AB and CD mark boundaries of the flow segments. The shaded region corresponds to the flow from the closest tube and the central section ABCD corresponds to the flow from the farthest tube.

Let f_1 and f_3 be the flow fractions from the closest and farthest tubes respectively. For segment 1, we can determine the coordinates of points A, B and M using the procedure as described above for flow fraction f_1. We also get the center of gravity for region 1. If we repeat the process with a fraction $(f_1 + f_3)$, we get coordinates for points C, D and M'. We also get the center of gravity of the combined regions 1 and 3. This also gives us the center of the gravity for segment 2. Let d_1, d_2 and d_3 be the distances of the centers of gravity of the three segments from the center. We have obtained d_1 and d_3 explicitly. Taking moment around the center we get,

$d_3 = (f_1 d_1 - f_2 d_2)/ f_3$.

The center of gravity for the third region will lie on the line joining CG_1 and the center.

$$CG_3 = CG_1 - CG_1 \times \frac{d_1 + d_3}{d_1}.$$

A4. DETERMINING RELATIVE DISTANCE FROM BOUNDARY AND ANGLE FROM REFERENCE VECTOR

(i) For the Circular Segments

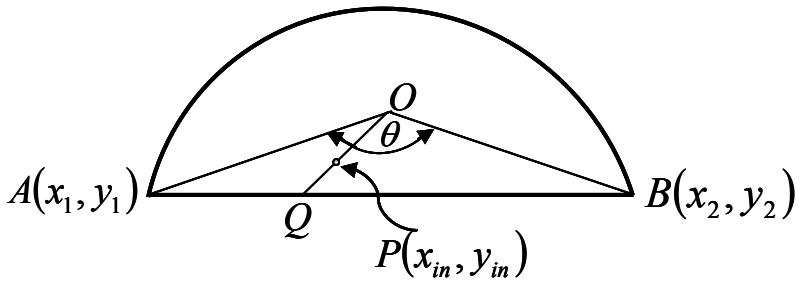

Figure A.5: Determining relative distance of a point from chord.

Figure shows a point *P* in a segment. We need to determine the relative distance of the point to the boundary of the segment and the angle its position vector makes with the reference vector.

We have shifted the entire segment of the circle so that its geometric center lies at the origin.

Equation of line AB is

$$(x_2 - x_1)(y - y_1) = (y_2 - y_1)(x - x_1).$$

This form of equation works even when $x_2 = x_1$.

Let $P(x_{in}, y_{in})$ denote the incoming point.

We also denote $\vec{OA} = \vec{v}_1$, $\vec{OB} = \vec{v}_2$ and $\vec{OP} = \vec{v}_{in}$.

$$\theta = \angle AOB = \cos^{-1}\left(\frac{\vec{v}_1.\vec{v}_2}{|\vec{v}_1|.|\vec{v}_2|}\right),$$

$$\theta_1 = \angle AOP = \cos^{-1}\left(\frac{\vec{v}_1.\vec{v}_{in}}{|\vec{v}_1|.|\vec{v}_{in}|}\right),$$

$$\theta_2 = \angle BOP = \cos^{-1}\left(\frac{\vec{v}_2.\vec{v}_{in}}{|\vec{v}_2|.|\vec{v}_{in}|}\right),$$

If $\theta_1 + \theta_2 = \theta$, then the extended line joining the point *P* to the center will intersect the line *AB*, otherwise it will intersect the circular portion of the segment.

If the extended line OP meets line segment AB

Equation of the line OP

$$y = \frac{y_{in}}{x_{in}} x.$$

The coordinates of the point of intersection *Q* is given by

$$x = \frac{(x_2 - x_1)y_1 - (y_2 - y_1)x_1}{(x_2 - x_1)\frac{y_{in}}{x_{in}} - (y_2 - y_1)}$$

and

$$y = \frac{y_{in}}{x_{in}} x.$$

Therefore the distance to the boundary

$$R = \sqrt{x^2 + y^2}.$$

Relative radial distance of point *P* to the boundary = $\sqrt{x_{in}^2 + y_{in}^2} / \sqrt{x^2 + y^2}$.

The angle between *OP* and the reference vector can be calculated by the difference between the azimuth angles of the two in polar coordinate system.

If the extended line OP meets the circular arc

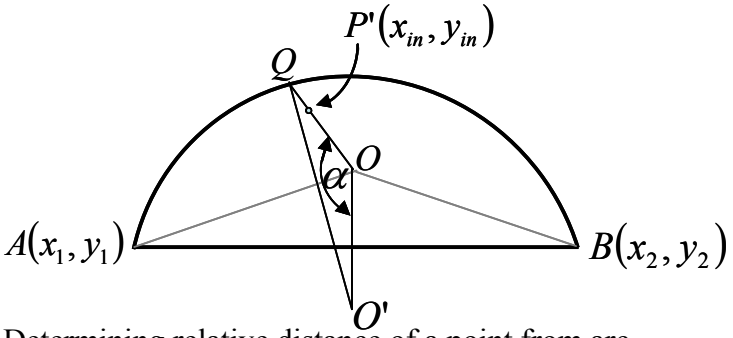

Figure A.6: Determining relative distance of a point from arc.

O' denotes the center of the circle.

$\vec{OO'} = \vec{v}_1$ and $\vec{OP'} = \vec{v}_{in}$,

$$\alpha = \angle O'OQ = \cos^{-1}\left(\frac{\vec{v}_1 . \vec{v}_{in}}{|\vec{v}_1| . |\vec{v}_{in}|}\right).$$

In $\Delta O'OQ$, $O'Q = r$, radius of the circle.

Let's call $O'O = d$ and $OQ = x$.

From cosine rule

$$r^2 = d^2 + x^2 - 2\,d\,x\cos\alpha \ .$$

We solve this equation for *x* to determine the maximum distance to boundary in the direction of position vector *OP'*.

As before, the angle between *OP'* and the reference vector can be calculated by the difference between the azimuth angles of the two in polar coordinate system.

(ii) For the Mid-Section of a Circular Tube

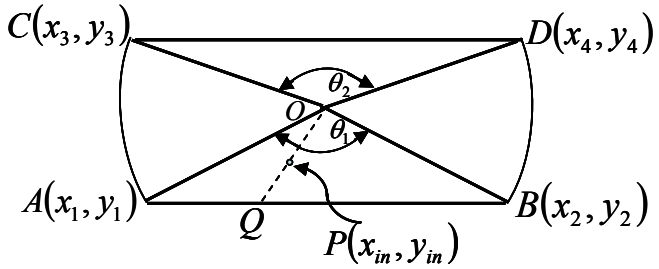

Figure A.7: Determining relative distance of a point in the mid-section of a circular tube.

As before, we shift all the points so that the geometric center of the segment lies at the origin.

Let $P(x_{in}, y_{in})$ denote the incoming point.

Let's say $\vec{OA} = \vec{v}_1$, $\vec{OB} = \vec{v}_2$, $\vec{OC} = \vec{v}_3$, $\vec{OD} = \vec{v}_4$ and $\vec{OP} = \vec{v}_{in}$.

$$\theta_1 = \angle AOB = \cos^{-1}\left(\frac{\vec{v}_1.\vec{v}_2}{|\vec{v}_1|.|\vec{v}_2|}\right),$$

$$\theta_2 = \angle COD = \cos^{-1}\left(\frac{\vec{v}_3.\vec{v}_4}{|\vec{v}_3|.|\vec{v}_4|}\right),$$

$$\theta_{11} = \angle AOP = \cos^{-1}\left(\frac{\vec{v}_1.\vec{v}_{in}}{|\vec{v}_1|.|\vec{v}_{in}|}\right),$$

$$\theta_{12} = \angle BOP = \cos^{-1}\left(\frac{\vec{v}_2.\vec{v}_{in}}{|\vec{v}_2|.|\vec{v}_{in}|}\right),$$

$$\theta_{21} = \angle COP = \cos^{-1}\left(\frac{\vec{v}_3.\vec{v}_{in}}{|\vec{v}_3|.|\vec{v}_{in}|}\right),$$

$$\theta_{22} = \angle DOP = \cos^{-1}\left(\frac{\vec{v}_4.\vec{v}_{in}}{|\vec{v}_4|.|\vec{v}_{in}|}\right).$$

If $\theta_{11} + \theta_{12} = \theta_1$, then the extended line joining the point P to the center will intersect the line AB, if $\theta_{21} + \theta_{22} = \theta_2$, then the extended line joining the point P to the center will intersect the line CD, otherwise it will intersect the circular portion of the segment.

The procedure for calculating the relative distance to the boundary and the angle of position vector with the reference vector for both the cases has already been described.

A5. ROTATING A POINT ON A HORIZONTAL CIRCLE IN ANY ARBITRARY DIRECTION AND VICE VERSA

Our network model is three dimensional having randomly oriented cylindrical bonds. Faces of the cylinders where solute particles exit and enter next bond are circles in three dimensions.

Mathematics is a lot easier in two dimensions as compared to three dimensions. Therefore, we rotate three dimensional, randomly oriented, inflowing and out-flowing circular faces to the x-y plane. After doing the required calculations to map the in-flowing point to an out-flowing point in x-y plane, we rotate the points back to mark their

positions in three dimensions. In this section, we describe rotation of points from x-y plane to a plane in arbitrary direction and vice versa.

We consider a point in a horizontal circle whose axis points in the positive z-direction. In other words, unit vector along the axis of the circle is $\vec{k}$. We need to rotate it so that its axis points in the direction of unit vector $\vec{d} = a\vec{i} + b\vec{j} + c\vec{k}$. Let ϕ be the angle of rotation.

$\vec{k}.\vec{d} = \left|\vec{k}\right|\left|\vec{d}\right|\cos\phi$,

$\Rightarrow c = \cos\phi$ since $\left|\vec{k}\right| = \left|\vec{d}\right| = 1$.

Taking cross product,

$$\vec{k}\times\vec{d} = \begin{vmatrix} \vec{i} & \vec{j} & \vec{k} \\ 0 & 0 & 1 \\ a & b & c \end{vmatrix} = -b\vec{i} + a\vec{j}\,.$$

Taking magnitudes,

$\left|\vec{k}\right|\left|\vec{d}\right|\sin\phi = \sqrt{a^2 + b^2}$.

Let $\vec{w}$ be unit vector along the axis of rotation. It will be perpendicular to both the normals $\vec{k}$ and $\vec{d}$.

$$\vec{w} = \frac{\vec{k}\times\vec{d}}{\left|\vec{k}\times\vec{d}\right|} = \frac{-b\vec{i} + a\vec{j}}{\sqrt{a^2 + b^2}}$$

For any vector in 3D space $\vec{v} = x\vec{i} + y\vec{j} + z\vec{k}$, we need to derive the rotated vector $\vec{V} = X\vec{i} + Y\vec{j} + Z\vec{k}$.

$\vec{v}$ can be expressed as the sum of the component along the $\vec{w}$ and the component orthogonal to $\vec{w}$.

The component along the $\vec{w}$ direction is $(\vec{v}.\vec{w})\cdot\vec{w}$.

$(\vec{w}\times\vec{v})$ is a vector with magnitude of the second component, but it is orthogonal to both the components. The vector $(\vec{w}\times\vec{v})\times\vec{w}$ is the second component itself.

If $\vec{v}$ is rotated through the angle ϕ about $\vec{w}$ to $\vec{V}$, we can express $\vec{V}$ in terms of following three vectors

$$\vec{V} = (\vec{v}.\vec{w})\vec{w} + \{(\vec{w}\times\vec{v})\times\vec{w}\}\cos\phi + (\vec{w}\times\vec{v})\sin\phi.$$

We evaluate the three vectors

$$(\vec{v}.\vec{w})\vec{w} = \left\{\left(x\vec{i} + y\vec{j} + z\vec{k}\right).\left(\frac{-b\vec{i} + a\vec{j}}{\sqrt{a^2+b^2}}\right)\right\}\left(\frac{-b\vec{i} + a\vec{j}}{\sqrt{a^2+b^2}}\right),$$
$$= \left(\frac{-bx + ay}{a^2+b^2}\right)\left(-b\vec{i} + a\vec{j}\right)$$

$$\vec{w}\times\vec{v} = \begin{vmatrix} \vec{i} & \vec{j} & \vec{k} \\ \dfrac{-b}{\sqrt{a^2+b^2}} & \dfrac{a}{\sqrt{a^2+b^2}} & 0 \\ x & y & z \end{vmatrix} = \frac{1}{\sqrt{a^2+b^2}}\left\{a\,z\,\vec{i} + b\,z\,\vec{j} - (b\,y + a\,x)\vec{k}\right\},$$

$$(\vec{w}\times\vec{v})\times\vec{w} = \frac{1}{a^2+b^2}\begin{vmatrix} \vec{i} & \vec{j} & \vec{k} \\ a\,z & b\,z & -(b\,y+a\,x) \\ -b & a & 0 \end{vmatrix}$$

$$= \frac{1}{a^2+b^2}\left\{a(b\,y+a\,x)\vec{i} + b(b\,y+a\,x)\vec{j} + (a^2+b^2)z\,\vec{k}\right\}$$

$$= \frac{(a\,x+b\,y)(a\,\vec{i}+b\,\vec{j})}{a^2+b^2} + z\,\vec{k}$$

, $\vec{V} = (\vec{v}.\vec{w})\vec{w} + \{(\vec{w}\times\vec{v})\times\vec{w}\}\cos\phi + (\vec{w}\times\vec{v})\sin\phi$.

Substituting the values and rearranging,

$$\vec{V} = \left\{\frac{b^2x - a\,b\,y}{a^2+b^2} + \frac{a^2c\,x + a\,b\,c\,y}{a^2+b^2} + a\,z\right\}\vec{i} + \left\{\frac{-a\,b\,x + a^2\,y}{a^2+b^2} + \frac{a\,b\,c\,x + b^2\,c\,y}{a^2+b^2} + b\,z\right\}\vec{j}$$

$$+ \{z\,c - a\,x - b\,y\}\vec{k}$$

$$= \frac{1}{a^2+b^2}\left\{\left(b^2+a^2c\right)x + a\,b(c-1)y + a\left(a^2+b^2\right)\right\}\vec{i} + \frac{1}{a^2+b^2}\left\{a\,b(c-1)x + \left(a^2+b^2c\right)y + b\left(a^2+b^2\right)\right\}\vec{j}$$

$$+ \{-a\,x - b\,y + c\,z\}\vec{k}$$

$$\begin{bmatrix} X \\ Y \\ Z \end{bmatrix} = \begin{bmatrix} \frac{b^2+a^2c}{a^2+b^2} & \frac{a\,b(c-1)}{a^2+b^2} & a \\ \frac{a\,b(c-1)}{a^2+b^2} & \frac{a^2+b^2c}{a^2+b^2} & b \\ -a & -b & c \end{bmatrix}\begin{bmatrix} x \\ y \\ z \end{bmatrix}.$$

Conversely, to rotate a point on circle with axis (a,b,c) to the horizontal direction with axis (0,0,1) we can follow the previous steps. Only the sign of $\vec{w}$ will change in this case. Everything else remains the same.

$$\vec{w} = \frac{b\vec{i} - a\vec{j}}{\sqrt{a^2 + b^2}}.$$

Following the steps we can show that

$$\begin{bmatrix} x \\ y \\ z \end{bmatrix} = \begin{bmatrix} \dfrac{b^2 + a^2 c}{a^2 + b^2} & \dfrac{ab(c-1)}{a^2 + b^2} & -a \\ \dfrac{ab(c-1)}{a^2 + b^2} & \dfrac{a^2 + b^2 c}{a^2 + b^2} & -b \\ a & b & c \end{bmatrix} \begin{bmatrix} X \\ Y \\ Z \end{bmatrix}.$$

List of Symbols

β	Power law coefficient characterizing dependence of dispersion coefficient on Peclet number.
C	Solute concentration, moles/m^3.
D_L	Longitudinal dispersion coefficient, m^2/s.
D_{mech}	Mechanical dispersion coefficient, m^2/s.
D_p	Particle diameter, m.
D_o	Molecular diffusion coefficient, m^2/s.
F	Formation resistivity factor.
g	Hydraulic conductivity of a bond, m^3/s/Pa.
J	Diffusive flux, mol/m^2.s
l	Length of a bond connecting two neighbors, m.
L_t	Mean path length of solute particles in the medium, m.
Le	Length of the medium, m.
μ	Fluid viscosity, Pa.s.
ϕ	Porosity.
Pe	Pore scale Peclet number, $Pe=vD_p/D_o$.
Pe_L	Longitudinal Peclet number, $Pe_{L=}\overline{v}L / D_L$
q	Flow rate through a bond, m^3/s.

r_{diff}	Magnitude of diffusive jump, m
r_c	Radius of the largest circle to fit in a pore throat, m.
r_e	Radius of a circle having same area as a pore throat, m.
Re	Reynolds number.
σ_z^2	Variance of solute particles in z-direction, m^2.
τ	Tortuosity.
v	Interstitial fluid velocity, m/s.
$\overline{v}$	Average fluid velocity through a bond, m/s.
V	Hydraulic potential, Pa.

Bibliography

Acharya, R. C., van Dijke, M. I. J., Sorbie, K. S., Van der Zee, S. E. A. T. M. and Leijnse, A.: "Quantification of dispersion by upscaling Brownian motion of tracer displacement in a 3D pore-scale network model", Advances in Water Resources, 30 (2), 199 – 213, (2007).

Aris, R.: "On the dispersion of a solute in fluid flowing through a tube", Proc. R. Soc. London, Ser. A, 235, 67-77 (1956).

Aris, R.: "Dispersion of a solute by diffusion, convection, and exchange between phases." Proc. Roy. Soc. (London) A252: 538-50, (1959).

Aris, R. and Amundson, N.R.: "Some remarks on longitudinal mixing or diffusion in fixed beds", AIChE Journal (Jun. 1957).

Auset, M. and Keller, A.A.: "Pore scale processes that control dispersion of colloids in saturated porous media", Water Resources Research, Volume 40 (2004).

Baudet, C., Chertcoff, R. and Hulin, J.P.: "Effets de de´sordre de structure sur la dispersion d'un traceur dans un milieu poreux mode`le" *C. R. Acad. Sci*., Ser. II, *305*, 327–330, (1987).

Bear, Jacob: *Dynamics of Fluids in Porous Media*, Elsevier, New York, (1972).

Bijeljic, B., Muggeridge, A. H. and Blunt, M. J.: "Pore-scale modeling of longitudinal dispersion", Water Resources Research, Vol. 40, W11501 (2004).

Brenner, H.: "Dispersion resulting from flow through spatially periodic porous media", Phil. Trans. R. Soc. Lon., A, 297, 81-133, (1980).

Bruderer, C. and Y. Bernabe: “Network modeling of dispersion: Transition from Taylor dispersion in homogeneous networks to mechanical dispersion in very heterogeneous ones”, Water Resources Research 37(4): 897-908 (2001).

Bryant, S. L. and Blunt, M.: “Prediction of relative permeability in simple porous media”, Physical Review A, 46 (4), (Aug. 1992).

Bryant, S. L., King, P. R. and Mellor, D. W.: “Network model evaluation of permeability and spatial correlation in a real random sphere packing”, Transport in Porous Media, 11, 53-70, (1993).

Buyuktas, D. and Wallender, W.W.: “Dispersion in spatially periodic porous media”, Heat and Mass Transfer, Volume 40, 261-270 (2004).

Carman, P. C.: “Fluid flow through a granular bed”, Trans. Inst. Chem. Eng. London, 15, 150-156 (1937).

Cenedese, A. and Viotti, P.: “Lagrangian analysis of nonreactive pollutant dispersion in porous media by means of particle image velocimetry technique”, Water Resources Research, 32 (8), 2329-2343, (Aug., 1996).

Chandrasekhar, S.: “Stochastic problems in physics and astronomy”, Rev. Mod. Phys., 15, 1-89, (1943).

Cherette, V. J., Evangelista E., Chertcoff R., Auradou, H., Hulin, J. P. and Ippolito, I.: “Influence of the disorder on solute dispersion in a flow channel”, Eur. Phys. J. Appl Phys., 39, 267-274, (2007).

Cirpka, O. A. and Kitanidis, P. K.: “Characterization of mixing and dilution in heterogeneous aquifers by means of local temporal moments”, Water Resources Research, 36 (5), 1211-1236, (May 2000).

Coats, K. H., C. H. Whitson and L.K. Thomas: "Modeling conformance as dispersion", paper SPE 90390 presented at the SPE Annual Technical Conference and Exhibition, Houston, TX, (Sep 26-29 2004).

Deans, H.A.: “A mathematical model for dispersion in the direction of flow in porous media”, SPE Journal (Mar. 1962).

Dullien, F. A. L., Porous Media: “*Fluid Transport and Pore Structure*”, Academic, San Diego, Calif, (1992).

Duplay, R. and Sen, P.N.: “Influence of local geometry and transition to dispersive regime by mechanical mixing in porous media”, Physical Review E, 066309, (2004).

Eidsath, A., Carbonell, R. G., Whitkar, S. and Herrmann, L. R.: “Dispersion in pulsed systems, III, Comparison between theory and experiments for packed beds, Chem. Eng. Sci., 38, 1803-1816 (1983).

FEMLAB Chemical Engineering Module Users Guide, (Oct. 2004).

Finney, J.: “Random packings and the structure of simple liquids. I. The geometry of random close Packing”, Proc. Roy. Soc. 319A, 479 494, (1970).

Flekkoy, E.G., Oxaal, U., Feder, J. and Jossang, T.: “Hydrodynamic dispersion at stagnant points: simulations and experiments”, Physics Review E, Volume 52, Number 5, (Nov. 1995).

Flekkoy, E.G., Rage, T., Oxaal, U. and Feder, J.: “Hydrodynamic irreversibility in creeping flow”, Physical Review Letters, Volume 77, Number 20, (Nov. 1996).

Frosch, G. P., Tillich, J. E., Haselmeier, R., Holz, M. and Althaus E.: “Probing the pore space of geothermal reservoir sandstones by nuclear magnetic resonance”, Geothermics, 29(6), 671– 687 (2000).

Garmeh, G., Johns R. T. and Lake, L. W.: “Pore scale simulation of dispersion in porous media”, SPE 110228 presented at SPE ATCE held at Anaheim, California, (Nov. 2007).

Gist, G. A., Thompson, A. H., Katz, A. J. and Higgins R. L. :“Hydrodynamic dispersion and pore geometry in consolidated rock”, Phys. Fluids A, 2(9), 1533–1544, (1990).

Graton, L. C. and Fraser, H. J.: “Systematic packing of spheres”, Journal of Geology (Nov-Dec. 1935).

Greenkorn, R.A. and Kesseler, D.P.: “Dispersion in heterogeneous nonuniform anisotropic porous media”, Industrial and Engineering Chemistry, 61, 33, (1969).

Heller, J. P.: "An Unmixing Demonstration", American J Phys, 28 (4), 348-353, (1960).

Hiby, J. W. "Longitudinal and transverse mixing during single-phase flow through granular beds." Symposium on the interaction between fluids and particles, Institute of Chemical Engineers, London, (1962).

Hoagland, D. A. and Prud'homme R. K.: "Taylor-Aris dispersion arising from flow in a sinusoidal tube", AIChE Journal, 31 (2), 2, 236-243, (1985).

Hulin, J. P. and T. J. Plona: "Echo tracer dispersion in porous media." Physics of Fluids A: Fluid Dynamics 1(8): 1341-7, (1989).

Jha, R. K. : *Pore Level Investigation of Dispersivity*, MS Thesis, The University of Texas at Austin, (May, 2005).

Jha, R.K., Bryant, S.L., Lake, L.W. and John, A.: "Investigation of pore-scale (local) mixing**",** paper SPE - 99782 presented at SPE Improved Oil Recovery Symposium, Tulsa, Oklahoma, (Apr. 2006).

Jha, R.K., John, A. K., Bryant, S. L. and Lake L. W.: "Flow reversal and mixing", SPE 103054 presented at SPE ATCE held at San Antonio, Texas, (Sep. 2006). To be published in SPE Journal (Sep., 2008).

Jha, R.K., Bryant, S. L. and Lake L. W.: "Influence of local mixing on core scale mixing", SPE 115961 to be presented at SPE ATCE held at Denver, Colorado, (Sep. 2008).

John, A. K., Lake, L. W., Bryant, S. L. and Jennings, J. W.: "Investigation of field scale dispersion", paper SPE - 113429 presented at SPE Improved Oil Recovery Symposium, Tulsa, Oklahoma, (Apr. 2008).

Johns, R. T., Sah, P. and Subramanian, S.: "Effect of Gas Enrichment above the MME on Oil Recovery in Enriched-Gas Floods," paper SPE 56826 presented at SPE ATCE held at Houston, Texas, (Oct. 1999).

Johns, R. T., Sah, P. and Solano, R.: "Effect of Dispersion on Local Displacement Efficiency for Multicomponent Enriched-Gas Floods above the MME",

paper SPE 64725 presented at SPE International Oil and Gas Conference and Exhibition in China held in Beijing, (Nov. 2000).

Kandhai, D., Hlushkou, D., Hoekstra, A. G., Sloot, P. M. A.,. Van As, H. and Tallarek U.: "Influence of stagnant zones on transient and asymptotic dispersion in macroscopically homogeneous porous media", Phys. Rev. Lett., 88(23), (2002).

Khrapitchev, A. A. and Callaghan, P. T.: "Reversible and irreversible dispersion in a porous medium", Phys. Fluids, 15(9), 2649– 2660, (2003).

Kitanidis, P. K.: "The concept of dilution index", Water Resources Research, 30 (7), 2011-2026, (Jul. 1994).

Koch, D. L. and Brady, J. F.: "Dispersion in fixed beds", J. Fluid Mech., 154, 399-427, (1985).

Koch, D. L. and Brady, J. F.: "A non-local description of advection-diffusion with application to dispersion in porous media", J. Fluid Mech., 180, 387-403, (1987).

Lake, L. W.: *Enhanced Oil Recovery*, Prentice Hall, NJ, (1989). Available through the author.

Lebon, L., Leblond, J. and Hulin, J. P.: "Experimental measurement of dispersion processes at short times using a pulsed gradient NMR technique", Physics of Fluids, 9(3), 481-490, (Mar., 1997).

Legatski, M. W. and Katz, D. L.:" Dispersion coefficients for gases flowing in consolidated porous media", SPE Journal, 7, 43–53, (1967).

Mahadevan, J., Lake, L. W. and Johns, R. T.: "Estimation of true dispersivity in field-scale permeable media**",** SPE Journal, (Sep. 2003).

Manz, B., Alexander, P. and Gladden, L.F.: "Correlations between dispersion and structure in porous media probed by nuclear magnetic resonance", Physics of Fluids, 11(2), 259-267, (Feb., 1999).

Mellor, D. W.: "*Random close packing (RCP) of equal spheres: structure and implications for use as a model porous medium*", PhD dissertation, Dept. of Earth Sciences, Open University, (1989).

Moroni, M. and Cushman, J. H.: "Three dimensional particle tracking velocimetry studies of the transition from pore dispersion to Fickian dispersion for homogeneous porous media", Water Resources Research, 37(4), 873-884, (Apr., 2001).

Muzzio, F.J., Swanson, P.D. and Ottino, J.M.: "Mixing distributions produced by multiplicative stretching in chaotic flows", International Journal of Bifurcation and Chaos, Volume 2, Number 1 37-50, (1992).

Ottino, J. M.: "Mixing, chaotic advection and turbulence", Annu. Rev. Fluid Mech., 22, 207-253, (1990).

Perkins, T. K. and Johnston, O. C.: "A Review of Diffusion and Dispersion in Porous Media"**,** SPE 480, SPE Journal, 3(3), 70-84, (Mar., 1963).

Pfannkuch, H. O.: "Contribution a l' etude des deplacements de fluiedes miscibles dans un milieu poreux", Rev. Inst. Fr. Pet., 18, 215–270,(1963).

Rigord, P., Calvo, A. and Hulin, J.P.: "Transition to irreversibility for the dispersion of a tracer in porous media", Physics of Fluids, 681 (May 1990).

Rigord, P., Leroy, C., Charlaix, E., Baudet, C., Guyon, E. and Hulin, J.P.: “Reversible and irreversible tracer dispersion in porous media”, Journal of Physics, Condens. Matter 2, (1990) , SA437-SA442.

Saffman, P. G.: “A theory of dispersion in a porous medium”, Journal of Fluid Mech., 6, 321-349, (1959).

Sahimi, M., Hughes, B.D., Scriven, L. E. and Davis, H. T.:” Dispersion in flow through porous media, I, One-phase flow, *Chem. Eng. Sci*., *41*, 2103–2122, (1986).

Salles J., Thovert, R., Delannay, R., Prevors, L., Auriault, J. L. and Adler, P. M.: “Taylor dispersion in porous media. Determination of the dispersion tensor”, Phys. Fluids A , 5 (10), 2348-2376, (Oct. 1993).

Seymour, J. D. and Callaghan, P. T.: Generalized approach to NMR analysis of flow and dispersion in porous media, AIChE J., 43, 2096, (1997).

Solano, R., Johns, R.T. and Lake, L.W.: “Impact of reservoir mixing on recovery in enriched-gas drives above the minimum miscibility enrichment”, SPE Reservoir Evaluation and Engineering, Volume 4, Number 5, (Oct. 2001).

Sto¨hr, M.: “*Analysis of flow and transport in refractive index matched porous media*”, Ph.D. thesis, Univ. of Heidelberg, Heidelberg, Germany, (2003).

Taylor, G.:"Dispersion of soluble matter in solvent flowing slowly through a tube." Proc. Roy. Soc. (London) A219: 186-203. (1953).

Taylor, G.I. : "*Low Reynolds Number Flows",* The National Committee for Fluid Mechanics Films. Released by Encyclopedia Britannica Educational Corp., Chicago, IL, (1972).

Thane, C.: Personal communication (2006).

Thane, C.: *Geometry and Topology of Model Sediments and Their Influence on Sediment Properties*, M.S. Thesis, The University of Texas at Austin (2006).

Vita

Raman Kumar Jha was born at Bhagalpur, Bihar, India to Mr. Niranjan Kumar Jha and Mrs. Shaila Jha. After completing his high school at Railway High School, Jamalpur, Monghyr, he entered Indian School of Mines, Dhanbad, India in June 1996. He received the degree of Bachelor of Technology in Petroleum Engineering in June 2000. Starting July 2000, he worked as a reservoir engineer in Oil and Natural Gas Corporation Limited, Karaikal, India for three years. In August 2003, he entered the Graduate School at The University of Texas at Austin. In May 2005 he received his MS in Petroleum Engineering and subsequently he entered the Ph. D. program.

Permanent Address:
C/O Sri Ramdhari Jha
Vill. – Gosaindaspur,
Nathnagar, Champanagar,
Dist. - Bhagalpur, Bihar
INDIA

This dissertation was typed by the author.